Deciphering Cell Specific Metabolic Programs in the Tumor Microenvironment

By
Bradley Isaac Reinfeld

Dissertation
Submitted to the Faculty of the
Graduate School of Vanderbilt University
in partial fulfillment of the requirements
for the degree of

DOCTOR OF PHILOSOPHY
in

Cancer Biology
May 31, 2022
Nashville, Tennessee

Approved:

Jeffrey C Rathmell Ph.D

Mary Philip M.D., Ph.D.

Alexander Bick M.D., Ph.D.

Volker Haase M.D.

Volker Haase M.D.

W. Kimryn Rathmell M.D., Ph.D.

Acknowledgements

This unique collaborative environment of the Rathmell allowed me to take part in great science at the intersection of immunobiology and cancer biology. I would first like to acknowledge the co-authors who helped published my major publications (Chapter 1 Reinfeld, Rathmell, Kim and Rathmell 2021, Chapter 2 Reinfeld and Madden et al. 2021) as well as the unpublished work on Hexokinase three in chapter 3. There are many potential coauthors of unpublished work in Chapter 3, Dr. Emily Arner, Dr. Aguirre De Cubas, Logan Vlatch, Dr. Scott Haake, Dr. Aleks Obradovic, Dr. Charles Drake, Dr. Brian Rini, Dr. Katy Beckermann Dr. Margret Axelrod, Dr. Justin Balko, Dr. Houssein Ardehali, Dr. P Brent Ferrell Jr, and Dr. Henrique Serezani. Patients treated at Vanderbilt University Medical Center generously contributed samples for analyses (Figures 2.1, 2.10, 2.11, Table 2.1, 3.11C,D,K, 3.12 I,J).

I am most grateful for the opportunity to train in Kim and Jeff's labs. They create an open environment where any student or post doc can thrive. It is a testament to their unique leadership abilities and scientific acumen. As they now direct large multi-institutional programs and departments, their laboratories remain hubs of scientific innovation and patient changing discoveries. At the end of many days, I often find myself saying, again we prove Kim and Jeff's fundamental discoveries about VHL in RCC and glucose's role in T cells. This is evidence of their decades long commitment to scientific rigor that I hope I have gained as a trainee in their orbit. One day, I hope to establish a lab/research team that emulates Jeff and Kim's success furthers scientific research and improves cancer patient outcomes.

This scientific work is made possible by the primary tumor collection conducted over the years by Dr. Katy Beckermann, Dr. Peter Siska, Kirsten Young, Rachel Hongo and Maddie Landis. I learned first-hand how to do much bench work as a young graduate student from Dr. Jamie Weyandt and Anna Chytil. Without Anna's remarkable knowledge and expertise for mouse work, western blotting cell culture and other cornerstones of molecular biology, I would not have made it to completing this document. I also have immense appreciation for Dr. Frank Mason, who has helped guide this project and brought his diverse perspective in order to improve this work on a day-in-day-out basis. Melissa Wolf both as her time as a technician in J Rathmell's lab and also as a graduate student in our group has helped me conduct many of these experiences With Dr. Agi De Cubas' bioinformatics skills, I have been able to tackle the second portion of my thesis. It has been wonderful working a new Post-Doctoral fellow in our lab, Dr. Emily Arner who has been a large help in the work in chapter 4. From Dr. J Rathmell lab, I have learned an immense amount of immmunometabolism from highly talented scientist like Dr. Marc Johnson, Dr. Ayaka Sugiura, Dr. Jackie Bader, Dr. Andrew Patterson, and Dr. Kelsey Voss. My science has improved from discussions and perspectives informed by how they do and think about science. A special thanks to Gabe Needle, a new member of Dr. J Rathmell's group for his tremendous help in organizing the large datasets in this document.

None of the work presented in the future pages could be done without the team science approach at Vanderbilt. I am the biggest beneficiary of working side by side day-by-day with, Dr. Matthew Z Madden. Matt and I interviewed for the MSTP on the same day in early January 2015 as both students from NESCAC schools with an appreciation

for great rec league basketball and were ultimately both wait-listed. We both ultimately choose to complete our PhDs in the Rathmell labs working side by side for many long mouse take down days. To say I was privileged to work with him over the last 5 years closely is an understatement. Matt's thoughtful approach to scientific questions at the bench mixed with his excitement on finding new biological truths has made me a better scientist in every dimension. This project's success relied on many skills Matt obtained, and I am forever grateful that he shared them with me on this scientific journey. I look forward to a career where I can continue to seek out his expertise.

Thank you to the physician scientists and translational scientists on the sixth floor of PRB who provided me with their insights and treated me as their peer. Special thanks to Drs. Balko, Johnson, Massion, Hurley, Moslehi and Park. Drs. Serezani, Ferrell ,and Bick have been unappareled resources in uncovering the role of HK3 in myeloid cells. Dr. Chris William's support for MSTP students allowed me to be successful at the bench and in my personal life. I am tremendously grateful to have a series of mentors outside of Vanderbilt that I have gained Playing in The Checkpoints. I would also like to thank my committee members for their consistent feedback and encouragement throughout this entire process.

My scientific success today would not be possible without my earliest scientific mentors. In high school, Mr. Eric Sloate and Dr. Arbetman permitted my growth and interest in scientific approach. With their help, I went to Tufts University with the undying passion to work in a science lab. Under the guidance of Dr. Susan Koegel, she directed me to Dr. Steve Fuchs' lab where I gained many skills to be a successful bench scientist and a better person. Their unwavering support gave me significant confidence that I could

one day in fact be a physician scientist. Additionally, my immunology professor, Harry Bernheim was a constant source of knowledge, excitement, and encouragement. I must thank Dr. Jessica Sims, and Dr. Lali Medina Kauwe for letting me spend a summer in a translational breast cancer lab at Cedars Sinai Medical Center.

This work has been funded by a handful of sources directly. I would like to thank the NIH/NCI for their support with my F30 (CA247202), our groups collaborative RO1 to study metabolic disturbances in RCC (R01CA217987) and the AACR Kure it Kidney Cancer Grant. From attending kidney cancer meetings and through social media engagement, I have gained an appreciation for the immense lengths patient advocates go to, and now appreciate that our great science would not be possible their tireless dedication to the field.

There are many Vanderbilt institutional entities to thank for this work. The image core run by Dr. Peterson, Dr. Tantawy and Fu Xie helped perform almost all the radioactive experiments. The Flow Cytometry core helped on studies in chapter 2. TPSR conducted IHC staining while CHTN consented and collected many of our human tissues. The Vanderbilt Institute for Advanced Genomics (VANTAGE) for library preparation and conducting of the NanoString study in chapter 2 and 3. Many figures in this dissertation were created using Biorender.com.

I would like to acknowledge the many people who helped me grow as a physician and a scientist who I have had the pleasure to work with and learn from over the last 7 years. I'd like to also thank Dean Dr. Amy Fleming, Dr. Yakes and Dr. Clair for being voices of reason through a hectic new age medical curriculum. I am grateful for the mentorship of Dr. Pierre Massion, Dr. Michael Fowler, and Dr. Geoffrey Fleming who have

passed prior to this thesis completeion. I will be forever grateful for the way in which all these excellent physicians treated me as a peer and shared their expertise with trainees. I am especially grateful to Ling Geng, a research scientist from H. Charles Manning Lab who lost his life to COVID in the winter of 2020 and helped perform autoradiography experiments in chapter 2. Ling and I often crossed paths on his way from the imaging institute to the mouse house. His constant kindness and helpful attitude are some of the examples of the supportive scientific environment at the Vanderbilt University Medical School. I am additionally grateful for the time I spent mentoring and learning from Zach Jones, an MSTP student.

This day would not be possible without the wonderful group of friends and colleagues I made here. There is no doubt that I am better for the friendship of Dr. Margaret Axelrod: She is an ideal friend and collaborator. She has always been there for me and helped me with some of my vexing scientific problems. Dr. Michael Raddatz has been a great sounding board for scientific ideas but more importantly someone whose perspective I always admire. Drs. Beebout, Reisman and Peek were all wonderful roommates and scientific collaborators. There are more friends in medical school classes past and present who enriched my learning and my clinical experience.

Last but certainly not least, I would like to thank my family for supporting me on this journey. While pursuing my PhD, I lost incredibly important role models in my personal life. Both of my grandmothers passed away, both of whom were fierce advocates for themselves and their grandchildren. Each possessed their own different perspectives and styles (one east coast, one west coast), but were unwavering in their pride for my personal and academic accomplishments. Tina Banos raised my mother, my brother, and I. In the

process, this proud women from Pachua, Mexico loved each one of us as if we were her own children. I am so privileged that she spent 28 years of my life mentoring me, teaching me and supporting me. I wish I could give her some of it back, but I hope to have a similar impact in the lives of those who I work and cross paths with. My parents, Ilene and Elliot, my rocks through every step on this long journey. The curriculum my mother crafted decades ago when she was my elementary school principal led to this crowning achievement today. To my brother Walker, thank you for supporting my aspirations, my work, and for being a source of laughter in my life. Though, my Reinfeld family has minimal exposure to science and medicine, their unwavering support of failed mouse experiments and western blots is commendable. I also want to thank the two men who came into my life during the COVID pandemic. My canine companion, RigaToni Reinfeld who always greets me with a kind smile upon returning from lab and helped me get through the revisions of our paper in the Winter of 2021. My partner Julian has been along for the wild ride as a long-distance relationship, and hopefully for the next scientific and personal journey, we can be side by side.

Table of Contents

List of Figures

List of Tables

CHAPTER 1: INTRODUCTION

This chapter is significant compromised of published review in *Cellular and Molecular Immunology*.

Reinfeld, B.I., Rathmell, W.K., Kim, T.K. and Rathmell, J.C. The therapeutic implications of immunosuppressive tumor aerobic glycolysis. *Cell Mol Immunol* **19,** 46–58 (2022). https://doi.org/10.1038/s41423-021-00727-3

It has been reproduced with the permission of the publisher and my co-authors Drs. TK Kim, W. Kimryn Rathmell, and Jeffrey C. Rathmell. Additional sections on metabolism of non-T cells and the metabolic implications of transforming mutations have been added for completeness.

In 2011, Hanahan and Weinberg added “Deregulating Cellular Energetics” and “Avoiding Immune Destruction” to the six previous Hallmarks of Cancer. These hallmarks remained at the revision of this document in 2022. Since this seminal paper, there is a growing consensus that these new hallmarks are not mutually exclusive but rather interdependent. The following introduction will summarize how founding genetic events for tumorigenesis ultimately increase tumor cell glycolysis that not only supports the metabolic demands of malignancy but also provides an immunoprotective niche, promoting malignant cell proliferation, maintenance, and progression. Mechanisms by which altered metabolism contribute to immune impairment are multifactorial: (1) the metabolic demands of proliferating tumor cells and activated immune cells are similar, thus creating a situation where immune cells may be in competition for key nutrients. (2) the metabolic byproducts of aerobic glycolysis directly inhibit anti-tumor immunity while promoting a regulatory immune phenotype. (3) The gene programs associated with upregulation of glycolysis also result in the generation of immunosuppressive cytokines and metabolites. With this perspective, we will shed light onto important considerations for development of new classes of agents targeting cancer metabolism. These types of therapies can impair tumor growth, but also pose a significant risk to stifle anti-tumor immunity.

The fundamental discovery that led to the field of tumor metabolism is Otto Warburg’s description that tumor tissues utilize glucose and produce lactate in the presence of oxygen (Warburg et al., 1924). Based on these findings Warburg proposed the cancer cell-centric model that the disruption of the mitochondrial electron transport chain was necessary for tumorigenesis and thus a commonality between all cancer

cells (Warburg, 1956). However, these early studies failed to recognize the duality of metabolic demands by both the tumor cells themselves and other resident cells in the tumor microenvironment (TME). Importantly, more recent established literature implicates reprogramming of cell metabolism as essential for immune cell fates. In the context of a tumor, metabolic networks are crucial for immune cells ability to eliminate tumors (Andrejeva & Rathmell, 2017).

It is now clear that all dividing cells upregulate glucose metabolism to meet the biosynthetic demands of proliferation(Vander Heiden et al., 2009). Even though glycolysis produces limited ATP, this metabolic program supports the necessary pathways for *de novo* lipid, nucleotide, and amino acid synthesis with great efficiency. This applies to both proliferating tumor cells with deregulated cell cycle and to the activation of immune cells, which undergo rapid transitions from quiescent to proliferative when confronted with appropriate stimuli. Further, the field of immunometabolism demonstrated that different immune subsets implement and require distinctive metabolic programs to accomplish their diverse effector functions, indicating that the metabolism of proliferating cells share some but not all features (O'Neill et al., 2016). Because both tumors and immune cells implement generally similar metabolic programs, this review will evaluate possible synergistic interactions between cancer metabolism targeting therapies and cancer-modulating immunotherapies. Inhibitors developed to target cancer metabolism may therefore, counterproductively, hinder immunotherapy efficacy.

Common signaling and mutational events that regulate glycolysis

The structure of metabolic signaling is shared amongst most mammalian cells. Critically, the phosphoinositide 3 kinase (PI3K)/Akt/mechanistic Target of Rapamycin

Complex 1 (mTORC1) pathway plays a key role to induce anabolic metabolism for cell growth(Orozco et al., 2020; Saxton & Sabatini, 2017; Ward & Thompson, 2012) (**Figure 1.1**). Canonically, this pathway becomes activated when growth factors bind to receptor tyrosine kinases (RTKs), or g-coupled protein receptors (GPCRs). Class 1A PI3K are activated via binding of their regulatory SH2 containing domains to phosphorylated tyrosines on the cytoplasmic tails of RTKs**.** The regulatory domain of Class IB PI3K interact with the beta and gamma subunits of the activated G proteins in the presence of activating ligand. In both situations, conformational changes in these regulatory PI3K proteins promote activation of the PI3K catalytic kinase domain, p110 (Fruman et al., 2017). Active p110 in turn phosphorylates membrane phosphoinositides, increasing levels of AKT activating PIP_3(3,4,5). Additionally, active Ras bound GTP can drive PIP_3(3,4,5) accumulation via binding to p110 kinase within the Ras binding domain of PI3K (Rodriguez-Viciana et al., 1996). AKT ultimately recognizes PIP_3(3,4,5) via its PH domain leading to subsequent activation by PDK1, and mTORC2, via phosphorylation at threonine 308 (Alessi et al., 1997) and serine 473 (Sarbassov et al., 2005), respectively. With these two posttranslational modifications, AKT becomes active and is therefore able to increase cellular glycolysis (Elstrom et al., 2004).

AKT has a diverse collection of cellular targets that promote cell growth and prevent apoptosis. AKT activation results in the phosphorylation of Glut1 (Rathmell et al., 2003) and GLUT4 (Kohn et al., 1998), allowing for translocation of these glucose transporters to the cellular membrane where they promote glucose uptake. Hexokinase (HK), the first commitment step of glycolysis, is also regulated by AKT (Rathmell et al., 2003) HK is rate limiting for glycolysis, and its activity irreversibly fixes glucose inside the

cell. When HK is phosphorylated, it associates with the mitochondria to become more active (Majewski et al., 2004) . Additionally, active AKT directly regulates phosphofructokinase 2, which in turn increases cellular fructose 2,6 bisphosphate(F2,6BP) (Deprez et al., 1997). This metabolite acts a positive regulator of the rate-limiting step of glycolysis, phosphofructokinase 1, which is responsible for making fructose 1,6 bisphosphate. Therefore, AKT activation promotes glycolytic flux via increased glucose uptake and elevating basal glycolytic rate.

Ultimately, mTORC1 is the key cellular metabolic signaling hub. **(Figure 1.1)**. This protein complex integrating metabolite availability and growth factor signaling. The AKT can increases mTOR signaling by phosphorylating TSC2 (Inoki et al., 2002) and PRAS40 (Kovacina et al., 2003), two separate negative regulators of mTOR. The role of these pathways has been reviewed extensively in many cell types (Saxton & Sabatini, 2017; Waickman & Powell, 2012) mTORC1 activity promotes anabolic metabolism. Downstream of mTORC1, glucose-dependent synthesis of nucleotides and lipids occurs via phosphorylation of p70S6 kinase (pS6K) and 4EBP1. Activated mTOR promotes transcription of Hypoxia Inducible Factor 1 (HIF1α), the main transcriptional regulator of glycolysis (Land & Tee, 2007)**,** and then CAP-dependent translation of this key protein (Duvel et al., 2010). Other key downstream transcriptional effectors of mTORC1 signal are the transcriptional regulator of lipid metabolism, Sterol Regulatory Element Binding Protein (SREBP), and c-Myc. To ensure proliferation in the presence of sufficient metabolic substrate, mTORC1 induces this anabolic program only when sensing adequate intracellular levels of essential amino acids from its position on the surface of the lysosome (Wolfson & Sabatini, 2017).

The transcription factors HIF1α, HIF2α and c-Myc play crucial roles to promote glycolysis at a transcriptional level **(Figure 1.1**). HIF1α and HIF2α are oxygen dependent transcription factors which bind to HIF response elements throughout the genome to induce a glycolytic gene expression program. In normoxia, HIF1α is inactivated by prolyl hydroxylase enzymes (PHDs). The PHDs hydroxylate HIF1α at proline residues 402 and 562, which then promote ubiquitination and ultimately degradation via the E3 ubiquitin ligase VBC complex containing the von Hippel Lindau (VHL) tumor suppressor as the targeting component (Epstein et al., 2001; Ivan et al., 2001; Jaakkola et al., 2001; Yu et al., 2001). In hypoxia, the PHDs are inhibited and therefore VHL can no longer recognize the HIF family of transcription factors. Then, the αHIF subunit accumulates, binds to HIF1β/ARNT (a homolog with DNA binding capacity) and translocates to the nucleus (Semenza & Wang, 1992). HIF1α, together with the transcriptional co-activator p300, promotes transcription of glycolytic genes including Glut1, HK2, aldolase, and lactate dehydrogenase (LDH), to increase cellular uptake and utilization of glucose. Active HIF1α elevates Vascular Endothelial Growth Factor (VEGF), leading to increased cellular oxygenation and metabolic substrate availability through formation of new blood vessels.

It is worth noting that HIF1α has a closely related homolog seen in multicellular eukaryotes, HIF2α. These two proteins have non-redundant functions. HIF1α and HIF2α predominate at different oxygen tensions (Holmquist-Mengelbier et al., 2006). Additionally, these two transcription factors bind an overlapping and yet unique set of genes. For example, both HIF1α and HIF2α regulate Glut1 and VEGF expression but HIF1α specifically regulates hexokinase expression while erythropoietin is only

responsive to HIF2α levels (Keith et al., 2011). In different human cancers, either HIF1α or HIF2α or in some cases both factors can be negative prognostic indicators of outcome (Keith et al., 2011)**.** Currently, we do not understand what extrinsic/tissue specific factors govern the wide variety of transcription control that is HIF-dependent across tissues or disease contexts. Therefore because of the pleiotropic effects of these two key hypoxia transcriptional regulators (especially in cancer cells), we will reference genes regulated by either of these factors as hypoxia regulated genes.

Glycolytic genes are also regulated by the myc family of oncogenes. Myc proteins heterodimerize with Max and bind to gene promoter containing E boxes to ultimately drive glycolytic gene transcription. Myc is unusual as a transcription factor because it interacts broadly across the genome and can associate with paused RNA polymerase II to increase transcript elongation (Rahl et al., 2010). Therefore, it can amplify expression of a diverse set of active genes with easily accessible chromatin. It comes as no surprise that the Myc family of transcription factors can regulate most of the enzymes related to glycolysis given that these proteins are expressed basally in most cell types. Of the many glycolytic genes myc regulates, myc accumulation can also increase the expression levels of Glut1, PFK, Glyceraldehyde 3-Phosphate Dehydrogenase, Phosphoglycerate Kinase, Enolase and Phosphoglucose Isomerase (Osthus et al., 2000). Additionally, many promoters of glycolytic genes were found via chromatin immunoprecipitation to contain Myc-Max bound E-boxes (Kim et al., 2004). Active Myc is known to also promoting glutaminolysis, which can maintain mitochondrial anaplerosis (Wise et al., 2008) in addition to increasing ribosome and mitochondrial biogenesis (Kim et al., 2008).

p53 opposes aerobic glycolysis

p53 is generally viewed as an antagonist of Warburg metabolism (Napoli & Flores, 2017) **(Figure 1.1**). Typically, cellular levels of p53 are low given that MDM2 ubiquitinates p53, marking it for proteasomal degradation. However, upon a wide variety of cellular stressors, MDM2 is inhibited, p53 is stabilized and exerts its senescent/proapoptotic function via binding to DNA and changing cellular gene expression. By increasing SCO2 expression, p53 is viewed a key regulator of oxidative metabolism. SCO2 is necessary for the assembly of the cytochrome C complex where O2 is the final electron acceptor (Matoba et al., 2006). p53 negatively regulates glycolysis through inhibiting transcription of Glut1 and Glut4 (Schwartzenberg-Bar-Yoseph et al., 2004) in addition to blocking Glut3 mobilization via decreasing active levels of NF-kB (Kawauchi et al., 2008). Active p53 also results in the accumulation of TIGAR, a protein whose activity shunts glucose into the pentose phosphate pathway (PPP) in addition to inhibiting PFK1 by decreasing available pools of F2,6BP (Bensaad et al., 2006). At times of high levels of cellular stress, p53 directly binds and inhibits the activity of glucose-6-phosphate dehydrogenase, the rate limiting enzyme of the PPP (Jiang et al., 2011). Blocking G6PD prevents *de novo* nucleotide synthesis and promotes apoptosis via limiting pools of necessary nucleotides for DNA repair.

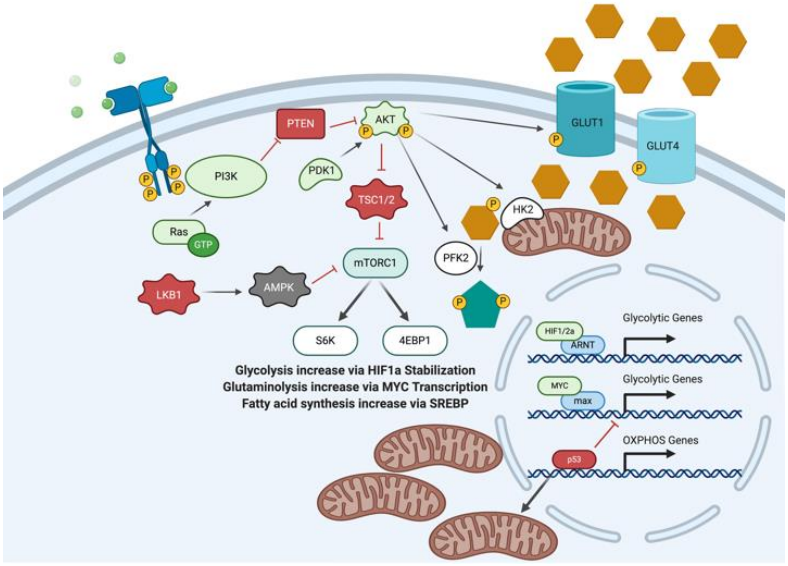

Figure 1.1: **Activation of classical oncogenes and loss of canonical tumor suppressors results in elevated tumor glycolysis**. Oncogenes are depicted in green, while tumor suppressors are depicted in red. White gene products are not implicated in malignancy through genetic events. Ultimately, genetic activation of the PI3K/AKT/mTOR pathway increases the glycolytic transcription factors HIF1α and myc. phospho-AKT also promotes increase glycolytic rate by phosphorylating/hyperactivating a myriad of glycolysis associated substrates, Glut1/4, Hexokinase 2 (HK2) and Phosphofructose Kinase 2 (PFK2). The oncogenic transcription factors HIF1α and Myc bind promoters of genes related to glycolysis. HIFs can be stabilized through mutations that result in Krebs cycle dysfunction or inactivate machinery required for proteasomal degradation. Active p53 prevents the transcription of these genes in addition to shunting glucose into the PPP.

Activating oncogenic mutations increase PI3K/mTOR signaling tone and tumor glycolysis

Mutations causing constitutive activation of growth factor receptor pathways can stimulate increased cancer cell glycolysis (**Figure 1.1**)**.** An often mutated or overexpressed protein in cancer is the epidermal growth factor receptor (EGFR) and its 3 homologs (HER2, HER3 and HER4) (**Table 1.1**). Via their extracellular domain (which HER2 lacks), this receptor family binds to the epidermal growth factor family of ligands, promoting dimerization. In this dimerized conformation, the intracellular kinase phosphorylates their intracellular domains at tyrosine residues. These phosphotyrosine residues act as docking sites for proteins with SH2 domains like the regulatory subunit of PI3K. Signaling through this family of receptors is thought to canonically activate both

the mitogen activated protein kinase pathways (MAPK) and the PI3K/mTOR pathway (Yarden, 2001). In most cases, mutations in these receptors promote phosphorylation of these intracellular tyrosines without binding ligand. Additionally, in some tumor types, there are amplifications of one of these receptors, increasing the total amount of phosphotyrosine and signaling tone through this pathway. For example, 15-20% of non-small cell lung cancer patients contain activating mutation in EGFR (da Cunha Santos et al., 2011). Blocking glycolysis, with 2-DG (an inhibitor of HK) restored sensitivity to tyrosine kinase inhibitors for cell lines harboring EGFR T790M mutations (TKIs) (Kim et al., 2013). Additionally, over 25-30% of all breast cancer patients have amplifications of HER2 (Loibl & Gianni, 2017). As expected, HER2 amplified mouse mammary tumors demonstrate increased radiolabeled glucose uptake via F18-Florodeoxyglucose (FDG) positron emission tomography (PET) and inhibition of HER2 either with a monoclonal antibody or TKI decreases tumor FDG-PET avidity (Miller et al., 2009).

As mentioned earlier, activated Ras can increase PI3K activity directly by binding to the p110 subunit (**Figure 1.1**) Activating Ras mutations are key features of lung (Roman et al., 2018) and pancreatic cancer (Bryant et al., 2014) (where 90% of patients have K-Ras G12X mutations) (**Table 1.1**). It has been shown overexpressing oncogenic Ras in fibroblasts increases VEGF expression. This increase of VEGF is dependent on the HRE in the 5' promoter, indicating that activated Ras increases glycolytic HIF signaling (Mazure et al., 1996).

Increases in PI3K related signaling can also originate from amplifications of the kinase itself, or mutations that remove regulatory control of this kinase **(Figure 1.1).** *PIK3CA* is amplified in a number of tumor types including breast, cervical, gastric, lung,

ovarian, and prostate (Courtney et al., 2010) (**Table 1.1**). Additionally, there are three hotspot mutations, two commonly found in the helical domain (E542K, E545K). These mutations prevent the regulatory p85 from repressing p110s kinase activity. The other common mutation (H1047R) occurs in the kinase domain, which promotes constitutive activation. There are also gain of function mutations in the p85 regulatory subunit that promote activation of p110 without engaging phosphotyrosines or activated G proteins (Courtney et al., 2010). Mutations that activate the downstream kinase, AKT, follow a similar structural pattern (**Figure 1.1, Table 1.1**). All three variants of AKT can have gain of function mutations, which promote membrane localization and increased activity without changes in membrane levels of PIP_3(3,4,5). AKT2 appears to be the only variant of this protein that is amplified across cancer types. In colorectal cancer, groups have described gain of function mutations in the AKT activating enzyme, PDK1 (Parsons et al., 2005). Through these mutations and amplifications of PI3K and AKT, increased signaling tone resulting in elevated mTOR activation contributes to enhanced tumor glycolysis.

Myc's role as an oncogene is supported by the fact that it is the 3rd most amplified gene in all human cancer (**Figure 1.1, Table 1.1**) (Zack et al., 2013). A classic example of myc driven oncogenesis occurs in Burkitt's Lymphoma. The molecular diagnostic hallmark of this disease is the t(8;14) chromosomal translocation that results in the myc oncogene located downstream of the immunoglobulin heavy chain promoter (Haluska et al., 1986)**.** This genetic event results in myc accumulation. Ectopic overexpression of myc in glioblastoma cells results in the expected increase in glucose uptake, and lactate production. However, by increasing cellular glycolysis, these cells become

vulnerable to NAPMT inhibition. NAPMT is the rate limiting step in the NAD salvage pathway, and therefore inhibiting this enzyme in myc high cells induces death due to limited availability of NAD (Tateishi et al., 2016).

Table 1.1:**Across tumor types, gain of function mutations drive increase cellular glycolysis**

Gain of Function	Type of mutations	Tumor Type	Role in metabolism	Evidence of mutations impacting cell metabolism
Myc	Amplification Translocations	Ewing's Sarcoma Lymphoma Neuroblastoma	Promotes glucose utilization via transcription of GLUT1, PFK, G3PD, PGK, enolase, and Pgi,	1:.Deregulation of glucose transporter 1 and glycolytic gene expression by c-Myc[1] 2:Evaluation of Myc E-Box Phylogenetic Footprints in Glycolytic Genes by Chromatin Immunoprecipitation[2] 3:Myc-Driven glycolysis is a therapeutic target in glioblastoma[3] 4:Global metabolic reprogramming of colorectal cancer occurs at adenoma stage and is induced by MYC[4]
AKT	Amplification, Point mutation	Breast Colon Endometrial Melanoma Ovarian	Translocation of GLUT1/3, HK activation, PFK2 activation mTOR activation via inhibition of TSC1/2,	1:Akt Stimulates Aerobic Glycolysis in Cancer Cells[5] 2:Akt Maintains Cell Size and Survival by Increasing mTOR-dependent Nutrient Uptake[6] 3:Akt regulation of glycolysis mediates bioenergetic stability in epithelial cells[7] 4:Selective eradication of cancer displaying hyperactive Akt by exploiting the metabolic consequences of Akt activation[8]
PDK1	Amplification	Breast Gastric Colorectal Lung Prostate Thyroid	Activates AKT at S374	1:PDK1-dependent Metabolic reprogramming dictates metastatic potential in breast cancer[9] 2:PDK1 potentiates upstream lesions on the PI3K pathway in breast carcinoma[10] 3:Pyruvate Dehydrogenase Complex Activity Controls Metabolic and Malignant Phenotype in Cancer Cell[11]
PI3K	Amplification, Point Mutation	Breast Cervical Endometrial Gastric Glioma Head and Neck carcinoma Lymphoma Liver Lung Prostate Pancreas Thyroid	Essential for AKT activation	1:Oncogenic PIK3CA mutations reprogram glutamine metabolism in colorectal cancer[12] 2:Suppression of insulin feedback enhances the efficacy of PI3K inhibitors[13] 3:PIK3CA Mutational Status Is Associated with High Glycolytic Activity in ER+/HER2,âí Early Invasive Breast Cancer: a Molecular Imaging Study Using [18F]FDG PET/CT[14] 4:The PIK3CA E542K and E545K mutations promote glycolysis and proliferation via induction of the b-catenin/SIRT3 signaling pathway in cervical cancer[15] 5:Phosphoinositide 3-Kinase p110β activity: Key Role in Metabolism and Mammary Gland Cancer but not Development[16] 6:Kinase-dependent and -independent functions of the p110β phosphoinositide-3-kinase in cell growth, metabolic regulation and oncogenic transformation[17] 7:PI3Kδ inhibition by idelalisib in patients with relapsed indolent lymphoma[18].
HER2	Amplification, Point Mutation	Breast Cholangiocarcinoma Colon Lung Ovarian Salivary Duct,	Upstream activator of PI3K/AKT/mTOR	1:Inhibition of mammalian target of rapamycin is required for optimal antitumor effect of HER2 inhibitors against HER2-overexpressing cancer cells. 2:Optical Imaging of Glucose Uptake and Mitochondrial Membrane Potential to Characterize Her2 Breast Tumor Metabolic Phenotypes 3:Tyrosine Phosphorylation of Mitochondrial Creatine Kinase 1 Enhances a Druggable Tumor Energy Shuttle Pathway[19]
EGFR	Amplification, Point Mutation	Colon Lung Glioma	Upstream activator of PI3K/AKT/mTOR	1:Glycolysis Inhibition Sensitizes Non-Small Cell Lung Cancer with T790M Mutation to Irreversible EGFR Inhibitors via Translational Suppression of Mcl-1 by AMPK Activation[20]. 2:Enhanced Glycolysis Supports Cell Survival in EGFR-Mutant Lung Adenocarcinoma by Inhibiting Autophagy-Mediated EGFR Degradation[21] 3: EGFR-Induced and PKCε Monoubiquitylation-Dependent NF-κB Activation Upregulates PKM2 Expression and Promotes Tumorigenesis[22]
RAS	Mutation	Colon Lung Rectal Pancreas	Activator of PI3K signaling cascade via RBD	1:Oncogenic transformation and hypoxia synergistically act to modulate vascular endothelial growth factor expression[23] 2:Oncogenic KRAS supports pancreatic cancer through regulation of nucleotide synthesis[24] 3:Oncogene ablation-resistant pancreatic cancer cells depend on mitochondrial function[25]

Loss of tumor suppressors also increases tumor glycolysis

Loss of function mutations in tumor suppressors can lead to increased PI3K/AKT/mTOR tone in transformed cells **(Table 1.2)** PTEN is a negative regulator of

the PI3K/AKT/mTOR pathway. PTEN is a lipid phosphatase that catalyzes the transformation of AKT-activating PIP_3(3,4,5) to PIP_2(3,4). PIP_2(3,4) is not recognized by the PH domain of AKT and therefore limits downstream mTOR signaling (**Figure 1.1**). Therefore, PTEN loss results in accumulation of PIP_3(3,4,5) and excess activation of AKT (Myers et al., 1998). PTEN loss is the most common aberration in the PI3K pathway seen across cancer patients. This gene can be inactivated by loss of function mutations, deletions, or epigenetic silencing of the loci. Ingenuity pathway analysis examining transcripts from PTEN depleted melanoma cells, demonstrates an increase in glycolysis is secondary to losing this tumor suppressor (Cascone et al., 2018).

Another protein known to negatively regulate the mTOR pathway is LKB1/STK11. This kinase phosphorylates AMPK (Saxton & Sabatini, 2017), which is a kinase that directly inhibits mTOR via phosphorylation of TSC2 and RAPTOR. AMPK and mTOR have opposing effects in cells. mTOR integrates proliferative signals (i.e. growth factors) and nutrients (i.e. amino acids), to ultimately promote a proliferative and glycolytic metabolic program (Saxton & Sabatini, 2017) **.** AMPK, conversely, is active at high AMP/ATP ratio, indicating a need to replenish cellular energy sources, promoting oxidative phosphorylation and fatty acid oxidation. In Peutz Jurgers, a familial hamartomatous syndrome, patients have germ line mutations inactivating LKB1. Additionally, 15-30% of NSCLC and 20% of cervical cancers harbor loss of function mutations in LKB1. As expected, cells with LKB1 loss have high levels of HIF1α, increased glucose uptake and lactate production (Faubert et al., 2014).

Not surprisingly, loss of another negative regulatory complex of mTOR, the tuberous sclerosis complex (compromised of the proteins TSC1/TSC2) results in the

familial tumor syndrome, tuberous sclerosis (**Table 1.2**). TSC1/2 under normal physiological conditions suppress mTOR activation by acting as a GTPase activating protein for RHEB (Tee et al., 2003; Zhang et al., 2003), the necessary co-activator for mTORC1 (Tabancay et al., 2003) (**Figure 1.1**). Mouse embryonic fibroblasts (MEFs) deficient in TSC1 or TSC2 have increased glucose uptake, lactate production which is dependent on mTOR activation and transcription of the oncogenic pyruvate kinase isoform (PKM2) downstream of HIF1α. These TSC2 deficient MEFs are more sensitive to glycolysis inhibition or rapamycin then their WT control (Sun et al., 2011). Additionally, a new model of lymphangiosarcoma, where TSC1 is specifically deleted in endothelial cells, results in the development of tumors reliant on autocrine VEGF signaling. From this mouse model, Sun and colleagues uncovered a positive correlation between mTORC1 activation with HIF1α, VEGF, c-myc and Ki67 levels in a collection of human lymphangiosarcoma samples (Sun et al., 2015).

Loss of p53 is the most common event in human cancer (**Figure 1.1**). As discussed earlier, this protein has a unique ability to promote oxidative metabolism and promote usage of the PPP. A group used a novel chemical activator of p53 to show that by re-activating p53 in transformed cells, glycolytic genes like HK as well as glycolytic transcriptions factors myc and HIF1α could be repressed. However, this ability was abolished in Tp53 null cell lines, illustrating that activating wild type p53 alone can decrease tumor glycolysis (Zawacka-Pankau et al., 2011).

Genetic elevation HIF1α is another hallmark of cancer

Through a variety of genetic mechanisms, The HIFs can be permanently stabilized, promoting constant aerobic glycolysis (**Table 1.2**). In over 90% of clear cell renal cell

carcinoma (ccRCC), VHL is lost most. This most commonly occurs commonly by deletion of chromosomal arm 3p or inactivating mutation but can also occur by promoter hypermethylation (Cancer Genome Atlas Research, 2013; Turajlic et al., 2018). Without this ubiquitin ligase, the HIFs become hydroxylated but cannot be degraded in normoxia. Loss of VHL results in decrease in mitochondrial biogenesis (Zhang et al., 2007) and an increase in FDG PET signal (Thomas et al., 2006) in pre-clinical models of ccRCC.

Additionally, aberrations in Krebs cycle can stabilize HIFs. There are a host of familial paraganglioma/pheochromocytoma syndromes where patients have germline mutations in different members of the succinate dehydrogenase complex (Malinoc et al., 2012; Vanharanta et al., 2004) in addition to Hereditary Leiomyomatosis and Renal Cell Carcinoma syndrome where patients harbor loss of function mutation in another Krebs cycle enzyme, fumarate hydratase (Tomlinson et al., 2002) (**Table 1.2**). Both succinate (Selak et al., 2005) and fumarate (Isaacs et al., 2005; Pollard et al., 2005) accumulate in these cancer syndromes, inhibiting the diverse family of alpha ketoglutarate dependent dioxygenases like the PHDs. Therefore, the HIFs cannot be hydroxylated and thus are not recognized by VHL. In the FH deficient RCCs, this accumulated fumarate increases glycolysis via two additional mechanism: (1) inhibition of PTEN (Ge et al., 2022) and (2) mitochondrial replication (Crooks et al., 2021). There is also growing appreciation for the transforming properties of IDH1/2 mutant tumors, seen most often in gliomas and myeloid malignancies. With these neomorphic IDH mutations, tumor cells accumulate the onco-metabolite 2HG, which also inhibits alpha ketoglutarate dependent dioxygenases and raises cellular HIF levels (Xu et al., 2011).

Over 75% of cancers harbor mutations predicted to result in a glycolytic phenotype (Meric-Bernstam et al., 2015) when re-analyzing sequencing data from over 2000 patients. It comes as no surprise, therefore, that altered metabolism and increased glucose uptake are intimately associated with transformation and are both central cancer hallmarks(Hanahan & Weinberg, 2011; Pavlova & Thompson, 2016). Nevertheless, most measurements of tumor metabolism are conducted on cell lines *in vitro* or in bulk chunks of heterogeneous tumor tissues *in vivo*. These *in vitro* or bulk measurements may simplify or miss key aspects of the metabolism of individual cells due to the altered nutrients

Table 1.2: **Common loss of function mutations in tumor suppressors promote glycolytic upregulation in human malignancies**

Loss of Function	Type of mutations	Tumor Type	Role in metabolism	Evidence of mutations impacting cell metabolism
VHL	Inactivating promoter hypermethylation, chromosomal deletion	ccRCC PNETs paraganglioma	Negative regulator HIF TFs	1.HIF-1 Inhibits Mitochondrial Biogenesis and Cellular Respiration in VHL-Deficient Renal Cell Carcinoma by Repression of C-MYC[26] 2.Hypoxia-inducible factor determines sensitivity to inhibitors of mTOR in kidney cancer[27] I3.sotope Tracing of Human Clear Cell Renal Cell Carcinomas Demonstrates Suppressed Glucose Oxidation In Vivo[28]
p53	Inactivating, Dominant negative	Bladder Breast Colon Esophageal Lung Li-Fraumeni Ovarian Pancreas Prostate	Promotes cytochrome C assembly, negative regulator of GLUT1/3/4 G6PD, activates TIGAR to inhibit 2,6FBP	1.P53 Regulates Mitochondrial Respiration[29] 2.The Tumor Suppressor p53 Down-Regulates Glucose Transporters GLUT1 and GLUT4 Gene Expression[30] 3.p53 regulates glucose metabolism through an IKK-NF-kappaB pathway and inhibits cell transformation[31]. 4.TIGAR, a p53-Inducible Regulator of Glycolysis and Apoptosis[32] 5.P53 regulates biosynthesis through direct inactivation of glucose-6-phosphate dehydrogenase[33] 6.Regulation of monocarboxylate transporter MCT1 expression by p53 mediates inward and outward lactate fluxes in tumors[34]
TSC1 TSC2	Inactivating Deletion	Bladder Endometrial Lung Melanoma Renal Tuberous Sclerosis Syndromes	Negative regulator of mTOR	1.Constitutive Activation of mTORC1 in Endothelial Cells Leads to the Development and Progression of Lymphangiosarcoma through VEGF Autocrine Signaling[35] 2.Mammalian target of rapamycin up-regulation of pyruvate kinase isoenzyme type M2 is critical for aerobic glycolysis and tumor growth[36] 3.Glucose deprivation in tuberous sclerosis complex-related tumors[37] 4.Autophagy-Dependent Metabolic Reprogramming Sensitizes TSC2-Deficient Cells to the Antimetabolite 6-Aminonicotinamide[38]
LKB1/ STK11	Inactivating	IO resitant Lung Cancer Peutz-Jegher Syndrome	Positive regulator of AMPK	1.Loss of the tumor suppressor LKB1 promotes metabolic reprogramming of cancer cells via HIF-1[39] 2.LKB1/KRAS mutant lung cancers constitute a genetic subset of NSCLC with increased sensitivity to MAPK and mTOR signaling inhibition[40] 3.LKB1 deficiency in T cells promotes the development of gastrointestinal polyposis[41]
FH SDH IDH1/2	Inactivating	Acute Myeloid Leukemia Cholangiocarcinoma Gliomas Paragangliomas Familial Renal Carcinoma	Key enzymes in the Krebs Cycle Accumulation of aKG-like oncometaboilte s which stabilize HIFs	1.UOK 262 cell line, fumarate hydratase deficient (FH-/FH-) hereditary leiomyomatosis renal cell carcinoma: in vitro and in vivo model of an aberrant energy metabolic pathway in human cancer[42] 2.Mutations in SDHD, a mitochondrial complex II gene, in hereditary paragnaglioma[43] 3.Cancer-associated IDH1 mutations produce 2-hydroxyglutarate[44] 4.Suppression of antitumor T cell immunity by the oncometabolite (R)-2-hydroxyglutarate[45]
PTEN	Inactivating Chromosomal del etion	Breast Endometrial Glioma Melanoma	Negative regulator of AKT, increasing membrane bound activating PIP3	1. Increased Tumor Glycolysis Characterizes Immune Resistance to Adoptive T Cell Therapy[46] 2.Inhibiting PI3KB with AZD8186 regulates key metabolic pathways in PTEN-null tumors[47] I3.ncreased Concentrations of Fructose 2,6-Bisphosphate Contribute to the Warburg Effect in Phosphatase and Tensin Homolog (PTEN)-deficient Cells[48] 4.Hexokinase 2-Mediated Warburg Effect Is Required for PTEN and p53-Deficiency Driven Prostate Cancer Growth[49] 5.PTEN Suppresses Glycolysis by Dephosphorylating and Inhibiting Autophosphorylated PGK1[50]

available *in vitro* and the diversity of cellular components and spatial heterogeneity in the whole tissues. The interplay of cancer cell, stromal, and immune cell metabolism *in vivo*, therefore, has not been well disentangled and displays the challenges and opportunities to dissect this arena to better treat this heterogenous disease.

Warburg Metabolism as essential feature of infiltrating immune cells

Previous reviews have extensively discussed the steps required to generate anti-tumor immunity (Chen & Mellman, 2013) as well as the conditions for efficacious immunotherapy (Galluzzi et al., 2018). To have proper antigen shedding, antigen presentation, immune cell activation, immune effector function and ultimately memory generation, the anti-tumor compartment of tissue resident dendritic cell (DC), M1 macrophages, Natural Killer (NK) Cells and Th1/CTLs requires complex metabolic reprogramming. The field of immunometabolism now provides a framework to understand the necessary metabolic changes that promote the effective T cell response to cancer and how cancer cells and immune cells may interact in the tumor microenvironment. These studies illustrate the similarities and differences among these diverse cell types, and how nutrient limitations and molecular cues in the TME promote immune cell dysfunction, regulatory immune cell subsets, and a niche for tumor maintenance and proliferation. The same set of principles have also been applied to myeloid maturation, tumor cell phagocytosis, NK cell licensing, and DC antigen presentation where ultimate immune cell fate and function are inextricably linked to unique metabolic programs that produce targetable vulnerabilities.

Metabolic diversity underlies divergent T cell phenotypes and function

Consistent with aerobic glycolysis as a program for proliferative metabolism, activated anti-tumor cells employ the same aerobic glycolysis as transformed tumor cells to perform their function (Andrejeva & Rathmell, 2017). T cells must express the master regulator of glycolysis, HIF1α, in addition to the main glucose transporter, Glut1 (Macintyre et al., 2014) to perform their anti-tumor function. In T cells, HIF1α and c-Myc protein abundance increases with activation. T cells are unable to proliferate in response to activation with loss of c-Myc but can proliferate with loss of HIF1α (Wang et al., 2011) (**Figure 1.2A**). HIF1α is not dispensable for sustained effector function, as this transcription factor is essential for anti-tumor immune responses in adoptive cell transfer (ACT) models and immune checkpoint blockade (ICB) (Palazon et al., 2017) (Doedens et al., 2013). In line with these observations, T cells with genetically constitutive HIF activation via loss of the hydroxylation proteins (PHD1/2/3), have increased glycolytic rate and have increased ability to eliminate lung metastasis in a metastatic model of melanoma (Clever et al., 2016).

Not only is glycolysis essential for T cell proliferation and activation, but each T cell subsets employs a different metabolic program to gain differential effector functions (Kaymak et al., 2021). Th1 and CD8 cytotoxic T cells, for example, are dependent on uptake of glucose and glutamine through Glut1 and ASCT2 but may be independent of the glutamine metabolism enzyme Glutaminase (GLS). All the while, Th17 cells rely on both uptake and GLS (Johnson et al., 2018). Conversely, regulatory T cells may be enhanced when glutamine uptake is suppressed. It is important, therefore, to consider

how the metabolic constraints of the TME may promote one T cell or myeloid subset over the other. (**Figure 1.2B**). Additionally, forced expression of the canonical T_{reg} Transcription factor, FoxP3, decreases active AKT and Glut1 cell surface mobilization, illustrating that lineage and metabolic function are intricately linked (Basu et al., 2015). Recent data supports that oxidative metabolism is necessary for T_{reg} function in the TME. Strikingly, mice with T_{reg} specific mitochondrial complex three deficiency have potent anti-tumor immunity due to loss of functionality of these suppressive cells (Weinberg et al., 2019) **(Figure 1.2B).** This oxidative program includes the uptake of TME lactate to sustain Treg suppressive function (Watson et al., 2021).

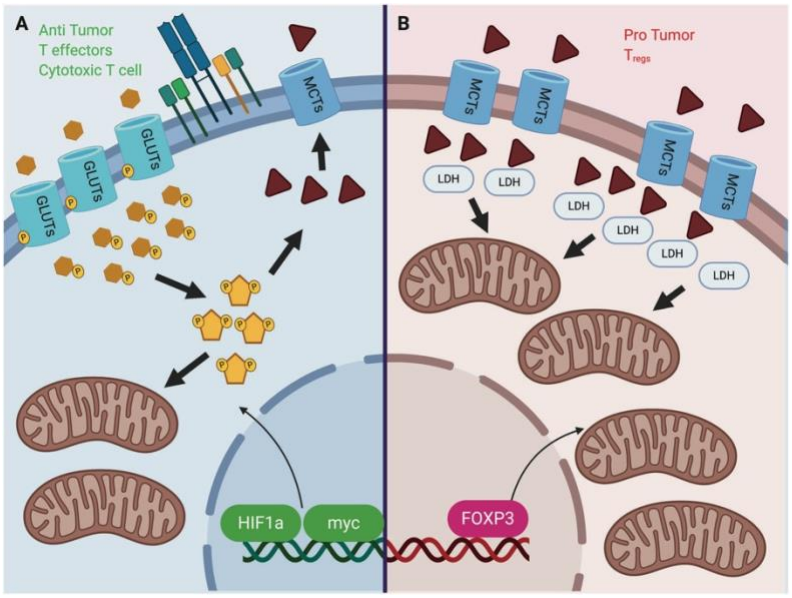

Figure 1.2*:* **The unique metabolic features of T cell subsets**. **A**: T cell activation via the TCR results in glycolytic reprogramming and a significant increase in mitochondrial metabolism. Recent tracing experiments demonstrates that glucose is metabolized into both lactate and into Krebs cycle intermediates *in vivo.* These metabolic changes are dictated by the oncogenic transcription factors HIF and myc. **B**: Pro tumor T_{regs} are more oxidative in comparison to their anti-tumor counterparts. These tumor promoting cells can metabolize lactate in the TME, convert it to pyruvate via LDH and use this substrate as mitochondrial fuel. The T_{reg} identity marker FOXP3 drives this substantial increase in mitochondrial biogenesis and function while recently mitochondrial complex 3 has been shown to be crucial for ultimate T_{reg} suppressive function.

Co-receptor engagement alters metabolism in the tumor microenvironment

Often overlooked is that the two most clinically relevant checkpoints, CTLA4 and PD-1, are negative regulators of T cell glycolysis (**Fig 1.3**). Engagement of the T-cell

co-stimulatory receptor CD28 by the ligands B7.1 or B7.2 leads to mobilization of Glut1 and reprogramming for anabolic metabolism via PI3K-AKT and mTORC1. Conversely, CTLA4 both competes for binding with B7.1 and B7.2 and can directly recruit the phosphate SHP2 to inhibit CD28 and TCR signaling and restrict Glut1 translocation, glucose uptake and T cell activation (Frauwirth et al., 2002). Thus, blockade of CTLA4 in ICB removes an inhibitory brake to result in increased CD28 and TCR signaling and greater levels of T cell aerobic glycolysis. Recent work from Zappasodi et al. demonstrates that CTLA4 inhibition on TME resident Tregs alters their oxidative program to promote a more glycolytic phenotype. With this shift in metabolism towards increase glucose utilization, Tregs become functionally impaired and thus create a more pro-inflammatory, anti-tumor microenvironment (Zappasodi et al., 2021). Similar phenotypes have been shown when Tregs have been exposed to pathogen association molecular patterns, where engagement with immunogenic substrates results in increase Treg glycolysis and compromised suppressive activity (Gerriets et al., 2016). This shift is consistent with enhanced PI3K-Akt-mTORC1 signaling, as genetic deletion of the lipid phosphatase, PTEN, led to enhanced Akt-mTORC1 signaling that destabilized Treg and led to an inflammatory autoimmunity (Huynh et al., 2015; Shrestha et al., 2015).

PD-1, another critical immune T cell checkpoint with that has been successfully targeted in the clinic, also negatively regulates T cell glycolysis and mitochondrial metabolism (Patsoukis et al., 2015). The interaction of PD-1 with PD-1 ligand (PD-L1) blocks glycolysis through the inhibition of PI3K/PKB/mTOR pathway and the downregulation of Glut1 (Boussiotis et al., 2014). However, PD-1 ligation can also

activate AMPK, that triggers fatty acid B-oxidation (FAO) while restraining utilization of and branched chain amino acids (Patsoukis et al., 2015; Sharpe & Pauken, 2018). T cell differentiation into effectors requires glycolysis as described above in CD28, so PD-1 may block terminal differentiation by inhibiting glycolysis. In contrast, CTLA-4 inhibits glycolysis but not FAO (Patsoukis et al., 2015). PD-1 blockade restores T cell glycolysis and IFNγ production in T cells (Staron et al., 2014). These two negative regulatory pathways do differ in their mechanism of mTORC suppression **(Figure 1.3A)**. PD-1 decreases upstream PI3K activity where as CTLA4 increases Protein Phosphatase 2a and SHP activity to inactive AKT(Parry et al., 2005). While the metabolic implications of CTLA4 and PD-1 blockade remain under study, the direct role to suppress anabolic Akt-mTORC1 directed signaling suggests that metabolic reinvigoration may be a contributory mechanism of action **(Figure 1.3C)**.

Unsurprisingly, other T cell inhibitory checkpoints also impact metabolic fate of tumor infiltrating T Cells (**Figure 1.3A/B**). In line with the suppressive role of PD-1/CTLA4 on T cell metabolism, inhibitory co-receptors are now known to decrease the metabolic rate of activated T cells. Lymphocyte activation gene 3 (LAG-3) deficient naïve CD4 T cells reveal increased oxygen consumption and enhanced glycolysis via activated STAT5 signaling (Previte et al., 2019). The interaction of TIGIT on T cells with CD155 on stomach cancer dampens glucose uptake, decreases T Cell glycolysis and the expression of Glut1 and hexokinase 2 (HK2) (He et al., 2017). Additionally, TIM3 engagement down-regulates glucose uptake and consumption by down-regulating Glut1 expression (Lee et al., 2020). Stimulation of GITR, a co-inhibitory receptor,

augments metabolic activities in T cells (Sabharwal et al., 2018). Thus, each co-receptor has distinct function on T cell metabolism.

Activating T Cell co-receptors, conversely, can improve metabolic fitness of activated T Cells. 4-1BB agonism activates the liver kinase B1 (LKB1)-AMP-activated protein kinase (AMPK)-acetyl-CoA carboxylase (ACC) signaling pathway, which is important for the metabolism of glucose and fatty acids (Choi et al., 2017) . Although 4-1BB co-signaling contributes glycolysis, it induces a higher mitochondrial oxidative phosphorylation leading to the generation of memory T cells rather than the differentiation into effector cells by CD28. 4-1BB signaling also enhances mitochondrial capacity even in exhausted T cells via p38-MAPK activation (Menk et al., 2018). Recent studies demonstrate that the 4-1BB intracellular signaling domain in chimeric antigen receptor T cells promotes mitochondrial biogenesis and improves oxidative metabolism (Kawalekar et al., 2016; Long et al., 2015). In line with the metabolic reprogramming described above, 4-1BB ligation induces Glut1 expression (Choi et al., 2017). The stimulation of ICOS, another immunoglobulin superfamily member, enhances glycolysis via activation of mTORC1 and mTORC2 as well as Glut1 induction (Zeng et al., 2016). Another TNF receptor superfamily member, OX40 is highly expressed with Glut1 in metabolically active CD4+ T cells (Palmer et al., 2017). OX40 regulates glycolysis and lipid metabolism in Tregs and promotes T cell expansion and the differentiation of memory T cells (Pacella et al., 2018). CD27, normally expressed in resting T cells provides strong co-stimulation. CD27 agonism induces the expression of genes for glycolysis, glutaminolysis and fatty acid synthesis (Buchan et al., 2018).

The increased expression of Pim-1 by CD27 co-signaling may play the role on glycolysis (Beharry et al., 2011; Peperzak et al., 2010).

Ligands for these T cell checkpoints have metabolic implications on the TME. PD-L1 (also known as B7-H1) has been known as a ligand (Dong et al., 2002; Freeman et al., 2000) but it can receive signals as a receptor (Azuma et al., 2008; Jalali et al., 2019) impacting cancer cell biology agnostic of the immune system. PD-L1 expression on tumor cells may activate AKT-mTOR pathway and in turn glycolysis in cancer cells to increase cancer cell glucose uptake (Chang et al., 2015). Interestingly, this type of metabolic reprogramming and resultant microenvironmental acidosis by lactate secretion combined with hypoxia can further up-regulate cancer cell PD-L1 expression via HIF1α, and directly lead to inhibition of T cell mediated cytotoxicity (Barsoum et al., 2014; Fischer et al., 2007) . PD-L1 blockade restores glucose levels in the tumor microenvironment, supporting adequate T cell function in the TME may be hampered by lactate (Huang et al., 2017). Among co-inhibitory ligands besides PD-L1, the immunological function of B7-H3, also known as CD276, remains to be elucidated. B7-H3 has conflicting co-stimulatory and co-inhibitory molecules depending on different contexts (Wang et al., 2014). Non-immunological roles of B7-H3 include cancer invasion, metastasis, drug resistance in multiple different cancer (Chen et al., 2008; Liu et al., 2011; Tekle et al., 2012; Zhao, Li, et al., 2013; Zhao, Zhang, et al., 2013) . Additionally, B7-H3 intrinsically regulates cancer cell metabolism. B7-H3 expression positively regulates HIF1α, leading to glycolysis, lactate production and tumor growth (Lim et al., 2016). B7-H3 also activates AKT/mTOR pathway, that enhances glycolysis in breast cancers (Nunes-Xavier et al., 2016) and STAT3 pathway that promotes

hexokinase 2 (HK2) in colorectal cancers (Shi et al., 2019). It raises a possibility that co-inhibitory ligands such as B7-H3 enhance glucose metabolism in cancer cells, ultimately converting the TME to an overall more suppressive immune environment. Another B7 family member, B7-H4 is a co-inhibitory ligand although its binding partner has not been fully established (Sica et al., 2003). B7-H4 on donor or host immune cells prevents graft-versus-host disease lethality in MHC mismatched bone marrow transplantation models (Saha et al., 2019). The genetic deletion of B7-H4 in donor T cells or recipient immune cells enhances mitochondrial activity, superoxide production, Glut1 expression, glucose uptake and metabolism. FAO and fatty acid uptake also increased in B7-H4$^{-/-}$ T cells in murine GVHD models (Saha et al., 2019)

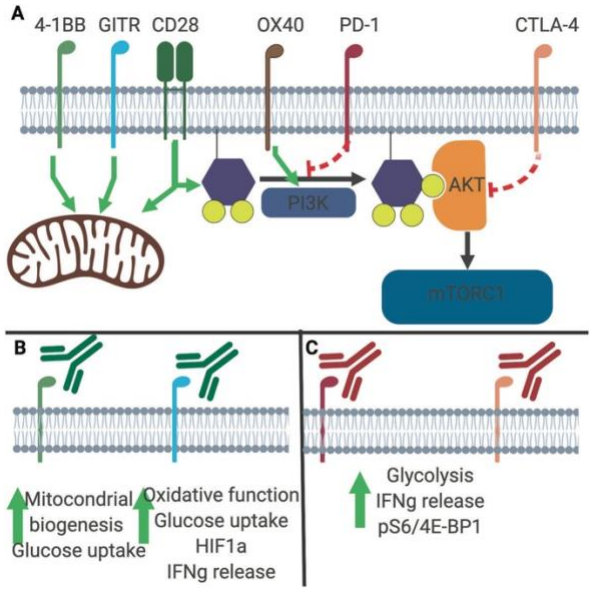

Figure 1.3: **Immunometabolic consequences of checkpoint blockade**. **A:** Ligation of CD28, 4-1BB, OX40 promote increased mitochondrial metabolism and augment PI3K signaling tone. PD-1 and CTLA4 directly suppressive mTOR activation through distinct mechanism. **B**: Using stimulatory antibodies against 4-1BB and OX40 to improve T cell metabolism and enhance tumor elimination. **C**: Inhibition of T cell co-stimulation via CTLA4 and PD-1 results in increased mTOR signaling. The clinical success of immune checkpoint blockade via of PD-1 and CTLA4 inhibition may be in the ability of these therapies to enhance/reinvigorate T cell metabolism in the TME.

The work above supports a model where glycolytic metabolism is a component of anti-tumor T cells and oxidative metabolism is crucial to T_{reg} suppressive capacity.

Adaptation of T cells to the TME, however, can lead to shifts in metabolism and defects in both glycolysis and mitochondria can directly contribute to impaired immune function. T cells from clear cell renal cell carcinoma (RCC) samples were found to have reduced glucose uptake as well as fragmented and inefficient mitochondria. Surprisingly, when supplemented with pyruvate, antioxidants, or potent co-stimulation through CD28 could rescue effector function (Beckermann et al., 2020; Siska et al., 2017). Similarly, T cells from mouse tumors were found to rapidly develop mitochondrial and functional defects and anti-tumor immunity could be restored by enhancing mitochondrial biogenesis or promoting lipid uptake to support more efficient mitochondrial metabolism (Zhang et al., 2017). These data suggest that T cells may adopt multiple metabolic states in the TME. Enhancing aerobic glycolysis may be only one path towards anti-tumor immunity while enhancing mitochondrial function can be another. The mechanism through which multiple signal checkpoint ligands are integrated and ultimately alter the metabolic capacity of these crucial cells is yet to be fully elucidated. However, each pathway endows unique signaling and metabolic programs that can impact therapeutic efficacy and patient outcomes. It remains challenging with current technologies to fully dissociate these models, as glucose uptake may play a role to both support glycolysis as well as support mitochondrial metabolism through pyruvate oxidation. The key distinction yet to be established may be not if T cells utilize glucose metabolism, but instead if pyruvate is converted to lactate or provides a mitochondrial fuel. Future therapeutic success will be predicated on understanding how TILs use metabolic substrate to support differentiation and support their anti-tumor function.

Metabolic differences underlie diverse TME myeloid biology

In the TME, myeloid cells are quite heterogeneous (Katzenelenbogen et al., 2020; Molgora et al., 2020; Song et al., 2019; Tcyganov et al., 2018; Zhang et al., 2020). A majority of the myeloid infiltrate in mouse tumor models and the human TME are thought to be of monocyte origin. These cells are recruited to the TME due to tumor associated inflammation and tumor glycolytic gene transcription (Cai et al., 2017; W. Li et al., 2018). In the development from monocyte to macrophage or granulocyte precursor to neutrophil, these cells exist in a variety of premature cell state, typically referred to as the myeloid derived suppressor cell (MDSC) or immature myeloid cell (iMC). Regardless of their ultimate fate, the maturation from blood monocyte to a more mature, yet suppressive cell via M-CSF or GM-CSF, requires an PI3K/AKT/mTOR dependent upregulation of glycolysis (Goffaux et al., 2017; Hammami et al., 2012; Karmaus et al., 2017; Kelley et al., 1999; Ribechini et al., 2017; Tavakoli et al., 2017). Intriguingly, hyperglycemia alone can increase myelopoiesis and a peripheral accumulation of these suppressor cells (Nagareddy et al., 2013). Suppressive MDSCs and iMCs both increase expression of glycolytic machinery while residing in the TME (Jian et al., 2017; Wu et al., 2019). For MDSCs infiltration in the TME, HIF2α is needed to support their glycolytic metabolism (Imtiyaz et al., 2010). Recently it has been appreciated that the transcription factor, RORγT is essential for MDSC maintenance (Strauss et al., 2015). Active RORγT has been shown to increase glycolytic metabolism in bladder cancer (D. Cao et al., 2019) and in the glucose addicted Th17 cells (Gerriets et al., 2016; Hochrein et al., 2022; Johnson et al., 2018). To support the glycolytic nature of MDSCs, mTOR signaling tone is elevated in TME infiltrating MDSCs, and treatment with rapamycin inhibits their suppressive

function (Deng et al., 2018). Myeloid specific mTOR deletion impairs MDSC maintenance in the TME and results in concomitate infiltration by anti-tumor IFNγ+ CTLs (T. Wu et al., 2016). Increased glycolytic rate related promotes MDSC cell fate as well as supports the suppressive functionality of these cells. MDSC are dependent on extracellular glucose to restrict T cell proliferation (Jian et al., 2017) while iMCs require exogenous glutamine (Wu et al., 2019). HIF1α stabilization in MDSCs promotes PD-L1 surface expression (Noman et al., 2014) as well as expression of immunosuppressive enzyme, iNOS and ARG*1* (Corzo et al., 2010). It has been recently appreciated that MDSCs use glycolysis derived methylglyoxal, a non-enzymatic reactive species, to impair T cell proliferation and activation (Baumann et al., 2020).

Once monocyte derived myeloid cells mature into macrophages, there are canonically thought to possess either anti-tumor (M1-like) or protumor (M2-like) effector programs. It is worth noting that these two phenotypes are not truly discrete entities but rather a continuum of phenotypes that are quite plastic. Additionally, based on the tumor type and treatment modality, the prognostic significance and/or molecular phenotype of tumor associated macrophages (TAMs) may be quite divergent (Dannenmann et al., 2013; Fakih et al., 2019; Fridman et al., 2017). It is well appreciated that TAM infiltration is correlated to an increase in glycolytic enzyme expression (D. Liu et al., 2017) and increased in whole tumor glucose uptake (Jeong et al., 2019). Via transcriptomic and metabolic labeling studies, it is appreciated that M1-like macrophages are incredibly glycolytic while M2-like macrophages utilize a more oxidative program (Geeraerts et al., 2021; Jha et al., 2015; Puchalska et al., 2018; Rodriguez-Prados et al., 2010). Fitting this model, constitutive genetic mTOR activation increases M1 phenotypes and impairs M2

phenotypes (Byles et al., 2013). M1 macrophages are canonically induced with exposure to LPS/IFNγ, which have extensively been shown to stabilize HIF1α, secondary to NF-kB activation (Blouin et al., 2004; Cramer et al., 2003; C. Li et al., 2018; Liu et al., 2016; Rius et al., 2008; T. Wang et al., 2017). HIF1α is stabilized in these M1-like cells due to their unique metabolic program, which contains a broken Tricarboxylic acid cycle (TCA) (Jha et al., 2015) With this program, M1 cells accumulate and oxidize succinate. This TCA intermediate directly modifies both HIF1α and the glycolytic transcriptional coactivator PKM2 to increase glycolytic gene transcription and inflammatory cytokines like IL1ß (Mills et al., 2016; Palsson-McDermott et al., 2015; T. Wang et al., 2017). Therefore, as one would expect, LPS/IFNγ stimulation results in a profound increase Glut1 and MCT4 expression (Freemerman et al., 2014; Fukuzumi et al., 1996; Z. Tan, N. Xie, S. Banerjee, et al., 2015). These metabolic transporters ultimately promote glucose uptake and lactate venting (Hard, 1970). Diverting excess glucose into the mitochondria via pyruvate dehydrogenase kinase knockdown in LPS stimulated M1-like cells decreases inflammatory cytokine response (TNFα, IL1ß) while increasing M2-like phenotypes (Arg1 and IL10 expression) (Z. Tan, N. Xie, H. Cui, et al., 2015). Even though the TCA cycle does not complete in full in M1-like cells, and PDK pyruvate dehydrogenase kinase is necessary for M1-like function, citrate is a key molecule these inflammatory macrophages. Transport of citrate out of the mitochondrion via acetylated SLC25a1 (Infantino et al., 2014; Palmieri et al., 2015) and its conversion to acetate via ATP-citrate lyase (ACYL) is crucial for maintenance of the M1-like phenotype and inflammatory cytokine expression (Lauterbach et al., 2019). This increase in acetate drives *de novo* lipid synthesis via SREBP mediated transcription (Im et al., 2011).

Both the process of phagocytosis (Michl et al., 1976; Morioka et al., 2018) as well as antigen presentation (Acosta-Iborra et al., 2009) require an increase in macrophage glycolysis. Vaccine responses can be enhanced by specifically stabilizing HIF1α in macrophages (Bhandari et al., 2013). In inflammatory models of carcinogenesis, increasing mTORC1 signaling genetically in macrophages increases tumor size and multiplicity (Katholnig et al., 2019) while mTORC1 deletion prevents TAM infiltration into subcutaneous tumor models (Ding et al., 2019). Prolonged HIF1α stabilization in macrophages promotes TAM tumor residency (Liu et al., 2014). Like MDSCs, TAMs require HIF1α to suppress the anti-tumor T cell response (Doedens et al., 2010)**.** The anti-tumor effect of rapamycin analogs may be in part due to suppressing the activity of these glycolytic myeloid cells (Wenes et al., 2016). These data support a model where glucose utilization and signaling is at the core of both the anti-tumor and pro-tumor effectors of macrophages in the TME.

As alluded to earlier, M2-like macrophages have a divergent metabolic program. IL4 stimulation increases mitochondrial biogenesis via PCG1ß transcription, while forced over expression of this factor prevents M1-like polarization (Vats et al., 2006). The mitochondrial fusion and oxidative metabolism secondary to IL4 stimulation is so significant that it prevents M1 repolarization (Van den Bossche et al., 2016). Differing from their inflammatory counterpart, M2 macrophages implement the non-oxidative pentose phosphate pathway. Glucose derived G6PD is metabolized by CARKL, while deleting this enzyme pushes macrophage to a more M1-like fate (Haschemi et al., 2012). Interestingly, *in vitro* glucose depletion has no effect on generation of M2-like macrophages (Wang et al., 2018). In comparison to M1-like cells, M2-like macrophages have a profound reliance

on extracellular glutamine, which is ultimately used to UDP-GlnNac important fate proteins like CD206 as well as increasing cellular alpha-ketoglutarate (Hinshaw et al., 2021; Jha et al., 2015; P. S. Liu et al., 2017). It is now appreciated that the transcription factor C-maf drives these oxidative and anaplerotic programs, which dictate the suppressive functions of this subtype of macrophage (M. Liu et al., 2020)**.** This glutamine utilization is so significant, that M2-like cells employ the cataplerotic enzyme Glutamine synthetase (GS) to increase intracellular glutamine pools from glutamate. This may be a metabolic vulnerability of these protumor cells given that deleting GS in myeloid cells prevents M2-like maturation and decreases tumor burden/tumor metastasis *in vivo* (Palmieri et al., 2017). Unlike M1 macrophages, M2 macrophages upregulate the lipid transport protein, CD36 when activated. M2-like cells appear to have increased reliance on extracellular lipids (Huang et al., 2014) where as M1-like cells synthesize their own lipids via SREBP as mentioned approve.

Metabolic alterations support DC cross presentation

Like antigen presenting macrophages, DCs demonstrate a wide variety of phenotypes, which have district roles in tissue homeostasis, inflammation and the TME (Brown et al., 2019; Guilliams et al., 2016) **.** Recent research in both treatment naïve, and ICB treated patients indicate that the most active anti-tumor DC is the tissue resident CD103+ IRF8, BATF3 conventional DCs1 (cDC1, (Durai et al., 2019; Fuertes et al., 2011; Hubert et al., 2020; Kurotaki et al., 2019; Meyer et al., 2018; Spranger et al., 2015; Spranger et al., 2017)). The human markers of cDC1 are CD141, Clec9a, XCR1 (Bachem et al., 2010; Crozat et al., 2010; Poulin et al., 2010). cDC1s mature in the presence of FLT3L and have the unique ability to cross present antigens to anti-tumor CTLs (Mayer

et al., 2014; Naik et al., 2005; Waskow et al., 2008). Strong evidence now exists to support vaccines FLT3L induced cDC1 are more efficacious than previous generations of GM-CSF derived DCs (Hammerich et al., 2019; Laoui et al., 2016; Wculek et al., 2019). Therefore, it is essential to understand the metabolic pathways that govern fate and function of cDC1s in the tissues to effectively generate anti-tumor immunity.

There is significant heterogeneity in our understanding of DC metabolism, underlying the many different culture and *in vivo* techniques in which to study these cells. The following work summarizes what is known about cDC1 biology given the prognostic role of these cells in cancer. *In vitro* generation of cDC1s with FLT3L is accompanied with an increase in glucose uptake, and Glut1 surface expression. Successful generation of functional cDC1 in culture is dependent on glycolysis (Kratchmarov et al., 2018). Not surprisingly, FLT3L activates the PI3K/mTOR pathway while treatment with rapamycin inhibits FLT3L driven cDC1 generation both *in vivo* and *in vitro* (Hackstein et al., 2003). mTORC1 deletion specifically impairs cDC1 infiltration and function in the lungs while promoting a more inflammatory DC phenotype (Sinclair et al., 2017). Genetic hyperactivation of mTOR (via PTEN or LAMPTOR deletion) results in an accumulation of cDC1s in mice (Sathaliyawala et al., 2010; Scheffler et al., 2014). Supporting the glycolytic nature of cDC1s, hexokinase inhibition in models of inflammation specifically impair DC infiltration into the lungs (Guak et al., 2018).

Other metabolic transcriptional activators regulate cDC1 glycolytic fate. L-myc is found to be specifically upregulated with FLT3L differentiation and DC migration into the tissue. Deletion of l-myc, impairs DC infiltration of a wide variety of tissues and results in a decreased vaccine response (Kc et al., 2014). The hippo pathway is also known to

support the increased oxidative and glycolytic metabolism required for successful antigen cross presentation by cDC1s. DC specific loss of hippo results impaired glycolytic and mitochondrial reprogramming, thus decreasing IL12 expression and restricting T cell proliferation and activation (Du et al., 2018). Exposure to IFNα and Poly(I:C) results in stabilization of HIF1α and thus increases DC glycolysis (Pantel et al., 2014). LPS stimulation of cDC1s induces rapid glycolysis that is mediated by a unique axis, Tank Binding Kinase 1/AKT/HK. Here we appreciate that DCs bypasses PI3K/mTORs regulation of glycolysis (at least in early activation), typically seen in tumor cells, macrophages, and T cells. The metabolic consequence of increased DC glycolysis and mitochondrial biogenesis is to generate additional citrate and NADPH (Everts et al., 2014; D. Wu et al., 2016). These metabolites are crucial for the synthesis of new lipids, which DCs require for their exquisite increased antigen presentation (Everts et al., 2014). Further evidence to support the key role of lipid generation in cDC1s is that cytoplasmic lipid bodies are seen in more immunogenic subsets of DCs with enhanced cross presentation (Bougneres et al., 2009; den Brok et al., 2016; Ibrahim et al., 2012).

In a similar vein to Tregs and suppressive myeloid cells, immunosuppressive tolerogenic DCs have unique metabolic features that may underlie the dysfunctional immune response seen in cancer patients. Tumor derived WNT5a induces a fatty acid oxidation program that increases DC IDO activity and suppresses DC IL12 expression (Zhao et al., 2018). Interestingly, dysfunctional tumor infiltrating DCs also have substantial lipid droplets (Herber et al., 2010). However, in TME resident dendritic cells, these structures are enriched with triglycerides and oxidized lipids, which ultimately restrict antigen presentation (Ramakrishnan et al., 2014; Veglia et al., 2017) The origin of these

oxidized lipids is currently unknown (potentially consumed from the oxidative milieu of the TME or from the fatty acid oxidation program seen in Zhao (Zhao et al., 2018). These oxidized lipid species are known to activate the XBP1 axis in cDCs and ultimately prevent the T cell activation needed for tumor elimination (Cubillos-Ruiz et al., 2015; Osorio et al., 2014).

NK cells activation and licensing requires metabolic re-wiring

NK cells in the TME can demonstrate substantial anti-tumor efficacy. NK cells become activated when engaged with stimulatory ligands in the absence of inhibitory ligands like MHC class one. NK cells also contribute to the anti-tumor efficacy of therapeutic monoclonal antibodies via antibody dependent cellular cytotoxicity and their surface Fcγ receptor, CD16. Recently, it has been appreciated that NK cells are also crucial for the efficacy of PD-1 blockade (Hsu et al., 2018). Activated NK cells release significant amounts of anti-tumor cytokines like IFNγ as well as kill directly through release of Granzyme B and Perforin. Recent evidence also has demonstrated that NK cells release FLT3L in the TME that promote recruitment and generation of crucial glycolytic anti-tumor cDCs (Barry et al., 2018; Bottcher et al., 2018). Therefore, understanding their metabolic reprogramming is important to elimination cancer cells as well as perpetuating the cancer-immune cell cycle (Chen & Mellman, 2013).

In line with T cells, mTORC1 activation is crucial for NK cell activation in response to activating receptors (Keppel et al., 2015) and the response to anti-tumor cytokines IL2, IL12, and IL15 (Donnelly et al., 2014; Keating et al., 2016; Marcais et al., 2014). Genetic deletion of mTORC1, over expression of PTEN, or acute pharmacological inhibition of mTORC1 in NK cells impairs granzyme B expression and cytotoxicity. Additionally, NK

cells stimulated in glucose-deficient media, or treated with the glycolysis inhibitor 2-deoxyglucose (2DG) decrease pS6K levels and anti-tumor effector molecules (Briercheck et al., 2015; Donnelly et al., 2014; Mah et al., 2017). NK cell expression of PDK1 is needed for *in vivo* elimination of metastatic tumors (He et al., 2019; Yang et al., 2015). Further supporting mTORC1's central role in NK cell activation are observations that ligation of the NK inhibitory receptor KLRG1 activates AMPK, a key negative regulator of mTORC1. Engagement of the inhibitory receptor KLRG1 prevents NK cells from proliferating in an AMPK dependent manner (Muller-Durovic et al., 2016). Oncolytic virus therapy that increases NK cell glycolysis have been shown to synergize with IL15 treatment, indicating that increased NK cell glycolysis can be used to generate improved NK cell immunotherapy (Samudio et al., 2016) (which is a growing area of adoptive cell therapy based on recent clinical trial excitement (E. Liu et al., 2020). Metabolic dysfunction may underlie defective NK cell function in the TME. Recent evidence supports that tumor derived TGFß can cause NK cell utilization of the gluconeogenic enzyme fructose 1,6-bisphosphatase. Upregulation of this enzyme ultimately impairs NK mediated cytotoxicity by limiting the glycolytic capacity of infiltrating NK cells (Cong et al., 2018; Slattery et al., 2021).

NK cells demonstrate unique metabolic features when compared to other anti-tumor immune cells. The anabolic fatty acid transcription factor SREBP has been shown to be a crucial regulator of NK cell glycolysis via inducing the citrate-malate shuttle. Surprisingly, SREBP-deficient NK cells have compromised oxidative and glycolytic metabolism and are unable to proliferate while producing significantly reduced levels of Granzyme B and IFNγ. The impairment is mediated by a decrease in the necessary citrate

malate shuttle enzyme, ACLY. NK cell deficits specific to SREBP loss were phenocopied with ACLY loss (Assmann et al., 2017). Consistent with this model, adoptive NK cell therapy in the B16 melanoma model was compromised with NK cell SREBP inhibition (Assmann et al., 2017). More recent work demonstrated that the citrate malate shuttle is sufficient to support active NK cell OXPHOS, while glutaminolysis appears dispensary for mitochondrial metabolism. Even though glutamine catabolism is not essential, glutamine remains an important nutrient for NK cell function. Upon IL2/IL12 stimulation, myc is stabilized only in the presence of extracellular glutamine. The cellular uptake of glutamine improves NK cell activation and tumor lysis. Surprisingly, the anti-tumor effect of glutamine inhibition was not dependent glutaminolysis, suggesting that the role of glutamine may be in part through in non-enzymatic mechanisms, such as a cofactor in the hexosamine pathway or as an antiporter substrate for uptake of other key immune activating nutrients (Loftus et al., 2018).

Like other immune cell lineages, NK cells also demonstrate subset specific metabolic programs. Licensed NK cells, which recognized MHC-I deficient tumors, have been shown to have an increased reliance on glycolytic metabolism and glutaminolysis (Schafer et al., 2019), while unlicensed NK cells are more reliant on mitochondrial OXPHOS. These metabolic discrepancies may, however, be related to differences in mouse and human NK cells or that the previous interrogations of glutamine metabolism in mouse T cells (Loftus et al., 2018) did not subdivide NK cell phenotypes by licensed or unlicensed.

Tumor cells subvert anti-tumor immunity via production of inhibitory metabolites and depletion of essential metabolites in the microenvironment

Lactic acid and pH as immunosuppressants:

For aerobic glycolysis to proceed at elevated rates, both tumor and immune cells must dispose of intracellular lactate to maintain cytosolic redox balance and glycolytic flux. It comes as no surprise then that the main transporters for lactate, MCT1 (Miranda-Goncalves et al., 2016) and MCT4 (Ullah et al., 2006) are transcriptional targets of HIF1α (**Figure 1.4).** With hypoxic induction of lactate generating enzyme, LDH (Firth et al., 1995), the TME is rich with extracellular lactate acidic protons. These H^+ ions are exported into the extracellular space by MCT1, 3, and 4 and the Na^+/H^+ symporter, NHE1, which is also a HIF1α target (Shimoda et al., 2006). The CO_2 produced from pyruvate oxidation becomes hydrated extracellularly and transformed into carbonic acid and a free proton via another HIF responsive gene, Carbonic Anhydrase IX (CAIX)(Mookerjee et al., 2015; Svastova et al., 2004). Therefore, the TME can be rich in extracellular lactate (Siska et al., 2017; Sullivan et al., 2019) have a pH as low as 6.0 as well as depleted of oxygen. Multiplex immunohistochemistry has confirmed that hypoxic areas of tumors are high in Glut1, LDH, CAIX, and MCT4 to demonstrate that these lactate rich, low pH environments are truly present in the TME (**Figure 1.4)** (Rademakers et al., 2011). There is now evidence that these harsh metabolic environments actively evade the immune system. The depletion of oxygen in tumors can have negative consequences on T cell fitness. Hypoxia experienced CD8 T cells have compromised mitochondrial metabolism and ROS tolerance, which prevent tumor clearance (Scharping et al., 2021). Cancer cell expression of HIF response CAIX can recruit suppressive myeloid cells via expression of G-CSF (Chafe et al., 2015) while

melanoma patients who have high bulk glycolysis transcriptomic signature have worse progression free survival on PD-1 blockade (Renner et al., 2019) as well as adoptive cell therapy(Cascone et al., 2018) . Tumors resistant to combined ICB demonstrate hypermetabolic phenotypes where they produce much more lactate in vivo then their parental sensitive line (Jaiswal et al., 2020). Intriguingly, increasing ambient oxygen to 60% decreases tumor cell metastasis while increasing T Cell recruitment (Hatfield et al., 2015).

Lactic acid is also now recognized as a directly immunosuppressive molecule to all anti-tumor immune cell types. Human and mouse effector T cells divide less, produce less cytokine and are less able to kill cancer cells in physiologically relevant lactic acid (Brand et al., 2016; Fischer et al., 2007; Mendler et al., 2012). This inhibition of effector activity is mediated through decreased NFAT translocation to the nucleus secondary to high lactate concentrations (Brand et al., 2016), decrease in intracellular pH(Fischer et al., 2007) and less active p38 and c-JNK/c-JUN (Mendler et al., 2012). High levels of lactate also promote more regulatory T cells (Angelin et al., 2017; Watson et al., 2021) whose presence in the TME promotes tumor progression and metastasis across many tumor types (Fridman et al., 2012). These tumors promoting CD4+ T regulatory cells (T^{-}_{regs}) appear to use lactate for their oxidative metabolic program, endowing them survival benefit in the TME rich of lactate (Angelin et al., 2017; Brand et al., 2016; Cortese et al., 2020; Siska et al., 2017). Loss of the lactate importer MCT1 in a Treg specific manner resulted in improved anti-tumor function, illustrating that this metabolite acts as fuel for these suppressive cells (Watson et al., 2021). Recently it has been shown that lactate can increase Treg PD1 levels while decreasing T effector PD1, thus redirecting PD1

blockade to paradoxically promote Treg function (Kumagai et al., 2022). High levels of lactate are also able to polarize macrophages into a more immunosuppressive M2 like phenotypes (Colegio et al., 2014), as demonstrated by expression of *Arg1, Vegf, Fizz1, Mgl1 and Mgl2*. The mechanism of lactate's immunosuppressive action is unclear in myeloid cells, as the immune modulatory effects of lactate do not appear governed by macrophage expression of GPR81, a GPCR that binds lactate (Errea et al., 2016). Lactic acid has been shown to inhibit the professional antigen presenting DC cytokine production in organoid coculture models (Gottfried et al., 2006). Like other lymphoid derived immune cells, NK cells cultured in physiologically relevant lactate had compromised cytokine release (Brand et al., 2016). To increase NK cell activity in the TME, tumor specific knock down of tumor LDHa correlated with increased NK tumor infiltration and IFNγ+ NK cells. The inhibitory nature of lactate in multiple classes of immune cells may be reminiscent of both PD-1 and CTLA4 ligation in T cells. Lactate may directly decrease the rate of immune cell glycolysis. One study demonstrated that high extracellular lactate decreased immune cell glycolysis, and limited cellular production of TNFα in macrophages (Dietl et al., 2010). High levels of extracellular lactate may prevent lactate efflux out of the infiltrating immune cells to suppress continued flux through the glycolytic program requisite for anti-tumor function.

Tumor acidity may be an important modulator of immune response given that low intra-lymph node pH regulates T cell proliferation and activation (Wu et al., 2020) (**Figure 1.4)**. *Ex vivo* studies in acidic media show that low pH directly inhibits proliferation of melanoma TILs, limits activation markers like intracellular p-STAT5 and p-ERK, in addition to restricting production of IL2, TNFα, and IFNγ. Treatment with

proton pump inhibitors led to in an increase in intratumoral pH from 6.5 to 7 and increased the efficacy of ACT (Calcinotto et al., 2012). Further, mice drinking bicarbonate *ad libitum* had decreased tumor volume with an observed increase in CD8+ T cell infiltrate. Bicarbonate ultimately did improve the efficacy of ACT and ICB therapy in mouse models of melanoma (Pilon-Thomas et al., 2016). Modifying TME pH via inhibition of CAIX also increases response rates to ICB (Chafe et al., 2019). Giving credence to the metabolic complexity of the TME, mouse lymphomas overexpressing glycolytic/glutaminolytic transcription factor Myc, generate fewer tumor resident IFNγ positive NK cells. Providing these MYC^{hi} mice with exogenous bicarbonate reversed the acidic TME pH, and increased NK cell infiltration, NK cell phosphorylation of JNK, number of IFNγ expressing NK cells. In concordance with increased NK cell activity, mouse survival is increased with excess bicarbonate (Potzl et al., 2017). These studies suggest that mitigating the acidic TME may improve anti-tumor immune cell functionality and activity.

Competition for nutrients

While intra-tumoral glucose levels may be maintained in some settings (Cortese et al., 2020; Siska et al., 2017; Sullivan et al., 2019) metabolic competition for glucose between cells in the TME may contribute to TIL dysfunction in other contexts (Chang et al., 2015). Supporting a model that increased aerobic glycolysis of cancer cells can restrain TIL, overexpression of Pdk1, Hk2, Glut1, or c-Myc, allowed tumors that were normally rejected to instead grow to palpable masses (Chang et al., 2015). T cells purified from those glycolytic tumors had reduced ability to uptake glucose as assessed by the fluorescent dye 2NBDG (D'Souza et al., 2021; Sinclair et al., 2020) and express

inflammatory cytokines than T cells from less glycolytic tumors. Similarly, nuclear translocation of NFAT, a crucial T cell activation transcription factor, is dependent on the glycolytic intermediate, phosphoenolpyruvate (PEP) (Ho et al., 2015). In a glucose limited TME, this necessary event may not occur. Conversely, overexpressing the gluconeogenic enzyme PEPCK1, increased T cell intracellular PEP, and promoted increased T cell activation along with increased tumor clearance. These findings support a model where increasing T cell glucose availability may improve tumor eradication and glucose limitation may act as a tumor immunosuppressive mechanism. It is unclear, however, if the T cell dysfunction in these cases is due to direct metabolic limitations and poor access to nutrients or due to alterations in the immune infiltrate that occurred secondarily to a change in cancer cell physiology. It thus is not fully established if changes to cancer cell metabolism directly alter cancer cells fitness that can indirectly influence T cell function independent of glucose competition.

Recent work has demonstrated that glucose is present in appreciable concentrations in many mouse models of cancer in addition to human RCC to support a model in which glucose is generally not a limiting feature of tumor biology. Using radiolabeled Positron Emission Tomography (PET) tracers, we found that myeloid cells surprisingly consume for per cell glucose than either cancer cells or T cells (Reinfeld et al., 2021). Importantly, inhibition of glutamine uptake could further increase glucose uptake, indicating that glucose uptake in the TME was limited by cell intrinsic metabolic pathways rather than limiting access to glucose. While microenvironmental glucose limitations may occur, this work questions the widespread nature of glucose limitation and competition in the TME. When nutrients are limiting and competition does occur, it

may be multifactorial in that there are many diverse cell types attempting to attain and consume metabolic substrate. To overcome such potential resource barrier when it may occur, immunotherapy may improve T cell competitiveness to uptake glucose or promote alternative pathways and approaches to increase T cell mitochondrial metabolism have been shown to enhance tumor clearance (Beckermann et al., 2020; Siska et al., 2017). However, glucose availability across tumors may be heterogeneous and the degree to which glucose competition restricts TIL as a whole remains uncertain, as bulk measurements of glucose in tumor interstitial fluids have found that glucose can be readily available in diverse settings in both mouse and human tumors (Beckermann et al., 2020; Cortese et al., 2020; Reinfeld et al., 2021; Siska et al., 2017; Sullivan et al., 2019).

Where the evidence for glucose competition is mixed, availability of some nutrients may become limiting in tumor microenvironments for anti-tumor immune cells. There is evidence, for example, that tumors and T cells may compete for the amino acid methionine. For proper T cell activation and cytokine production, methionine must be present (Sinclair et al., 2019). This essential amino acid is crucial for T cell generation of SAM/SAH, which are the key methyl donors in mammalian cells. With decreased methionine uptake, T cells demonstrate an exhausted gene signature and less p-STAT5 signaling. This increase in TME resident T cell apoptosis and T cell exhaustion in the TME is dependent on tumor cell expression of the methionine transporter SLC43a2. Intriguingly, in a small trial of human cancer patient's exogenous methionine supplementation significantly improved T cell cytokine production and activation supporting this model where anti-tumor T cells require this amino acid for

function (Bian et al., 2020). Only one year prior, another group published (in the same journal no less) that dietary methionine restriction was an effective therapy for cancer (Gao et al., 2019). What could drive such divergent findings? (Gao et al., 2019) only evaluated xenograft human tumors in immune compromised animals which crucially lacked the methionine dependent anti tumor T cells. This series of studies emphasizes the crucial role immunocompetent models play in understanding TME metabolism.

Glycolytic tumor cells influence anti-tumor immunity via inhibitory gene networks

HIF driven VEGF stimulates suppressive TME

HIF1α/HIF2α not only promote expression of glycolytic genes that can lead to lactate accumulation, reduced pH, and glucose restriction in the TME, but also promote expression of soluble immunosuppressive factors in the TME. VEGF is considered a canonical HIF target (**Figure 1.4)** (Mazure et al., 1996). Its induction is thought to promote oxygenation and deliver vital nutrients to hypoxic tissues via generation of new blood vessels. However, physiological VEGF concentrations prevent dendritic cell-induced T cell activation and promote increased differentiation of tumor suppressive Gr-1+ myeloid derived suppressor cells (Gabrilovich et al., 1998). VEGF signaling through T cell VEGFR2 restricts T cell proliferation, viability, and cytotoxicity (Gavalas et al., 2012). Elevated VEGF also promotes high levels of the negative checkpoints, PD-1, TIM3 and CTLA4 on tumor infiltrating T lymphocytes (Voron et al., 2015). Myeloid cell VEGF suppresses NK cell activity in the TME (Klose et al., 2016). As expected, treating RCC patients with the VEGF receptor inhibitor, sunitinib, decreases MDSC number, promotes more IFNγ^+ T cells and depletes FoxP3$^+$ T_{regs} (Ko et al., 2009). With these studies, it should come as no surprise that clinical trials combining VEGF

inhibitors and ICB are demonstrating an increased response rate than either therapy alone in multiple disease types (Huang et al., 2020; Rini et al., 2019). Intriguingly, patients with high T cell and high myeloid gene signatures appear to benefit the most from this combination therapy, illustrating that pre-existing immunosuppression may be a predictive biomarker of successful immunotherapy (McDermott et al., 2018).

Immunosuppressive adenosine generation in the TME is secondary to HIF stabilization

Throughout tumorigenesis, the constant cell turnover should be recognized as not merely consuming, but also creating a milieu replete with additional metabolites, including ATP and adenosine. Immunostimulatory ATP is released by dying and necrotic cells and can be hydrolyzed to immunosuppressive adenosine by CD39 and CD73 **(Figure 1.4),** both ecto-nucleases and targets of HIF1α (Chiu et al., 2017; Synnestvedt et al., 2002). Highly glycolytic tumors will convert a majority of extracellular ATP from apoptotic and necrotic cells into adenosine. This conversion of ATP to extracellular adenosine has several negative consequences on anti-tumor immunity. ATP itself is a damage-associated molecular pattern, (DAMP), that can activate the P2RX7 receptor on tissue resident CD103+ T cells to promote inflammation and survival of this key cell population via mitochondrial fusion (Borges da Silva et al., 2018). Engagement of the ATP purinergic receptors on DCs increases vaccination response and cell surface expression of co-stimulatory molecules CD80/86 (Granstein et al., 2005). Conversely, engagement of adenosine receptors A2AR is anti-inflammatory and compromises T cell proliferation (Ohta et al., 2006; Ohta et al., 2009), T cell cytokine release and increases inhibitory checkpoint molecules expression (CTLA4 and PD-1) (Sevigny et al., 2007). A2AR activation has similar negative effects

on NK cell proliferation and activation (Lokshin et al., 2006; Young et al., 2018). Genetic depletion of the A2AR receptor specifically in NK cells increased NK cell proliferation, tissue invasion and ultimately improved tumor elimination in multiple models (Young et al., 2018). In renal cell carcinoma, single agent A2AR blockade may be successful (Fong et al., 2020) in part due to HIF stabilization that is necessary for tumorigenesis in this tumor, thus creating a TME rich with adenosine (Linehan et al., 2019). Activation of the alternate immunosuppressive adenosine receptor, A2BR, can also suppress anti-tumor immunity by increasing MDSC infiltration, maintenance, and myeloid VEGF expression (Iannone et al., 2013; Sorrentino et al., 2015). Consistent with an immune suppressive role for intra-tumoral conversion of ATP to adenosine, combining CD73 blockade with ICB results in synergistic inhibition of tumor growth in preclinical models (Allard et al., 2013).

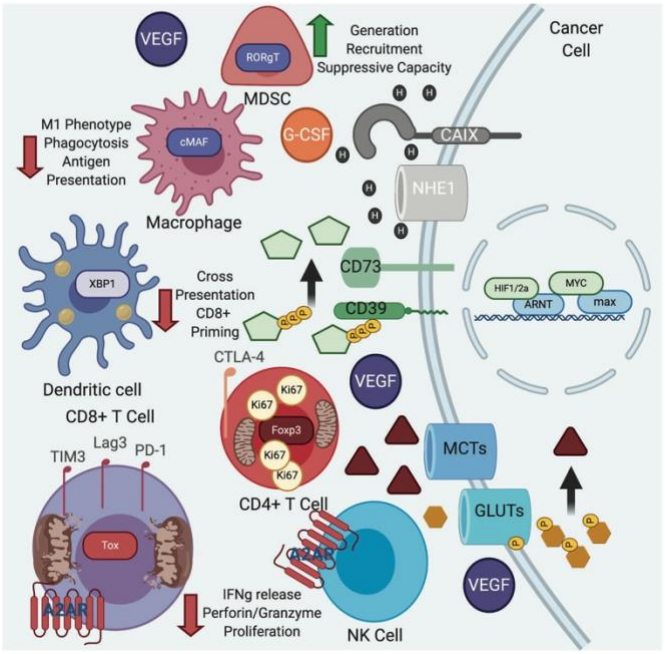

Figure 1.4: **A hostile immunosuppressive tumor microenvironment occurs secondary to tumorigenic mutations**. High levels of nuclear myc and HIF increase tumor cell glycolysis resulting in a TME rich in immunosuppressive molecules. Lactate is produced as byproduct of oncogene activation. This transcriptional program also decreases intratumor pH, increases secretion of suppressive cytokine like VEGF, recruits suppressive myeloid cells via G-CSF and promotes the extracellular degradation of ATP

into adenosine. The combination of the metabolic perturbations and TME alterations decrease the ability of the anti-tumor immune compartment to conduct their requisite function (seen in less cytokine and granzymes in anti-tumor CD8s and NK cells). This oxidative microenvironment creates a niche where Tregs, lipid filled tolerogenic DCs, and suppressive myeloid cells thrive, thus promoting immune evasion and tumor progression.

Combining metabolic agents with immunotherapy

ICB has revolutionized the treatment of many metastatic cancers (Gandhi et al., 2018; Larkin et al., 2015; Motzer et al., 2018). However, there remains a significant need to enhance the activity of these treatments to drive durable remissions both in more patients and across more disease types. The high rates of resistance to single agent ICB therapies across all tumor types has led to the development of many trials to combine targeted therapies, chemotherapies, and other metabolism-based therapies with ICB in efforts to increase responses (Sharma & Allison, 2015; Xin Yu et al., 2020), yet agents that target cancer metabolism may also impair anti-tumor immunity. Because *in vivo* metabolism and heterogeneity can confound *in vitro* modeling, we propose that using immune-competent models of cancer will be critical to identify metabolism- and TME-targeting agents to limit tumor proliferation that simultaneously retain the capability of the immune system to eliminate tumors.

Warburg targeting agents can harm or augment the anti-tumor response

To support the increase glucose demand of TME resident cells, glutamine is consumed by both transformed and infiltrating cells (Altman et al., 2016; Andrejeva & Rathmell, 2017; Pan et al., 2016). As an anaplerotic source to maintain mitochondrial metabolism, amino acid pools, and to increase glutathione stores, glutamine metabolism is often coupled to aerobic glycolysis in proliferative cells. Broad inhibition of glutamine metabolism or selective inhibition of Glutaminase (GLS)/glutamine uptake can result in reduced tumor glycolysis and growth (Byun et al., 2020; Edwards et al.,

2021; Leone et al., 2019; Meric-Bernstam et al., 2019; Schulte et al., 2018) **(Figure 1.5)**. Importantly, while some T cells subsets rely on GLS, others, including anti-tumor CD4 T_h1 and CD8 cytotoxic cells appear to adapt to glutamine depletion through increased glucose and acetate metabolism. By blocking glutamine metabolism, these anti-tumor cells can increase effector function (Byun et al., 2020; Edwards et al., 2021; Johnson et al., 2018; Leone et al., 2019; Schulte et al., 2018) while tumor cell undergo apoptosis due to overwhelming levels of ROS. It appears that tumor cell glutamine demand (Reinfeld et al., 2021) may itself restrict T cell activity in the TME . Deletion of GLS in triple negative breast cancer, resulted in marked increase in active TME T cells who acquired the excess glutamine via Slc6a14 (Edwards et al., 2021). Likewise, inhibition of glutamine metabolism in the TME can promote inflammatory M1 phenotype macrophages (P. S. Liu et al., 2017; Palmieri et al., 2017) and impair MDSC infiltration and function via decreased kynurenine generation (Oh et al., 2020). In both T cells and macrophages, the mechanism of increased differentiation with inhibition of glutamine appears to be in part through alteration in levels of the glutamine-derived metabolite α-ketoglutarate, which is required for many de-methylation reactions that influence chromatin accessibility and gene expression (Johnson et al., 2018; P. S. Liu et al., 2017). A potential drawback, however, may be terminal differentiation or exhaustion of T cells with inhibition of glutamine metabolism (Johnson et al., 2018) and GLS inhibition can have anti-inflammatory effects in a variety of settings (Johnson et al., 2018; Kono et al., 2019) that may also impair anti-tumor immunity. Combining glutamine metabolism antagonists with immunotherapy agents now has the potential to hinder

cancer cell proliferation while promoting inflammatory metabolic programs in T cells and macrophages, although further studies are necessary.

Given that elevated PI3K/mTOR signaling is a commonality of all tumor types, Glut1 is often over expressed in cancer and expression of this transporter is correlated to poor patient outcome across tumor types (J. Wang et al., 2017; Yu et al., 2017). Glut1 inhibition have shown effective in many preclinical models of cancer (Chan et al., 2011; Contat et al., 2020). However, these studies have been conducted in *in vitro* and xenografted *in vivo* models that lack the adaptive immune system. Glut1 deficiency may ultimately also prevent anti-tumor immune cell function **(Figure 1.5)**. Effector CD4 and CD8 cells have decreased ability to proliferate or secrete effector cytokines and promote inflammation with genetic deletion of Glut1. T_{regs}, however, can be Glut1 independent and remain suppressive with Glut1 loss (Macintyre et al., 2014). Additionally myeloid Glut1 loss results in a decrease in M1-like enzyme iNOS and an increase expression of M2 marker CD206 (Freemerman et al., 2019). CD11c+ DCs rely on glucose to differentiate and perform their crucial functions (Du et al., 2018). Careful preclinical evaluation is needed to test if Glut1 inhibitors would compromise anti-tumor immunity and promote regulatory Tregs and M2 like cells. A therapeutic window may exist where tumor Glut1 levels are relatively high in the cancer cell compartment when compared to immune cells. An appropriate dosing strategy would need to be developed to evaluate an approach where a Glut1 inhibitor could impair tumor growth and metabolism without overly impeding cDC1 and TIL function. Alternatively, Glut1 treatment may promote long lived memory T cells with capacity for prolonged control of tumors, in line with the effects of 2-deoxyglucose and AKT inhibition in models of

adoptive cell transfer (Crompton et al., 2015; Sukumar et al., 2013). Therefore, future studies should be rigorously conducted to properly evaluate if Glut1 inhibition in vivo limits T cell glycolysis or instead synergizes with ICB.

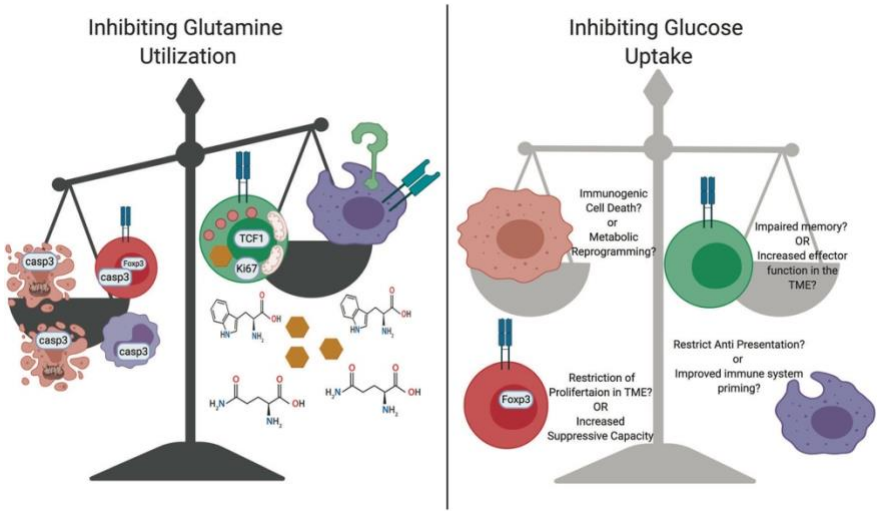

Figure 1.5: **Targeting metabolic pathways may hamper anti-tumor immunity.** Inhibition of glutamine pathways with antagonists like DON or GLS with CB839 promotes anti-tumor immunity. TME becomes enriched with glutamine, glucose, and tryptophan secondary to these pharmacologic interventions. T cell metabolic reprogramming with glutamine perturbations results in increased expression of anti-tumor molecules like granzyme B and perforin as well as improvements in mitochondrial function and increased glucose utilization. Glutamine starvation promotes tumor cell death in addition to death and decrease function of myeloid-derived suppressor cells and Tregs. Anti-tumor M1-like macrophages increase antigen presentation machinery and inflammatory cytokine production in response to alterations to glutamine metabolism. It is currently unknown how blocking glucose uptake will alter immune and tumor cell function in malignancy. It is possible that this therapeutic targeting of glucose metabolism may restrict anti-tumor immunity while inducing increase tumor growth. Or T Cells metabolic function may improve by limiting the metabolic stress they experience in the TME. Glucose metabolism is important for macrophage phagocytosis and antigen presentation, and it is currently unknown how restricting glucose will aid or inhibit anti-tumor function.

Unique isoform usage creates metabolic vulnerabilities in suppressive immune cells

Recent work has elucidated that infiltrating immune cells are more similar transcriptomically and metabolically than malignant cells across patients (Tirosh et al., 2016; Xiao et al., 2019). This may be because phenotype of these infiltrating cells is inextricably linked to a signaling program that is shared by all patients while each patient's tumors has developed their own metabolic features while responding to unique selective pressures in each host. These shared metabolic programs may then be

targeted across patients rather than developing personalized metabolic therapies for each patient's disease.

Whole genome sequencing of patients with immunodeficiency has led to the discovery that PI3Kγ and PI3K**δ** both play important roles for immune cell maintenance. Combined with the host of mutational data of other PI3K isoforms in solid tumors, targeting this pathway with small molecules has become a large area of scientific research. Recent advances in medicinal chemistry now allow for specific isoform targeting and thus have provided new insights into augmenting anti-tumor immunity without impairing anti-tumor immune cell glycolysis (Evans et al., 2016). PI3K isoform usage allows for cell type specific targeting: Malignant epithelial cells express PI3K isoforms α and β, while myeloid cells express the γ isoform (Kaneda, Cappello, et al., 2016) **(Figure 1.6)**. In evaluating these PI3Kγ compounds, it has become clear that robust anti-tumor immunity can be induced via inhibiting glycolytic immature suppressor cells through this unique PI3k variant usage. Myeloid PI3kγ activation is secondary to upstream activation by RTKs, TLRs, and IL1ß (Foubert et al., 2017; Schmid et al., 2011). These ligand binding events mobilize the integrin α1ß4 and release IL10 allowing for MDSC tissue infiltration and tumor promotion (Schmid et al., 2011). Genetic deletion or pharmacological inhibition of PI3Kγ increases host immune response to both spontaneous (Kaneda, Cappello, et al., 2016; Torres et al., 2019) and inflammatory tumors models (Gonzalez-Garcia et al., 2010). Additionally, PI3kγ inhibitors synergize with ICB administration (De Henau et al., 2016; Kaneda, Messer, et al., 2016). Secondary to myeloid PI3Kγ loss, there is both a robust change in infiltrate as well as cytokines in the TME. By perturbing TME PI3Kγ, an increase in infiltrating CD8 T cells and the anti-tumor conventional DC1s is observed while

depleting suppressive MDSCs, B regulatory cells and Foxp3+ T_{regs}. (X. Zhang et al., 2019) The MDSCs in PI3kγ null tumors or inhibitor treated mice are less able to suppress T cells and less likely to mature into M2-like macrophages (Joshi et al., 2019). T cells in these PI3Kγ depleted tumors also demonstrate a more active phenotype and a larger anti-tumor TCR repitoire (De Henau et al., 2016). Secondary to inhibition of the PI3Kγ, the TME becomes enriched with anti-tumor factors like IFNγ and IL12 and depleted of immunosuppressive VEGF (Qin et al., 2019).

These preclinical studies referenced above have led to late-stage clinical trials using PI3Kγ inhibitors in solid tumors in combination with ICB (NCT03961698, NCT03711058, NCT02637531). However, it is worth noting that excessive PI3Kγ inhibition may ultimately impair the anti-tumor response. PI3Kγ is known to be expressed in lymphoid cells like T and NK cells as well as dendritic cells and to a lesser extent than myeloid cells (Gyori et al., 2017; Kaneda, Cappello, et al., 2016). Thymocyte development and mature CD4 cells are eliminated in PI3Kγ KO mice (Sasaki et al., 2000). T cells are unable to upregulate the crucial chemokine receptor, CXCR3 (Chow et al., 2019), with PI3Kγ KO (Barbi et al., 2008). In models of autoimmunity, PI3γ KO T cells delayed graft rejection (Uehara et al., 2017), illustrating that this protein may be responsible for developing T cell responses. Interestingly, adoptive cell transfer of PI3kγ KO T cells or PI3kγ inhibitor pretreated T cells generates more memory like T cells and more robust anti-tumor responses in multiple cancer models (Dwyer et al., 2020; Foubert et al., 2017). This work Illustrates that anti-tumor immunity may not rely on T cell PI3Kγ even though this isoform seems important *for de novo* T cell generation. Like T cells, genetic PI3Kγ deletion in NK cell impairs IFNγ release(Tassi et al., 2007) and tissue infiltration

(Saudemont et al., 2009). PI3kγ loss also impairs cDC1 generation in models of viral immunity, preventing effective CD8 responses. However, current immunotherapies do not require *de novo* thymic T cell generation or peripheral DC maturation.

Together, these studies support alterations to the traditional pharmacological approach in oncology. Instead of evaluating metabolic immuno-oncology agents for maximum tolerable doses, the focus should be on developing pharmacodynamic metrics that measure the dose required to receive maximal effective immune response to cancer. A recent publication supports this notion in that high dose (50 mg/kg) PI3kγ/**δ** inhibition with the clinically approved Duvalisib (IPI-145) impairs the generation and proliferation of anti-tumor T lymphocytes. This CTL impairment ultimately counteracts the efficacy of PD-L1 treatment in mouse models of breast cancer. Low dose treatment (15 mg/kg) with the same compound synergizes with PD-L1 treatment via inhibiting MDSC infiltration and function while promoting more active tumor specific T cells in the TME (Davis et al., 2017). The efficacy from this combination may come from anti-myeloid effect of the PI3kγ inhibition combined with anti Treg component of the low dose PI3k**δ** inhibition. It is now appreciated that Tregs are uniquely inhibited with PI3k**δ** inhibition when compared to other T cells in mouse and human tumors (Abu-Eid et al., 2014; Chellappa et al., 2019). These therapeutic windows may exist because of the basal differences between immunosuppressive cells and cytotoxic CD8s in protein isoform usage noted above.

Differential regulation of glycolysis in tumor and immune cells may also offer an opportunity to selectively suppress tumor glucose metabolism while leaving immune cells intact. Uniquely in clear cell renal cell carcinoma (ccRCC), HIF2α can fully compensate for HIF1α loss (Shen et al., 2011). This has led to the development of

HIF2α specific inhibitors for the treatment of ccRCC. Preclinical xenograft models(Chen et al., 2016; Cho et al., 2016) and early phase clinical trials (Choueiri et al., 2021; Courtney, Infante, et al., 2018) demonstrate efficacy of targeting this transcription factor *in vivo* in patients. This is a promising agent to combine with immunotherapy because HIF2α is dispersible for T cell anti-tumor immune responses in adoptive cell therapy models (Palazon et al., 2017). Additionally, myeloid-specific deletion of HIF2α decreased tumor infiltration by tumor associated macrophages in hepatocellular carcinoma and resulted in decreased tumor cell proliferation (Imtiyaz et al., 2010) so these compounds may have beneficial immunostimulotory effects **(Figure 1.6**). This type of approach would allow for anti-tumor immune cells to still upregulate glycolysis via HIF1α without significant impairment, while halting cancer cell glycolysis.

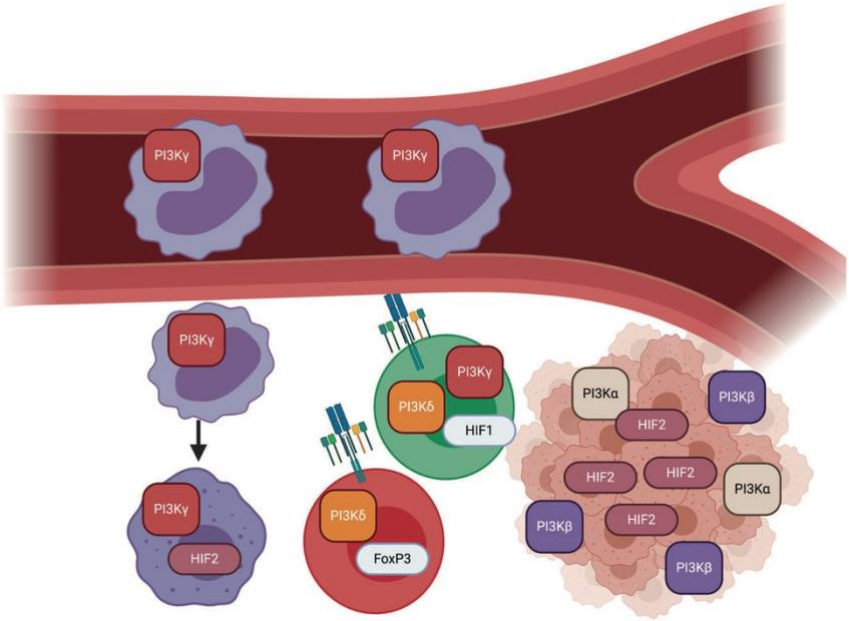

Figure 1.6*:* **Isoform targeting as a strategy to hamper suppressive immune cell metabolism while enhancing anti-tumor immunity.** PI3kγ is a crucial aspect of inflammatory myeloid cell recruitment into tumors, MDSC suppressor function and ultimate lineage commit to a M2-like macrophage. HIF2a (in ccRCC) and in certain myeloid subsets is key to sustaining glycolytic function. Specific inhibition of PI3Kγ or HIF2a remodels the tumor microenvironment in that there is significant tumor cell death, a depletion of regulatory CD4s and suppressive myeloid cells, while enhancing CTL activation and cytokine release.

Conclusion

In the pursuit of more efficacious cancer therapies, what is becoming increasingly clear is that immune cells in the TME implement discrete metabolic programs to promote tumor elimination or augment tumor progression, offering unique windows to selective therapeutic interventions. A variety of metabolic interventions can preferentially selectively eliminate tumor cells or subsets of pro-tumor immune cells, providing an opportunity for metabolic interventions to serve as strategies to augment checkpoint immunotherapy or in the future, by benefitting cellular therapy products. Many of the pathways that support immune function are well-established pathways, such as mTOR and PI3K, with increasingly selective agents available for sophisticated tuning of the immune cells in the TME to eradicate tumor cells. The differential dependencies on such metabolites as glutamine and glucose are also huge opportunities. What is further clear is that these strategies offer a sophisticated strategy to harness the immune system, harkening for more immune competent animal models that support cancer biology studies. Together with these tools and insights, we are poised to make substantive inroads in the treatment of cancer by understanding metabolite consumption patterns in the diverse cell which infiltrate tumors.

CHAPTER 2: Cell Programmed Nutrient Partitioning in the Tumor Microenvironment

This chapter is adapted from “Cell-programmed nutrient partitioning in the tumour microenvironment” published in *Nature*.

Reinfeld, B. I., Madden, M. Z., Wolf, M. M., Chytil, A., Bader, J. E., Patterson, A. R., Sugiura, A., Cohen, A. S., Ali, A., Do, B. T., Muir, A., Lewis, C. A., Hongo, R. A., Young, K. L., Brown, R. E., Todd, V. M., Huffstater, T., Abraham, A., O'Neil, R. T., Wilson, M. H., Xin, F., Tantawy, M. N., Merryman, W. D., Johnson, R. W., Williams, C. S., Mason, E. F., Mason, F. M., Beckermann, K. E., Vander Heiden, M. G., Manning, H. C., Rathmell, J. C. and Rathmell, W. K. Cell-programmed nutrient partitioning in the tumour microenvironment. Nature, 593 (7858), 282-288.

Introduction

Cancer cells characteristically consume glucose through Warburg metabolism (Vander Heiden & DeBerardinis, 2017) a process forming the basis of tumor imaging by positron emission tomography (PET). Tumor infiltrating immune cells also rely on glucose, and impaired immune cell metabolism in the tumor microenvironment (TME) contributes to tumor immunological evasion (Chang et al., 2015; Ho et al., 2015; Siska et al., 2017). It remains uncertain, however, if immune cell metabolism is dysregulated in the TME by cell intrinsic programs or by competition with cancer cells for limiting nutrients. Here we used PET tracers to measure access and uptake of glucose and glutamine by specific cell subsets in the TME. Surprisingly, myeloid cells had the greatest capacity to uptake intra-tumoral glucose, followed by T cells and cancer cells across a range of cancer models. Cancer cells, in contrast, demonstrated the highest glutamine uptake. This distinct nutrient partitioning was cell intrinsically programmed through mTORC1 signaling and glucose and glutamine-related gene expression. Inhibiting glutamine uptake enhanced glucose uptake across tumor resident cell types, demonstrating that glutamine metabolism suppresses glucose uptake without glucose being limiting in the TME. Thus, cell intrinsic programs drive the preferential immune and cancer cell acquisition of glucose and glutamine, respectively. Cell selective partitioning of these nutrients may be exploited to develop therapies and imaging strategies to enhance or monitor the metabolic programs and activities of specific cell populations in the TME.

The founding observation in cancer metabolism was that tumors consume glucose to produce lactate in the presence of oxygen. Aerobic glycolysis is widely observed in rapidly proliferating cells, including activated immune cells, to support biosynthetic

demands (Vander Heiden & DeBerardinis, 2017). *In vivo* carbon labeling studies have confirmed that glucose supports anabolic metabolism in transformed cells and T cells. (Faubert et al., 2017; Ma et al., 2019). Glutamine metabolism provides anaplerotic fuel and restrains glucose-dependent differentiation and function of macrophages and T cells (Johnson et al., 2018; Leone et al., 2019; P. S. Liu et al., 2017). These metabolic pathways may become disrupted in immune cells in the TME to prevent anti-tumor immunity (Chang et al., 2015; Ho et al., 2015; Scharping et al., 2021; Siska et al., 2017) although the relative uptake and use of nutrients by diverse cells populations in the intact TME has not previously been directly examined.

Glucose uptake can be measured using [18F]-fluorodeoxyglucose (FDG) positron emission tomography (PET) imaging to detect cancers and monitor therapeutic responses. Based on the metabolic needs of cancer and immune cells, depletion of TME glucose by cancer cells may drive nutrient competition as a metabolic mechanism of immunosuppression (Chang et al., 2015; Ho et al., 2015). Recent publications, however, have measured high micromolar to millimolar glucose concentration in the mouse and human TME (Cortese et al., 2020; Siska et al., 2017; Sullivan et al., 2019). Further, the metabolic phenotypes of T cells can persist even after removal from the TME with activation in monoculture with nutrient-replete media. These aberrations can be reversed after the specific addition of pyruvate suggesting dysfunctional glycolysis is programmed in these cells, rather than driven by the presense of proliferating cancer cell (Gemta et al., 2019; Siska et al., 2017). The extent of intrinsic metabolic programming or nutrient competition for limited nutrients between cancer cells and immune cells remains uncertain. Here we used PET probes to analyze the accessibility of glucose and

glutamine to specific cell subsets in the TME and show that metabolites partition into distinct cell populations based on cell intrinsic metabolic programs.

Nutrients partition in the TME

Immune cells may contribute significantly to glucose consumption in the TME. We measured nutrient abundance in the tissue interstitial fluid (IF) from freshly resected human renal cell carcinoma (RCC) specimens and subcutaneous murine MC38 tumors using mass spectrometry (**Figure 2.1a-b, Table 2.1**). Glucose, glutamine, and lactate were all detectable in the TME at similar concentrations to matched normal kidney tissue or plasma. *In vivo* glucose uptake was next directly measured to quantify the accessibility of glucose to distinct cell populations in the TME. Subcutaneous MC38 tumors were visualized by FDG-PET imaging and per cell *in vivo* 18F radioactivity was measured in fractionated tumor cell subsets **(Figure 2.1c, d).** CD45 positive selection magnetic microbeads fractionated tumor cells into enriched CD45-, predominantly cancer cell, and CD45+ immune cell populations (**Figure 2.1e, Figure 2.2a**). Unfractionated tumor cells demonstrated higher FDG avidity than control tissue splenocytes (**Figure 2.1f**). Strikingly, tumor infiltrating CD45+ immune cells had greater per cell FDG uptake than CD45- cells. FDG autoradiography and immunohistochemistry demonstrated homogenous distribution of FDG and CD45+ cells, showing differential uptake was not due to spatial distribution favoring immune cells (**Figure 2.1g-h**). Immune cells also had higher FDG avidity in CT26 and Renca subcutaneous tumors (**Figure 2.1i-j, Figure 2.2b-c**) and orthotopic Renca tumors demonstrated higher per cell FDG avidity in immune cells (**Figure 2.1k, Figure 2.2d**). Infiltrating immune cells had higher FDG uptake than EPCAM+ cancer cells in both azoxymethane/dextran sodium sulfate-induced (AOM/DSS) inflammatory colon cancer

tumors and PyMT genetically engineered mouse model (GEMM) breast cancer models (**Figure 2.1l-m, Figure 2.2e-g**). These results show that glucose is available in the TME and preferentially partitions into infiltrating immune cells more than cancer cells across multiple models.

Table 2.1: Human kidney cancer patient characteristics.
Patients 170-248 were used for TIF analysis, 295-345 were used for pS6 analysis. N/R= not reported

Patient #	Patient ID	Histology	Grade	Age	Race Ethnicity	Size (cm)	Mechanism of Attainment
1	170	ccRCC	G3	66	White	N/R	Primary Nephrectomy at VUMC
2	192	ccRCC	G3	65	Black	5.4	Primary Nephrectomy at VUMC
6	213	ccRCC	G4	59	White	10	Primary Nephrectomy at VUMC
9	218	ccRCC	G3	56	White	6	Primary Nephrectomy at VUMC
10	219	ccRCC	G1	33	White	5.6	Primary Nephrectomy at VUMC
11	220	ccRCC	G3	44	White	9	Primary Nephrectomy at VUMC
12	225	ccRCC	G3	79	White	7	Primary Nephrectomy at VUMC
14	227	ccRCC	G3	62	White	13	Primary Nephrectomy at VUMC
15	228	ccRCC	G3	67	Hispanic	8.5	Primary Nephrectomy at VUMC
16	229	ccRCC	G2	74	White	5	Primary Nephrectomy at VUMC
17	231	ccRCC	G2	62	White	3.5	Primary Nephrectomy at VUMC
18	234	ccRCC	G4	79	White	3.5	Primary Nephrectomy at VUMC
19	235	ccRCC	G2	45	White	12	Primary Nephrectomy at VUMC
20	247	ccRCC	G3	38	White	6	Primary Nephrectomy at VUMC
21	248	ccRCC	G2	66	White	7.6	Primary Nephrectomy at VUMC
1	295	ccRCC	G1	65	White	4	Primary Nephrectomy at VUMC
2	323	ccRCC	G4	84	White	8	Primary Nephrectomy at VUMC
3	333	ccRCC	G3	43	White	9.7	Primary Nephrectomy at VUMC
4	345	ccRCC	G2	45	White	14	Primary Nephrectomy at VUMC

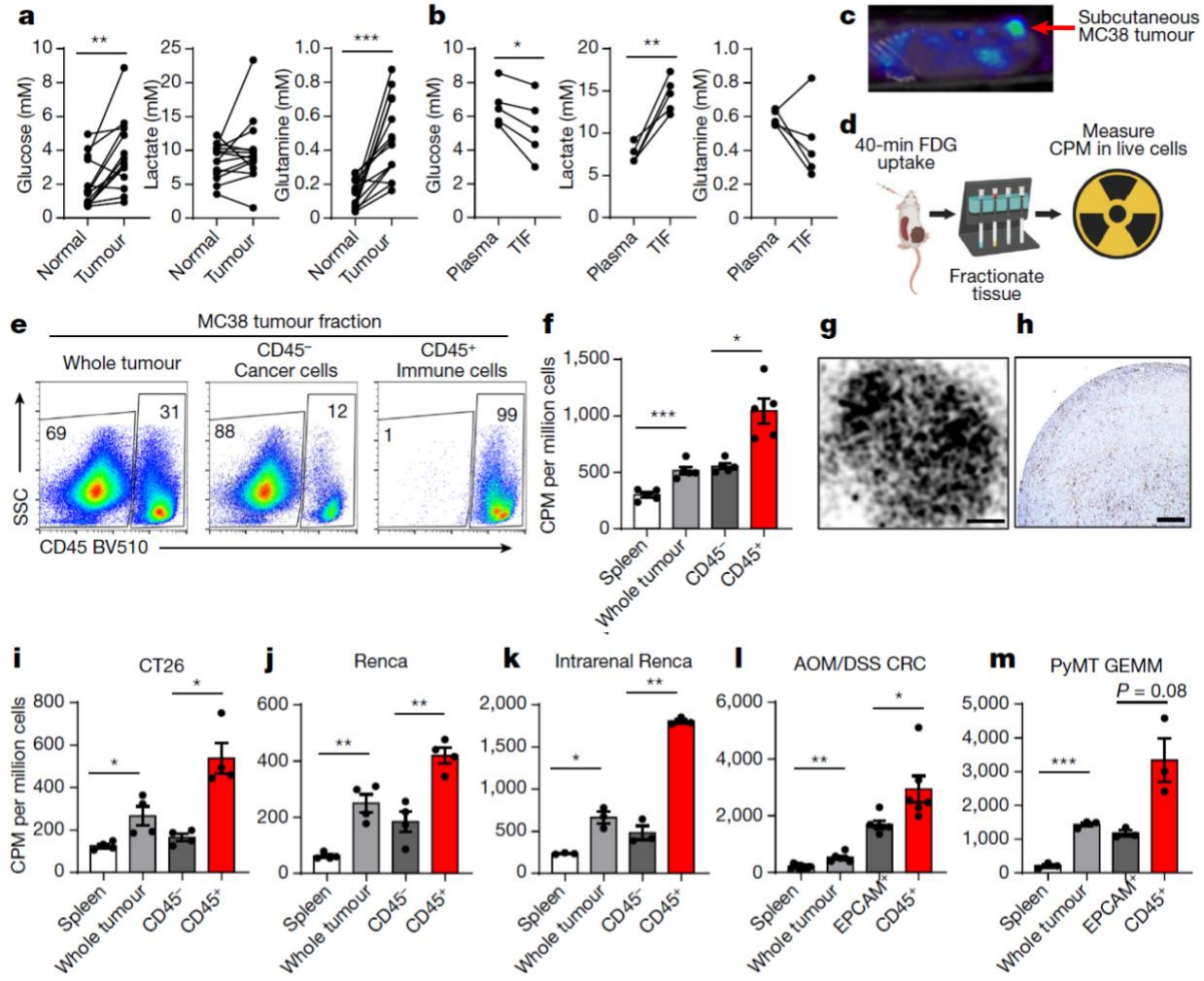

Figure 2.1: Glucose is preferentially consumed by immune cells over cancer cells. a,b Quantification of IF metabolites from (**a**) human ccRCC tumors and matched adjacent normal kidney (n=14 patients) and (**b**) murine MC38 subcutaneous tumor IF and matched plasma (n=5 mice). (**c**), Representative (of n>20 mice) FDG PET image of MC38 tumor. (**d**) Experimental schema. (**e**) Representative flow cytometry analysis of MC38 whole tumor, $CD45^+$, and $CD45^-$ cell fractions gated on live cells. (**f**) FDG avidity in designated cell fractions from MC38 tumors (n=5 mice). (**g**) Representative (of n=3 mice) tissue autoradiography of MC38 tumor (scale bar = 800μm). (**h**) Representative (of n=5 mice) IHC for CD45 in MC38 tumor (scale bar = 200μm). **i-m,** FDG avidity in designated tumor cell fractions from subcutaneous CT26 (n=4 mice) (**i**) and Renca (n=4 mice) (**j**) tumors; intrarenal Renca tumors (n=3 mice) (**k**); AOM/DSS-induced CRC tumors (n=6 for tumor, n=11 mice for spleen) **(l);** and PyMT GEMM tumors (n=3 mice) (**m**). Each data point represents a biological replicate and graphs show mean and SEM. (b-c, e-m) are data from representative studies performed independently at least twice. P values were calculated using paired 2-tailed t-test for (a-b) and Welch's 2-tailed t-test for (f, i-m). * p<0.05, ** p<0.01, *** p<0.001. AOM/DSS CRC: azoxymethane/dextran sodium sulfate-induced colorectal cancer; ccRCC: clear cell renal cell carcinoma; CPM: counts per minute; FDG PET: 18-fluorodeoxyglucose positron emission tomography; GEMM:

genetically engineered mouse model; IF: interstitial fluid; PyMT: Polyoma virus middle T antigen; TIF: tumor interstitial fluid; TME: tumor microenvironment

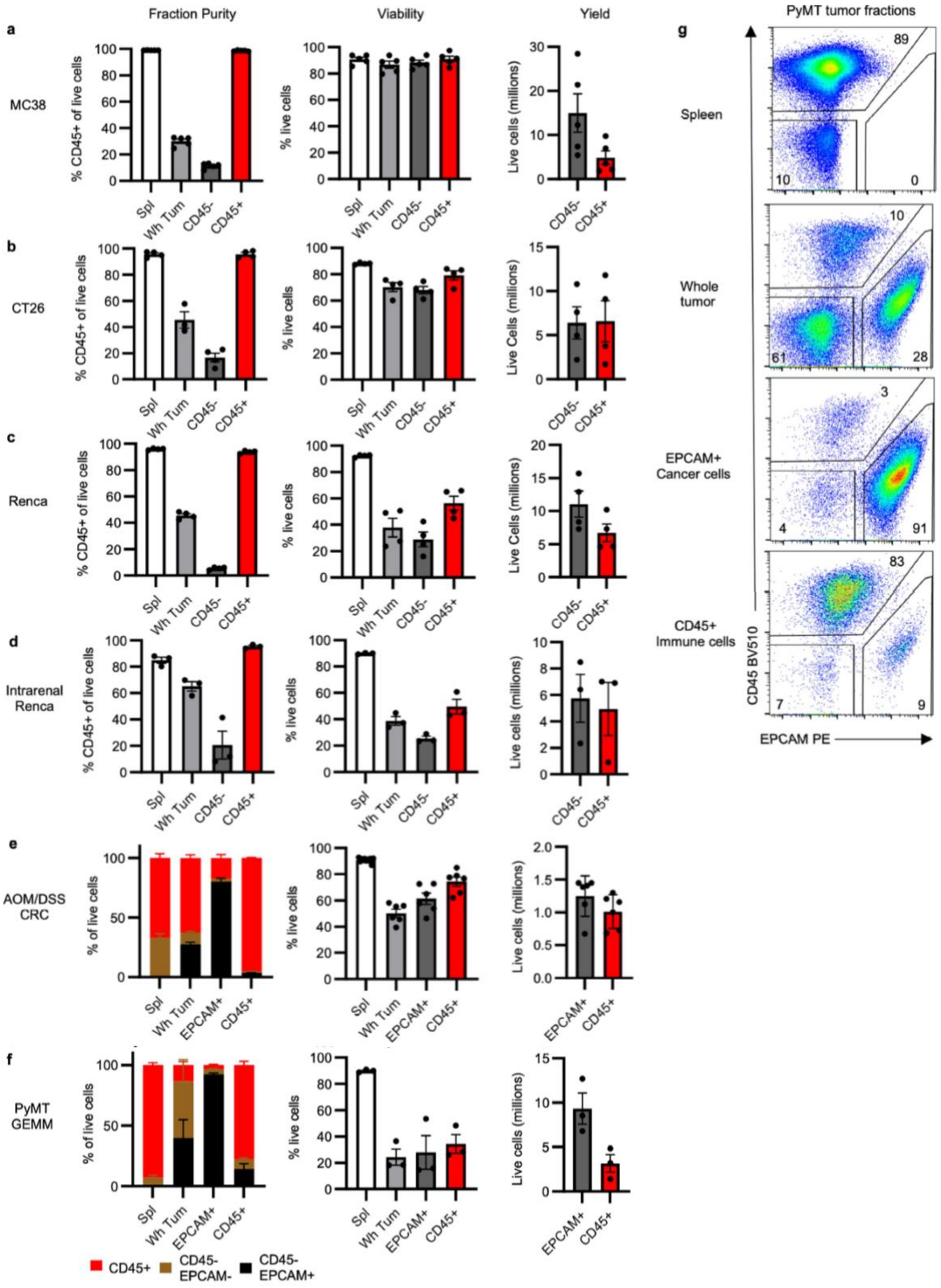

Figure 2.2: Purity, viability, and yield of isolated tumor cell populations. a-f, Fraction purity, viability, and yield for (**a**) MC38 (n=5 mice), (**b**) CT26 (n=4 mice), and (**c**) Renca (n=4 mice) subcutaneous tumors; (**d**) intrarenal Renca tumors (n=3 mice); (**e**) AOM/DSS-induced CRC tumors (n=6 for tumors, n=11 mice for spleens); and (**f**) spontaneous PyMT GEMM (n=3 mice) tumors. (**g**) Representative flow cytometry analysis of PyMT and AOM/DSS CRC whole tumor, $CD45^+$ immune cell, and $EPCAM^+$ cancer cell fractions gated on live cells. Each data point represents a biological replicate and graphs show mean and SEM. Data are representative studies performed independently at least twice. AOM/DSS CRC: azoxymethane/dextran sodium sulfate-induced colorectal cancer; GEMM: genetically engineered mouse model; PyMT: polyoma virus middle T antigen.

Multiple strategies validated that this approach accurately measures *in vivo* per cell glucose uptake. Immune cells isolated from MC38 tumors were confirmed as tumor-infiltrating based on minimal labeling following intravenous administration of fluorescent anti-CD45 antibody that efficiently labeled immune cells in blood and spleen (**Figure 2.3a**). FDG uptake had a dynamic range with a multiple-log scale of linearity (**Figure 2.3b**) and was independent of sample viability, cell yield, and tumor mass across biological replicates and tumor models (**Figure 2.3c**). To confirm that FDG uptake did not occur during tumor processing, unlabeled MC38 tumor single cell suspensions were incubated with supernatants from FDG-labeled tumors. *Ex vivo* FDG uptake did not substantially contribute to the final FDG signal (**Figure 2.3d-e**). Finally, to specifically examine cancer cells apart from other $CD45^-$ cells, $Thy1.1^+$ MC38 cells were implanted in $Thy1.1^-$ hosts and isolated using Thy1.1 positive selection microbeads. Negatively selected $Thy1.1^-$ immune cells demonstrated higher FDG avidity than $Thy1.1^+$ cancer cells (**Figure 2.3f-h**). This approach thus specifically and quantitatively measures *in vivo* glucose uptake of cancer and immune cells in the TME. We also tested the fluorescent glucose analog 2NBDG (N-(7-Nitrobenz-2-oxa-1,3-diazol-4-yl)Amino)-2-Deoxyglucose). Consistent with other *in vitro* findings (D'Souza et al., 2021; Sinclair et al., 2020), 2NBDG was not specific for glucose uptake *in vivo*. We observed higher 2NBDG in naïve CD4 and CD8 cells in comparisons to effector memory cells. This finding is in contrast to the litany of literature

that supports T cell receptor activation drives glucose uptake. Naïve T Cells (which have not experienced antigen) were 2NBDG^{hi}. Addiitonally, comparative measures of radioactive FDG and 2NBDG uptake in T cells from mice co-injected with both tracers showed no correlation of FDG radioactivity with 2NBDG (**Figure 2.4, Figure 2.5**).

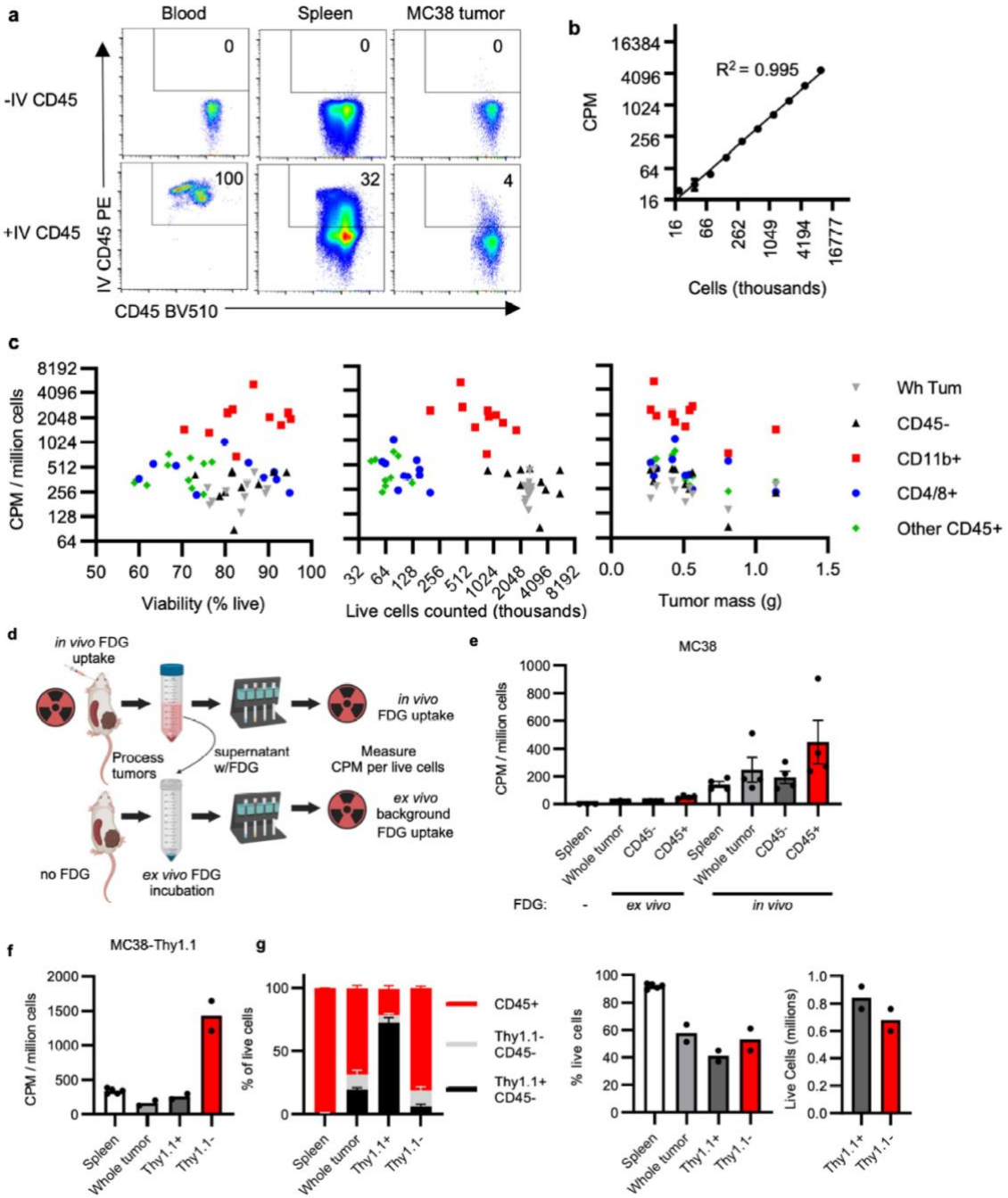

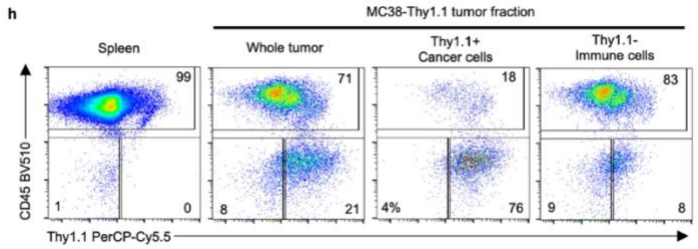

Figure 2.3: Validation of *in vivo* cellular FDG uptake assay. (a) Intravenous (IV) anti-CD45 PE staining of leukocytes from designated tissues gated on live CD45$^+$ cells. (**b**) Demonstration of dynamic range of ^{18}F quantification using serially diluted *in vivo* FDG-labelled splenocytes. (**c**) Correlation plots of CPM/live cell versus cell viability, cells counted, and tumor mass across multiple tumor cell populations. Only "CD45$^-$" and "Other CD45$^+$" simple linear regressions had slopes significantly different than 0 for tumor mass (n=10 mice). (**d**), FDG-labelled digest supernatant from *in vivo* labelled MC38 tumors was applied to FDG-naïve MC38 tumor single cell suspensions to determine *ex vivo* background FDG uptake contribution to final signal. (**e**), Cellular FDG avidity in designated *ex vivo* and *in vivo* labelled MC38 tumor cell populations (n=4 mice/group). (**f**), Cellular FDG avidity in designated tumor cell fractions from MC38-Thy1.1 tumors (n=2 mice). (**g**) Proportion of CD45$^+$ and Thy1.1$^+$ cells, cell viability, and live cell yield from MC38-Thy1.1 tumors (n=2 for tumors, n=5 mice for spleens). (**h**) Representative flow cytometry analysis of MC38-Thy1.1 tumor fractions. Each data point represents a biological replicate and graphs show mean and SEM. (b, d-h) are data from a representative study performed independently at least twice. * p<0.05, ** p<0.01, *** p<0.001. CPM: counts per minute.

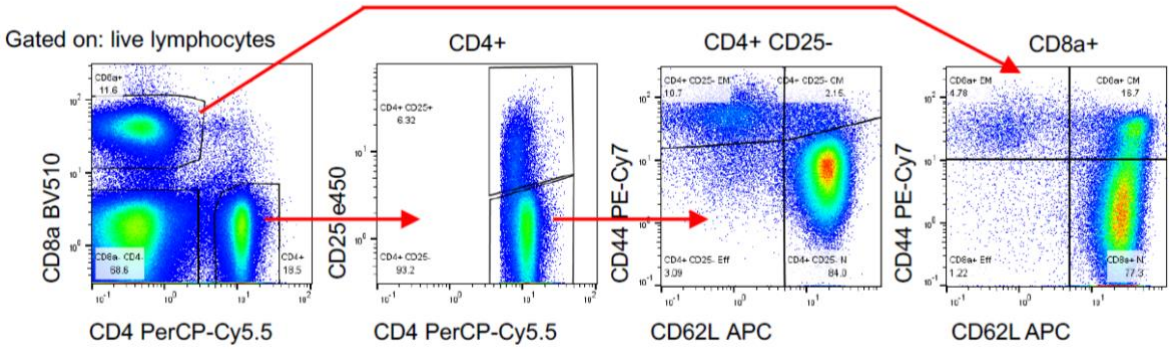

Figure 2.4: Flow cytometry gating scheme for *in vivo* 2NBDG T cell uptake.

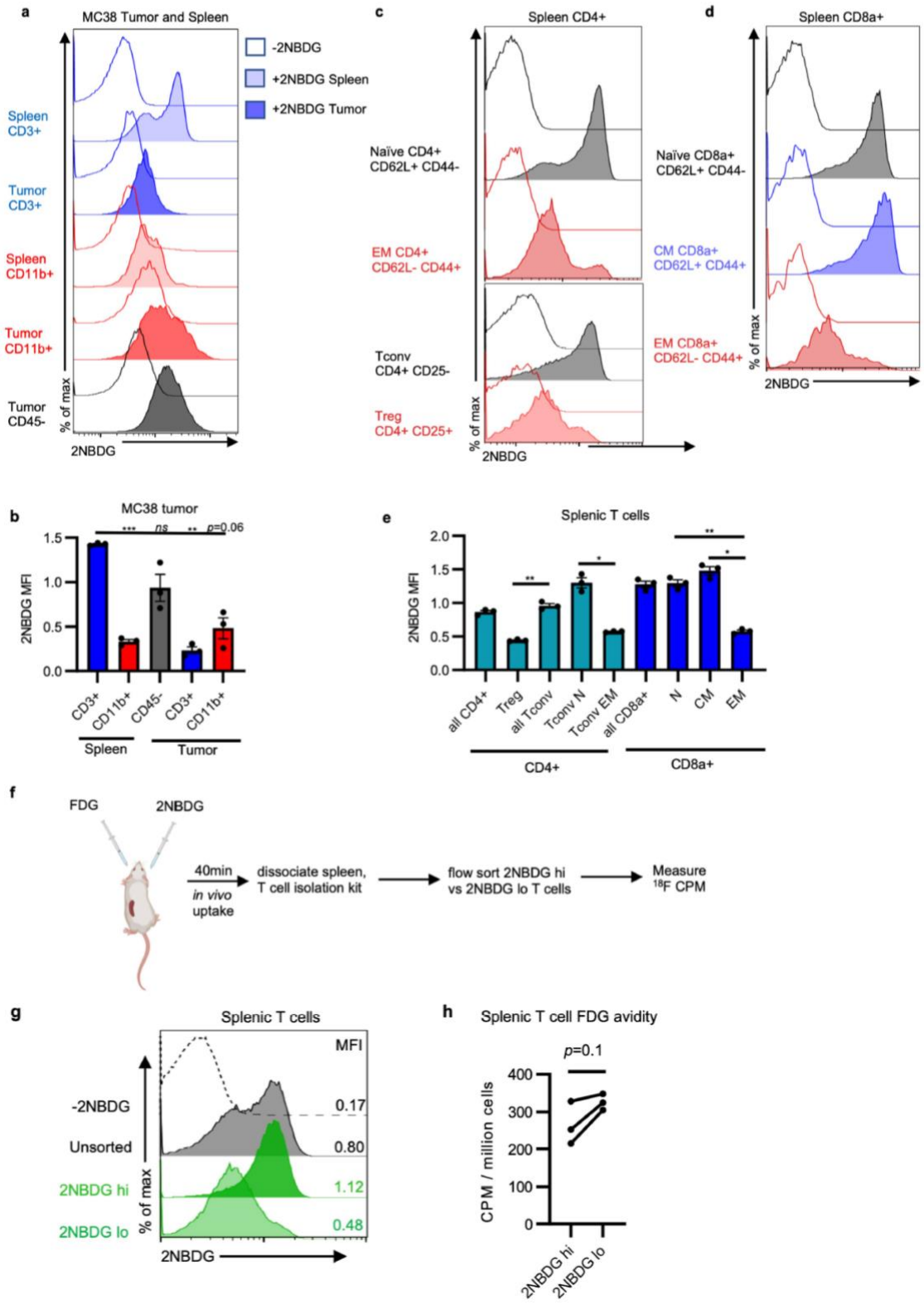

Figure 2.5: *In vivo* 2NBDG uptake does not mirror FDG uptake. (**a**) Representative histograms of *in vivo* 2NBDG uptake in splenic and MC38 tumor cell subsets. (**b**) MFI of *in vivo* 2NBDG uptake across spleen and MC38 tumor cells (n=3 mice). **c-d,** Representative histograms of *in vivo* splenic CD4 **(c)** and CD8 (**d**) T cell 2NBDG uptake. (**e**) 2NBDG staining in splenic $CD4^+$ and $CD8^+$ subsets (n=3 mice). (**f**) Schema for

2NBDG/FDG co-injection experiment. (**g**) Representative histogram of 2NBDG hi and 2NBDG lo populations collected via flow sorting. (**h**) Per cell FDG avidity of flow-sorted $2NBDG^{lo}$ versus $2NBDG^{ho}$ splenic T cells (n=3 mice). Each data point represents a biological replicate and graphs show mean and SEM. Data are from representative studies performed independently at least twice. P values were calculated using the Brown-Forsythe and Welch ANOVA with Dunnett's T3 for multiple comparison tests for (b,e), 2-tailed Welch's t test for CD4 comparisons in (e), and a paired t-test for (h). * $p<0.05$, ** $p<0.01$, *** $p<0.001$. 2NBDG: 2-(N-(7-Nitrobenz-2-oxa-1,3-diazol-4-yl)Amino)-2-Deoxyglucose); CM: central memory; CPM: counts per million; EM: effector memory; FDG: fluorodeoxyglucose; Tconv; conventional CD4 T cell; Treg: regulatory CD4 T cell

Myeloid cells uptake the most glucose in the tumor microenvironment

Effector T cells and inflammatory myeloid cells both use glycolysis and are subjects for immunotherapeutic strategies in the TME (Andrejeva & Rathmell, 2017). $CD3^+$ T cells, $CD11b^+$ myeloid cells, and $F4/80^+$ macrophages were abundant in MC38 tumors without clear differences in spatial distribution or proximity to $CD31^+$ endothelial cells that would suggest differential nutrient access (**Figure 2.6**). Characterization of immune infiltrates across various tumor models demonstrated diversity in immune cell composition (**Figure 2.7)**. We next sought to compare the FDG uptake between tumor T cells, myeloid cells, and cancer cells in the MC38 model using microbeads to isolate each population. T cells in the TME had greater *in vivo* FDG avidity than resting splenic T cells and similar FDG avidity to cancer cells (**Figure 2.8a-b, Figure 2.9a**), suggesting that these cells are not glucose deprived. T cell glucose uptake was significantly lower, however, than that of the remaining $CD45^+$ non-T cells.

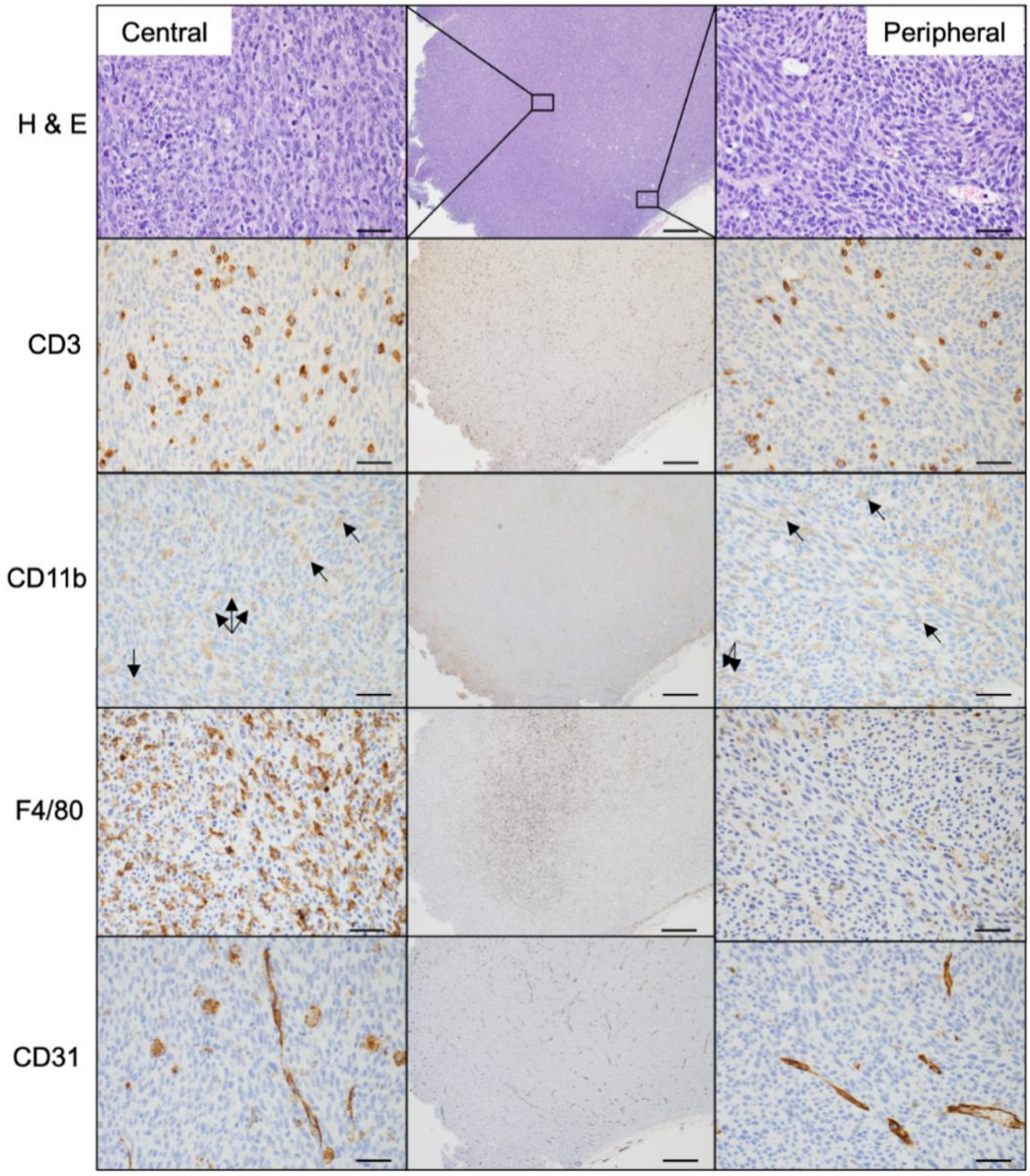

Figure 2.6: Spatial organization of immune cells in subcutaneous MC38 tumors. Representative micrographs of H&E and indicated immunohistochemistry (IHC) stains of subcutaneous MC38 tumors. Arrows indicate positive cells on faint CD11b stain. Center column is low power overview (scale bar = 200μm). Insets demonstrate high power images from central (left) and peripheral (right) tumor locations (scale bar = 20μm). Images are representative from 5 biological replicates.

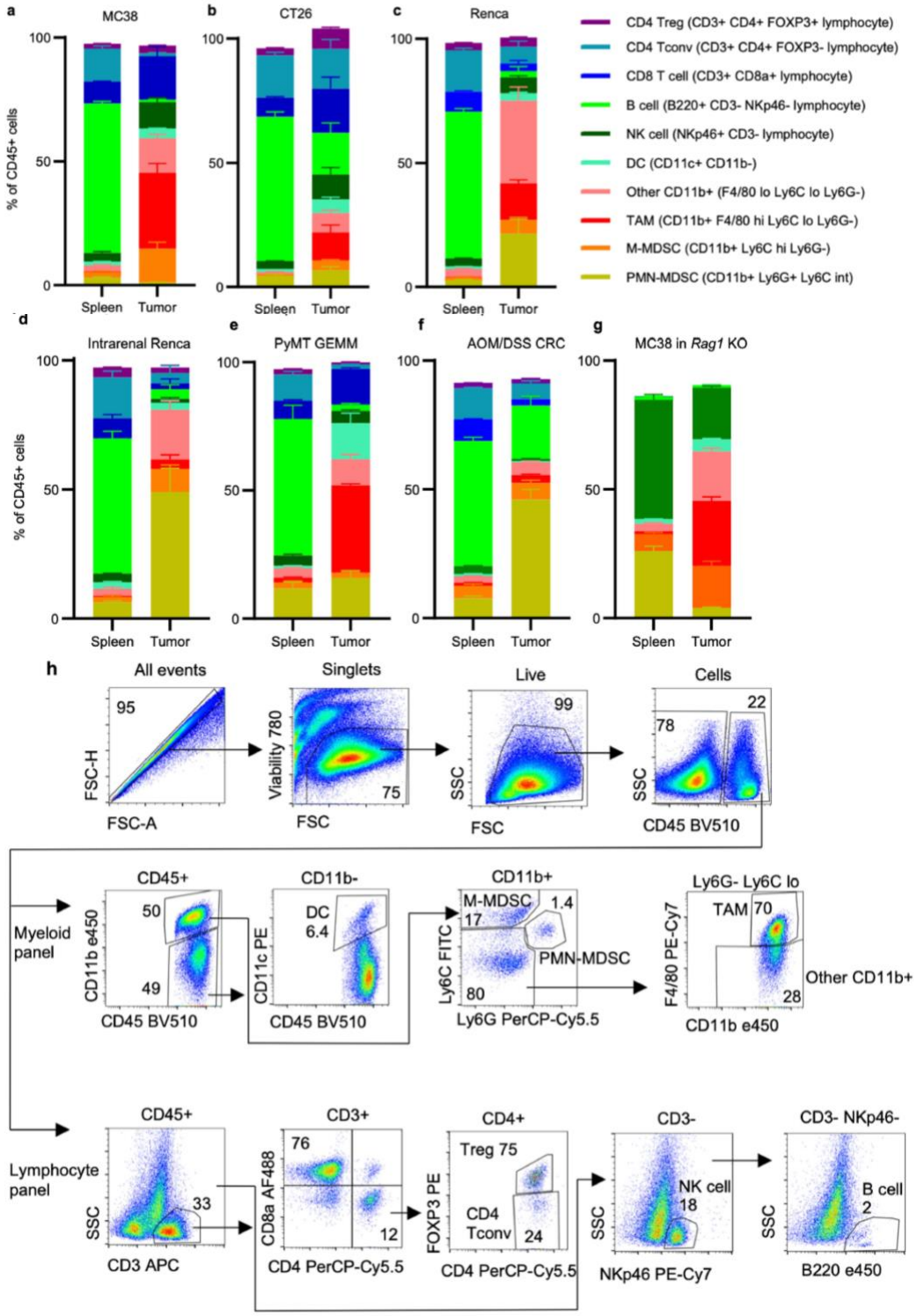

Figure 2.7: Tumor model characterizations by flow cytometry. a-g, Spleen and tumor CD45^{+} immune cell populations from MC38 (**a**) (n=3 mice), CT26 (**b**) (n=4 mice), and Renca (**c**) (n=4 mice) subcutaneous tumors; intrarenal Renca tumors (**d**) (n=3 mice); spontaneous PyMT GEMM tumors (**e**) (n=3 mice); AOM/DSS CRC tumors (**f**) (n=6 for tumors, n=11 mice for spleens); and MC38 subcutaneous tumors grown in *Rag1*$^{-/-}$ mice (**g**) (n=6 mice). (**h**) Gating strategy for immune cell identification using lymphocyte and myeloid-focused antibody panels. Each data point represents a biological replicate and graphs show mean and SEM. Data from a-f are representative of independent experiments performed at least twice. DC:

dendritic cell; M-MDSC: monocytic myeloid-derived suppressor cell; NK cell: natural killer cell; PMN-MDSC: polymorphonuclear myeloid-derived suppressor cell; PyMT: polyoma virus middle T antigen; TAM: tumor-associated macrophage

To characterize the non-T cell $CD45^+$ cells, myeloid cells were isolated using CD11b positive selection beads (**Figure 2.8c-d, Figure 2.9b**). Notably, $CD11b^+$ myeloid cells displayed higher FDG uptake per cell than cancer cells and other immune cells in MC38 tumors. Myeloid cells from CT26 tumors displayed a similar phenotype (**Figure 2.9c-d**), consistent with recent reports (Hesketh et al., 2019; Nair-Gill et al., 2010). Flow cytometry analysis of $CD45^+$ $CD11b^+$ cells from MC38 tumors demonstrated two dominant cell populations: $Ly6G^-Ly6C^{hi}$ cells consistent with monocytic myeloid-derived suppressor cells (M-MDSC), and $Ly6G^-Ly6C^{lo}F4/80^{hi}CD68^+CD206^{hi}$ cells consistent with tumor associated macrophages (TAM) (**Figure 2.8e**). Isolated $F4/80^{hi}$ cells had histiocytic morphology (**Figure 2.8f**), concordant with TAM classification. Both M-MDSC isolated using Gr1 positive selection beads and TAM isolated using F4/80 positive selection beads demonstrated high FDG avidity (**Figure 2.8g-h, Figure 2.9e-f**). $CD11b^+$ cells demonstrated high glucose uptake even in B- and T cell-deficient *Rag1*$^{-/-}$ (**Figure 2.7g**), showing that high glucose uptake in myeloid cells is independent of adaptive immunity (**Figure 2.9g**). Conventional type 1 dendritic cells (cDC1) are critical to support anti-tumor CD8 T cell activity (Spranger et al., 2017). $CD11b^-CD11c^+$ cDC, displaying a $MHCII^+CD103^+Ly6C^-$ phenotype consistent with cDC1, had lower glucose uptake than $CD11b^+$ myeloid cells but greater glucose uptake than cancer cells and non-myeloid immune cells in the TME (**Figure 2.9h-j**).

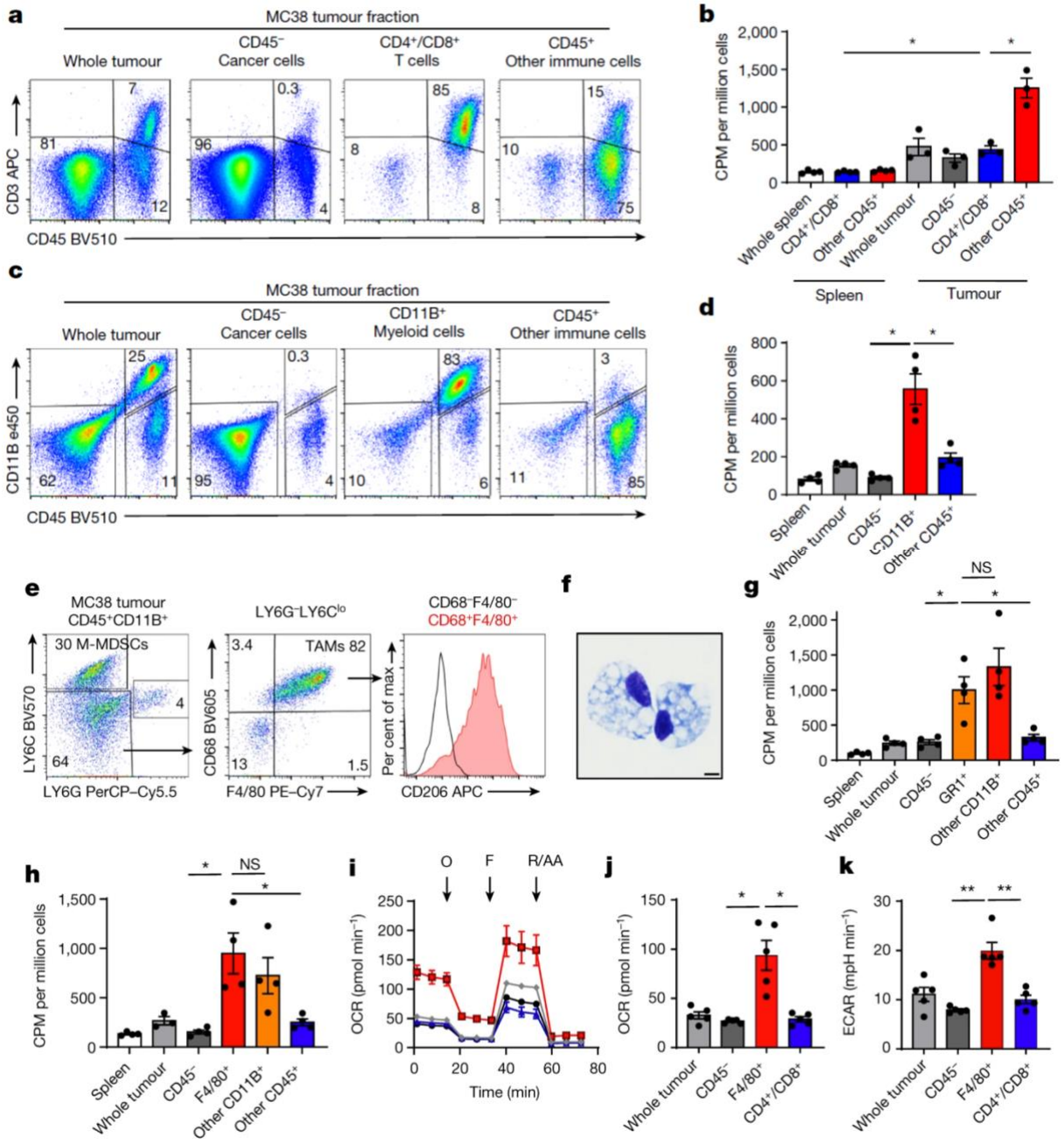

Figure. 2.8: TME myeloid cells uptake more glucose than cancer cells. (**a**) Representative flow cytometry from CD4/8 microbead fractionated MC38 tumors gated on live cells. (**b**) FDG avidity in designated cell fractions (n=3 for tumor, n=4 mice for spleen). (**c**) Representative flow from CD11b microbead fractionated MC38 tumor gated on live cells. (**d**) FDG avidity in designated cell fractions (n=4 mice). (**e**) Representative flow cytometry plots of MC38 tumor CD11b$^+$ myeloid cells. (**f**) Representative (of n=2 mice) H&E-stained micrograph of F4/80 microbead-isolated TAM (scale bar = 5μm). (**g-h**), FDG avidity in designated MC38 tumor cell fractions using Gr1 (n=4 except Wh Tum n=3 mice) (g) or F4/80 microbeads (n=4 mice) (h). **i,** Representative (of n=5 mice) OCR tracings from MC38 tumor cell fractions with oligomycin (O), FCCP (F), and rotenone and antimycin A (R/AA). (**j-k**) Basal mitochondrial OCR (**j**) and cellular ECAR (**k**) of MC38 tumor fractions (n=5 mice). Each data point represents a biological replicate except for (i) which shows technical replicates of a single biological replicate, and graphs show mean and SEM. Independent representative studies were performed at least twice. P values were calculated using Welch's 2-tailed t-

test. * $p<0.05$, ** $p<0.01$, *** $p<0.001$. ECAR: extracellular acidification rate; M-MDSC: monocytic myeloid-derived suppressor cell; OCR: oxygen consumption rate; TAM: tumor-associated macrophage

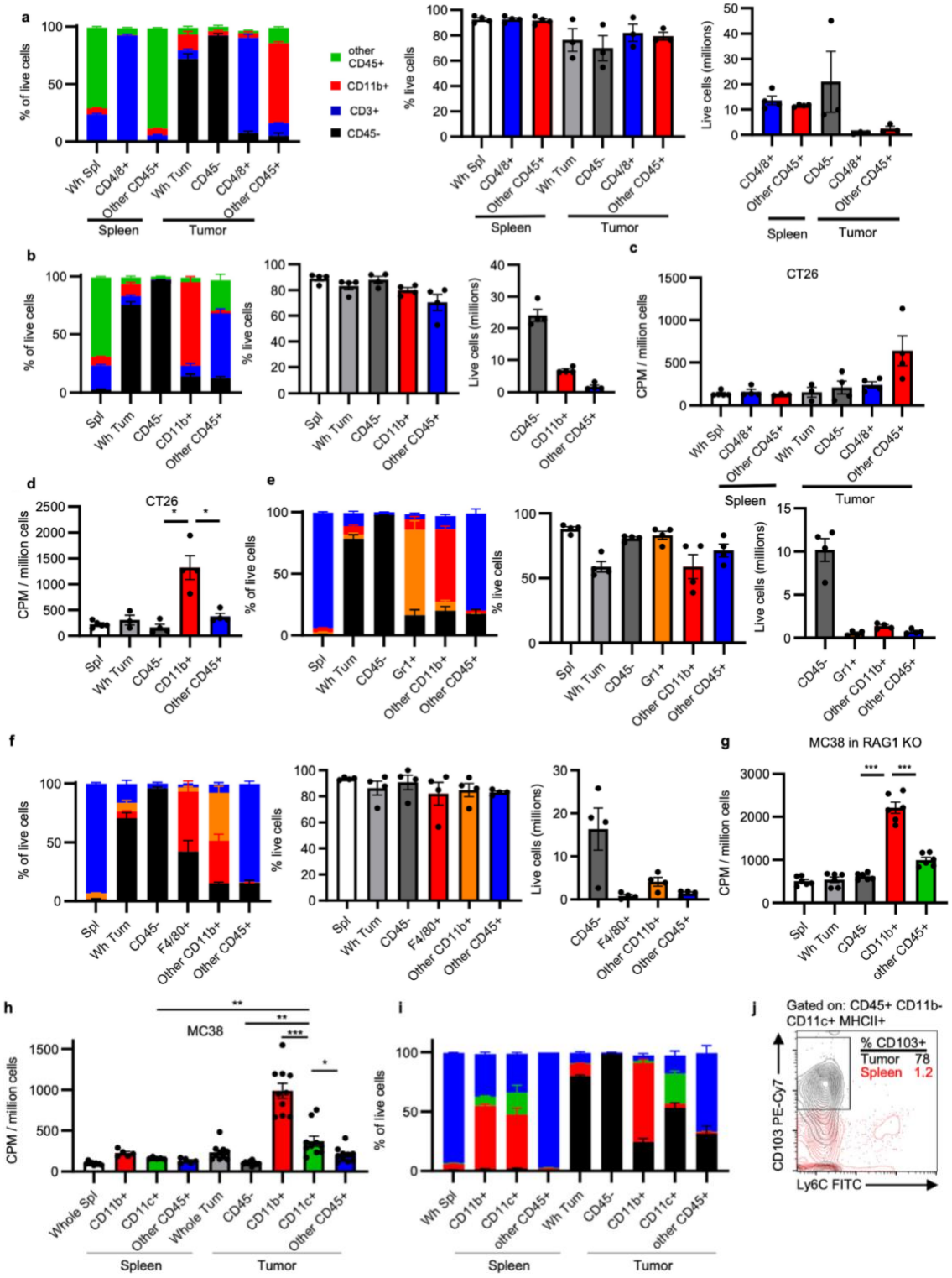

Figure 2.9: MC38 and CT26 cell isolation characterization and glucose uptake in RAG1 KO mice and in cDC. **a-b**, Fraction composition, viability, and live cell yield from MC38 tumor fractions isolated using CD4/8 microbeads (n=3 for tumors, n=4 mice for spleens) (**a**) and CD11b microbeads (n=4 mice) (**b**). **c-d**, Cellular FDG avidity in designated CT26 tumor cell fractions using CD4/8 microbeads (n=5 for Wh Spl, n=3

for Spl other CD45+ and Wh Tum, n=4 mice for all others) (**c**) and CD11b microbeads (n=5 for spleens, n=3 for Wh Tum, and n=4 mice for all others) (**d**). **c-f**, Fraction composition, viability, and live cell yield from MC38 tumor fractions isolated using Gr1 microbeads (**e**) and F4/80 microbeads (**f**) (n=4 mice). (**g**) Cellular FDG avidity in designated MC38 tumor cell fractions from *Rag1* KO mice (n=6 mice). **h,** Cellular FDG avidity in MC38 tumor cell fractions using CD11b and CD11c microbeads (n= 9 for Wh Spl, n=5 for spleen fraction, n=10 mice for all others). **i,** Fraction composition of CD11c purification (n= 9 for Wh Spl, n=5 for spleen fraction, n=10 mice for all others). **j,** Representative flow cytometry illustrating CD103 and Ly6C staining of cDC ($CD45^+$ $CD11b^-$ $CD11c^+$ $MHCII^+$ cells) from MC38 tumor and spleen. Each data point represents a biological replicate and graphs show mean and SEM. Data are representative of independent experiments performed at least twice. (h) includes data from two independent experiments. P values were calculated using Welch's 2-tailed t-test. * $p<0.05$. ** $p<0.01$, *** $p<0.001$. cDC1: type 1 conventional dendritic cell

We conducted extracellular flux assays on microbead-fractionated MC38 tumors to validate metabolic activity of cells in the TME. Isolated $F4/80^+$ TAM maintained higher basal cellular extracellular acidification rate (ECAR) and mitochondrial oxygen consumption rate (OCR) than tumor infiltrating T cells and cancer cells (**Figure 2.8i-k**). These studies show TAM and M-MDSC consume the most per cell glucose in the TME and maintain active glucose metabolism. Consistently, myeloid infiltration has been correlated with FDG avidity in non-tumor bearing lymph nodes in human and mouse gynecological malignancies (Mabuchi et al., 2020). Our data extend these findings directly to the TME and reveal the relative metabolic phenotypes of heterogeneous cells in the TME.

mTORC1 and transcription programs support metabolism in the tumor microenvironment

Mechanistic target of rapamycin complex 1 (mTORC1) supports anabolic metabolism and nutrient uptake (Saxton & Sabatini, 2017). We observed mTORC1 pathway activity by higher levels of phosphorylated ribosomal protein S6 (pS6) in tumor myeloid cells compared to other tumor cell subsets in human ccRCC, murine MC38, and murine CT26 tumors (**Figure 2.10, Figure 2.11a-c, Figure 2.12a, Table 2.1**). To determine whether mTORC1 supports glucose uptake in the TME, we treated MC38 tumor-bearing mice with rapamycin for four days and measured FDG uptake in tumor cell

populations. Rapamycin did not affect tumor weights, glucose, glutamine, or lactate concentration in the TME, but significantly decreased pS6 levels, T cell infiltration, Ki67 levels in cancer cells and T cells, and TAM cell size (**Figure 2.11d, Figure 2.12b-f**). Rapamycin treatment led to significant decreases in myeloid and cancer cell FDG uptake (**Figure 2.11e**). Extracellular flux demonstrated that *in vivo* rapamycin treatment decreased myeloid cell metabolism *ex vivo*, while cancer cells and T cells remained unchanged (**Figure 2.11f-h**). Tumor CD8 T cells and TAM retained phenotypic markers after rapamycin treatment, but CD8 T cells displayed a functionally less activated phenotype (**Figure 2.12g-n, Figure 2.13**).

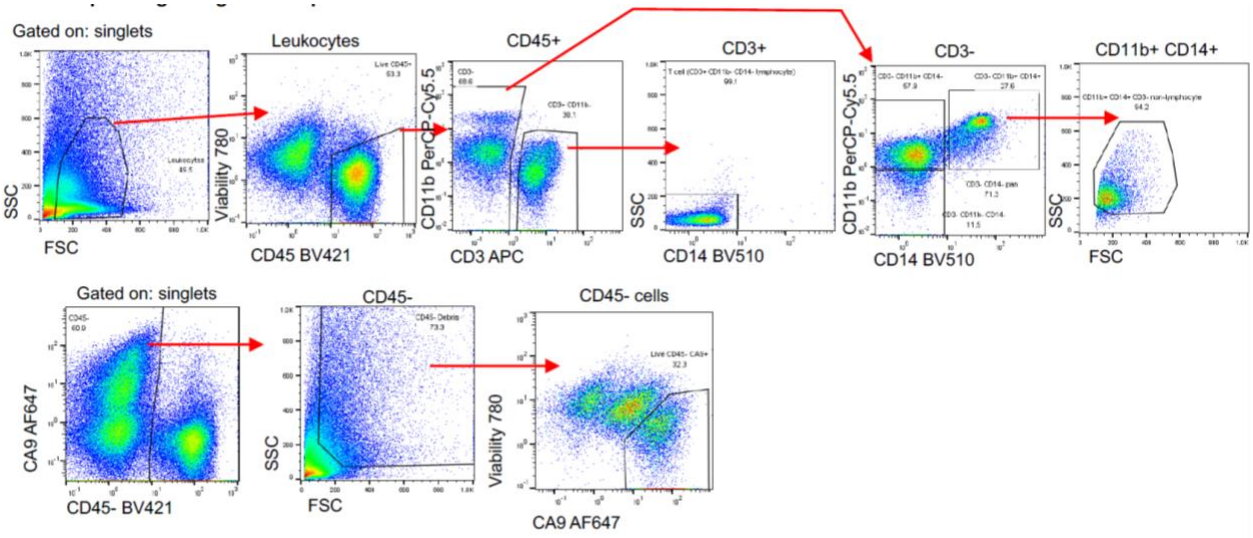

Figure 2.10: Flow cytometry gating scheme for pS6 analysis of human ccRCC tumors.

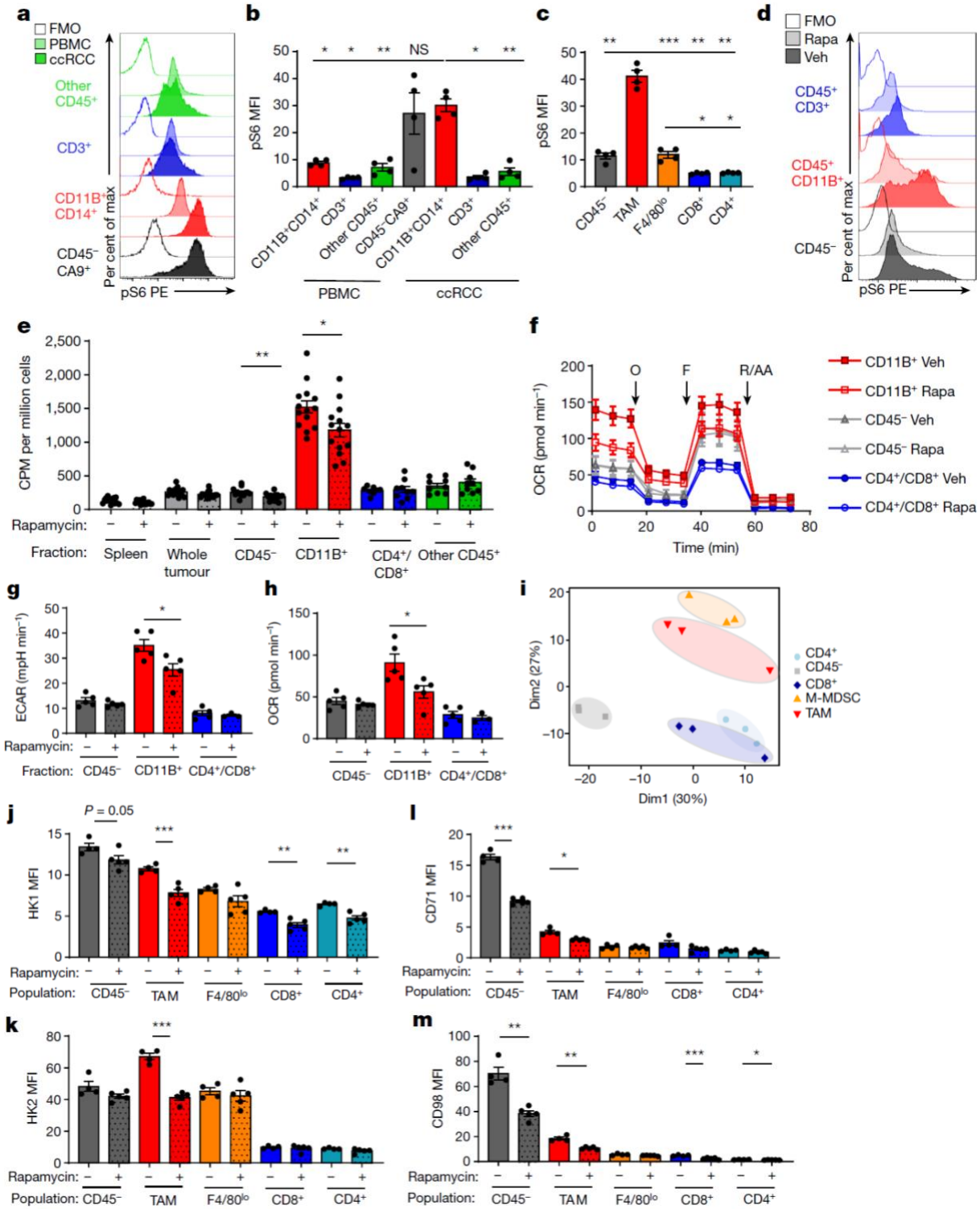

Figure 2.11: mTORC1 supports glucose uptake and metabolism in the TME. a-c, Phosphorylated S6 (pS6) levels in indicated cell populations by flow cytometry in human peripheral blood mononuclear cells (PBMC) and matched ccRCC (representative histograms (**a**), quantification (**b**) (n=4 patients) and MC38 tumors (**c**) (n=4 mice). (**d**) Representative histograms of pS6 levels in MC38 tumor cells from mice treated

with rapamycin or vehicle. (**e**) FDG avidity in designated MC38 tumor cell fractions with rapamycin treatment (n=15 for Spl Veh, n=8 for $CD4/8^+$ veh, n=9 for $CD4/8^+$ rapa and other $CD45^+$, and n=14 mice for all other groups). (**f**) Representative (of n=5 mice/group) OCR tracings from fractionated MC38 tumors from mice treated with rapamycin or vehicle with indicated injections of oligomycin (O), FCCP (F), and rotenone and antimycin A (R/AA). **g-h,** Basal cellular ECAR (**g**) and mitochondrial OCR (**h**) of MC38 tumor fractions from mice treated with rapamycin or vehicle (n=5 except for $CD4/8^+$ rapa n=3 mice/group). **i,** PCA plot of metabolism-related mRNA transcripts from $CD45^-$, TAM, M-MDSC, CD8 T cell, and CD4 T cell flow-sorted populations from MC38 tumors (n=3 mice). **j-m**, Flow cytometry quantification of HK1 (**j**), HK2 (**k**), CD71 (**l**), and CD98 (**m**) in MC38 tumor cell populations from mice treated with rapamycin or vehicle (n=4 for veh, n=5 mice for rapa). **c-d, i-m** are representative of at least two independent experiments. (e**)** is the combined data of three independent experiments. Each data point represents a biological replicate except for (f) which shows technical replicates of a single biological replicate, and graphs show mean and SEM. P values were calculated using Brown-Forsythe and Welch ANOVA with Dunnett's T3 for multiple comparison tests for (b-c) and Welch's 2-tailed t-test for (e-m). * $p<0.05$, ** $p<0.01$, *** $p<0.001$. FMO: fluorescence minus one; MFI: median fluorescence intensity; M-MDSC, monocytic myeloid derived suppressor cell; PBMC: peripheral blood mononuclear cell; pS6: phosphorylated ribosomal protein S6 (Ser235/236); Rapa: rapamycin

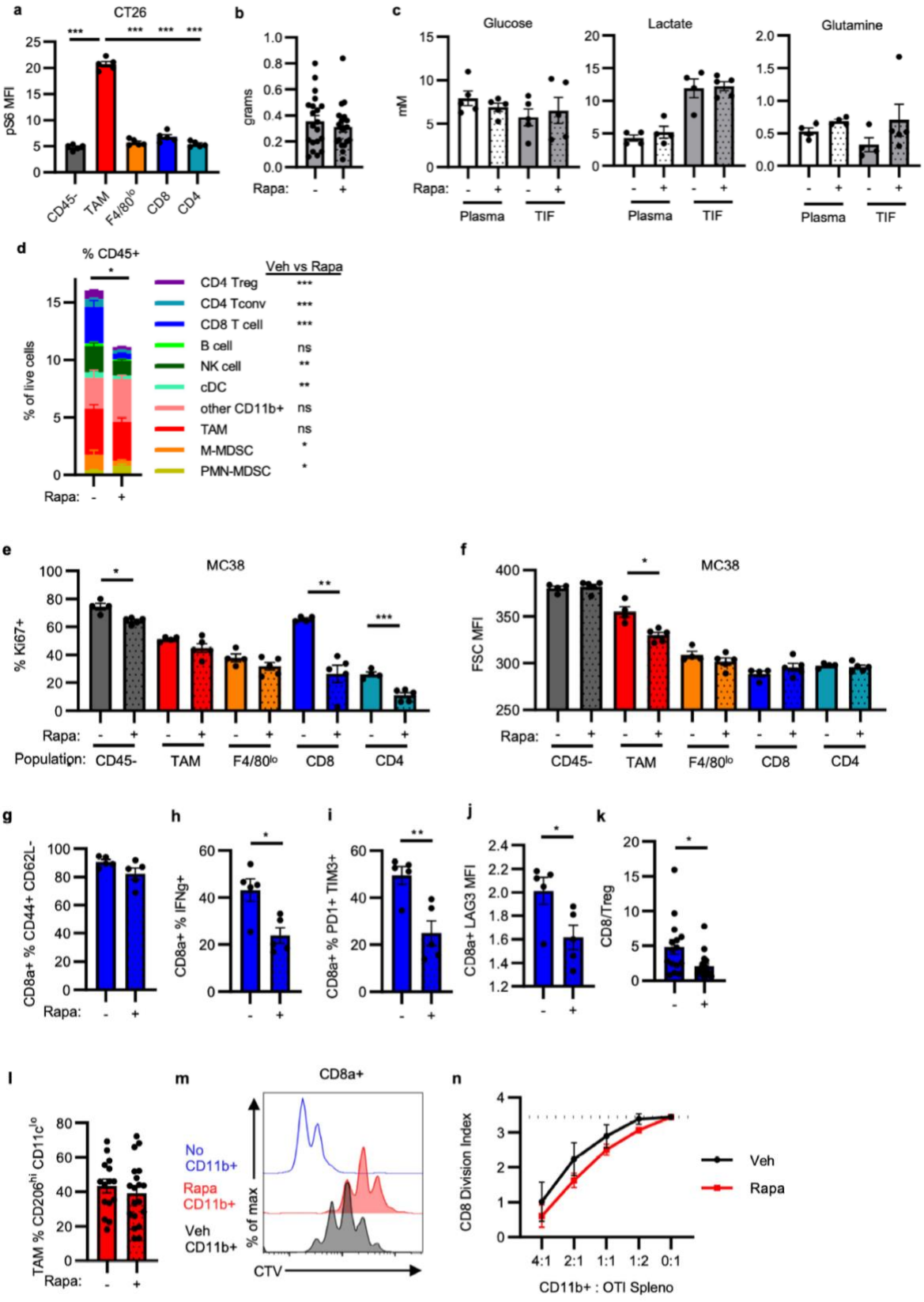
a
CT26
pS6 MFI
CD45-
TAM
F4/80lo
CD8
CD4
b
grams
Rapa:
c
Glucose
Lactate
Glutamine
mM
Plasma
TIF
d
% CD45+
% of live cells
Veh vs Rapa
CD4 Treg
CD4 Tconv
CD8 T cell
B cell
NK cell
cDC
other CD11b+
TAM
M-MDSC
PMN-MDSC
e
MC38
% Ki67+
Population:
f
FSC MFI
g
CD8a+ % CD44+ CD62L-
h
CD8a+ % IFNg+
i
CD8a+ % PD1+ TIM3+
j
CD8a+ LAG3 MFI
k
CD8/Treg
l
TAM % CD206hi CD11clo
m
CD8a+
No CD11b+
Rapa CD11b+
Veh CD11b+
% of max
CTV
n
CD8 Division Index
Veh
Rapa
4:1
2:1
1:1
1:2
0:1
CD11b+ : OTI Spleno

Figure 2.12: Effect of rapamycin treatment on the MC38 TME. (**a**) pS6 levels in CT26 tumor populations (n=5 mice). (**b**) MC38 tumor mass at study endpoint with rapamycin (n=20 for veh, n=19 mice for rapa). (**c**) Metabolite concentrations in tumor interstitial fluid (TIF) and matched plasma from MC38 tumor-bearing mice treated with rapamycin or vehicle (n=5, except for lactate and glutamine plasma and TIF veh n=4 mice). (**d**) Immune cell infiltration of MC38 tumors from mice treated with rapamycin or vehicle (n=15 for veh, n=19 mice for rapa). Significance between rapamycin and vehicle treatment for individual populations indicated in legend. Significant decrease in total $CD45^+$ cell infiltration is noted. **e-f,** Flow cytometry quantification of Ki67 positivity (**e**) and cell size (forward scatter, FSC) (**f**) from MC38 tumor populations in mice treated with rapamycin or vehicle (n=4 for veh, n=5 mice for rapa). **g-k** MC38 tumor $CD3^+CD8a^+$ T cell phenotypes from rapamycin or vehicle treated mice for effector memory phenotype (**g**), *ex vivo* IFNγ production (**h**), PD1 and TIM3 expression (**i**), LAG3 expression (**j**) (n=5 mice/group), and ratio of CD8 T cells to $CD4^+FOXP3^+$ Treg (**k**) (n=15 for veh, n=19 mice for rapa). (**l**) % M2-like TAM ($CD11c^{lo}CD206^{hi}$) in MC38 tumors from mice treated with rapamycin or vehicle (n=15 for veh, n=19 mice for rapa). **m-n**, Myeloid suppression assay representative histogram of $CD8a^+$ OT-I T cell dilution of CellTrace Violet (CTV) indicative of proliferation (**m**) and quantification of division index (**n**) for MC38 tumor myeloid cells isolated using CD11b microbeads from rapamycin and vehicle-treated mice (n=5 mice/group). Each data point represents a biological replicate and graphs show mean and SEM. Data in (a, e-j) are representative of independent experiments performed at least twice. (b, d, k-l) display data merged from 4 independent experiments. P values were calculated using the Brown-Forsythe and Welch ANOVA with Dunnett's T3 for multiple comparison tests (a) and Welch's 2-tailed t-test (b-l, n). * p<0.05. ** p<0.01, *** p<0.001. pS6: phosphorylated ribosomal protein S6 (Ser235/236); Rapa: rapamycin; TIF: tumor interstitial fluid.

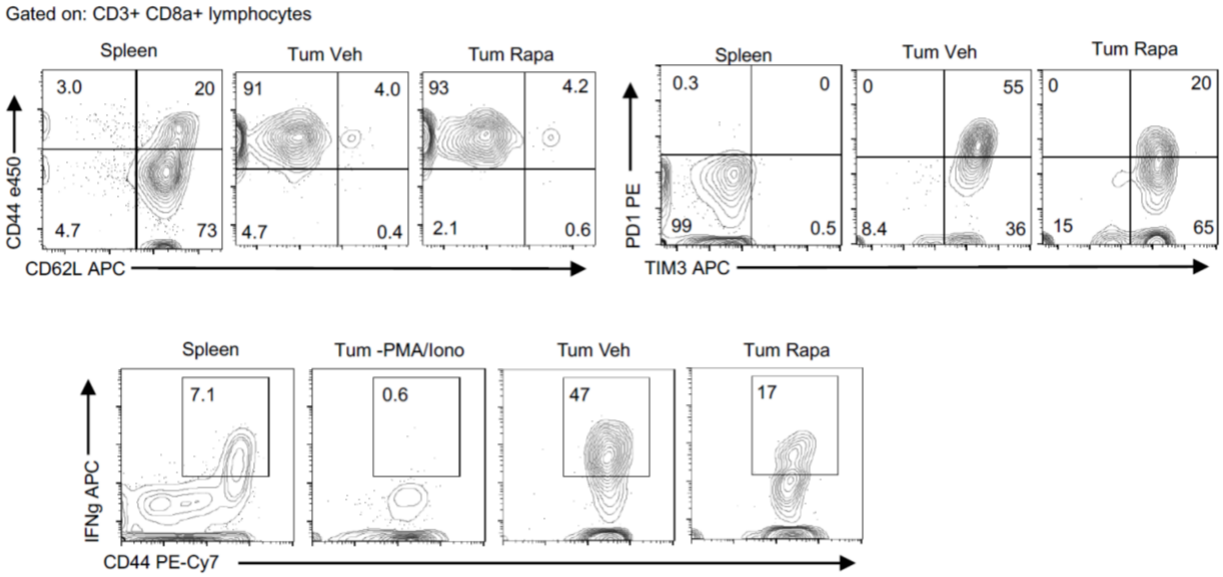

Figure 2.13: Flow cytometry gating strategy of tumor-infiltrating T cells from rapamycin-treated tumors.

Flow-sorted $CD45^-$ cancer cells, TAM, M-MDSC, CD8 T cells, and CD4 T cells from MC38 tumors were transcriptionally profiled (**Figure 2.14a**). In untreated tumors, principal component analysis and unbiased clustering based on only metabolism-related transcripts grouped samples by cell identity (**Figure 2.11i, Figure 2.14b**). Corresponding with increased glucose uptake in myeloid cells, gene set enrichment analysis revealed

relative enrichment of glucose-related pathways in M-MDSC and TAM (**Figure 2.14c, Table 2.2**). Glucose transporters demonstrated population-specific expression, with cancer cells and myeloid cells expressing high transcript levels of *Slc2a1* (GLUT1) and T cells expressing high levels of *Slc2a3* (GLUT3). Hexokinase isoforms *Hk2* and *Hk3*, which catalyze glucose phosphorylation in cells as the rate-limiting initial phosphorylation of glucose in glycolysis, were most highly expressed in myeloid cells in contrast to broadly expressed *Hk1.* $CD45^-$ cancer cells displayed amino acid, lipid, and signaling-related transcripts, and CD8 T cells were enriched in nucleotide-related transcripts (**Figure 2.14c**). Rapamycin increased glycolysis-related transcript levels, particularly in $CD45^-$ cancer cells, while other metabolic gene transcripts decreased, including amino acid-related transcripts (**Figures 2.15a-e**). Gene expression levels and changes after rapamycin treatment were confirmed at protein levels by flow cytometry. Rapamycin treatment reduced HK1 across tumor cell populations and HK2 specifically in TAM, potentially underlying differences in glucose uptake and glucose flux **(Figure 2.11j-k)**. GLUT1 levels remained unchanged (**Figure 2.15f**), yet iron transporter CD71 and amino acid transporter CD98 protein levels decreased with rapamycin treatment (**Figure 2.11l-m**).

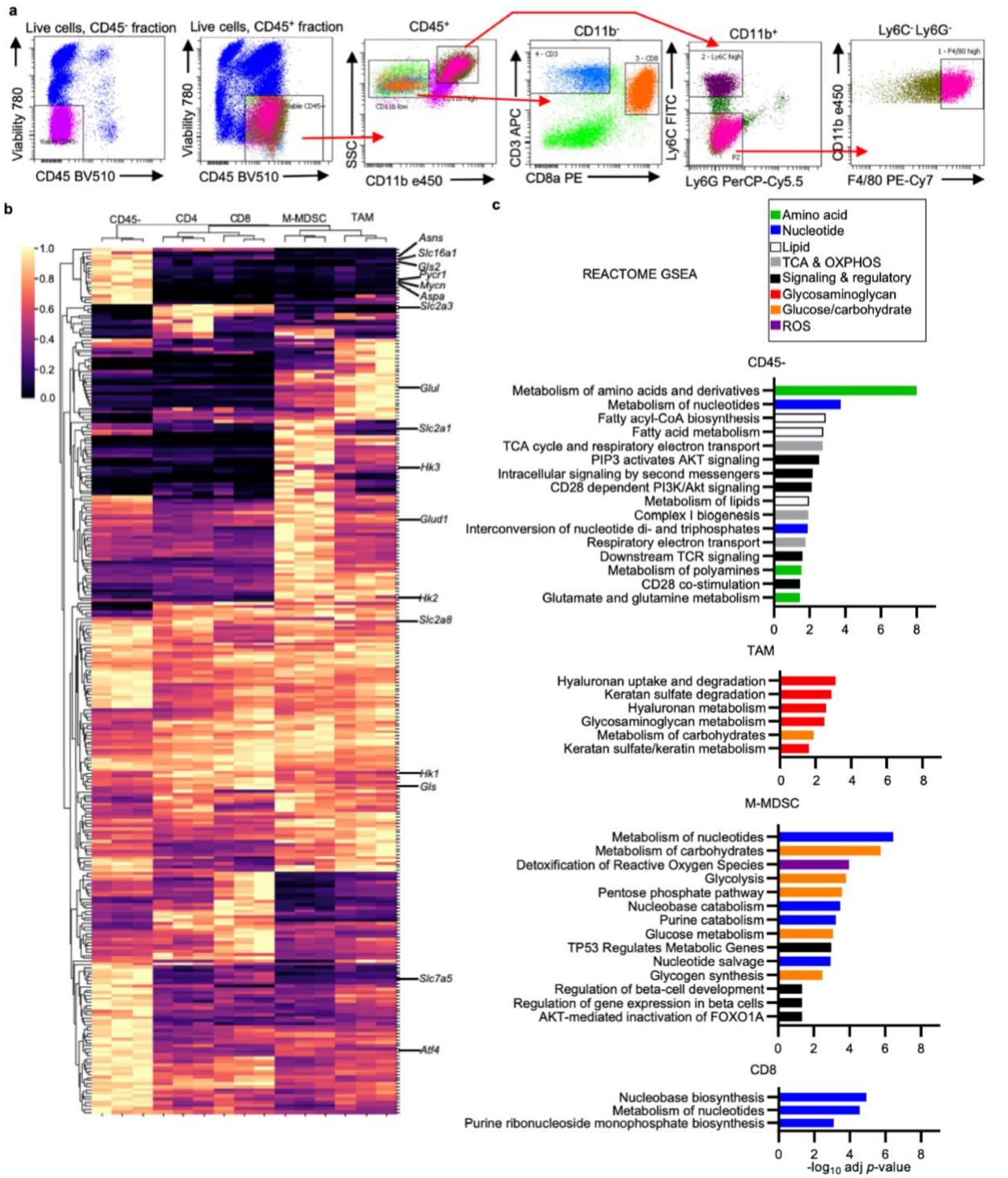

Figure 2.14: Metabolic transcriptional signatures of MC38 tumor cell populations. (**a**) Cell sorting scheme of MC38 tumor cell populations used for mRNA transcript analyses. (**b**) Clustering analysis heatmap of differentially expressed metabolic genes from MC38 tumor cell populations. Select genes annotated. (**c**) Reactome gene set enrichment analysis for genes most highly expressed in each MC38 tumor population. Significantly enriched gene sets are shown and colored according to metabolic pathway. OXPHOS; oxidative phosphorylation; TCA; tricarboxylic acid cycle

Table 2.2: Genes most highly expressed in distinct MC38 tumor populations.
Gene lists were generated based on clustering analysis of differentially expressed genes (FDR <0.01) and were subsequently used for gene set enrichment analysis.

CD45-		TAM	M-MDSC	CD8	CD4
Fah	Prdx1	Slc27a1	Ass1	Fdx1	Slc2a3
Aox1	Akt1s1	Idh2	Nt5e	Psph	Adora2a
Asns	Fahd1	Naglu	Haa0	Eno3	Hsd11b1
Slc16a1	Nadk2	Ada	Slc16a3	Rrm1	Ehhadh
Gls2	Pck2	Gmpr	Slc3a1	Rrm2	Pparg
Mapk8ip1	Acat2	Ptgs1	Upp1	Ppat	Nos1
Ptges	Fasn	Apoe	Vegfa	Cad	Odc1
Ak5	Sqstm1	Gatm	Cybb	Shmt1	Glrx
Pycr1	Pemt	Alox5	Apoc2	Tfrc	Hif1a
Mycn	Pfkm	Trf	Deptor	Bcl2	
Aspa	Psmb10	Idh1	Prdx5	Afmid	
Adh7	Txn1	Fnip2	Atox1	Pfkb1	
Scd1	Nme2	Car9	Gpx1	Impdh1	
Thbs2	Psma7	Dglucy	Pgd	Slc1a5	
Sardh	Acaca	Tbxas1	Ampd3	Kmt2a	
Mras	Prkaa1	Glul	Gda	Plcg1	
Pik3r2	Gpx4	Hexa	Hk3	Pik3r1	
Atg101	Atf4	Slc16a7	Nfe2l2	Cab39	
Ndufa7	H6pd	Gns	Slc7a11	Rpia	
Cox7c	Ppm1a	Gusb	Ptgs2	Lta4h	
Ndufa6	Impdh2	Hexb	Thbs1	Me2	
Acat1	Pycrl	Pla2g15	Kynu	Mycn	
Ndufa12	Agk	Aldob	Gad1	Gart	
Ndufb10	Gmps	Acy1	Kmo	Idh3a	
Ndufb2	Ampd2	Fabp5	Hdc	Acadl	
Mat2a	Mrps5	Slc16a6	Nat8l	Prps1	
Psmc1	Ndufa4		Aldh2	H2-Ke6	
Psma3	Sod1		Mgst3	Tfam	
Uqcr10	Ak3		Aprt		
Wdr45	Tecr		Eno1		
Map3k12	Adk		Uck2		
Prr5	Hadh		Pdk3		
Psat1	Rptor		Akt1		
Slc7a5	Srr		Glud1		
Ctps	Mcat		Pgm1		
Pebp1	Shmt2		Txnrd1		
Insr	Pdp1		Ern1		
Cbr4	Rictor		Nadk		
Srm			Akt3		
			Psmb10		
			Slc3a2		
			Pfkl		
			Pkm		
			Aloa		
			Mpc1		
			Pgk1		
			Xdh		
			Taldo1		
			G6pdx		
			Map2k1		
			Sod2		

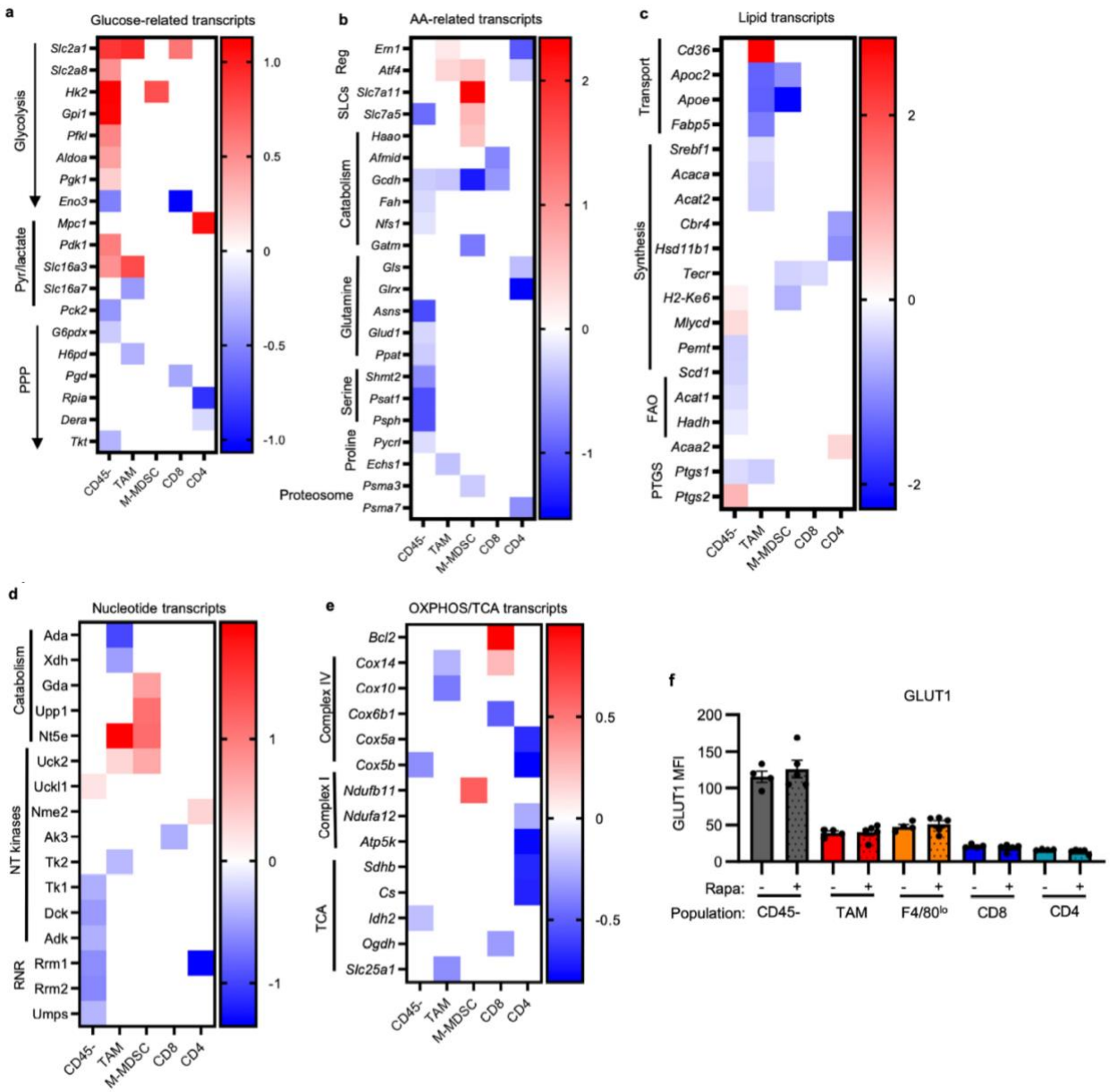

Figure 2.15: Effects of rapamycin on MC38 tumor population metabolic markers. a-e, Heatmaps of significantly altered metabolic genes between rapamycin and vehicle-treated MC38 tumor cell populations for indicated metabolic pathways: (**a)** glycolysis (**b**) amino acid metabolism (**c**) lipid metabolism (**d**) Nucleotide metabolism (**e**) oxidative phosphorylation. White spaces indicate non-significant changes with rapamycin treatment for that gene and tumor cell population. **(**Genes were grouped and classified manually. (n=3/group, except n=2 for rapamycin treated M-MDSC and CD4) (**f),** Flow cytometry quantification of GLUT1 expression in MC38 tumor populations from mice treated with rapamycin or vehicle (n=4 for veh, n=5 mice for rapa). Each data point represents a biological replicate and graphs show mean and SEM. AA: amino acid; FAO: fatty acid oxidation; NT: nucleotide; OXPHOS: oxidative phosphorylation; PPP: pentose phosphate pathway; PTGS: prostaglandin synthases; Reg: regulatory genes; RNR: ribonucleotide reductase; SLCs: solute carrier proteins; TCA tricarboxylic acid cycle

Cancer cells uptake relatively more glutamine and lipids in the tumor microenvironment

Having shown that systemic glucose is preferentially consumed by tumor-infiltrating myeloid cells, we hypothesized that other nutrients also have distinct patterns of uptake in the TME. *Ex vivo* uptake of fluorescently labelled palmitate (C16 BODIPY) was highest in $CD45^-$ cancer cells, corroborating transcript enrichment data and showing that other nutrients may partition differently than glucose in the TME (**Figure 2.17a-c**). We postulated based on transcript data that glutamine uptake would also be greatest in $CD45^-$ cancer cells. TME glutamine metabolism has been shown to promote cancer cell growth while impairing anti-tumor immunity(Leone et al., 2019). MYCN and ATF4 drive glutamine utilization (Yoshida, 2020), and *Mycn* and *Atf4* were more highly expressed in MC38 cancer cells than immune cells (**Figure 2.16a-b**). Glutamine metabolism enzymes *Aspa*, *Asns*, and *Gls2* were also specifically expressed in the MC38 cancer cells, as well as other amino acid-related transcripts *Pycr1* and *Slc7a5* (**Figure 2.14b**). Tumor-bearing mice were injected with ^{18}F-(2S,4R)4-Fluoroglutamine (^{18}F-Gln) (Zhou et al., 2017) to measure glutamine pool size and uptake in the TME. Subcutaneous MC38 tumors were ^{18}F-Gln avid (**Figure 2.16c, d**). In contrast to FDG, however, $CD45^-$ cancer cells demonstrated greater ^{18}F-Gln avidity than $CD45^+$ immune cells in MC38 (**Figure 2.16e**), CT26, Renca, and spontaneous AOM/DSS tumor models (**Figure 2.17d-f**).

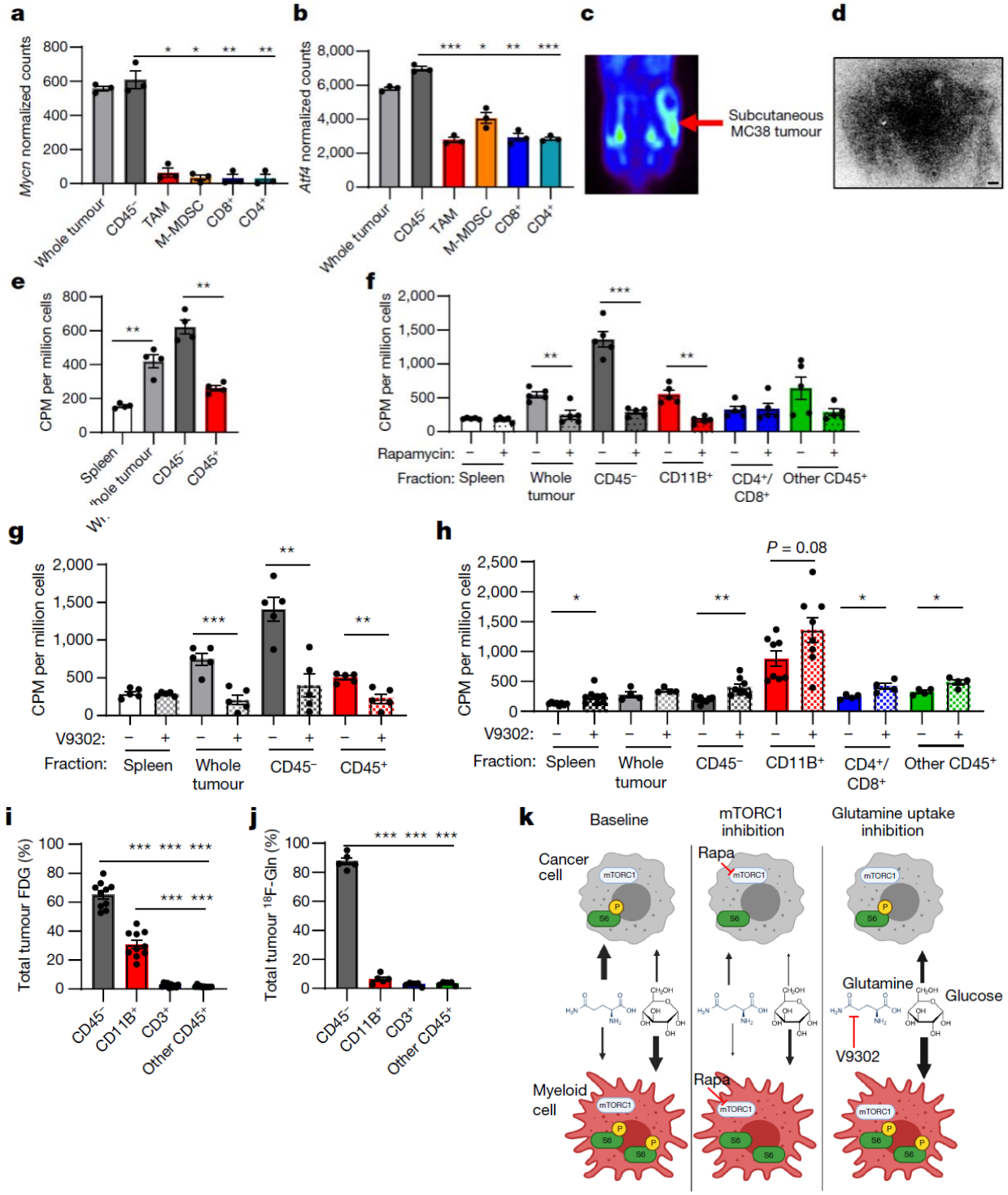

Figure 2.16: Glutamine partitions into cancer cells in the TME. a-b, Glutamine-related transcription factor mRNA transcript levels of flow-sorted MC38 tumor cell populations (n=3 mice), (**a**) *Mycn*, (**b**) *Atf4*. (**c**)**,** Representative ^{18}F-Gln image of subcutaneous MC38 tumor. (**d**) ^{18}F-Gln autoradiography image of subcutaneous MC38 tumor (scale bar = 800μm). (**e**) Cellular ^{18}F-Gln avidity in designated MC38 tumor cell fractions (n=4 mice). **f-g,** Cellular ^{18}F-Gln avidity in MC38 tumor cell fractions from mice treated with vehicle or rapamycin (**f**) or V9302 (**g**) (n=5 mice/group). (**h**) FDG avidity in MC38 tumor cell fractions from mice treated with V9302 or DMSO (n=4 for Wh Tum, CD4/8^{+}, and other CD45^{+}; n=8 mice for all others). **i-j** Contribution of cell populations to total MC38 tumor FDG (**i**) (n=10 mice) and ^{18}F-Gln signal (n=5 mice) (**j**).

(**k**) Model for nutrient partitioning in the TME. Each data point represents a biological replicate and graphs show mean and SEM. Data are representative of at least two independent experiments. (h) shows combined data of two independent experiments. P values were calculated using Welch's 2-tailed t-test for (e-h) and Brown-Forsythe and Welch ANOVA with Dunnett's T3 for multiple comparison tests for (a-b, i-j). * $p<0.05$, ** $p<0.01$, *** $p<0.001$. ^{18}F-Gln: ^{18}F-4-fluoroglutamine; DMSO: Dimethyl sulfoxide; V9302: ASCT2 inhibitor.

Rapamycin reduced amino acid-related transcripts and CD98 protein levels. Correspondingly, rapamycin treatment sharply decreased ^{18}F-Gln uptake in CD45^{-} and myeloid cells (**Figure 2.16f**). To assess the relationship between glutamine and glucose uptake, tumor-bearing mice were treated with V9302, a small molecule inhibitor of the glutamine transporter ASCT2 (Schulte et al., 2018). V9302 broadly decreased glutamine uptake by cells in the TME (**Figure 2.16g**), but increased glucose uptake in all tumor cell populations in the TME (**Figure 2.16h**). V9302 also decreased MC38 tumor mass and T cell infiltration (**Figure 2.17g, h**) and increased the frequency of tumor M2-like macrophages (**Figure 2.17i, j**). Together these data demonstrate that glutamine uptake and metabolism actively restrain glucose metabolism *in vivo* and that tumor infiltrating cells can access and increase glucose uptake beyond basal levels when glutamine is restricted. Cell-intrinsic programs of distinct tumor cell subsets thus dictate glucose and glutamine uptake in the TME.

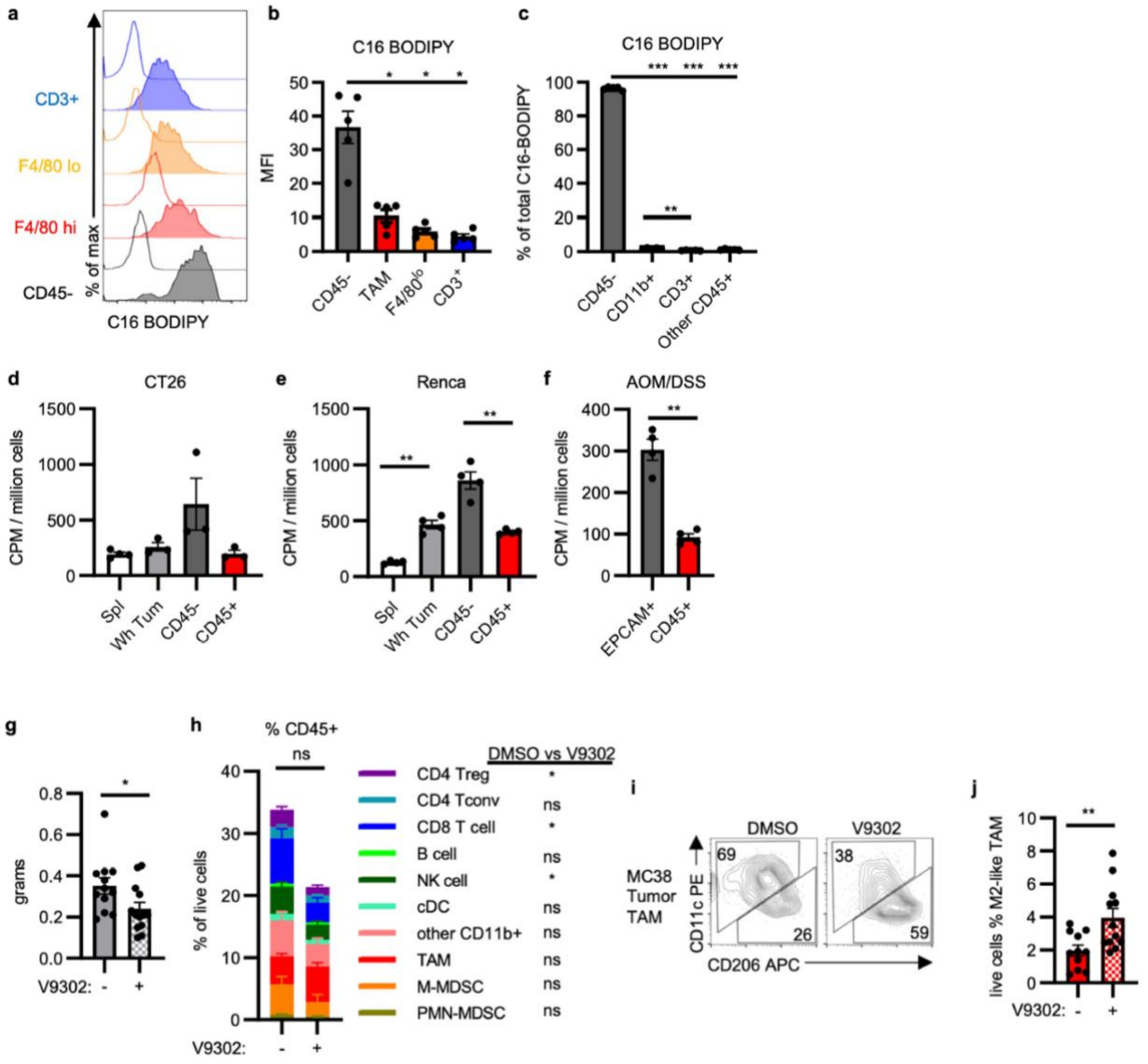

Figure 2.17: Fatty acid and glutamine uptake and the effect of V9302 treatment on the TME. a-b, Representative histograms (**a**) and quantification (**b**) for *ex vivo* staining of C16 BODIPY by indicated MC38 tumor cell populations from tumor single cell suspensions (n=5 mice). (**c**) Percent contribution to total tumor C16 BODIPY signal from indicated tumor cell populations (n=5 mice). **d-f,** Cellular ^{18}F-Gln avidity in designated tumor cell fractions in CT26 (n=4 for spleen, n=3 mice for tumor) (**d**) and Renca (n=5 mice) (**e**) subcutaneous tumors and AOM/DSS spontaneous tumors (n=4 mice) (**f**). (**g**) MC38 tumor mass from mice treated with V9302 or DMSO (n=13 for V9302, n=12 mice for DMSO). (**h**) Immune cell infiltration of MC38 tumors from mice treated with V9302 or DMSO (n=13 for V9302, n=12 mice for DMSO). Significance between V9302 and DMSO treatment in distinct populations is indicated in legend. There is no significant change in total CD45$^+$ cell infiltration (n=13 for V9302, n=12 mice for DMSO). **i-j,** Representative plot (**i**) and abundance (**j**) of MC38 M2-like TAM from mice treated with V9302 or DMSO (n=13 for V9302, n=12 mice for DMSO). Each data point represents a biological replicate and graphs show mean and SEM. Data are representative of at least two independent experiments. (g-j) are data combined from two experiments. P values were calculated using the Brown-Forsythe and Welch ANOVA with Dunnett's T3 for multiple comparison tests (b,c) or Welch's 2-tailed t-test (d-j). * p<0.05, ** p<0.01, *** p<0.001. C16 BODIPY: C16 (4,4-Difluoro-5,7-Dimethyl-4-Bora-3a,4a-Diaza-s-Indacene-3-Hexadecanoic Acid) (fluorescent analog of palmitate); V9302: glutamine uptake inhibitor

Selective nutrient partitioning

Our findings demonstrate discrete metabolic signaling regulate glucose and glutamine uptake within different cell subsets across the TME. In the context of the whole tumor, multiplying the per cell glucose uptake by the abundance of each cell type showed that cancer cells accounted overall for approximately 2/3 of glucose uptake, with myeloid cells accounting for another 1/3. Other immune cells contributing negligibly to TME FDG uptake (**Figure 2.16i**). In contrast, glutamine and lipid per-cell and total tumor uptake were dominated by cancer cells (**Figure 2.16j, Figure 2.17c**). These results support the notion that glucose is not grossly limiting in the TME, and utilization is instead modulated by cell intrinsic programs and glutamine uptake (**Figure 2.16k**).

This work reveals that diverse cell populations preferentially acquire distinct metabolites from a common pool of metabolites available in the TME (Kilgour et al., 2021; Sullivan et al., 2019). Tumor myeloid cells consume markedly more glucose than do tumor-infiltrating T cells or cancer cells on a per-cell basis. Additionally, tumor-infiltrating immune cells are more active than those in the spleen. This has implications for metabolism-targeting agents as well as myeloid targeting therapies. These new agents have the potential to either enhance or impair tumor-related inflammation. These data also support targeting glutamine metabolism as a specific strategy to hamper cancer cell growth while also increasing glucose consumption and altering immunophenotype in the TME as a result. Given the interest in glutamine-targeting therapeutics, our findings contribute a model of nutrient partitioning that supports their further development.

Previous studies have suggested competition for glucose in the TME between cancer cells and T cells contributes to immunosuppression (Cascone et al., 2018; Chang

et al., 2015; Ho et al., 2015). Our data, however, show that glucose is not broadly limiting, and TME resident cells have the capacity to increase glucose uptake *in vivo* when glutamine uptake is restricted. This cell-intrinsic programming provides a new level of insight into the innerworkings of the TME. Here, a program of mTORC1-driven glutamine uptake in the CD45- cancer may suppress glycolytic gene expression and glucose metabolism in these cells. There is also growing evidence that glycolytic cancer cell transcriptional programs are associated with immunosuppressive TMEs and directly recruit suppressive myeloid cells (Chafe et al., 2019; C. Li et al., 2018) while TAM glycolysis may drive hypoxia via endothelial dysfunction (Wenes et al., 2016) and cytokine production (Jeong et al., 2019). Our work supports a model where glycolytic tumors are immunoinhibitory not directly due to nutrient deficiencies but rather because of large scale microenvironmental changes which alter intrinsic cellular programming of immune cells. We observe that different nutrients may follow distinct, but cell and tumor-type specific patterns.

Myeloid cells directly consume FDG out of proportion to the cancer cells and thus account for a significant fraction (30%) of measured tumor glucose uptake in PET imaging. These data challenge the expectation that FDG tumor avidity is primarily reflective of cancer cell metabolism and illustrate that FDG-PET imaging of immune checkpoint blockade responses reflect a significant non-tumor component. The FDG imaging features of a tumor may also be dependent on the type and activation state of a patient's tumor immune infiltrate. Supporting this, recent work has shown increased FDG avidity in lung cancer is associated with $CD68^{+}$ TAM, which was interpreted as an increase in cancer cell glycolysis due to macrophage secretion of TNFα (Jeong et al.,

2019), not glucose uptake by TAM. Our data support the model where TAM directly consume FDG and thus account for a significant portion of the measured tumor glucose uptake. The DeBerardinis group at UTSW has also recently demonstrated that FDG uptake does not correlate with C13 labeling in non-small cell lung cancer patients. However, maximal FDG intensity does correlate with tumor proliferation and size, which often correlate with suppressive myeloid infiltrate (L. Cao et al., 2019; Hirayama et al., 2012; Kernstine et al., 2020; Zhang et al., 2011). These findings also help explain intratumoral regional variability in FDG avidity observed on PET imaging as well as the PET avid nature of Hodgkin's lymphoma, a disease entity with far more inflammatory cells than transformed tumor cells. Understanding the biology of distinct cell types in the complex TME has contributed substantially to shaping models of tumorigenesis. Our studies extend these approaches to evaluate *in vivo* metabolic features of tumor cell types and show that individual cell populations have distinct nutrient uptake programs that may play an important role in therapy response or resistance.

CHAPTER 3: HK3 as a myeloid specific interferon gamma stimulated gene with prognostic significance in clear cell renal cell carcinoma

Introduction

The manner in which cells metabolize glucose ultimately impacts their cellular fate and function. Glucose can be used for the generation of more energy (ATP), reduced electron donors (NADH), as well as biosynthetic substrate for new macromolecules (Vander Heiden et al., 2009). Additionally, glucose can suppress apoptotic signals from the mitochondria (Danial et al., 2003; Rathmell et al., 2003) .

T cell subsets with divergent lineage markers and transcription factors employ different metabolic programs to ultimately gain their diverse effector function (Gerriets et al., 2015). Recently, it has been appreciated that different members of the glucose transporter family contribute differentially to T Cells subsets where Glut3 promotes the pathogenicity of Th17 cells, but not other T cell subsets (Hochrein et al., 2022)

Glucose enters cells via the aforementioned family of SLC2a transporters by a passive process, facilitated diffusion. However, for glucose to remain inside the cell, and thus be utilized in cellular processes, it must be phosphorylated by a hexokinase (HK). There are four main glucose HKs (three with low K_ms) that allow cells to fix glucose intracellularly. The high Km HK (glucokinase, GCK) is used almost exclusively by pancreatic beta cells to sense blood glucose and thus drive insulin secretion, demonstrating that the unique biochemical properties of these enzymes can be inextricably linked to cell function and organismal physiology (MacDonald et al., 2005). This is in marked contrast to *HK1* expression, which is known as a house keeping gene and expressed throughout tissues in the body. *HK2* expression is regulated by mTOR/hypoxia signaling, playing a key role in tumorigenesis and metastasis (Ciscato et

al., 2021). *HK3* expression on the other hand has been often overlooked, mostly due to a lack of isoform specific reagents. Previous studies show that HK3 has the highest affinity for glucose while uniquely demonstrating both substrate and product inhibition, where HK1 and HK2 only demonstrate end production inhibition(Su & Wilson, 2002) (Cardenas et al., 1998). HK3 was originally thought as a liver specific isoform (Katzen & Schimke, 1965). In today's literature, HK3 is denoted as white blood cell specific hexokinase. However, it remains unknown which white blood cell(s) express this unique isoform.

Besides slight differences in biochemical characteristics, HK1 and HK2 are different than HK3 structurally (**Figure 3.1**). Even though these enzymes have similar duplications of kinase domains, HK1/2 contain N-terminal mitochondrial binding sequence (MBS) where as HK3 lacks this structure completely. This mitochondrial binding activity is essential for HK1 and HK2 given that these isoforms sense mitochondrial ATP pool to promote increase glucose retention and metabolism. Additionally, via this domain, these two HK isoforms bind BAX/BAK, actively suppressing apoptosis in the presence of glucose. The divergent N-terminal domain in HK3 is essential to protein folding and replacing it with the HK1 or HK2 MBD results in toxic protein aggregates (Wyatt et al., 2010). Recent work has demonstrated that eliminating HK1's mitochondrial binding leads to increased macrophage activity due to increased PPP flux (De Jesus et al., 2022). Given this finding, it can be hypothesized that the unique structural composition of HK3 (where it cannot bind the mitochondria) imparts altered function in the unknown cells that express this isoform.

Myeloid cell glucose metabolism has recently been shown to be a hallmark of both tumor microenvironments (TME) and in brain pathology. The most glucose consuming

cells in many tumor models as well as the brain appear to be the CD11b+ myeloid cells (Reinfeld et al., 2021), (Xiang et al., 2021). However, the underlying program that promotes this glucose uptake phenotype is not fully appreciated. Other groups have demonstrated different TAM subpopulations with divergent roles in tumor progression consume glucose and restock the Kreb's cycle in different patterns *in vitro* (Geeraerts et al., 2021). We observed increased pS6 levels in tumor myeloid cells. Rapamycin was able to lessen but not fully eliminate enhanced *in vivo* myeloid glucose uptake (Reinfeld et al., 2021). Therefore, understanding myeloid specific metabolic programs is important to uncovering tumor progression and novel therapeutic targets in this era of cancer immunotherapy.

In this work, we demonstrate that HK3 is a myeloid specific hexokinase in heterogenous tumor microenvironments, in healthy individuals and in inflammatory disease settings. Additionally, we show that HK3 expression is regulated the crucial anti-tumor cytokine interferon gamma (IFNγ). Because of the IFNγ responsive promoter of HK3, this gene is a poor prognosis indicator in clear cell Renal Cell Carcinoma (ccRCC). But since this tumor is now treated with immunotherapeutic agents that rely on functional IFNγ signalling, elevated *HK3* expression predicts better outcomes

Figure 3.1: **Structure and regulation of eukaryotic low K_m hexokinases**. HK: hexokinase, MBS: mitochondrial binding sequence, mTOR: mammalian target of rapamycin, HIF: hypoxia inducible factor

HK3/Hk3 expression is restricted to diverse myeloid cells in the TME

NanoString RNA transcriptomic analysis uncovered many glycolytic genes are enriched in flow sorted CD11b+ cell population ($GR1^+$ Myeloid Derived Suppressor cells (MDSCs), and $F4/80^+$ Tumor Associated (TAMs)) from the MCD38 tumor microenvironment (TME) (**Figures 2.11, 2.14**). We generated differently expressed genes between the two myeloid populations and the other three main tumor resident cell populations (CD45- cancer cells, CD4+ T cells, CD8+ T cells). Not surprisingly myeloid identity genes like *Arg1*, *Apoe*, *Cybb (*NOX2) and *H2.Aa* (MHCII) are highly enriched in these CD11b+ populations (**Figure 3.2A, Table 3.1**). Strikingly, *Hk3*, has a log fold enrichment (6.73) greater than many known myeloid genes like *Cd68*, *Tbxas1,* and other MHCII components (*H2.DMa*) in these MDSCs and TAMs . When comparing all three low Km HK isoforms across these tumor fractions, it is clear that HK3 is the dominate myeloid isoform and is not detected in the transformed cancer cells or the lymphoid compartment (**Figures. 3.2B-D**). Interestingly, *Hk1* is significantly enriched in the T lymphocytes.

Table 3.1: **Myeloid specific genes based on log fold enrichment in comparison to other TME resident cell types-** *Hk3* and *Hk2* are bolded in the chart for emphasis

Gene Name	p value	q value	fold change	Log Fold Change
Fcrlb	0.000706	0.00576066	2866.5	11.4850746
Apoe	4.00E-04	0.00329893	841.397959	9.71664451
Itgam	0.00176	0.00917291	804.238854	9.65148023
Fcrls	0.00177	0.00917291	565.813954	9.14418395
H2.Aa	4.00E-04	0.00329893	347.572926	8.4411719
Ly86	4.00E-04	0.00329893	299.306324	8.22547895
Arg1	4.00E-04	0.00329893	288.514286	8.17249895
Fcgr4	0.00177	0.00917291	220.321138	7.78346411
Kynu	0.000995	0.00713238	189.857143	7.56877047
Cybb	0.00172	0.00917291	186.09727	7.53991308
Cd14	4.00E-04	0.00329893	178.193333	7.47729955
H2.Eb1	4.00E-04	0.00329893	169.556075	7.40561866
Hk3	**4.00E-04**	**0.00329893**	**106.49434**	**6.73463294**
Btk	0.00177	0.00917291	85.4640719	6.41724615
Cd68	0.00177	0.00917291	85.0385662	6.41004537
Tbxas1	4.00E-04	0.00329893	81.9304636	6.35632807
Tlr2	4.00E-04	0.00329893	71.7306035	6.16451686

Cd180	0.00177	0.00917291	71.6861539	6.16362259
Trf	4.00E-04	0.00329893	71.2748032	6.15532025
Deptor	0.00126	0.00894833	61.7	5.94719858
Gatm	4.00E-04	0.00329893	47.8507614	5.58046998
H2.DMa	4.00E-04	0.00329893	46.2739726	5.53212905
Apoc2	4.00E-04	0.00329893	43.28125	5.43567026
Ctss	4.00E-04	0.00329893	42.4570509	5.40793226
Ms4a4a	4.00E-04	0.00329893	32.2667718	5.01197734
Cxcl9	0.00177	0.00917291	31.755571	4.98893781
Thbs1	4.00E-04	0.00329893	28.429311	4.82930723
Tlr7	4.00E-04	0.00329893	23.7519231	4.56997242
Cmklr1	4.00E-04	0.00329893	19.097653	4.25532344
Dglucy	0.00177	0.00917291	18.2307692	4.18830353
Car9	0.00172	0.00917291	17.612069	4.13849249
Gda	4.00E-04	0.00329893	16.750996	4.06617498
Slc16a7	4.00E-04	0.00329893	15.858209	3.98715794
Ptgs2	0.0111	0.04366	14.3429578	3.84227066
Csf3r	4.00E-04	0.00329893	12.9572368	3.69568619
Nod2	0.00177	0.00917291	11.9700855	3.58136155
Tlr4	4.00E-04	0.00329893	10.8411245	3.4384425
Alox5	4.00E-04	0.00329893	9.01156812	3.17177818
Hexb	4.00E-04	0.00329893	8.99082331	3.16845323
Hmox1	4.00E-04	0.00329893	8.86265477	3.14773892
Kmo	0.00172	0.00917291	8.82716049	3.14194943
Prdx5	4.00E-04	0.00329893	8.81264601	3.13957526
Pla2g15	4.00E-04	0.00329893	8.55169628	3.09621062
Ctsz	4.00E-04	0.00329893	8.34688675	3.0612382
Hexa	4.00E-04	0.00329893	8.12235133	3.02189743
Ampd3	0.00177	0.00917291	8.09708738	3.01740305
Cd36	0.000799	0.00578144	7.16612903	2.84119402
Slc7a11	0.00172	0.00917291	6.6097561	2.72459704
Gusb	4.00E-04	0.00329893	6.18519362	2.62881876
Gns	4.00E-04	0.00329893	6.13955929	2.6181351
Ly96	4.00E-04	0.00329893	5.68202765	2.50640585
Nfe2l2	4.00E-04	0.00329893	5.56469248	2.47630196
Tlr1	4.00E-04	0.00329893	5.55170576	2.47293111
Gpx1	4.00E-04	0.00329893	5.42443079	2.43947176
Gad1	4.00E-04	0.00329893	5.35667396	2.42133749
Flt1	0.00667	0.02842161	5.32215743	2.41201119
Fnip2	0.00177	0.00917291	5.27569061	2.39935996
Itgb5	0.00177	0.00917291	5.21439083	2.38249872
Ccl2	4.00E-04	0.00329893	5.20738689	2.3805596
Idh1	4.00E-04	0.00329893	5.00727435	2.3240255
Hk2	**4.00E-04**	**0.00329893**	**4.75357782**	**2.24901378**
Tnf	4.00E-04	0.00329893	4.67262093	2.224232

Cd84	4.00E-04	0.00329893	4.44319037	2.15159596
Myd88	4.00E-04	0.00329893	4.38220373	2.13165656
Fpr1	0.000799	0.00578144	4.23913044	2.08376836
Nat8l	0.0048	0.0208	4.23809524	2.08341601
Bcl2a1a	4.00E-04	0.00329893	4.16562909	2.05853439
Atox1	4.00E-04	0.00329893	4.07607025	2.02717892
Slc2a6	0.0111	0.04366	3.77755102	1.91745124
Neu1	4.00E-04	0.00329893	3.62313647	1.85723915
Pgd	4.00E-04	0.00329893	3.53292383	1.82086265
G6pdx	4.00E-04	0.00329893	3.4684123	1.79427541
Ctsa	0.0112	0.04382857	3.38855422	1.76066986
Cd274	0.0028	0.01325679	3.30876516	1.7262929
Glul	0.00177	0.00917291	3.29221626	1.71905911
Pik3cb	4.00E-04	0.00329893	3.2841185	1.71550619
Runx1	4.00E-04	0.00329893	3.14554589	1.65331041
Taldo1	4.00E-04	0.00329893	3.11566139	1.63953845
Dck	4.00E-04	0.00329893	3.10015728	1.63234141
Fabp5	4.00E-04	0.00329893	2.95888112	1.56505173
Sod2	4.00E-04	0.00329893	2.6017282	1.37947025
Tkt	4.00E-04	0.00329893	2.5191583	1.33294178
Ptger4	0.0028	0.01325679	2.51227496	1.32899437
Itgb2	0.0016	0.00917291	2.4651763	1.30169083
Xdh	0.0028	0.01325679	2.39870354	1.26225487
Slc16a6	0.000799	0.00578144	2.2908377	1.19587525
Gba	4.00E-04	0.00329893	2.2361194	1.16099723
Gmpr2	0.00177	0.00917291	2.2277512	1.15558812
Map2k1	4.00E-04	0.00329893	2.19071064	1.13139894
Cpt1a	0.00177	0.00917291	2.14877025	1.10351123
Ern1	0.0048	0.0208	2.12310455	1.08617542
Tet2	0.012	0.04403828	2.1215311	1.08510583
Prkab2	0.00759	0.03080175	2.09280501	1.0654379
Nadk	0.000799	0.00578144	2.07692308	1.05444778
Idh2	0.012	0.04403828	2.04166667	1.02974734
Ap2s1	4.00E-04	0.00329893	2.01261354	1.00907017
Washc4	0.000799	0.00578144	2.00624522	1.00449796
Fnip1	0.0016	0.00917291	1.97125371	0.97911347
Usp8	4.00E-04	0.00329893	1.94417266	0.95915635
Cbl	0.012	0.04403828	1.88552393	0.91496546
Echs1	4.00E-04	0.00329893	1.84115983	0.88061487
Slc3a2	4.00E-04	0.00329893	1.81728708	0.86178634
Psmb10	0.000799	0.00578144	1.80107527	0.84885847
Glud1	4.00E-04	0.00329893	1.79778242	0.84621843
Pfkl	0.00385	0.01789667	1.78237733	0.83380279
Acap2	4.00E-04	0.00329893	1.76764084	0.82182517
Bad	0.00795	0.03192487	1.7540633	0.81070081

Akt1	4.00E-04	0.00329893	1.73020264	0.79094102
Stat6	0.0016	0.00917291	1.72644099	0.78780102
Itch	4.00E-04	0.00329893	1.69871754	0.76444599
Pkm	0.00759	0.03080175	1.65939064	0.73065355
Traf6	0.0048	0.0208	1.65227396	0.72445292
Oat	0.012	0.04403828	1.6452215	0.71828183
H2.M3	0.0016	0.00917291	1.63752956	0.71152095
Sem1	0.0028	0.01325679	1.58751395	0.66676927
Sdhc	4.00E-04	0.00329893	1.56380922	0.64506452
Pgk1	0.0048	0.0208	1.55731032	0.63905646
Nedd8	4.00E-04	0.00329893	1.53791369	0.62097454
Lamtor2	4.00E-04	0.00329893	1.53349515	0.6168236
Tbc1d10b	4.00E-04	0.00329893	1.53293155	0.61629328
Lamtor5	4.00E-04	0.00329893	1.51940701	0.60350838
Vhl	0.00557	0.02386698	1.50287632	0.58772629
Pik3c2a	0.00319	0.01501061	1.48117625	0.56674332
Pgm1	0.00263	0.01325679	1.47712904	0.56279587
Ranbp2	4.00E-04	0.00329893	1.46234056	0.54827933
Selenok	0.00759	0.03080175	1.41585407	0.50167258
Cdk9	4.00E-04	0.00329893	1.40418397	0.48973196
Asl	0.00385	0.01789667	1.4018297	0.48731109
Mpc2	0.0016	0.00917291	1.39694381	0.48227399
Ndufb8	0.0048	0.0208	1.37169972	0.4559647
Atp6v1f	4.00E-04	0.00329893	1.37134806	0.45559478
Snf8	0.0028	0.01325679	1.35447304	0.43773168
Uqcr11	4.00E-04	0.00329893	1.32981159	0.41122185
Cat	0.012	0.04403828	1.32757415	0.40879245
Sdhb	0.0048	0.0208	1.31759785	0.39791011
Cox6b1	0.00759	0.03080175	1.3118848	0.39164104
Uqcrq	0.012	0.04403828	1.3040249	0.38297142
Mtf1	0.0048	0.0208	1.24022109	0.31059733
Ndufb4	0.012	0.04403828	1.21950791	0.28629911
Ndufs7	0.00759	0.03080175	1.21930791	0.2860625

Given this myeloid specific expression pattern of HK3, we evaluated HK3 expression in diverse cell types across mouse and human tumor models. In examining scRNAseq data from metastasizing mouse models of lung cancer (LaFave *Cancer Cell* 2020), *Hk3* is also a myeloid specific enzyme in this genetically engineered mouse model while *Hk2* is expressed both in cancer cells and immune cells (**Figures 3.3A-C**) (LaFave

et al., 2020). In both primary and metastatic brain malignancies (N=63 human patients,226 total fractions, (Klemm et al., 2020)), *HK3* transcripts are only detectable in the resident CD11b+ microglia, and infiltrating CD11b+ macrophages and neutrophils (**Figures 3.2E-F**)**.** We then analyzed the TISCH database (Sun et al., 2021) which contains RNA transcript prolife across 2x10^6 cells from 79 scRNAseq cancer studies. Again, we see that *HK3* is an immune specific gene (**Figure 3.3D**), however it is important to note that it is only expressed in the CD11b+ neutrophils, dendritic cells, and macrophages (**Figure 3.2G**). *HK3* was not expressed in either the lymphoid cells or the malignant cells in any of these tumor types, in line with our observation from the MC38 model. This myeloid specific expression pattern is unique to *HK3*, whereas *HK1* appears expressed to a similar level across cancer cells, immune cells and stromal cells (**Figure 3.3E**), in line with its description as a catabolic housekeeping gene. Expression of *HK2* is more variable across all cell types (**Figure 3.3E**). These data support that *HK3* is uniquely a myeloid specific hexokinase in the TME, not solely a white blood cell specific gene.

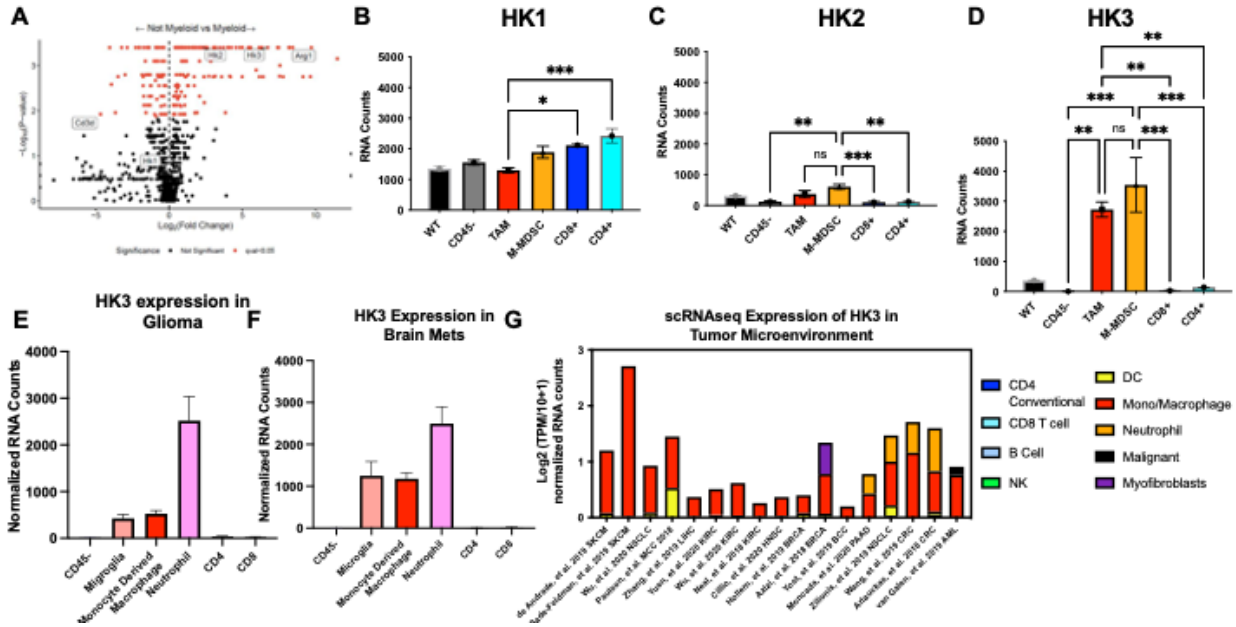

Figure 3.2: ***HK3* is a myeloid specific gene in the mouse and human tumor microenvironment**. (**A)** Volcano plot demonstrating myeloid specific genes from flow sorted CD11b+ populations in the MC38 tumor

microenvironment. Red dots represent genes that are significant with an FDR<.05 Normalized RNA expression of *Hk1* **(B)** *Hk2* **(C)** *Hk3* **(D**) across flow sorted fractions in the mouse tumor microenvironment. Experiement conducted in biological triplicate for each fraction. Normalized RNA expression of HK3 in human brain tumor microenvironment from surgically resected primary gliomas **(E)** or brain metastasis **(F).** Data from Klemm *Cell* 2020. For B through F, error bars indicate SEMs and middle point refers to mean. E/F have over 200 fractions taken from 50+ both New York City and Switzerland (**G**)**:** scRNA expression of HK3 across immune cells from 17 different scRNAseq experiments. Data take from TISCH online tool. Arg1: arginase 1, TAM: tumor associated macrophage, M-MDSC: monocyte myeloid derived suppressor cell, NK: natural killer, DC: dendritic cell, Mono:monocyte, sc: single cell. Figure 3.2G implements tumor naming scheme from TCGA (https://gdc.cancer.gov/resources-tcga-users/tcga-code-tables/tcga-study-abbreviations), Brown-Forythe One Way ANOVA with Welch test for multiple comparisons was conducted in panels B-D. * equals p<.05, ** equals p<.01=, ***equals p<.001.

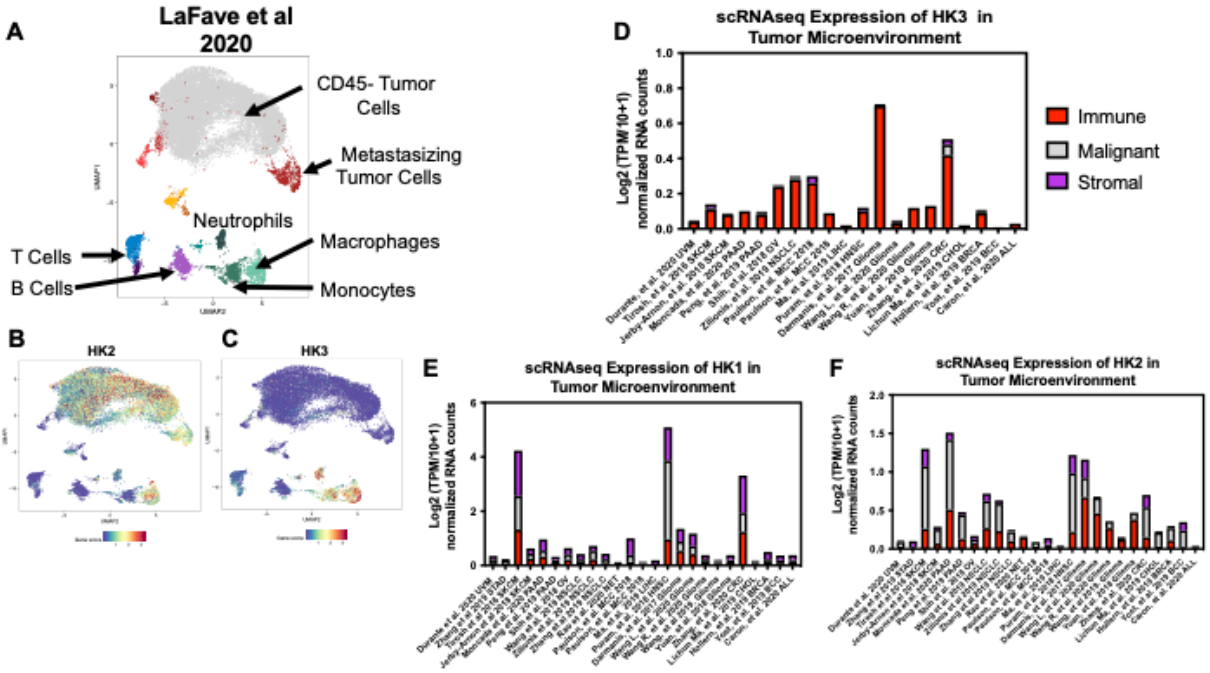

Figure 3.3*:* ***Hk3* differs in tumor cell subset expression from other low Km isoforms**. **(A)** UMAP from LeFeve *Cancer Cell* 2020 demonstrating cell cluster identity. Cell type specific expression of *Hk2* **(B**) and *Hk3* **(C**) from Lefeve *Cancer Cell* 2020. Broad cell type expression of HK3 (**D),** HK2 **(E)**, HK1 **(F)** from many human tumor types. Data taken from TISCH database for D-F. UMAP: Uniform Manifold Approximation and Projection for Dimension Reduction Figures 3.3D-F implements tumor naming scheme from TCGA (https://gdc.cancer.gov/resources-tcga-users/tcga-code-tables/tcga-study-abbreviations),

HK3/Hk3 is a myeloid specific metabolic gene in healthy individuals

Given the myeloid specific nature of *HK3* expression in the TME stands in contrast to previous observation of this gene as a pan white blood cell hexokinase, we evaluated whether this is the case in healthy individuals. Brain tissue from epileptic patients and healthy blood donors (Klemm *Cell* 2020), as well as PBMC control data collected by 10x

Genomics in TISCH also support the myeloid specific nature of this metabolic enzyme (**Figure**. **3.5A-C**). This strong concordance between the TME and healthy donors provides significant rationale to study HK3's expression across a wider swath of human biology.

By examining the GTEX dataset and normal from the TCGA (Tang et al., 2017), *HK3* is only detectable in lymphoid organs (lymph node, spleen, thymus) and the lung. (**Figures 3.4A and 3.5D**). Across the entire GTEX, *HK3* expression does correlate with the universal hematopoietic marker CD45 (*PTPRC*), (**Figure 3.4B**). This stands in contrast to *HK1* and *HK2*, which demonstrate minimal correlation with *PTPRC* across the entire GTEX (**Figure 3.5E**), supporting *HK3* as the white blood cell hexokinase. When conducting deeper correlation analysis in both lung tissue and across the entire dataset, it is clear that *HK3* expression correlates most strongly with myeloid genes like *ITGAM* (encoding CD11b) and not lymphoid genes *CD3*, *CD56* or *CD19* nor epithelial genes like *EPCAM* (**Figure 3.4C and 3.5F**). Interestingly, HK3 expression correlates better with *ITGAM* than *PTPRC*, further supporting that *HK3* is a myeloid specific gene in humans (Pearson R= 0.86, then CD45 = Pearson R = 0.76) (**Figures 3.4B and 3.4F**). Querying the human lung single nucleus RNAseq Atlas (Delorey et al., 2021), we observe the myeloid specific nature of this HK isoform, which stands in contrast to *HK2* (also detectable in the EPCAM+ epithelia) (**Figure 3.6A-E**). These data again are quite similar to our original observation in mouse tumor models (MC38 tumor model and (LaFave et al., 2020)).

We next sought to identify the time point at which *HK3* is transcribed during myeloid development. The data from Van Galen 2020 where transformed AML cells express less

HK3 than infiltrating myeloid cells suggests its associated with more mature myeloid cells (**Figure 3.2G**). By conducting scRNAseq and ATACseq on mouse methocult CD34+ cultures at D14, we find that *Hk3* chromatin openness is correlated with macrophage cell lineage and not precursor stem cell identity (**Figure 3.4D**). We also examined hexokinase isoform expression in publicly available human bone marrow scRNAseq (Hay et al., 2018). Additionally, we observe *HK3* expression is only detectable in monocytes, immature neutrophils, and neutrophils (versus the wide swath of precursor stages) in comparison to the widely expressed *HK1* and *HK2* this human bone marrow scRNA database. In fact, expression of *HK2* appears highest in the hypoxic stromal cells, in accordance with its known role as a HIF target (**Fig 3.5F**)(Parmar et al., 2007). These data suggest that *HK3* is solely engaged later in the myeloid development program.

Not surprisingly, in the UK Immune proteomics database, HK3 protein expression is only detectable in mouse myeloid cells, with greatest expression in M-CSF generated macrophages (Marchingo et al., 2020) (**Figure 3.4E**). To confirm this unique expression pattern, we performed qPCR on CD11b enriched bone marrow from healthy mice (**Figures. 3.4F and 3.6G**)**.** We observed a significant increase in *Hk3* RNA level in the CD11b+ bone marrow cells in comparison to the total marrow as well as the CD11b- cells (which are a heterogenous mixture of lymphoid and progenitor cell lineages (**Figure 3.4G**). Similar to our MC38 data and the human lung scRNAseq, *HK1* expression does not vary across bone marrow cell types (**Figure 3.5H**), and *HK2* expression is also elevated in these myeloid cells (**Figure 3.5I**)**.**

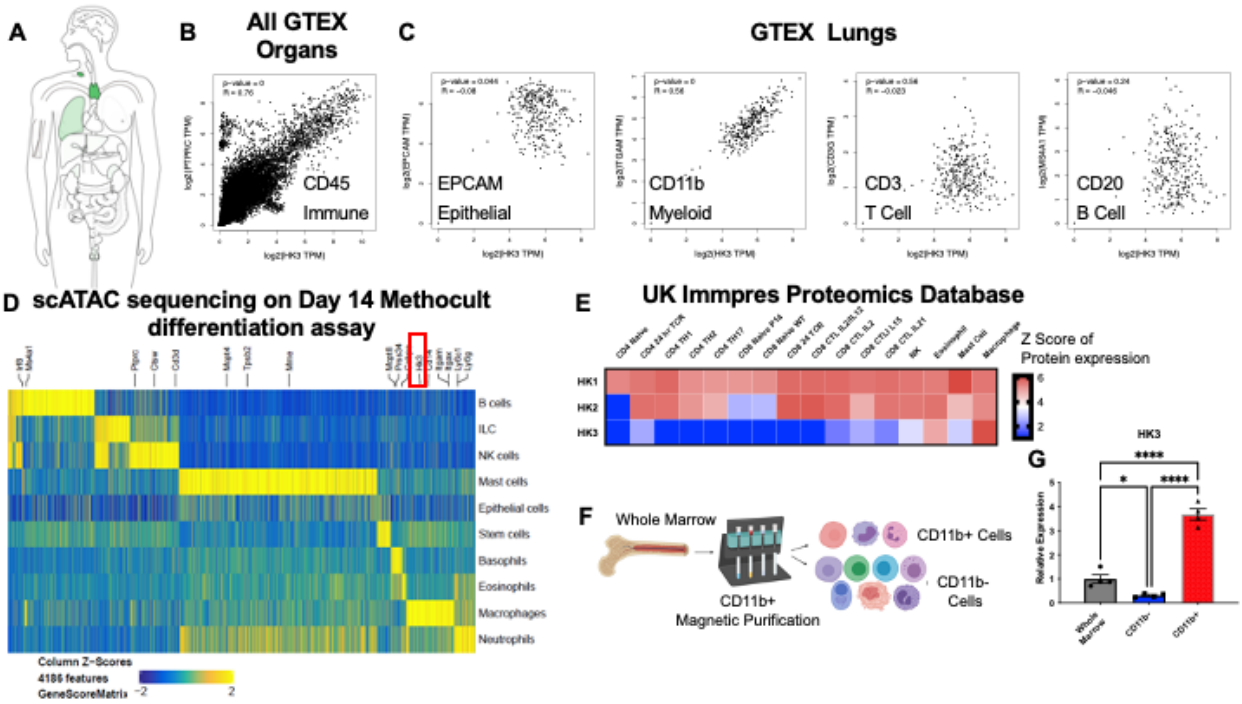

Figure 3.4: **In healthy individuals, HK3 is also a myeloid specific gene.** (**A**) Pictural representation of restricted HK3 expression. (**B**) HK3 and CD45 (*PTPRC*) correlation across all GTEX samples. (**C**) HK3 correlation with epithelial (*EpCAM*) myeloid (*ITGAM*) T cell (*CD3e*) or B cell (*MS4A1*) identity markers in the GTEX lung data set. (**D**) Heatmap from scATACseq on mouse Methocult cultures at day 14 demonstrate immune cell specific chromatin opening. (**E**) Heatmap developed from ImmPress proteomics database. Mass spectrometry was performed on mouse cultured immune cells and z scores were generated based on mass spectrometry peaks. (**F**) Experimental design for (generated in biorender) (**G**) qPCR for HK3 on CD11b+ enriched bone marrows. Pearson correlation used for b-c. P=0 indicatives $p<1*10^{-99}$ GTEX: the genotype tissue expression Panel G the midpoint on the bar graph references the mean and the error bars represent SEM. This experiment was done in biological quadruplicate. One Way ANOVA performed in panel G. * equals P<.05, **** equals p<.0001.

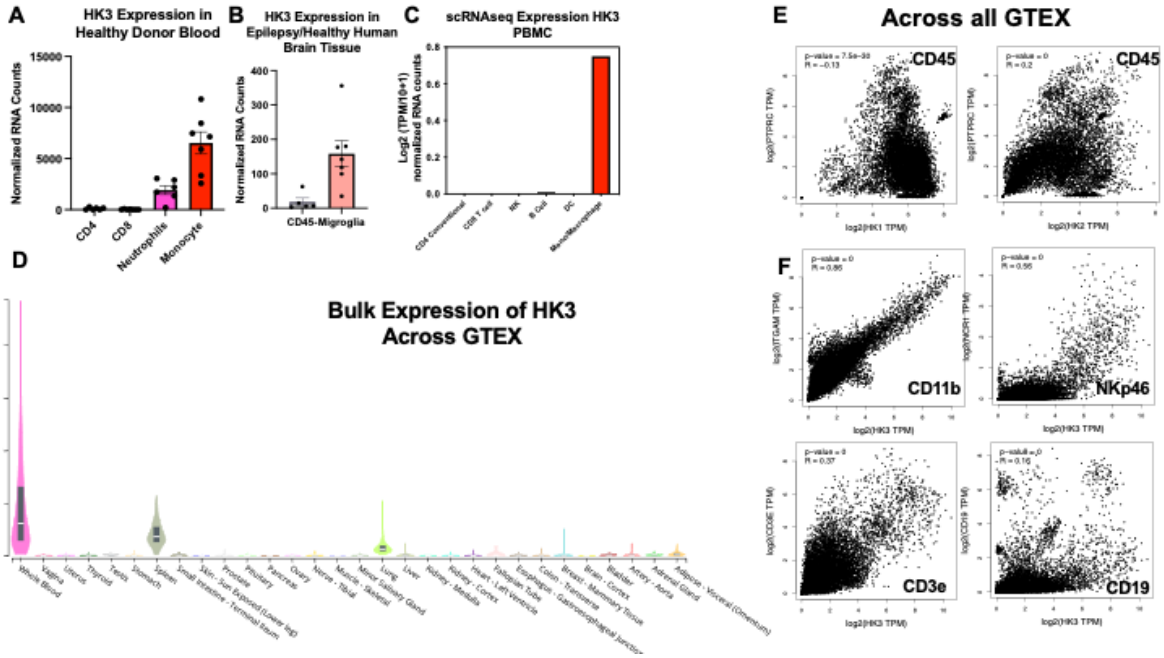

Figure 3.5: ***HK3* myeloid specific expressions occurs at homeostasis**. Bulk RNA seq *HK3* expression levels from FACS sorted cells from healthy donors blood (**A**) and epileptic brains (**B**) from Klemm *Cell* 2020. Panels A-B the mid point represents mean while the error bars represent SEM. For A n=7 patient PBMC and for B n=6 epileptic brain samples that were flow sorted. Each dot represents a biological replicate (**C**) *HK3* expression from 10x scRNAseq conducted on human PBMCs. Data taken from TISCH. (**D**) HK3 expression in GTEX database. (**E**) *HK1* and *HK2* correlation with CD45 (*PTPRC*) across entire GTEX dataset. (**F)** *HK3* correlation with myeloid (*ITGAM*,CD11b), NK Cell (*NCR1*, NKp46), T cell (*CD3e*) or B cell (*MS4A1*/CD20) identity markers in the entire GTEX data set. Pearson correlation used for b-c. P=0 indicative of $p<1*10^{-99}$.

Next, we examined what factors could be driving this cell subtype specific expression. In line with our mouse methocult data, scATAC sequencing data demonstrate that in human PBMCs, the *HK3* promoter is only open in CD11b+ myeloid cells (CD14+ classical monocytes, CD16+ non classical monocytes, cDC1/2s) in comparison to the broad subsets of lymphoid cells present in these cultures (Kartha et al., 2021) (**Figure 3.7**). Mouse enhancer network analysis further supports the four enhancers of *Hk3* are only active in HSCs and myeloid cells (**Figure 3.8C**), while *Hk2* **(Figure 3.8A**) and *Hk1* (**Figure 3.8B**) have one enhancer element which is active in almost all mature/immature lymphoid, myeloid, and bone marrow stromal cells. (Immungen Enhancer Network, (Yoshida et al., 2019))

These data suggest openness of the chromatin in both human and mouse myeloid cells, however, do not pin down regulatory factors that contribute to this relationship. The CHIPATLAS(Oki et al., 2018) contains approximately 15,000 chromatin immunoprecipitation experiments that can be unbiasedly quired to understand transcription factors (TFs) that bind promoters. From this data set, we observe that myeloid and inflammatory transcription factors can be found uniquely at the *HK3/Hk3* promoter in humans and mice. Of the 15000 human CHIP experiments in the human dataset, only 84 significant transcription factor specific binding events occur at the *HK3* promoter (significance=p value less $< 1.0 \times 10^{-5}$). Of those 84 significant studies, 77 occur

in blood cells supporting the original observation of *HK3* as a white blood cell specific enzyme. The recurrent blood binding transcription factors most strongly indicate basis for myeloid specific expression. In this dataset, the overwhelming recurrent binding factor is the myeloid determining transcription factor *SPI1* (encoding PU.1) (51/77 events). A similar pattern exists in mouse data where *Spi1* protein is found most frequently at the *Hk3* promoter, representing 116/261 significant blood transcription factor binding events (out of a total of 290 events across all tissue types). This is line with two publications in acute leukemias where PU.1 is described to bind the *HK3* promoter (Federzoni et al., 2014; Federzoni et al., 2012). Additionally, inflammatory transcriptions factors that bind *HK3* more often than *HK1* and *HK2* are Signal Traducer and Activator of Transcription 1 (STAT1) and many of the interferon regulatory factor (IRF) IRF proteins. For *HK1/Hk1* and *HK2/Hk2*, there are many more nonblood cell promoter binding interactions as well as interactions with more widespread transcriptions factors like CTCF, MYC, RAD21 **(Table 3.2)**. It is worth noting PU.1 can be found at the *HK2/Hk2* promoter in both mouse and humans. This is in line with much of the above data and our previous result where the expression of *HK2*, as well as many other cell types throughout eukaryotic organisms. That does not appear to be the case with *HK3* where its expression is restricted to myeloid cells. In concert, these findings support the cell programmed nature of *HK3* utilization in eukaryotic organismal homeostasis as a myeloid specific hexokinase.

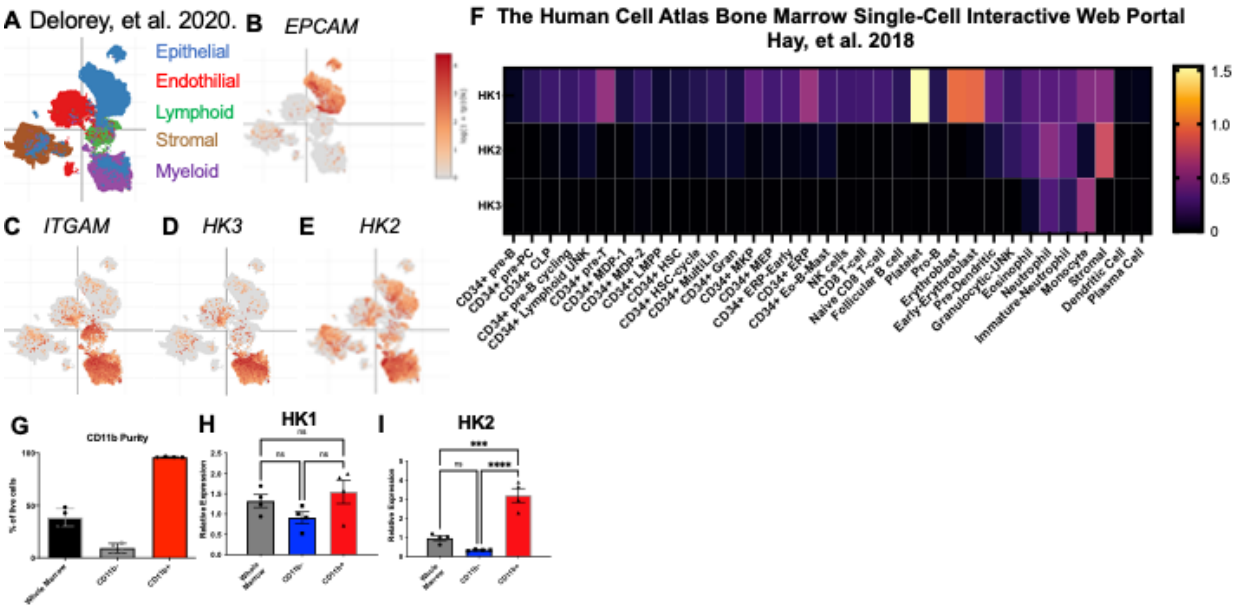

Figure 3.6: **In human lungs and bone marrow, *HK3* is expressed in mature myeloid cells in contrast to the other low K_m isoforms:** (**A**) UMAP of cell identities from Delray 2020 scNucSEQ of cadaver lungs. *EPCAM* (**B**), *ITGAM* (CD11b) (**C**) *HK3* (**D**) and *HK2* (**E**) expression across cell populations from Delorey et al. 2020 *Biorxiv*. **F:** Heatmap of low K_m HK isoforms from Hay et al. *Exp Hematology* 2018 which conducted scRNAseq on 8 healthy human BM donors. **F:** Enrichment of CD11b+ cells from qPCR experiments in figures 3.5/3.6**.** *HK1* **(G)** and *HK2* **(H)** expression in myeloid vs non myeloid bone marrow fractions. For panels G-I midpoint on the bar graph references the mean and the error bars represent SEM. This experiment was done in biological quadruplicate. Labels generated for F originate from Hay et al. 2018. One Way ANOVA performed in panel H/I, *** equals p=.0001, ****=, p<.0001

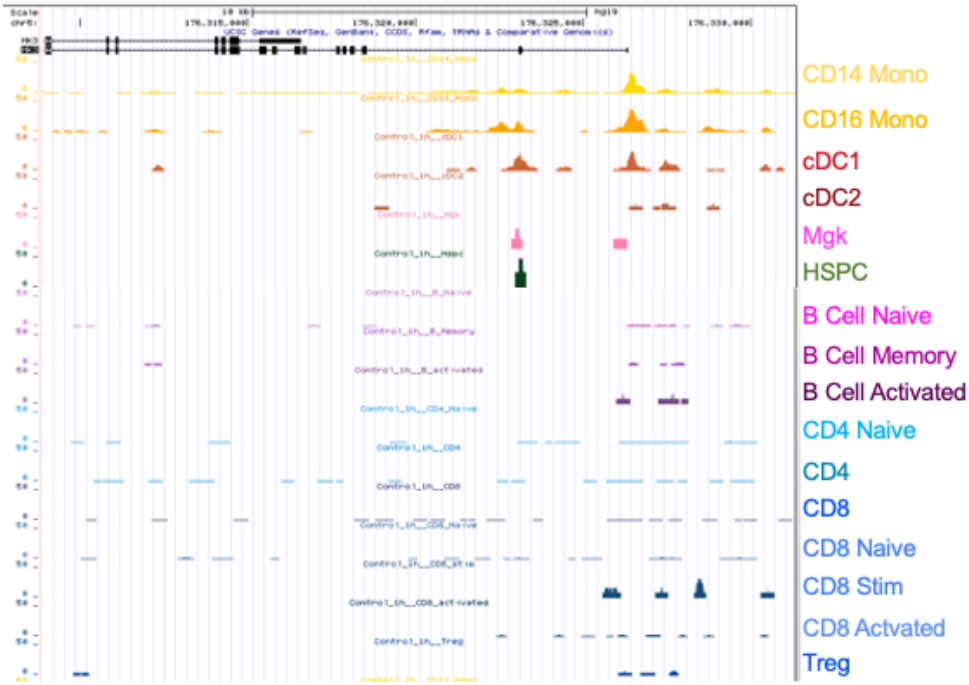

Figure 3.7: **Chromatin Openness at human HK3 promoter across immune cell types**. Tracks are from Katha et al. *biorvix.org* 2021 and are deposited at UCSC. cDC: conventional dendritic cell. Mgk: megakaryocyte. HSPC: hematopoietic stem progenitor cell, Treg: CD4+ T regulatory cell.

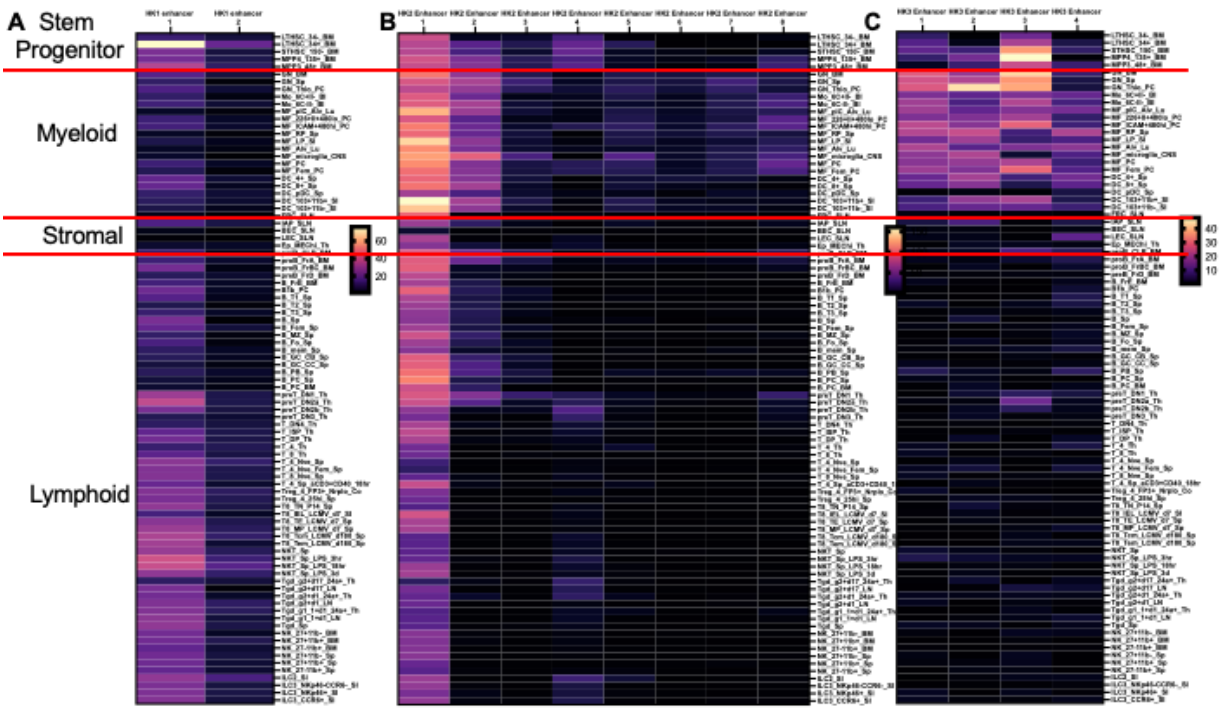

Figure 3.8: **Chromatin state of transcriptional elements from Low K_m HKs supports the myeloid specific nature of HK3.** Heatmap of enhancer elements from mouse (**A**) *Hk1* (**B**) *Hk2* (**C**) *Hk3* from Yoshida *Cell* 2019. Labels for each cell type generated by Yoshida *Cell* 2019. Red lines divide population into different lineages

Table 3.2- **CHIPATLAS summary data for TF binding interactions across human and mouse HK1/HK2/HK3**

Human	Significant Binding Studies	Significant Studies in Blood cells	Most Recurrent Event
HK1	866	141 (16%)	GATA1 (26x)
HK2	809	331(40%)	CTCF (166x)
HK3	87	76 (87%)	SPI1 (51x)
Mouse			
Hk1	124	76 (61%)	Rad21 (35x)
Hk2	676	305 (45%)	Ctcf (60x)
Hk3	290	261(90%)	Spi1(116x)

***HK3/Hk3* is an inflammation associated myeloid specific metabolic gene.**

In addition to our tumor studies, which demonstrate that myeloid cells consume the most glucose in the tumor microenvironment, another group has found that the brain resident phagocytic myeloid cells (CD11b+ microglia) in Alzheimer's Disease consume the most glucose (Xiang et al., 2021). These microglia also are the major expressor of *HK2/HK3* in the non-inflamed human epileptic brain (**Figures 3.3A-B**). Single-Nuc-sequencing from human spinal cords confirms that there is enhanced glucose fixing capacity of these supporting cells (**Figures 3.9A-C**) (Yadav et al., 2022) . With this evidence, we next evaluated glucose uptake in a model of asthma to see if this enhanced glucose consuming phenotype of myeloid occurs in additional tissues and inflammatory diseases. Using an *Alternaria* model, we find that CD11b+ myeloid cells consume the most per cell glucose in the inflamed asthmatic lung (**Figure 3.10A**). This finding in concert with recently published literatures supports the notion that in many inflammatory conditions, myeloid cells have an enhanced glucose uptake phenotype. (Reinfeld et al., 2021; Xiang et al., 2021)

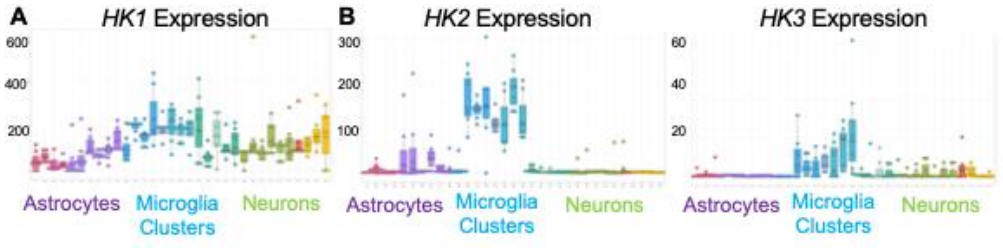

Figure 3.9: Human microglia express similar patterns of low K_m HKs to tumor associated myeloid cells: Expression of (**A**) *HK1* (**B**) *HK2* (**C)** *HK3* HK2 and HK3 in human spinal chord via single-nucRNAseq.. Light blue/teal groups are microglia. Groups on the left (red/purple) are supporting astrocytes, and groups on the right (green/yellow) different subpopulations of neurons

To address the role of *HK3* in glucose consuming inflammatory microenvironments, we evaluated *HK3/Hk3* levels across inflammatory diseases in

humans and mice. To our surprise, increased *Hk3* expression is not ubiquitously observed with inflammation. It is significantly increased in the hearts of mice who experienced heart attacks both during the repair phase (d7) and during fibrosis (d28) (**Figure 3.10B**). However, there is no significant no changes in *HK3* expression in a genetic model of immune checkpoint related myocarditis (**Figure 3.10C**), which is known to have significant myeloid infiltrate, (Balko, 2022; Wei et al., 2021). This suggests that specific inflammatory stimuli may regulate HK3's expression and utilization. In evaluating a meta-analysis of over 10,000 inflammatory bowel disease patients (Massimino et al., 2021), *HK3* is significantly elevated in the affected bowel tissue when compared to healthy control (in rectums colons and ileums from ulcerative colitis (UC) and Crohn's Disease (CD) patients **Figure 3.10D**). Additionally, *HK3* expression is elevated in monocytes from patients with CD when compared to monocytes from healthy controls demonstrating that this inflammatory factor driving *HK3* expression may be systemic and not localized to the tissue (nearly significant FDR is 1e-10, and p= 2*10-8). Therefore, we evaluated *HK3* expression in whole blood in a variety of inflammatory conditions in a previously published Vanderbilt cohort (Aune et al., 2017). What becomes apparent is that *HK3* is the dominate hexokinase expressed in human blood in healthy individuals and increases in inflammatory conditions like UC, CD, and Sjogren's syndrome (**Figure 3.10E**). This is in contrast to less inflammatory syndromes such as irritable bowel syndrome and fibromyalgia, where *HK3* expression is unaltered. Additionally, HK3 levels additionally with therapy in patients with multiple sclerosis. HK3's increase in this subgroup of immunopathologies stands in stark contrast to HK1 and HK2 as well as other canonical glycolytic genes associated with immune activation (*e.g., SLC2a1* and *GLUT1*).

Similarly, in COVID patients (julian.knight@well.ox.ac.uk & Consortium, 2022), it is apparent that *HK3* expression in the blood increases with COVID severity while *GLUT1* expression remains relatively stable (**Figure 3.10F**). *HK3* expression is the lowest in non-hospitalized COVID patients (community COVID) and highest in intubated critical COVID patients, again suggesting that a systemic factor can regulate *HK3* expression (**Figure 3.10G)**.

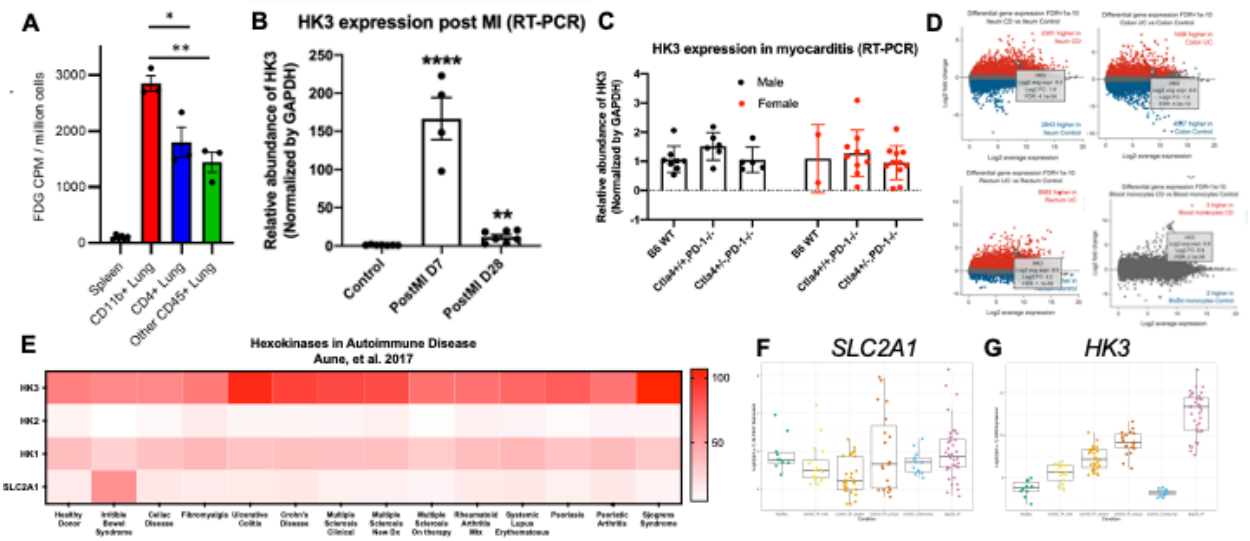

Figure 3.10: **Inflammatory myeloid cells increase *HK3 expression* both in disease sites and the blood**. (**A**) FDG uptake assay in mouse model of Asthma. N=3 biological replicates (**B**) qPCR conducted on mouse hearts after experimental induced myocardial ischemic injury. (**C**) qPCR conducted on 6-12 week old mice with genetic predisposition for myocarditis. (**D**) Volcano plots of HK3 expression in Ulcerative Colitis and Crohn's Disease across bowel tissue and blood monocytes. (**E**) Heatmap of blood-based RNA expression of glycolytic enzymes across inflammatory setting from Aune et al. *Autoimmnunity* 2017. Expression of *SLC2A1* (**F**) and *HK3* (**G**) in whole patient blood across COVID disease severity. FDR: false discovery rate, SLC2A1: Glut1 transcript name, IP: inpatient .P-values indicate result of Welch's 2-tailed t-test * equal p<0.05, ** equal p<0.01. for panel A. In panel B One Way ANOVA was performed with multiple comparison testing ** equals p=.0031,**** equals p<.0001. Error bars in A-C represent SEM, and midpoint represents mean. Box plots in F and G represent 25-75 quartile range. Midpoint is the median. Each point in this figure is a biological replicate.

HK3/Hk3 expression is regulated by IFNγ

Given the relationship between HK3 and inflammation, we stimulated myc immortalized mouse bone marrow derived macrophages (iBMDMs) with an array of cytokines. We observe that *Hk3* expression is induced by IFNγ stimulation (**Figure 3.11A**)

at 18 hours. This is consistent with the fact that STAT1 has been found to bind the *HK3/Hk3* promoter in mice and humans **(Table 3.2)**. *HK3* expression levels are unchanged with other inflammatory cytokines like IL-1ß, IL-4 and IL-6. We. Additionally, no significant changes in the other hexokinases were seen with these stimuli (**Figures 3.11B-C**). qPCR was validated by western blot at 24 hours (**Fig. 3.11D**)**,** where there is a large HK3 induction with IFNγ stimulation. Given that other cell types do not express *Hk3*, we wondered if IFNγ was sufficient to induce *HK3* expression in cancer cells. Strikingly, IFNγ driven HK3 expression only occurs in the CD11b+ iBMDMs. Colorectal, lung or melanoma cell lines do not express this hexokinase isoform with 24 hours of IFNγ treatment (**Figure 3.11E**). However, this is not due to loss of response to IFNγ in the cancer cells, however as these 3 mouse cancer cell lines upregulate PD-L1 after 24 hours of IFNγ stimulation (**Figure 3.1F**). This is in alignment with the CHIP-ATLAS data, because mouse STAT1 *HK3* promoter binding interaction was only observed in CD11b+ myeloid cells and not cells from solid organs (**Table 3.3**).

IFNγ is known to play a role in the metabolically active M1 macrophage. M1 macrophages are canonically stimulated with LPS and IFNγ to induce this phagocytic, anti-tumor gene transcriptional program. This classical stimulation results in a hyper metabolic cell that upregulates all three isoforms (**Figure 3.11 G-I**). From the cytokines tested, IFNγ alone induces *HK3* expression in contrast to HK1 and 2. Additionally, from examining human scATAC/RNA sequencing data from Kartha et al. 2021 (Kartha et al., 2021) IFNγ alone opens the chromatin in myeloid cells specifically at the HK3 promoter and thus drives HK3 expression. Chromatin opening and transcriptional engagement does not happen in the presence of other inflammatory stimuli like lipopolysaccharide or

Phorbol myristate acetate or in B or T cells with the same sample (**Figure 3.11J-L and Figure 3.12E**). Additionally, the expression of *HK3* is decreased in the presence of the JAK1/2 inhibitor Ruxolitinib (100 or 250 nM) at both the RNA and protein level (**Figures 3.11M-N**), confirming the regulation of *HK3* by IFNγ.

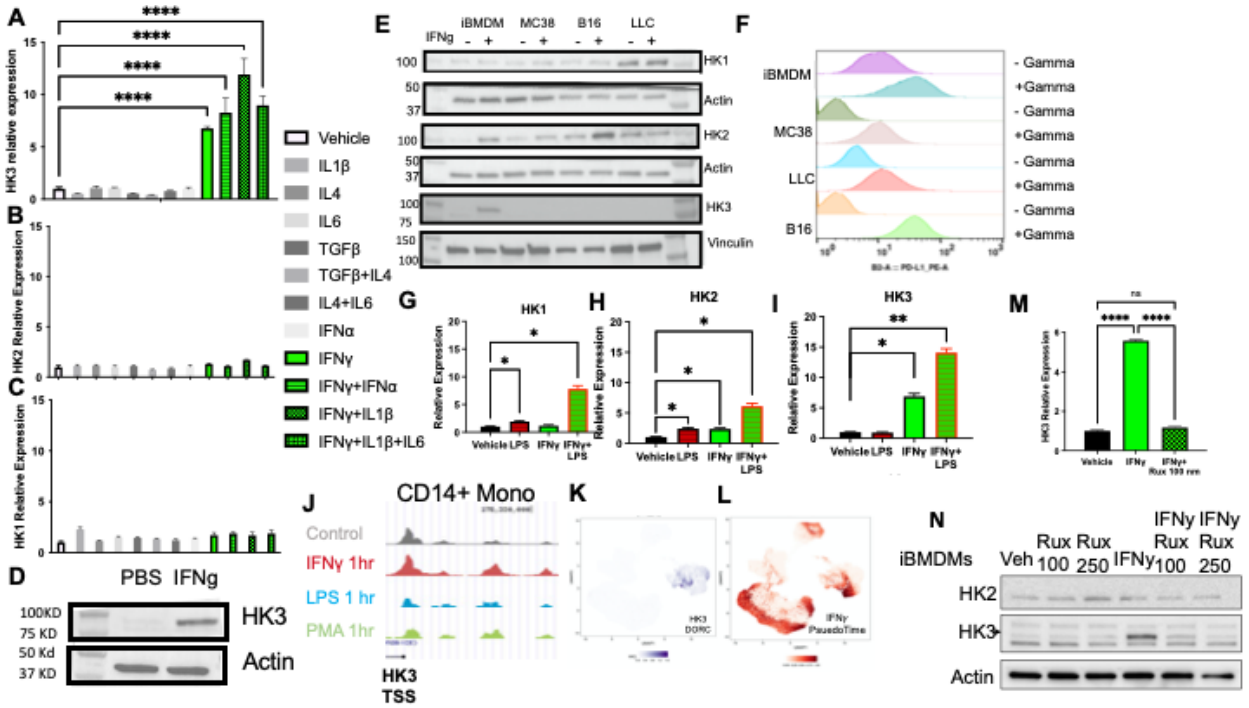

Figure 3.11: ***HK3/Hk3* as a bona-fide myeloid specific interferon gene in mouse and human cells.** qPCR for *Hk3* (**A**), *Hk2*(**B**), *Hk1*(**C**) with host of inflammatory stimuli at 18 hours post stim in iBMDMs. (**D**) Western blot of iBMDM lysates given IFNγ for 24hrs. (**E**) IFNγ effect on HK1, HK2, and HK3 protein across mouse cancer cell lines and iBMDMs. (**F**) PD-L1 protein expression examined by flow cytometry in mouse cancer cell lines and iBMDMs with 24 hours IFNγ. qPCR for *Hk1* **(G),** *Hk2* **(H)**, and **Hk3 (I)** with canonical M1 stimuli. (**J**) scATAC tracks from Kartha et al. 2021 from CD14+ monocytes stimulated with IFNγ, LPS or PMA. (**K**) Plotting of *HK3* chromatin opening on UMAP from Kartha et al. 2021: (**L**) IFNγ psuedotime from Kartha et al. 2021. Ruxolitinib effect on *HK3* expression at (**M**) RNA and (**N**) protein level at 100/250 nm doses. IL: interleukin TGF: transforming growth factor, IFN: Interferon LPS: lipopolysaccharide, PMA:Phorbol myristate acetate, DORC= domain of regulatory chromatin, Rux:ruxolitinib. In panel One Way ANOVA was conducted. All cytokine stims were compared to the vehicle **** equals p<.0001. In all bar graphs, error bars represent SEM, and midpoint represents mean. To generate the SEMs, experiments were conducted in technical triplicates. These panels have been repeated at least than and demonstrate identical trends. Western blots all have been replicated at least once and follow the same trends as qPCR data

Table 3.3-. **Significant STAT1-HK3 promoter interactions in human and mouse collected from CHIPAtlas Database**

Human	**Study ID**	**Antigen**	**Cell class**	**Cell**	**Fold Enrichment**
	SRX212648	STAT1	Blood	CD14+ Mono	2.61
	SRX212650	STAT1	Blood	CD14+ Mono	1.99

	SRX197292	Stat1	Blood	Macrophages	156.9
Mouse	SRX498829	Stat1	Blood	Macrophages	19.44
	SRX2417352	Stat1	Blood	Macrophages	17.57
	SRX109335	Stat1	Blood	Macrophages	16.69
	SRX109333	Stat1	Blood	Macrophages	15.91
	SRX109331	Stat1	Blood	Macrophages	15.27
	SRX109337	Stat1	Blood	Macrophages	14.31
	SRX109339	Stat1	Blood	Macrophages	12.62
	SRX5255298	Stat1	Blood	Macrophages	10.55
	SRX5255296	Stat1	Blood	Macrophages	9.53

Even though many of these mechanistic *in vitro* studies were performed in immortalized myeloid cells, we performed analogous studies in primary bone marrow macrophages and indeed found that *HK3* is uniquely elevated by IFNγ alone at the RNA and protein level (**Figure 3.12A-D**)**.** Additionally, examining previously reposited microarrary datasets (Immgen Gene Skyline). we find that *HK3* expression increases with IFNγ in myeloid cells where as IFNα has an intermediate to minimal effect on HK3 (**Figure 3.12F**). Expression of *HK1* and *HK2* are quite different in that IFNα can induce their expression and detection of these changes occurs in lymphoid cells (e.g., B cells for *HK2*) (**Figures 3.12G/H**). As mentioned previously, M1 macrophages are thought to be generated by IFNγ signalling. In the TISCH database, there are 7 studies that identify M1 and M2 populations in their human tumor scRNAseq dataset. In six of these seven datasets, the M1 macrophages have more *HK3* transcripts than the other myeloid cells found in the tumor microenvironment, supporting *HK3* as an IFNγ driven gene in human malignancy (**Figure 3.12I**).

In concert, these data suggest that IFNγ plays a strong role in inducing *HK3* expression in myeloid cells. This is in stark contrast to many of the other papers examining the impact of *HK3* in bulk tissues(Tuo et al., 2020; Xu et al., 2021). Groups have identified

HK3 expression as part of many poor prognostic signatures and thus attribute its role in tumor biology to increase in cancer cell. The data collected in this work argue instead that elevated *HK3* in bulk tissue is a marker of myeloid cell infiltration as well as interferon activation, which can in turn promote tumorigenesis, and metastasis.

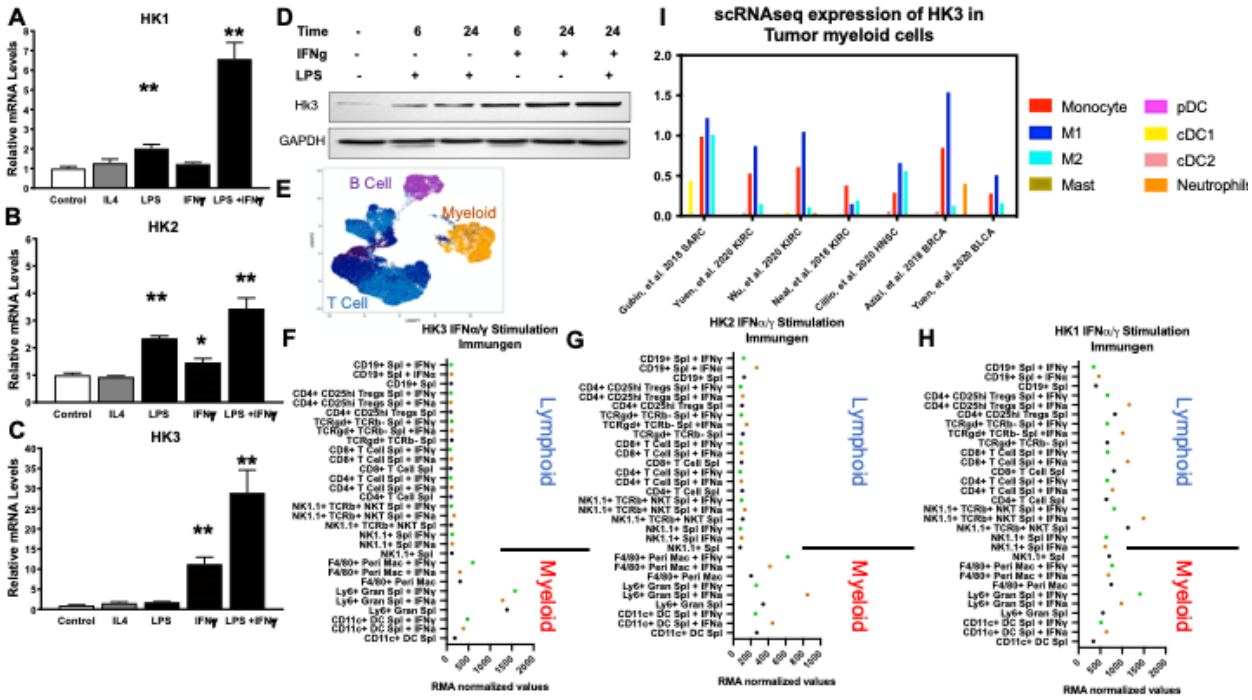

Figure 3.12*:* **Validation of *HK3* as a myeloid specific IFNγ regulated enzyme** qPCR conducted on mouse bone marrow derived macrophages, examining *Hk1* (**A**) *Hk2* **(B**) *Hk3* (**c**) expression. (**D**) Canonical M1 stimuli effect on human Hk3 protein levels. (**E**): UMAP from Kartha et al. 2021 *biorxiv.org* demonstrating cell identities. IFNg/a impact on *HK3* (**F**), *HK2* (**G**), *HK1* (**H**) expression elevated by RNA microarray. (**I**) 7 studies from the Tisch database where *HK3* expression can be compared across diverse myeloid subsets. F-H use labels generated by Immune Gene Skyline analysis. I implements tumor naming scheme from TCGA (https://gdc.cancer.gov/resources-tcga-users/tcga-code-tables/tcga-study-abbreviations), One Way ANOVA performed in panels A-C. * p<.05, ** p<.01 A-C plot the SEMs and mean. These experiments were done by a collaborator, the error bars are generated from biological replicates

Regulation of *HK3* supports it role as a biomarker in the inflammatory ccRCC

Our group has previously shown that ccRCC has the greatest amount of CD8 infiltrate of any solid tumor (Siska et al., 2017). Surprisingly, even though ccRCC patients have a low tumor mutational burden and this tumor type is not associated with chronic carcinogen exposure (in contrast to other immunotherapy responsive tumor types like bladder lung and melanoma), CD45 (*PTPRC*) as well as the pan macrophage marker

CD68 are expressed to the greatest degree of all solid tumors **(Figures. 3.13 A-B**) (GEPIA TCGA data). Using our 180 patient ccRCC tissue microarray, we validated this finding via CD68 immunofluorescence where we see macrophages are abundant in human ccRCC tissues (**Figure 3.13C**). Interestingly, CD68 protein level in this Vanderbilt cohort correlates with advanced tumor stage (**Figure 3.13D**).

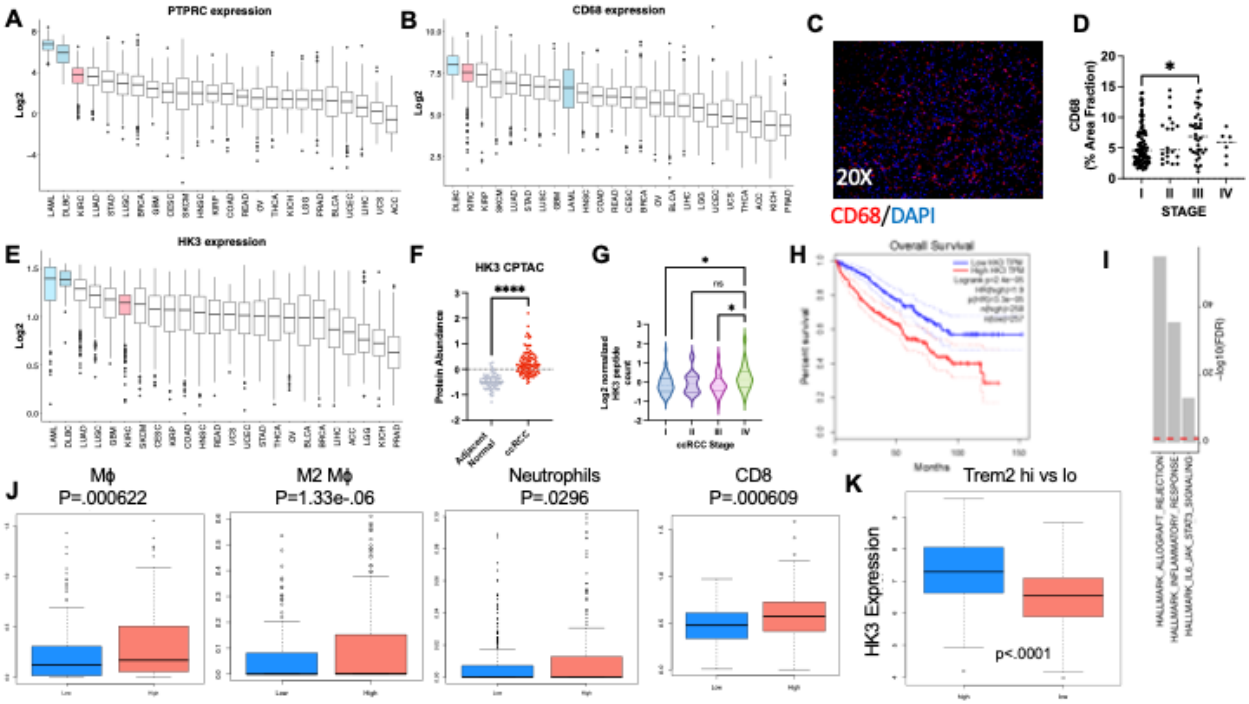

quartiles according to a confidence interval. KIRC box-and-whisker plot is indicated in light red, while LAML and DLBC box-and-whisker plots are shown in light blue (hematopoietic tumor types).(**C**) Representative Immunofluorescence for CD68 in ccRCC patient sample. (**D)** Correlation between CD68 protein level and outcomes in Vanderbilt 157 patient tissue microarray. (**E**): Expression level of HK3 across 24 TCGA cancer types (N=9264). Tumor types were sorted (descending) in function of the median expression. Box-and-whisker plot shows the sample median and lower and upper quartiles according to a confidence interval. KIRC box-and-whisker plot is indicated in light red, while LAML and DLBC box-and-whisker plots are shown in light blue (hematopoeitic tumor type).CPTAC ccRCC HK3 protein expression as determined by mass spectrometry compared to adjacent normal kidney tissue (**F**) as well as across different stages of ccRCC (**G**). (**H)** Kaplan Meier curve evaluating *HK3* expression level impact on patient overall survival**. (I)** Term Geneset Enrichment Analysis (GSEA) was performed using genes significantly expressed (FDR<0.05) between tumors expressing high and low levels HK3 (mean cutoff). All pathways had FDR<0.05 and significance represented as -log10(FDR). (**J-K**) ccRCC tumors were categorized according to high and low HK3 (N=9264). J) Box-and-whisker plots show CiberSortX profiles for M0 macrophages, M2 Macrophages, Neutrophils and CD8+ T cells for HK3 high (red) and low (blue) expressing ccRCCs TCGA samples. K) Box-and-whisker plot shows HK3 expression levels for TREM2 high (red) and low (blue) expressing ccRCCs (n=157 patients). Significance was assessed by two-sample Wilcoxon (Mann-Whitney)

test.Clinical Proteomic Technology Assessment for Cancer, ccRCC: clear cell renal cell carcinoma, TPM: transcript per million, Mϕ=macrophage, For A/B/E, tumor naming scheme from TCGA (https://gdc.cancer.gov/resources-tcga-users/tcga-code-tables/tcga-study-abbreviations), In panel A and G, One Way Anova performed. * equals p<.05. In panel F,J,K Mann Whitney test performed, **** equals p<.0001. P values listed for CiberSortX and TREM2 comparisons.

Given our data that suggests myeloid cells play a role in ccRCC progression, we wanted to evaluate the role of in this highly inflammatory malignancy. Median *HK3* RNA expression is higher than almost all solid tumors (**Figure 3.13E**). As shown in earlier figures, hematopoietic cells, the lung parenchymal macrophages as well as the CD11b+ microglia express *HK3* at baseline. Therefore, it is not surprising that tumors from those organs (including lymphomas and leukemias) have elevated *HK3* expression in comparison to ccRCC. In alignment with the RNA data from the TCGA, HK3 protein abundance is significantly elevated in ccRCC tumors when compared to adjacent normal kidney (**Figure 3.13F)** (Clark et al., 2019). Not surprisingly, given the glycolytic nature of ccRCC(Courtney, Bezwada, et al., 2018; Linehan et al., 2019), HK1 and HK2 are also significantly elevated at the protein level in ccRCC tumors (**Figures 3.14A-B**). HK3 levels are the highest in the metastatic stage IV tumors and demonstrate significant elevation in comparison to the localized stage I and stage III disease (**Figure 3.13G**). HK2 is not different among tumor stages while HK1 levels are similar between non metastatic stage III and metastatic stage IV tumors (Figures **3.14C-D**). These data suggest that HK3 and the cells which express it may promote ccRCC progression and metastasis.

Recently it has been reported that elevated *HK3* expression in the TCGA is associated with poor outcome in ccRCC (Xu et al., 2021). (**Figure 3.13H**). They documented that *HK3* expression level increases with known factors of aggressiveness (grade and stage) in both the TCGA and a new Chinese ccRCC cohort. What was overlooked in that publication is that this poor prognostic role is unique to *HK3* (**Figures**

3.14E-F) and not present in the other two low K_m isoforms. Additionally, there RNA analysis was not validated with CPTAC protein database expression from the same tumor. It is worth noting *HK3* expression is not prognostic in almost every other tumor type (including the two other common RCC histotypes, papillary and chromophobe (**Figures 3.14G-H**). Elevated *HK3* expression predicts worse overall survival in in only three tumor types: Prostate Adenocarcinoma, Uveal Melanoma and ccRCC. On the other hand, *HK3* expression is correlated with improved overall survival in cutaneous melanoma. This unique pattern of prognostic ability demonstrates a potential context specific role for this gene, in line with the *in vitro* observation that only one cytokine that we tested, IFNγ, can greatly dictate *HK3* expression.

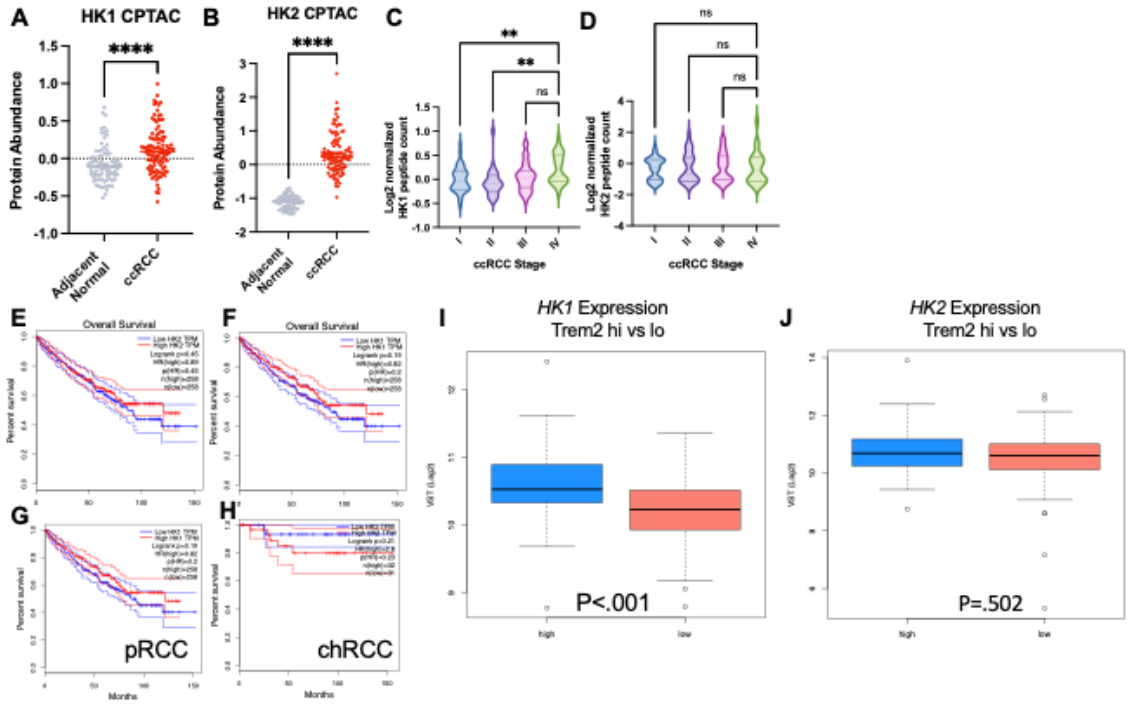

Figure 3.14*:* **HK3's poor prognostic features are unique when compared to other low K_m Hexokinases.** HK1 (**A**) HK2 (**B**) protein expression level between normal and tumor tissue. HK1 **(C)** and HK2 **(D)** protein expression as a function of ccRCC tumor stage. Kaplan Meier curves evaluating prognostic role of *HK1* (**E**), and *HK2* (**F**) in ccRCC. Kaplan Meier curve examining prognostic role of *HK3* in papillary RCC (**G)** and chromophobe RCC (**H).** *HK1* (**I**) and HK2 (**J**) levels in $Trem2^{hi}$ (blue) vs $TREM2^{lo}$ (red) patients. In panels A-B, I-J Mann Whitney test performed, **** p<.0001. In C-D, One Way ANOVA performed. P<.01=**

Recently, a model where *HK3* is expressed in the tumor cells and drives hyper inflammatory immune infiltrate has been proposed. To evaluate this possibility, we conducted hallmark pathway analysis comparing the *HK1*$^{Hi/Lo}$, *HK2*$^{Hi/Lo}$, *HK3*$^{Hi/Lo}$ to each other. We find that *HK3* elevated tumors are associated only significantly 3 gene sets: Allograft rejection, immune activation, and IL6-Stat3 signaling (**Figure 3.14I**). This stands in stark contrast to *HK1* and *HK2* where elevation of these two enzymes are associated with oncogenic, pro-proliferative hallmarks like mTORC signaling, EMT, and multiple immune activation pathways(see **Table 3.4**). These *HK3*^{hi} tumors have a unique infiltrate, significantly enriched with unpolarized macrophages, M2, neutrophils and CD8 T cells (as predicted by Cibersort) (**Figure 3.13J**). In support of the TCGA and CPTAC findings, we evaluated Vanderbilt related cohorts to interrogate the relationship between *HK3* expression and other known poor prognostic features. In our 180 patient TMA, we have previously reported that patients who have TREM2+, C1q+ macrophages have poor outcomes (Obradovic et al., 2021). We observe significantly higher *HK3* expression in the *TREM2*+ gene signature elevated patients further supporting *HK3* expression in poor outcome patients (**Figures 3.13K**). Interetsingly, *HK1* expression is significantly higher in the *TREM2*^{hi} patients but no differences in expression are seen in *HK2* **(Figures 3.14 I-J).**

Table 3.4: **GSEA terms generated in HK1^{hi}, HK2^{hi}, and HK3 ^{hi} tumors.** Red hallmarks are associated with metabolism. Green are associated with immune repones

HK1	HK2	HK3
HALLMARK_EPITHELIAL_MESENCHYMAL_TRANSITION	HALLMARK_EPITHELIAL_MESENCHYMAL_TRANSITION	HALLMARK_ALLOGRAFT_REJECTION
HALLMARK_INFLAMMATORY_RESPONSE	HALLMARK_HYPOXIA	HALLMARK_INFLAMATORY_RESPONE
HALLMARK_COMPLEMENT	HALLMARK_TNFA_SIGNALING_VIA_NFKB	HALLMARK_IL6_STAT3_SIGNALING
HALLMARK_G2M_CHECKPOINT	HALLMARK_ALLOGRAFT_REJECTION	

HALLMARK_MTORC1_SIGNALING	HALLMARK_INFLAMMATORY_RESPONSE	
HALLMARK_UV_RESPONSE_DN	HALLMARK_IL6_JAK_STAT3_SIGNALING	
HALLMARK_KRAS_SIGNALING_UP	HALLMARK_G2M_CHECKPOINT	
HALLMARK_TNFA_SIGNALING_VIA_NFKB	HALLMARK_COMPLEMENT	
HALLMARK_APOPTOSIS	HALLMARK_GLYCOLYSIS	
HALLMARK_HYPOXIA	HALLMARK_E2F_TARGETS	
HALLMARK_ESTROGEN_RESPONSE_EARLY	HALLMARK_COAGULATION	
HALLMARK_APICAL_JUNCTION	HALLMARK_APOPTOSIS	
HALLMARK_IL6_JAK_STAT3_SIGNALING	HALLMARK_MTORC1_SIGNALING	
HALLMARK_ESTROGEN_RESPONSE_LATE	HALLMARK_KRAS_SIGNALING_UP	
HALLMARK_ANGIOGENESIS	HALLMARK_ESTROGEN_RESPONSE_EARLY	
HALLMARK_ALLOGRAFT_REJECTION	HALLMARK_ESTROGEN_RESPONSE_LATE	
HALLMARK_GLYCOLYSIS	HALLMARK_INTERFERON_GAMMA_RESPONSE	
HALLMARK_E2F_TARGETS	HALLMARK_ANGIOGENESIS	
HALLMARK_PROTEIN_SECRETION	HALLMARK_UNFOLDED_PROTEIN_RESPONSE	
HALLMARK_UNFOLDED_PROTEIN_RESPONSE	HALLMARK_APICAL_JUNCTION	
HALLMARK_COAGULATION	HALLMARK_P53_PATHWAY	
HALLMARK_MITOTIC_SPINDLE	HALLMARK_MYC_TARGETS_V1	
HALLMARK_IL2_STAT5_SIGNALING	HALLMARK_IL2_STAT5_SIGNALING	
HALLMARK_MYC_TARGETS_V1	HALLMARK_MYC_TARGETS_V2	
HALLMARK_NOTCH_SIGNALING	HALLMARK_UV_RESPONSE_DN	
HALLMARK_MYOGENESIS	HALLMARK_KRAS_SIGNALING_DN	
HALLMARK_P53_PATHWAY	HALLMARK_MITOTIC_SPINDLE	
HALLMARK_INTERFERON_GAMMA_RESPONSE	HALLMARK_MYOGENESIS	
HALLMARK_MYC_TARGETS_V2		
HALLMARK_REACTIVE_OXYGEN_SPECIES_PATHWAY		
HALLMARK_TGF_BETA_SIGNALING		
HALLMARK_APICAL_SURFACE		

To further investigate the expression of HK3 in ccRCC cancer cells *HK3* expression, we examined a more recent scRNAseq ccRCC dataset in a conventional UMAP/Seurat approach (Bi et al., 2021). This contrasts with the three ccRCC experiments in the TISCH database that clearly demonstrate isolated *HK3* expression in monocytic macrophages **(Figure 3.2G**), Again, *HK3* is only detectable in the myeloid cells (**Figures 3.15A-B**) With the myeloid specific expression of *HK3*, this dataset was re-clustered just to examine the myeloid populations (**Figure 3.16A**). Myeloid cluster 9 is a *HK3* enriched cluster which also other myeloid defining genes like *FCG3a* (CD16), Cathepsin S (*CTSS*) *S100a4* and *FCN1* **(Figure 3.15C-D**). In line with our *in vitro* data, other genes that are unique to this cluster are *IFTIM2/3* which suggest these cells have elevated IFNγ signaling. Expression of *HK1* in the myeloid subcluster is ubiquitous, in line with its observation as a housekeeping gene (**Figure 3.16B**)**.** However, myeloid cluster 6 is *HK2*^{hi} along with other metabolic genes such *LDHA*, *GLUL* and *GAPDH* (**Figure 3.16C-D**). Correlation analysis across the entire ccRCC TCGA, *HK3* expression correlates better than *HK2* and *HK1* with other cluster 9 genes like *LST1*, *CD52*, *IFITM3*, *AIF* while *HK2* correlates more strongly with the metabolic genes found in cluster 6 (**Figs 3.15 E-F**). These data suggest that subset specific expression of these hexokinase isoforms and given the divergence in prognostic roles, the *HK3*+ myeloid may play large role in tumor progression and response to therapy.

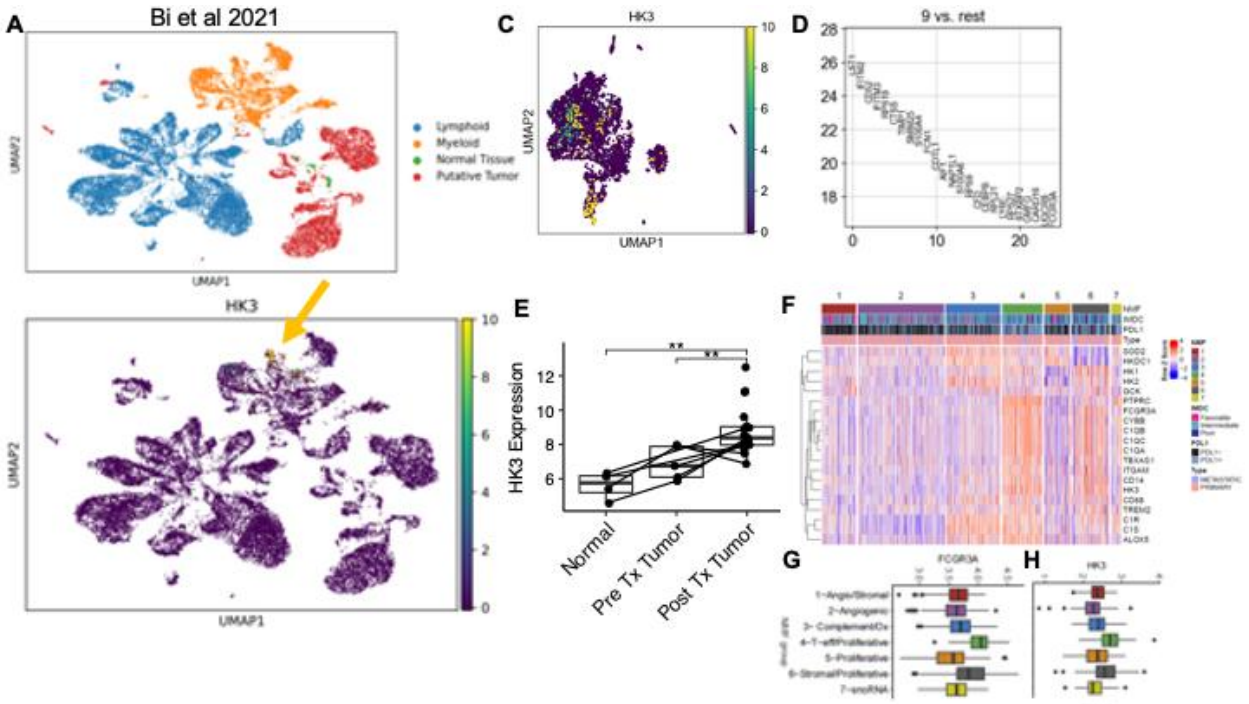

Figure 3.15: ***HK3+* myeloid cells in the ccRCC tumor microenvironment promote response to immune checkpoint blockade.** (**A**)/(**B**) scRNAseq expression of *HK3* Bi et al. 2021. (**C**) HK3 expression in myeloid subsets. (**D)** Cluster 9 (*HK3*^{hi}) specific gene set. (**E**) *HK3* levels via RNAseq in VEGFi neoadjuvant trial (Wood et al. JCI insight 2020). (**F)** Heatmap of a subset of myeloid relate genes and low Km hexokinases across NMF subtypes from Motzer *Cancer Cell* 2021 RNA expression of CD16 (*FCGR3a*) **(G)** and *HK3* (**H**) across seven unique RCC subtypes. Pre Tx: pre-pazopanib treatment, Post Tx: post-pazopanib treatment, NMF: non-negative matrix factorization, IMDC: International Metastatic Renal Cell Carcinoma Database Consortium, Angio:angiogenic, Ox: oxidative T-eff: T effector, snoRNA: small nucleolar RNAs. For E, Stats are Wilcoxon sign ranked tests with FDR correction. If no stars are on the plot, p-value is ns, ** equals 0.001<p<0.01, Box and whisker plots used for panel E. Connected dots in E demonstrate paired samples. Dots in G-H represent outlies

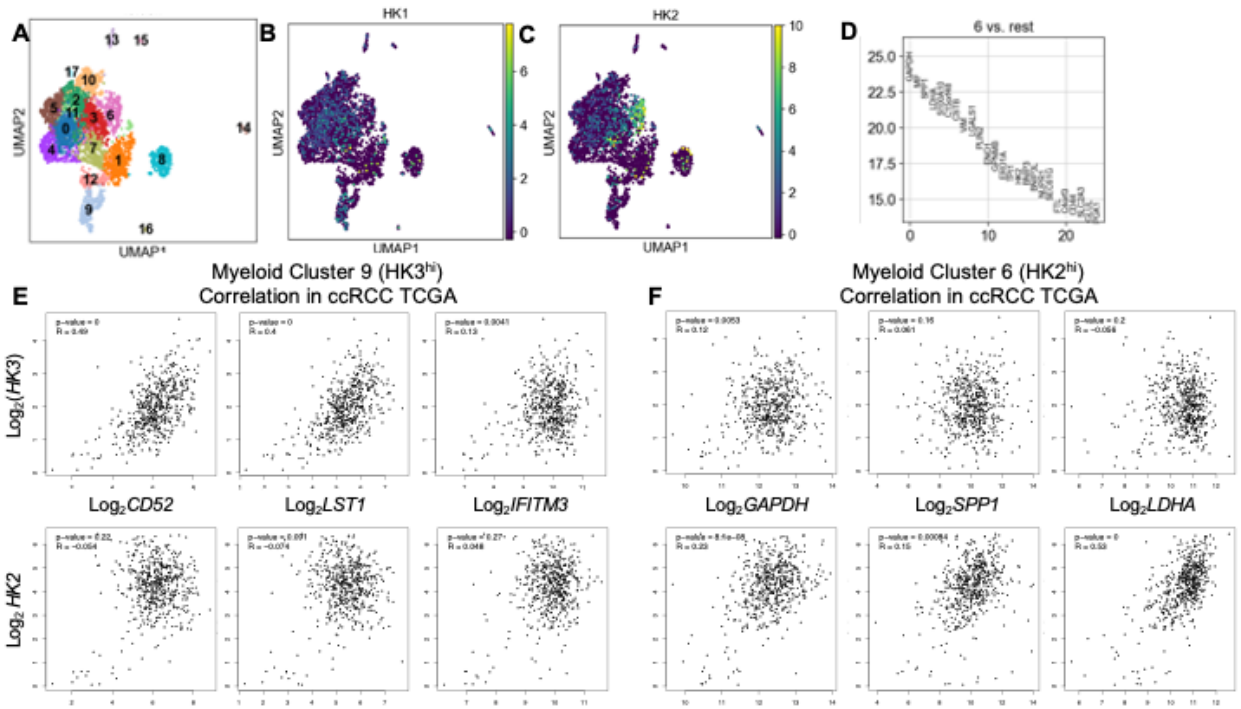

Figure 3.16: **HK2^{hi} and HK3^{hi} myeloid from the ccRCC TME, have distinct transcriptional programs**. (**A**) Myeloid sub-clustering from Bi et al. 2021. *HK1* (**B**) and *HK2* (**C**) expression in myeloid subclusters in this ccRCC dataset. (**D**) Gene expression program specific to cluster 6 (*HK2^{hi}* myeloid cells). (**E**) Correlation of *HK3* and *HK2* with myeloid cluster 9 specific genes across ccRCC TCGA data (**F**) Correlation of *HK3* and *HK2* with myeloid cluster 6 specific genes across ccRCC TCGA data. Pearson Correlation used for E-F. P-value=0 is when $p<1*10^{-99}$

A standard therapy for RCC patients is vascular endothelial growth factor tyrosine kinases inhibitor (TKI), however ultimately all patients develop resistance. Previous work suggests myeloid cells can contribute to this TKI resistance (Finke et al., 2011). Analyzing data from a neoadjuvant pazopinib study (Wood et al., 2020), we observe that *HK3* expression significantly increases with neoadjuvant VEGF blockade whereas *HK1* and *HK2* do not (**Figures 3.15E, 3.17A-B**). This indicates that this myeloid specific inflammatory hexokinase may be playing a role in TKI resistance. The latest treatment paradigm for ccRCC patients is combination VEGF and immune checkpoint blockade or combination checkpoint blockade. Motzer 2020 (Motzer et al., 2020) developed 7 NMFclusters that predict response to combination IO/TKI vs single agent TKI. In NMF cluster four (IFNγ^{hi} cluster who benefit from IO-TKI combo), have elevated expression of

HK3 as well as other myeloid genes in multiple datasets seen to be associated with *HK3* expression (*FCGR3a* (CD16), *C1q* isoforms, *TREM2*) (**Figure 3.15 F-H**). Interestingly, *HK1* demonstrates the highest expression in cluster 6 while *HK2* is elevated in cluster 3 (**Figure 3.17C-D**), both of which demonstrate the worst outcomes on either therapy. Interestingly, *HK3* expression does not appear to predict prognosis in a cohorts of melanoma patients treated with checkpoint blockade (Yang et al., 2021) (**Fig 3.17E**).

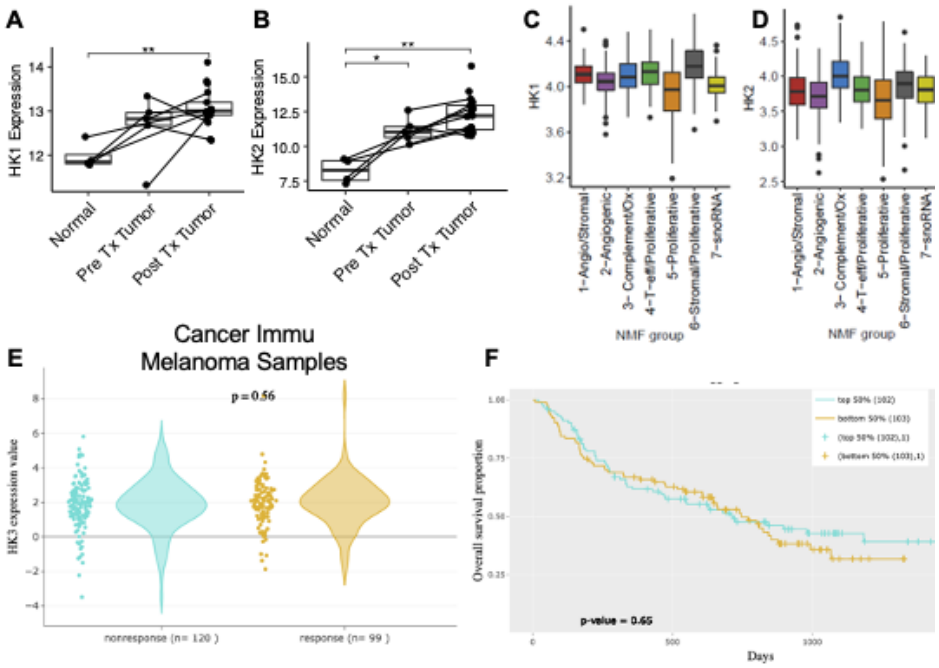

Figure 3.17: **Supplemental data to *HK3*+ myeloid cells in the ccRCC tumor microenvironment promote response to immune checkpoint blockade.** (**A**)*HK1* and (**B**)*HK2* expression in ccRCC patients receiving neoadjuvant TKI from Wood et al. *JCI Insight* 2020. (**C)** *HK1* and (**D**) *HK2* expression in metastatic ccRCC patients receiving VEGF TKI alone or TKI+ immune checkpoint blockade from Motzer et al. *Cancer Cell* 2021. (**E**) *HK3* level on pretreatment biopsy between responders and non-responders in combined Melanoma cohort receiving immune checkpoint blockade inhibitors. (**F**) Kaplan Meier curve examining impact of *HK3* expression on melanoma patients undergoing treatment with immune checkpoint blockade For A-B, Wilcoxon sign ranked test + FDR correction was performed. If no stars are displayed on plot, P-value is ns equals p>0.05, * equals 0.01<p< 0.05, ** equals 0.001<p<0.01. For panel E/F, p values are generated by Cancer Immu database. Unfortunately, in the publication and website there is no statement how this p values were generated. Connected dots in A-B demonstrate paired samples. Dots in C-D represent outliers. Box and whisker blots used for C-D.

In total these data support *HK3* as a unique biomarker due to its cell specific expression as well as its regulation by IFNγ. Thus, detecting *HK3* expression in ccRCC may indicate that a given patient has immune infiltrate rich in myeloid cells as well as the necessary anti-tumor cytokine IFNγ for response to checkpoint blockade.

Discussion

In this work, we validate our original finding of *HK3* as a myeloid specific gene across eukaryotic biology. This approach implements many different large datasets to confirm our initial observation from one mouse tumor model (MC38). By examining scRNAseq data from a host of mouse models and human TMEs, we confirmed the housekeeping function of *HK1*. *HK2* appears to be expressed in myeloid cells and proliferating tumor cells, whereas *HK3* is solely an immune specific gene. Diving further in the data indicates that HK3 is truly a myeloid specific gene, with no documented expression in lymphoid cells. There are two interesting examples of non-infiltrating immune cell *HK3* expression in the TISCH database. In Azizi et al., 2018, expression of *HK3* is found in “myofibroblasts”, however these cells express canonical TAM markers like CD11b+, CD163 indicating that these cells are most likely misannotated. Van Galen et al., 2020 documents *HK3* expression in the transformed myeloid cells from patients with acute myelogenous leukemia, however its expression is 4x less than in the infiltrating non mutated myeloid cells. This difference between cancer and infiltrating myeloid cells suggests *HK3* expression may be elevated in mature myeloid cells in comparison to the more primordial stem cells, which was further validated by analysis Hay et al. 2018.

This myeloid specific expression is endowed by binding of transcription factor, SPI1 to the *HK3* promoter. This has previously been observed in human leukemic cells,

but not examined in non-transformed immunocytes (Federzoni et al., 2014; Federzoni et al., 2012). Through scATAC sequencing, we observe that only myeloid cells have open chromatin surrounding *HK3* in both humans and mice whereas the other low K_m HKs can be expressed by all cell types throughout the organism. It is apparent, however that *HK2* also is enriched in myeloid cells. This mixed HK2+/HK3+ dual positivity in myeloid cells may underlie there persistent glycolytic phenotype multiple disease settings across different organs (Reinfeld et al., 2021; Xiang et al., 2021) Currently, it is unknown whether SPI1 plays a role in opening the surrounding chromatin in the HK2 and HK3 promoters or whether different components of the transcriptional machinery play a role in making these glucose fixing active in myeloid cells.

In examining expression of *HK3* in inflammatory microenvironments, we observe that certain inflammatory cues robustly induce HK3, both in the tissue of interest as well as the blood. This peripheral increase in *HK3* suggests that the factor is soluble. Following these observations, we stimulated myeloid cells with a host of cytokines *in vitro* and find that IFNγ alone can drive transcription and translation of HK3. This is in line with the significant elevation of *HK3* in patients with severe COVID, given that IFN high blood signatures predict poor outcomes (julian.knight@well.ox.ac.uk & Consortium, 2022). Mechanistically, we observe that STAT1 binds the HK3 promoter in mice and humans. This binding is restricted to myeloid cells. HK3 is reduced in the presence of the ruxolitinib, a clinical grade JAK1/JAK2 inhibitor. In total, these data support that *HK3* is a myeloid specific IFNγ stimulated gene. This fits a paradigm where many metabolic genes are upregulated to support the phenotype associated with anti-viral immunity. Two examples of metabolic genes that are also IFNγ targets are main M1 marker iNOS and SLC25a1,

which is known to be crucial for synthesis of acetyl-CoA in macrophages (Infantino et al., 2014). It is worth noting, that in these studies, we did not try type III interferons like lambda and other inflammatory cytokines like TNFα. Therefore, future work may take an even broader to understanding HK3 induction.

Given the direct role inflammation plays in *HK3* regulation, our group wondered if it could be used as a biomarker in ccRCC. This tumor type is highly inflamed and responds well to immune checkpoint blockade (Diaz-Montero et al., 2020). In support of the negative prognostic role of tumor inflammation in ccRCC, HK3 increases with stage of malignancy at a protein level, and high RNA expression predicts poor outcome (Xu et al., 2021). It appears that individual myeloid cell populations express these low K_m HKs preferentially. *HK2* is associated with a more mature glycolytic TAM (myeloid cluster 6), while *HK3* appears to be associated with more immature, potentially non-classical monocyte (myeloid cluster 9). Future work will implement flow sorting techniques to further investigate the myeloid subtype that expresses these enzymes to the greatest extent.

ccRCC is currently only treated with therapies that modify the TME. In the setting of VEGF TKI, HK3 is the only low K_m hexokinase that increases specifically with neoadjuvant treatment. This is in alignment with the knowledge that VEGF TKI resistance is associated with a myeloid infiltration program (Finke et al., 2011). Additionally, ccRCC patients with high IFNγ and high myeloid gene signatures are known to benefit from checkpoint blockade (McDermott et al., 2018; Motzer et al., 2020). In line with these prior observations, the IFNγ^{hi} NMF cluster 4 patients also have the highest level of HK3. This further supports IFNγ-HK3 relationship seen in our *in vitro* culture system. Intriguingly,

the other two low K_m HKs are elevated in the two worst subgroups of patients (clusters 3 and clusters 6) and do not cluster with the same myeloid genes as *HK3* (CD14, CD16 , C1q isoforms). This data provides rationale to inhibit TME glycolysis to make a more immunostimulatory microenvironment. However, that glycolysis inhibition must not limit the IFNγ network which is driving the increase in HK3 in these cluster 4 patients TME (Reinfeld et al., 2022).

CHAPTER 4: Materials and Methods

Prism was used for all bar graphs and heatmaps generated in this document unless otherwise noted. Hypothesis testing occurred in prism Biorender was used for the following figures 1.1,1.2,1.3,1.4,1.5,1.6, 3.1, 3.4F

Patient samples

Fresh histology-confirmed clear cell renal cell carcinoma (ccRCC) tumors and matched normal tissue were surgically removed from 14 patients. Supplementary Information Table 1 contains relevant patient and tumor information. Tumor and matched normal kidney were processed by mechanical dissociation (human tumor setting two on Miltenyi gentleMACS™) in HBSS with calcium chloride and magnesium chloride. Mechanical dissociation was followed by enzymatic digestion in 435U/mL deoxyribonuclease I (Sigma-Aldrich, D5025) and 218U/mL collagenase (Sigma-Aldrich, C2674) in RPMI supplemented with 10% FBS, 1% glutamine, 1% pen/strep, 1% Hepes, and 0.1% 2-Mercaptoethanol for 30-45min, depending on tissue toughness, at room temperature with 17 rpm agitation. Tissue digests were washed with HBSS without calcium chloride, magnesium chloride, or magnesium sulfate and then incubated in 5mM EDTA for 20min at room temperature with 17rpm agitation. Tumor and matched normal kidney digests were washed with HBSS with calcium chloride and magnesium chloride. Then they were passed through a 70µm filter and ACK-lysed. Patient peripheral blood mononuclear cells (PBMC) were isolated by density gradient centrifugation using Ficoll-Paque (GE Healthcare, 17144002) in SepMate-50 tubes (Stemcell Technologies, 85450) and subsequently ACK-lysed. Single cell suspensions were frozen in 90% FBS 10%

DMSO. Batched tumor and matched PBMC were thawed, rested for 10min at 37°C, counted, stained, and analyzed for flow cytometry. All studies were conducted in accordance with the Declaration of Helsinki principles under a protocol approved by the Vanderbilt University Medical Center (VUMC) Institutional Review Board (protocol #151549). Informed consent was received from all patients prior to inclusion in the study by the Cooperative Human Tissue Network at VUMC.

Interstitial fluid collection & LC/MS metabolite analysis

Tissue interstitial fluid (TIF) was collected from freshly resected ccRCC tumor and matched normal kidney tissue. Specimens were centrifuged against a 0.22μm nylon filter (Corning CLS8169) at 4°C for 5 minutes at 300g. Flow-through TIF was flash-frozen and stored at -80°C prior to batch analysis. Mouse blood was collected via submandibular vein, aliquoted immediately into EDTA, and centrifuged for 10min at 850g at 4°C. Plasma supernatant was collected and then cleared by centrifugation for 20min at 3000g at 4°C. Liquid chromatography/mass spectrometry (LC/MS) quantitation of metabolites was performed as described previously (Sullivan et al., 2019) .

Mice

C57BL/6J (000664), BALB/cJ (000651), and Rag1 KO (002216) were obtained from the Jackson Laboratory. All mouse procedures were performed under Institutional Animal Care and Use Committee (IACUC)-approved protocols from Vanderbilt University Medical Center and conformed to all relevant regulatory standards. Mice were housed in ventilated cages with at most 5 animals per cage and provided ad libitum food and water.

Mice were on 12 hour light/dark cycles which coincided with daylight in Nashville, TN. The mouse housing facility was maintained at 68-76°F and 30-70% humidity. For injectable tumor models, 8-20 week old male and female mice were used. Mice were euthanized if humane endpoint was reached (2cm dimension, ulceration, weight loss >10%). V9302 treatments were administered intraperitoneally twice daily for five days at 25mg/kg for FDG uptake or once at 75mg/kg 3hr prior to ^{18}F-Gln injection. Rapamycin treatments were administered intraperitoneally daily for four days at 2mg/kg dissolved in 2% DMSO 30% Polyethylene Glycol 300 (Sigma Aldrich 202371), and 5% Tween 80 (sigma Aldrich P1754).

Cell lines for chapter 2

The MC38 and CT26 cell lines were provided by Barbara Fingleton and grown in DMEM supplemented with 10% FBS. The RenCa cell line was obtained through ATCC and grown in RPMI 1640 supplemented with 10% FBS, 4mM glutamine, 25mM HEPES, essential amino acids, and sodium pyruvate. Cells were trypsinized, washed twice in PBS, and $1x10^6$ cells were injected subcutaneously in 100-200µL of PBS on mouse flanks. Subcutaneous tumors grew for 14 days prior to analysis. The MC38-EL-Thy1.1 cells were generated using a transposon based engineering approach with plasmids that were described previously (O'Neil et al., 2018). MC38 cells were electroporated using the NEON transfection system (ThermoFisher) according to manufacturer's recommendations for adherent cell lines. 5 million MC38 cells were suspended in electroporation buffer containing 5µg of the plasmid pCMV-M7PB and 15µg of the plasmid pT-EL-thy1.1, which is a bicistronic transposon vector driving expression of an

enhanced firefly luciferase as well as Thy1.1 antigen. Cells were magnetically sorted based on expression of Thy1.1 using magnetic beads (Miltenyi 130-121-273). MC38-OVA cells were generated and provided by Richard O'Neil. Cell lines were regularly tested for mycoplasma via PCR and all cells used in downstream assays were confirmed negative.

Orthotopic renal implantation

For intrarenal RenCa injections, survival mouse surgery was performed according to a method previously described (Tracz et al., 2014). Briefly, mice were anesthetized by isoflurane inhalation at 2-3% and placed on a warming recirculating water pad set at 37°C to maintain body temperature. Using sterile surgical techniques, a 1-cm incision was made in the skin running parallel to the spine, slightly below the ribcage on the right flank. Next, a 1-cm incision was made in the muscle layer in the same location. Using gentle pressure on the mouse abdomen, the right kidney was exteriorized. $5x10^4$ Renca cells resuspended in 100µL of PBS were injected using a 29-gauge needle inserted through the renal capsule into the cortical space. The injection site was swabbed using sterile gauze and the kidney was returned to the body cavity. The abdominal wall was closed using 6-0 monofilament absorbable sutures (AD Surgical; S-D618R13), and the skin was closed using wound clips. Analgesic was provided pre-surgery and 24 hours post-surgery in the form of ketoprofen injections at 5 mg/kg. Wound clips were removed 7 days following the surgery. Tumors were analyzed 28 days after cancer cell injection.

Spontaneous mouse tumor models

PyMT GEMM mice were bred by crossing male transgenic mice expressing the polyoma virus middle T antigen (PyMT) oncoprotein under the MMTV-LTR (Jackson

Laboratory 022974) with wildtype females on a similar B6/FVB mixed background. The GEMM mice were from a colony in which all mice expressed two *Vhl* alleles in which exon 1 is flanked by *loxP* sites (Jackson Laboratory 012933) but did not express a Cre transgene and were thus effectively wildtype. Once weaned, female mice were palpated twice a week and tumors were measured in three dimensions with digital calipers. Mice were collected when any tumor had grown to a size of 1 cm in diameter in any dimension, around 5 months of age. Virgin female littermates were used in these studies.

The AOM/DSS inflammatory colorectal cancer model was used as previously described (Becker et al., 2005; Parang et al., 2016). In brief, bedding was mixed to normalize microbiome two weeks prior to experimental initiation. 8-12 week-old C57BL/6J mice were intraperitoneally injected with 12.5 mg/kg AOM and exposed to three 4-day cycles of 3% to 4% DSS (TdB Labs 9011-18-1). Each DSS cycle was followed by a 16-day recovery period. Prior to sacrifice, colonoscopy was performed to confirm tumor development. Mice were weighed every other day throughout the experiment. Mice were euthanized 6-8wk after completing the last cycle of DSS. Colons were dissected and tumor tissue was isolated from the mucosa.

PET-CT imaging

For individual studies, a group of MC38 tumor-bearing mice were food-restricted overnight. Then the mice received a retro-orbital injection of ~ 37 MBq/0.1 mL of ^{18}F-FDG and were returned to plate-warmed cages. Forty minutes later, the mice were anesthetized under 2% isofluorane and imaged an Inveon microPET (Siemens Preclinical, Knoxville TN) for 20 min. Data from all possible lines of response (LOR) were

saved in the list mode raw data format. The raw data was then binned into 3D sinograms with a span of 3 and ring difference of 47. The images were reconstructed into transaxial slices (128 x 128 x 159) with voxel sizes of 0.0815 x 0.0815 x 0.0796 cm^3, using the MAP algorithm with 16 subsets, 4 iterations, and a beta of 0.0468. For anatomical co-registration, immediately following the PET scans, the mice received a CT scan in a NanoSPECT/CT (Mediso, Washington DC) at an x-ray beam intensity of 90 mAs and x-ray peak voltage of 45 kVp. The CT images were reconstructed into 170 x 170 x 186 voxels at a voxel size of 0.4 x 0.4 x 0.4 mm^3. The PET-CT images were uploaded into Amide (www.sourceforge.com) and volumetric regions-of-interest were drawn around the tumors. The PET images were normalized to the injected dose and the mean radiotracer concentration within the ROIs were determined.

^{18}F autoradiography

Mice were handled and injected similarly to previously described for the PET-CT imaging, but without overnight fasting. Tumors were harvested, embedded in optimal cutting temperature compound (OCT, Fisher 23-730-571), and frozen on dry ice. Tumors were cut into 10μm sections and imaged in a Beta Imager (Biospacelabs, France) for 1 hr. Regions-of-interest (ROIs) were drawn around the resulting tumor and spleen images and the counts in each ROI were compared.

In vivo ^{18}F-FDG and ^{18}F-Gln nutrient uptake assay

Tumor-bearing mice were retro-orbitally injected with 1mCi of FDG or ^{18}F-Gln synthesized at VUMC (Hassanein et al., 2016). During radiotracer uptake, mice were conscious and had access to food and water. Mice were euthanized and spleen and

tumors were harvested 40min after radiotracer administration. Single cell suspensions of splenocytes were prepared by physical dissociation followed by ACK-lysis. Tumors were chopped, mechanically dissociated on the Miltenyi gentleMACS™ Octo Dissociator with Heaters (setting implant tumor one) and digested in 435U/mL deoxyribonuclease I (Sigma-Aldrich, D5025) and 218U/mL collagenase (Sigma-Alrich, C2674) at 37°C for 30min. After enzyme treatment, tumors were passed through a 70μm filter and ACK-lysed. Cells were resuspended in MACS buffer (PBS +2% FBS +2mM EDTA) and counted using trypan blue with the TC20™ Automated Cell Counter (Bio-Rad). In some cases, tumors from different mice were pooled to achieve higher tumor cell number prior to fractionation to ensure sufficient ^{18}F signal and were ultimately analyzed as biological replicates. Next, tumor cell suspensions were fractionated using serial magnetic bead positive selection according to the manufacturer's instructions (all Miltenyi mouse kits: CD45 TIL 130-110-618, EPCAM 130-105-958, Thy1.1 130-121-273, CD4/8 TIL 130-116-480, CD11b 130-049-601, F4/80 130-110-443, Gr1 130-094-538, CD11c 130-125-835, CD8 TIL 130-116-478, CD4 TIL 130-116-475). Briefly, cells were resuspended at 10 million total cells/90μL MACS buffer and 10μL microbeads for 15min. Then, cell suspensions were applied to LS columns (Miltenyi 130-042-401) in Miltenyi QuadroMACS™ Separators, washed, and eluted according to manufacturer's instructions. Fractions were resuspended in 1mL of media; 10μL were used for trypan blue staining and TC20 cell count, ~50μL were stained for flow cytometry determination of fraction cellular composition, and 900μL were transferred into 5mL tubes to measure radioactivity. 900μL of 2mL splenocyte suspensions and 5 million total cells from the unfractionated whole tumor were also assayed for radioactivity. The Hidex Automatic

Gamma Counter was used with 1min read times to measure time-normalized ^{18}F counts per minute (CPM) for each sample. To determine per cell ^{18}F-nutrient avidity, time-normalized CPM was divided by the number of viable cells as determined by trypan count. Harvested tissues and cell fractions were kept on ice or at 4°C in RPMI 1640 supplemented with 10% FBS except when noted.

Flow cytometry

Single cell suspensions obtained from tumors and spleens were incubated in F_c block (1:50, BD 553142) for 10min at room temp, stained for surface markers for 15min at room temp, washed with FACS buffer (PBS +2% FBS) once, and resuspended in FACS buffer for analysis on a Miltenyi MACSQuant Analyzer 10 or 16. For intracellular staining, the eBioscience™ Foxp3/transcription factor staining buffer kit (Fisher 00-5523-00) was used. For intracellular cytokine staining, tumor single cell suspensions were incubated for 4hr at 37°C 5% CO_2 in supplemented RPMI with PMA (50ng/mL, Sigma Aldrich P8139-1MG), ionomycin (750ng/mL, Sigma Aldrich I0634-1MG), and GolgiPlug (1:1000, BD 555029), and processed using the BD Cytofix/Cytoperm™ Fixation and Permeabilization Solution (ThermoFisher BDB554722). Surface staining was performed as described above, cells were fix/permed for 20min at 4°C, and then stained for intracellular markers for at least 30min at 4°C. Ghost Dye Red 780 viability dye (1:4000, Cell Signaling 18452S) was used identically to surface antibodies. The anti-mouse and cross-reactive antibodies used were: CD45 BV510 (1:1600, 30-F11, Biolegend 103138), B220 e450 (1:400, RA3-6B2, ThermoFisher 48-0452-82), CD11b e450 (1:1600, M1/70, ThermoFisher 48-0112-82), CD11b FITC (1:1600, M1/70, Biolegend 101206), CD8a AF488 (1:1600, 53-6.7, Biolegend 100723), CD8a BV510 (1:600, 53-6.7, BD 563068), CD8a APC (1:200, 53.6-

7, BD 17-0081-82), Ly6C FITC (1:4000, HK1.4, Biolegend 128006), CD11c PE (1:1000, N418, BioLegend 117308), FOXP3 PE (1:125, FJK-16s, ThermoFisher 12-5773-82), pS6 Ser235/236 PE (1:100, D57.2.2E, Cell Signaling 5316S), CD4 PerCP-Cy5.5 (1:600, RM4-5, BioLegend 100540), Ly6G PerCP-Cy5.5 (1:800, 1A8, BioLegend 127616), F4/80 PE-Cy7 (1:800, BM8, BioLegend 123114), NKp46 PE-Cy7 (1:200, 29A1.4, BioLegend 137618), CD3 PE-Cy7 (1:200, 17A2, BioLegend 100220), CD3 FITC (1:200, 17A2, BioLegend 100204), CD3 APC (1:200 17A2, BioLegend 100236), CD206 APC (1:500, C068C2, BioLegend 141708), GLUT1 AF647 (1:500, EPR3915, Abcam ab195020), EPCAM PE (1:1500, G8.8, BioLegend 118206), Thy1.1 PerCP-Cy5.5 (1:2000, HIS51, ThermoFisher 45-0900-82), Thy1.1 FITC (1:2000, HIS51, ThermoFisher 11-0900-85), CD45 PE (1:1600, 30-F11, ThermoFisher 12-0451-83), Ly6C BV570 (1:400, HK1.4, BioLegend 128030), CD68 BV605 (1:200, FA-11, BioLegend 137021), HK1 AF647 (1:100, EPR10134(B), Abcam ab197864), HK2 AF647 (1:200, EPR20839, Abcam EPR20839), CD71 APC (1:100, RI7217, BioLegend 113820), CD98 PE (1:400, RL388, ThermoFisher 12-0981-81), MHCII I-A/I-E APC (1:4000, M5/114.15.2, BioLegend 107614), CD103 PE-Cy7 (1:200, 2E7, BioLegend 121425), LAG3 e450 (1:100, eBioC9B7W, ThermoFisher 48-2231-82), PD1 PE (1:100, 29F-1A12, BioLegend 135206), TIM3 APC (1:100, RMT3-23, BioLegend 119706), IFNγ APC (1:250, XMG1.2, BioLegend 505810), CD25 e450 (1:500, PD61.5, ThermoFisher 48-0251-82), CD44 PE-Cy7 (1:1000, IM7, BioLegend 103030), and CD62L APC (1:200, MEL-14, ThermoFisher 17-0621-82), CD69 FITC (1:200, H1.2F3, BioLegend), TCF1 AF647 (1:200, C64D9, Cell Signaling), TBET PE-Cy7 (1:100, eBio4B10, eBioscience 25-5825-82), EOMES PE (1:100, Dan11mag, eBioscience 12-4875-82), Perforin APC (1:100, eBioOMAK-D,

eBioscience 17939280), Granzyme B PE (1:100, NGZB, eBioscience 12-8898-80), IL-2 PE (1:100, BD 554428), and TNFα PE-Cy7 (1:200, MP6-XT22, BioLegend 506324). The anti-human antibodies used were: CD45 BV421 (1:400, HI30, BioLegend 304032), CD3 APC (1:200, UCHT1, BioLegend 300439), CD11b PerCP-Cy5.5 (1:200, ICRF44, BioLegend 301328), CD14 BV510 (1:200, M5E2, BioLegend 301842), CA9 AF647 (1:200, 303123, R&D Systems FAB2188R-100UG), and Human Fc Block (1:50, BD 564220). For *in vivo* intravenous CD45 PE labelling, MC38 tumor-bearing mice were injected with 5µg anti-CD45 PE diluted to 150 µL in PBS via tail vein and euthanized 5min later. For *ex vivo* fluorescent palmitate uptake, tumor single cell suspensions were incubated for 1hr in Krebs buffer (125mM NaCl, 2.5mM KCl, 25mM $NaHCO_3$, 1mM NaH_3PO_4, 1mM $MgCl_2$, 2.5mM $CaCl_2$, pH 7.2) at 37°C 5% CO_2, incubated with BODIPY™ FL C16 (1µM in Krebs buffer, Thermo D3821) for 45min, washed twice with FACS, and then stained for surface markers. For the myeloid suppression assay, microbead-isolated CD11b+ myeloid cells were co-incubated with 100,000 CellTrace Violet-labelled (CTV, Thermo C34557) OT-I splenocytes per well in a 96-well plate in the presence of 1µg/mL SIINFEKL peptide for 3 days prior to analysis by flow cytometry. Mitochondrial mass was measured with 200nM MitoTracker Green FM (Invitrogen M7514) and mitochondrial membrane potential was measured with 150nM TMRE (Lifetech T-669) staining for 30min at 37°C 5% CO_2 in complete media. Flow cytometry data were analyzed using FlowJo v10.7.1. NIH Tetramer Core Facility for provided the SIINFEKL PE tetramer (1:1000).

In vivo 2NBDG and flow sorting

2NBDG (Cayman Chemical 11046) was dissolved in PBS at 5 mM (1.71 mg/mL) and 100µL (500ng) was injected retro-orbitally. Mice were sacrificed 40 minutes later and tumor cells and splenocytes were harvested as indicated above. Splenic T cells were isolated according to manufacturer's instructions using the Pan T cell Isolation Kit (Miltenyi 130-095-130). 2NBDG$^{hi/lo}$ cells were collected on the Nanocellect (San Diego, USA) WOLF cell sorter and subsequently gamma counted as described in the ^{18}F-FDG and ^{18}F-Gln nutrient uptake assay.

Immunohistochemistry and light microscopy

MC38 tumors were fixed overnight in 10% formalin and then switched to 70% ethanol. Single color IHC was performed by Vanderbilt University Medical Center Translation Pathology Shared Resource. Staining was conducted on the Leica Bond Max IHC stainer. All steps besides dehydration, clearing and coverslipping are performed on the Bond Max. Slides were first deparaffinized. Antigen retrial and antibody dilution were altered for maximal staining with each antibody. For CD11b staining (Catalog # NB110-89474, Novus Biologicals, Centennial, CO) slides were placed in a Protein Block (Ref# x0909, DAKO, Carpinteria, CA) for 10min prior to staining. Then, the slides were incubated in epitope retrieval 2 solution for ten minutes, and subsequently stained (1:10,000 dilution). For CD3 staining (Ab16669, abcam, Cambridge, MA), epitope retrieval 2 solution for 10min prior to staining (1:250 dilution). For F4/80 staining (NB600-404, Novus Biologicals LLC, Littleton, CO), epitope retrieval was conducted in proteinase K for 5 minutes prior to primary antibody staining (1:300 dilution). Rabbit anti rat secondary (BA-4001, Vector Laboratories, Inc., Burlingame, CA) was used at a 1:2000

dilution for 15min for antigen detection. For CD31 staining (Cat.# DIA-310, Dianova, Hamburg, Germany,), epitope retrieval occurred in epitope retrieval 2 solution for 20min and then subsequently stained (1:75ul dilution). Staining with Biotinylated anti rat (Cat.# BA-4000, Vector Laboratories, Inc., Burlingame, CA) was used for antigen detection at a 1:2000 dilution for 15min. For CD45lca staining (cat# HS-427 017, SySy (Synaptic Systems), Goettingen, Germany) epitope retrieval occurred in epitope retrieval solution 2 for 20min, followed by primary antibody (1:500 dilution. Rabbit anti-rat secondary (BA-4001, Vector Laboratories, Inc., Burlingame, CA) was used at a 1:2000 dilution for 15min to detect the antigen. The Bond Refine (DS9800, Buffalo Grove, IL, USA) detection system was used for visualization. Images were captured using an Olympus BX53 microscope (Olympus Corporation, Center Valley, PA), an Olympus DP73 camera, and Olympus cellSens Standard imaging software version 1.17. Low-power images were captured with a 4X objective lens and high-power images were captured with a 40X objective lens.

MC38 anti-F4/80 microbead-fractionated TAM were mounted onto slides using Wescor Cytopro cytocentrifuge and stained with hematoxylin and eosin following manufacturer's guidelines (Fisher 23-122952). Images were captured under oil immersion (100x objective) using an Olympus BX53 microscope (Olympus Corporation, Center Valley, PA), an Olympus DP73 camera, and Olympus cellSens Standard imaging software.

Extracellular flux assay

Tumor cell fractions were obtained as described above. Each fraction was plated at 200,000 live cells/well in technical quadruplicate on a Cell-Tak-coated plate (Corning

354240) in Agilent Seahorse RPMI 1640 supplemented with 10mM glucose, 1mM sodium pyruvate, and 2mM glutamine. Cells were analyzed on a Seahorse XFe 96 bioanalyzer using the Mitostress assay (Agilent 103015–100) with 1μM oligomycin, 2μM FCCP, and 0.5μM rotenone/antimycin A. For *in vitro* activated T cells, 150,000 live cells/well were plated. Data were analyzed in Agilent Wave software version 2.6.

Cell sorting and mRNA transcript analysis

$CD45^+$ and $CD45^-$ tumor cell fractions were obtained as described above. Cell fractions were stained for the indicated surface markers and viability dye and sorted on a BD FACSAria III cell sorter. RNA was isolated from tumor cell populations and unstained whole tumor single cell suspensions using the Quick-RNA™ Microprep Kit (Zymo R1050) according to manufacturer's instructions. RNA transcripts were quantified using the NanoString nCounter Metabolic Pathways Gene Expression Panel (XT-CSO-MMP1-12) according to manufacturer's instructions. Transcript counts of 768 genes enriched in cellular metabolic pathways were analyzed using NACHOv1.0.1 (Canouil et al., 2020), an R package for parsing, visualization, quality control, and normalization designed for NanoString nCounter data. While parsing raw transcript counts, manufacturer-designated housekeeping genes were used to normalize between samples: *Abcf1*, *Agk*, *Cog7*, *Dhx16*, *Dnajc14*, *Edc3*, *Fcf1*, *G6Pdx*, *Mrps5*, *Nrde2*, *Oaz1*, *Polr2a*, *Sap130*, *Shda*, *Stk11ip*, *Tbc1d10b*, *Tbp*, *Tlk2*, *Ubb*, *Usp39*. Sample quality was evaluated based on normal ranges provided by the manufacture for 1) binding density (0.1-2.25), 2) Field of View (<75), 3) Positive Control Linearity (<0.95), and 4) limit of detection (<2). Samples were excluded if they failed any of the four conditions. The third replicates of M-MDSC Rapa and CD4 Rapa were excluded as outliers for abnormal positive control linearity and

limit of detection, respectively. Normalization was performed using geometric means based on housing genes, positive, and negative controls. The normalized data from this experiment has been deposited in Geo and can be accessed at GSE165223. Principal component analysis was performed using “FactoMineRv2.3”(LÍ et al., 2008) package in R. Differentially expressed metabolic genes were identified using a one-way ANOVA performed on transcript count across samples. P-values were adjusted for multiple testing using Benjamini & Hochberg false discovery rate using the “p.adjust” R function. For metabolic genes passing an adjusted p-value <0.01, we performed hierarchical clustering across samples and genes using default settings with the 'seaborn' package (version v0.11.0) in Python. Based on the hierarchical clustering, we grouped genes and performed gene set enrichment analyses using gProfiler (Raudvere et al., 2019) with Reactome gene sets compared to all genes. “Metabolism” was the most highly enriched pathway for each cell type and was excluded from bar graphs for space. Differentially expressed genes between the rapamycin and vehicle treated samples for each cell type were identified using “edgeR” (Robinson et al., 2010) (version 3.28.1). First, the dispersion (variance of transcript counts) was estimated using the function "estimateDisp". Next, the differential expression between conditions was evaluated using a likelihood ratio test for a negative binomial generalized log-linear model. We considered transcripts with a false discovery rate < 10% and/or a 2-tailed t-test p-value <0.01 as being differentially expressed. All analyses were performed using the R (version 4.0.2).

MC38 RNA analysis

Volcano plot and bar graphs (A/B/C/D generated in Figure 3.2 used data generated from (Reinfeld et al., 2021)). Briefly, RNA was purified from flow sorted populations CD8s, CD4, TAMs, MDSCs, and CD45- cancer cell from the MC38 model and then analyzed on the NanoString mouse metabolic panel. The data normalized using the n-counter software as described above. This data is publicly available at NCBI GEO GSE165223. Log fold changes of genes were computed by comparing enrichment in the two myeloid fractions (Ly6c^{hi} MDSCs, and F4/80^{hi} TAMS) in comparison to the TME resident cell types (CD45- tumor cells, CD4+ T Cells and CD8+ T Cells). Wilcox test done on each gene for differences between Myeloid vs not myeloid. FDR correction was done to adjust for multiple comparisons (reported as q-value). Red dots dominate genes that are significant after considering these multiple comparisons.

Brain TME RNA analysis

Data from 3.2E/F, 3.5A/B originates from Klemm et al. *Cell* 2020. Like our NanoString analysis, the Joyce group flow sorted for populations of interested across human PBMC, epileptic brain tissue, primary gliomas, and brain metastasis. After flow sorting, RNA was extracted and sequenced from each fraction. This data was generated to describe the unique immune environment in brain malignancies. Normalized data is available at this website https://joycelab.shinyapps.io/braintime/. *HK3* expression across all flow sorted populations was exported for analysis

Holistic single cell RNAseq data across multiple TMEs

Data from 3.2G, 3.3E/F/G, 3.12I originates from TISCH database (Sun et al., 2021) (http://tisch.comp-genomics.org/home/). This dataset contains 79 different scRNA experiments and allows for users to find unique patterns of cellular expression of genes of interest. To pair the data down, we filtered datasets that contained myeloid annotations for Figure 3.2G. This analysis excluded studies that had myeloid cell types but no documented HK3 expression. For Figure 3.3E-G, studies were filtered out when they did not contain three populations of interest (immune, stromal and malignant). Datasets annotated with the cell type "other" were excluded because it remains unclear what other cell annotation refers across these diverse studies. For Figure 3.10I, we filtered for studies that contained M0, M1, and M2 annotations so that we could directly compare *HK3* expression across different subtypes of macrophages. Figure 3.4C was taken from TISCH as well (data originates from experiment named PBMC_60K_10X).

scRNA expression from mouse lung cancer

Data for Figures 3.3A-C originates from LeFave et al. *Cancer Cell* 2020. This study performed scRNA/scATAC sequencing on mouse models of lung cancer as they metastasized. The R Shiny-based web application for data visualization is accessible here: https://buenrostrolab.shinyapps.io/lungATAC/. Expression of HK2 and HK3 were queried in this database. UMAP outputs with cell subtype clustering are included in the manuscript. The raw data is publicly available at Gene Expression Omnibus (GEO) under GSE134812, GSE145192, and GSE151403, GSE145194, GSE134812, GSE145192.

GTEX analysis

GEPIA (http://gepia.cancer-pku.cn/) was used to generate the pictorial representation of HK3 expression across adjacent normal human tissues taken for the the cancer genome atlas (TCGA) in Figure 3.3A**.** Violin plots generated for HK3 expression across organs was exported directly from the GTEX portal (https://gtexportal.org/home/gene/HK3). Data for this panel was filtered to excluded repeated samples from the same organ (i.e. multiple brain locations are deposited in GTEX, but only one was graphed for conciseness). Exclued tissues had no detectable *HK3* expression. GEPIA correlation analysis was used to perform correlations found in Figures 3.4B/C, 3.5E/F, 3.16E/F. Pearson's correlation co-efficient were used. GEPIA does not report small p values as number, but instead presents them as p=0. The low K_m HKs were correlated to either all GTEX data available on GEPIA, or solely the lung GTEX data (due to the lungs elevated *HK3* expression). These differences are denoted in the figures, legends, and text. Similar correlations were performed in Figures 3.15E/F. These figures examined Myeloid Cluster 6/9 specific genes and the correlation between these genes to HK2 and HK3. For this analysis in Figure 3.15, only the KIRC (ccRCC) tumor data was used.

MethoCult © assay

Hematopoietic progenitors were harvested from mouse femurs by flushing the marrow. From the single cell suspension, the Miltenyi HSC isolation was used. These Lin-,c-KIT+ cells were plated in Methocult© for 14 days. At day 14, the cells were collected from the methocult culture, resuspended appropriate to appropriate cell numbers and 10

scRNA/ATAC sequencing was performed by the Vantage core. Doctoral Dalton Greenwod performed the heatmap analysis.

ImPress proteomics data

TMT labeled Mass spectrometry was performed on cultured mouse immune cells given a variety of stimuli (Marchingo et al., 2020). Specific culture conditions are outlined at http://immpres.co.uk/. To make the heatmap in Figure 3.4E, Z scores for Hk1/2/3 protein expression were exported from this online database.

CD11b+ purification

Bone marrow cells were harvested from flushed mouse long bones from 6-12 week old WT C57B6 mice (purchased from Jacks). Myeloid cells were purified using CD11b+ magnetic bead isolation (130-049-601) from Miltenyi as previously described in Reinfeld Madden et al. 2021. Purification was verified using Miltenyi MACSquant10 flow cytometer. Cells were stained similarly to Reinfeld Madden Nature et al 2021.

qPCR protocol

RNA was isolated using Qiagen RNeasy kits. 10 uL of BME was added to 1 mL of RLT lysis buffer. Resulting RNA was quantified using NanoDrop. Meridian Bioscience cDNA sensi fast kit was used to generate cDNA from 1 ug of RNA (BIO-65053). This 20 uL reaction was diluted with 100 uL of H20. Subsequently, 10 uL of this diluted cDNA was further filuted in 190 uL of water. 5 uL of this 1:20 diluted stock cDNA was included in a 11 uL qPCR reaction using 5.5 uL of the 2x BioRad SSO qPCR mixture. 0.5 uL of 5uM

FWD and reverse qPCR primer were used for reaction. Real-time PCR was conducted with the SYBR Green PCR kit (Bio-Rad) using a Bio-Rad CFX Connect Real-time System, with the threshold cycle number determined by Bio-Rad CFX manager software V.3.0. Reactions were performed in technical triplicate and the threshold cycle numbers were averaged. Data normalized to GUSB or TBP expression. Repeat pipettor was used to aliquot both cDNA and primer containing master mix in 96 well plate.

Table 4.1: qPCR primer sequences for mouse low K_m Hexokinases

Gene	FWD	RVS
Hk1	GTGGACGGGACGCTCTAC	TTCACTGTTTGGTGCATGATT
Hk2	TGATCGCCTGCTTATTCACGG	AACCGCCTAGAAATCTCCAGA
Hk3	TGCTGCCCACATACGTGAG	GCCTGTCAGTGTTACCCACAA

GUSB/TBP primers provided by CS Williams lab. qPCR from freshly derived bone marrow macrophages were conducted by Dr. Farnaz Nejad in the Ardehali Lab at Northwester

Single nucleus lung sequencing

Single Nucleus sequencing on human lungs was conducted by the Delorey et al. 2021. The data available under accession number GSE16291. This data is an early release from (Delorey et al., 2021). Data is publicly available in this Broad single cell viewer (https://singlecell.broadinstitute.org/single_cell?type=study&page=1&terms=lung). Using this viewer, UMAPs demonstrating cell cluster identity and illustrating expression of *EPCAM*, *ITGAM*, *HK2* and *HK3* were exported.

scRNAseq on human bone marrow

Data for heatmap in Figure 3.6E originates from Hay, et al. *Exp Hematol* 2018. This study conducted scRNAseq on 8 bone marrow samples derived from healthy donors. It is publicly reposited at http://www.altanalyze.org/ICGS/HCA/Viewer.php. Normalized RNA counts for *Hk1/2/3* were exported and used to generate a heat map.

scATAC peaks from human PBMC

Kartha, et al. bioRxiv.org 2021 examines the role of inflammatory stimuli on chromatin openness in human PBMC. The scATAC tracks are deposited on the USCS genome browser. The following set of tracks (https://genome.ucsc.edu/s/vkartha/stimATAC_Control1h_cellTypes) were used in Figure 3.7 to examine *HK3* promoter openness across the 16 annotated cell types in this data set. The following sets of tracks (https://genome.ucsc.edu/s/vkartha/stimATAC_CD14_conditions) were used to generated Figure 3.11J. This set of tracks allows the viewer to examine *HK3* promoter openness with 1 hr of IFNγ, PMA or LPS stimulation. This data is reposited in a shinyapp (https://buenrostrolab.shinyapps.io/stimFigR/). The shinyapp was used to generate the UMAPs that were used in Figure 3.11 K/L to show domain domains of regulatory chromatin activation for *HK3* and IFNγ pseudotime in this data set. The shinyapp was used to generate the UMAP of cell indentities found in Figure 3.12E.

Enhancer network analysis of low K_m HKs

Data from Yoshida, et al. *Cell* 2019 is deposited on Immungen.com, under the enhancer network tool (http://rstats.immgen.org/EnhancerControl/index.html). For each

low K_m hexokinase, the data from “Open Chromatin Activity in Immune Cells” was exported and made into heatmaps (Figure 3.8A-C). This data differs from Kartha et al. 2021 because it originates from mouse scATAC sequencing, whereas Kartha, et al. implements human PBMC. The RNaseq and ATACseq data reported in Yoshida et al. 2019 can be found at GSE100738. Processed ATAC-seq data and called peaks can be found at: https://sharehost.hms.harvard.edu/immgen/ImmGenATAC18_AllOCRsInfo.csv

CHIP-ATLAS transcription factor binding analysis

Transcription factor enrichment analysis was conducted on the “ChIP:TF and others” data set across the Homo Sapiens (hg38) and mus musculus (mm10) across all cell types. Summarized data is found in Tables 3.2-3.3. This dataset has over 15155 transcription factor binding experiments for humans and 13000 for mice. Blood cells are comprised of a plurality of the cells studied in both specifies (4441/15155 human (29%), 3600/13,156 (27%)). All significant epitope tag-promoter binding interactions (GFP and biotin) were excluded from this analysis. All transcription factor promoter interactions reported in this paper have a $p<1*10^{-5}$. Enrichment analysis done for *HK1/Hk1, HK2/Hk2, HK3/Hk3* in both mouse and humans. The publication of this online tool can be found Oki Ohta, et al. EMBO Rep. 2018.

Single nucleus spinal cord sequencing

Data collected from Yadav and Matson, et al. bioRvix.org 2022 (https://vmenon.shinyapps.io/hsc_biorxiv/). The tissue for this study was collected from 7 organ donors. This dataset identifies 65 unique cell types in the human spinal cord. Like

the GTEX analysis above, repeating cell subtypes with no HK1/HK2/HK3 expression were filtered out to increase clarity. This data can be found in figure 3.9

Alternaria model of asthma

For Alternaria-induced lung inflammation, mice were anesthetized with isoflurane and challenged intranasally with 8μg Alternaria extract (Greer Laboratories) every 3 days for 4 total challenges before analyzing the day after the final challenge (Palmer et al., 2019). In order to perform the FDG uptake study, the mice were injected with tracer 40 minutes prior to sacrifice. The remainder of this experiment performed in a manner similar to prior publication Reinfeld Madden et al. 2021.

Hk3 expression in mouse myocardial infarctions

Cardiac tissue from *Pdcd1*,*Ctla4* KO mice was harvested similarly to {Wei, 2021 #358}. Myocardial infarctions were performed similar to {Terker, 2021 #627}. RNA was harvested from freshly isolated tissue, and qPCR was performed as described above.

IBD TAMMA analysis

Massimino et al. 2021 established on online tool to examine RNAseq data from 26 published Crohn' s Disease and Ulcerative Colitis studies, representing over 10,000 patients. On this tool, it is possible to compare RNA expression of human genes across many impacted tissues from patients with inflamatory bowel disease. Comparisons done in this analysis were between matched tissues in healthy and diseased patients. The four comparisons conducted in this analysis were HK3 levels in (1) Rectums in UC vs control,

(2) Colons in UC vs control, (3) Ileums in CD vs control, as well as (4) Blood monocytes from CD patient's vs blood monocytes from healthy controls. Padjusted is 7.2*10^-9 for HK3 in blood monocytes between CD and healthy. All the other p values are less than the FDR for this basal analysis ($1x10^{-10}$). This data appears in Figure 3.10D.

Glucose fixing enzyme expression in autoimmunity analysis

Data from Aune et al. 2017 is publicly available. This study evaluates blood RNA signatures from a host of VUMC patients with autoimmune diseases. The expression of the Low K_m HKs and GlUT1 were taken from Supplemental data file 1 in Aune *Autoimmunity* 2017. The GEO accession number for the raw data is GEO92472. This data appears in 3.10E

COMBAT COVID19 database RNA expression

The COMBAT COVID study examined blood RNA expression across different populations of patients who had the novel coronavirus (COVID19). Expression of *SLC2a1* (GlUT1) and *HK3* were quired in the COMBAT COVID database. This shiny app developed by the consortium authors (https://shiny.combat.ox.ac.uk/shiny/diffexpr/) was used to examine expression. Log Normalized RNA seq data can be seen here https://zenodo.org/record/6120249#.YlIBINPMIqw.

Culture conditions for cell line work in chapter 3

iBMDMs, B16, MC38, and LLC cell lines were grown in DMEM with 4.5 g/l glucose + 10% FBS and Pen/Strep. For stimulation assays, cells were plated $1x10^5$ in a six well

plate and allowed to grow for 36 hours. Then the cells were stimulated with cytokine from 8-24 hours. The dosing of the cytokines was performed at the following concentrations: IFNγ 50 ng/mL, LPS 10 ng/mL, IFNα 50 ng/mL, IL6 10 ng/mL, TGFβ 13.3 ng/mL, IL4 50 ng/mL, IL1β 20 ng/mL. Ruxolitinib was given at doses of 100 nm and 250 nm. The cells were given Ruxolitinib and IFNγ at the same time (8 hrs for RNA analysis, 24 for protein).

Protein Extraction/Western Blot Protocol

Whole cell lysate was extracted using radioimmunoprecipitation assay (RIPA) buffer supplemented with 1x Halt protease and phosphatase inhibitors (Thermo Fisher Scientific). Cells in 6 well plates were lysed in 100 uL of RIPA + Thermo Halt diluted 1:100. These tubes then sat on ice for 15 minutes. After lysis, cells were spun at 15,000g for 15 minute to pellet Protein concentration was quantified with a Pierce BCA assay (Thermo Fisher 23227). All lysates were quantified in technical triplicates at 1/10 dilution. Samples were boiled with 4x Laemmli buffer (BME 1:10 diluted). 20-40 ug of protein/lane were run in TGX 4-20% gels. They were run at 100v for approximately one hour (until the dye front reached the bottom of the cassette).

Transfers were conducted using the Transblot turbo multi-MW setting. Blots were blocked in 5% milk resuspended in TBST for at least 1 hour at room temperature. Primary antibodies were diluted as follows HK1 (Cell Signaling Technologies 1:1000), HK2 (Cell Signaling Technologies 1:1000), HK3 (curtsey of the Ardehali Lab (1:2000), actin (1:2500 Abcam) and stained at 4% overnight in 5% Milked resuspended in TBST. Blots were then washed at least three times for 10 minutes in TBST at room temperature. After sufficient washing, appropriate secondary antibodies were added at 1:40k dilution, resuspended in

5% milk in TBST. Secondary incubation occurred at room temperature for 45 minutes. Then the blots were washed at least 4 times in TBST and imaged on the BioRad Gel imager under the chemiluminescence protocol. The ThermoPhemto and Pico ECL reagents were used to visualize bands. These products are diluted 1:1 prior to placing on the blots for 5 minutes.

Immungen microarrary gene skyline analysis

Hk1,Hk2,Hk3 were queried at this online data portal that's examines the impact of IFNα/IFNγstimulation on transcription across a variety of CD45+ cell types from mice (http://rstats.immgen.org/Skyline_microarray/skyline.html). From this website, the data can export as a spreadsheet and the graphs were made in prism. Data is present in Figures 3.12F-H.

Pan TCGA expression of immune genes

Processed and normalized RNAseq data were obtained for 9264 tumor samples across 24 cancer types from The Cancer Genome Atlas (TCGA) (Rahman et al., 2015). These data and corresponding clinical data are available under Gene Expression Omnibus (GEO) accession number (GSE62944). Expression levels (log2(fpkm)) of select genes (*PTPRC*, *CD68* and *HK3*) Figures 3.13A-B,E respectively were assessed these genes between the 24 cancer types included in the TCGA dataset.

CD68 immunofluorescence

Human ccRCC TMA was provided by Scott Haake and VUMC pathology. Paraffin-embedded TMA slides were prepared for immunofluorescence and stained with CD68

(cell signaling #76437) as previously described (Sorrelle et al., 2019). Briefly, slides were deparaffined in xylene and rehydrated in serial ethanol dilutions. Antigen retrieval was performed by heating slides for 17 min in Tris EDTA buffer, pH 9 in a pressure cooker at 110˚c. Slides were cooled to room temperature and then blocked with 2.5% horse serum (vector labs). After blocking, slides were incubated overnight at 4˚c with anti-CD68, dilution 1:500 in 2.5% horse serum. Slides were then incubated in anti-rabbit HRP secondary (vector labs) for 1hr at room temperature the following day and subsequently incubated in 1:500 Opal 570 (akoya) for 10 minutes. Slides were then mounted and cover slipped using antifade gold mount with DAPI. Stained images were acquired using a Keyence digital microscope and analyzed with Fiji software for analysis. Quantification of CD68 was done by measuring total amount of CD68 divided by total area of tissue.

CPTAC data analysis

For tumor vs normal comparison, data was taken from https://cprosite.ccr.cancer.gov/#/. Expression of HK1/2/3 were queried in this database in ccRCC. This data can be seen in Figures 3.13F,3.14A-B. For normalized expression across kidney cancer stages, data was exported from https://pdc.cancer.gov/pdc/analysis/dbe94609-1fb3-11e9-b7f8-0a80fada099c?StudyName=CPTAC%20CCRCC%20Discovery%20Study%20-%20Proteome as a GCT data set, which allows stage information to be retained with normalized protein expression. This data can be found in Figures 3.13G, 3.14C-D.

Survival analysis in TCGA

Survival Analysis in TCGA performed in GEPIA. HK1, HK2, $HK3^{hi/lo}$ expression was set at the median value. The impact of HK1/HK2/HK3 on ccRCC survival was examined as well as the impact of HK3 on papillary and chromophobe survival. These analyses can be found in Figures 3.13H, 3.14E-H.

Hallmark analysis of $HK1^{hi}$/$HK2^{hi}$/$HK3^{hi}$ tumors

RNAseq data for the ccRCC TCGA samples (KIRC; N=485) was obtained from GSE62944 (Rahman et al., 2015). Differential gene expression analyses between *HK1*, *HK2* ,*HK3* high and low expressing tumors was calculated using the linear models (Limma) with correction for multiple testing (Ritchie et al., 2015). ccRCCs were categorized as high or low for *HK3* expression implemented the mean as the cutoff. Functional annotation of differentially expressed genes (FDR<0.05) was performed using Term Geneset Enrichment Analysis (GSEA)(Subramanian et al., 2005) (Mootha et al., 2003).This data can be found in Table 3.4 as well as Figure 3.13I.

CiberSortX on $HK3^{hi}$ tumors

Digital flow cytometry to estimate immune cell infiltration in each tumor was performed using CiberSortX (Newman et al., 2019). Significance for CiberSortX profiles between high and low *HK3* expressing tumors was assessed by two-sample Wilcoxon (Mann-Whitney) test. This data can be found in Figure 3.13J.

Analysis of genes in TREM2^{hi} tumors

For TREM2 analyses, RNAseq data for 157 ccRCC tumors was obtained from Obradovic et al. 2021. Raw counts were preprocessed and normalized (varianceStabilizingTransformation) using DESeq2 (Love et al., 2014). TREM2^{hi} tumors were identified based on the signature derived from Obradovic et al. 2021. Genes with an FDR<0.05 were considered significantly different in the TREM2^{hi} vs TREM2^{lo} cohort. This data can be found at Figures 3.13K, 3.14I-J.

Single cell analysis of Bi et al 2021.

Sample analysis was done using Scanpy. Scanpy is a scalable toolkit for analyzing single-cell gene expression data built jointly with anndata. It includes preprocessing, visualization, clustering, trajectory inference and differential expression testing. The processed single cell RNA-Seq data was deposited by Bi et al., 2021 and was accessed via the Single Cell Portal: https://singlecell.broadinstitute.org/single_cell/study/SCP1288/tumor-and-immune-reprogramming-during-immunotherapy-in-advanced-renal-cell-carcinoma#study-summary.

First, droplets with greater than 3000genes per count, and/or more than 5% of counts attributed to mitochondrial genes were removed prior to analysis. To normalize each cell by total counts over all genes, so that every cell has the same total count after normalization, counts per cells were then normalized to 10k counts per cell. The sample was next log transformed for further preprocessing. Lastly, droplets with less than 200 genes per cell, and genes in 3 or less cells were also removed in the preprocessing stage.

The resulting merged Anndata object dataset included 20,947 cells and 26516 genes detected genes across the eight samples.

Principal components analysis (PCA) was performed on the integration-transformed expression matrix, and the first 48 principal components were used for Leiden clustering of cells with a resolution parameter of 1. Uniform manifold approximation and projection (UMAP) was performed on the same PCs with 10 nearest neighbors for visualization in two dimensions. From here, figures provided demonstrating lineage and *HK1*, *HK2*, and *HK3* expression were generated using the previously demonstrated annotations by Bi et al. The lineage data can be found in Figures 3.15A-B.

To investigate the myeloid lineage further, an Anndata object was generated using the lineage characterization by Bi et al. generating a new Anndata object data set with 3938 cells and 26516 genes. To address batch effects across samples, the new Myeloid Lineage dataset was batch corrected using ComBAT. https://scanpy.readthedocs.io/en/stable/generated/scanpy.pp.combat.html. ComBAT corrects for batch effects by fitting linear models, gains statistical power via an EB framework where information is borrowed across genes. The Myeloid lineage data can be found at Figures 3.15C,3.16A-C.

Principal components analysis (PCA) was performed on the batch-corrected expression matrix, and the first 30 principal components were used for Leiden clustering of cells with a resolution parameter of 1. UMAP was performed on the same PCs with 10 nearest neighbors for visualization in two dimensions. From here, figures provided demonstrating leiden clusters, and expression patterns for HK1, HK2, and HK3 were

generated. Genes were then ranked leiden clusters of interest using the Wilcoxon rank-sum test. These gene lists can be found in Figures 3.15D,3.16D.

Low K_m HK expression in the setting of neoadjuvant TKI therapy

Wood CG et al. 2020 conducted a clinical trial of neoadjuvant pazoponib treatment in patients with non metastic ccRCC. RNAseq was performed on matched normal tissue, tumor prior to treatment and tumor post treatment. Log normalized data was provided by Dr. Ben Vincent.

IMmotion 151 data analysis

IMmotion 151 randomized patients to VEGF TKI alone (sutent) or VEGF inhibitor + aPDL1 anget (Bevicizumab+Atezolizumab). Tissue prior to treatment was collected and ultimately RNA was collected. Prior work performed RNAseq on these samples and generated 7 theranostic clusters using a non-negative matrix factorization algorithmn. For the heatmap in Figure 3.15F, the RNAseq data provided by Genetech was log transformed. Row normalized z scores are shown in the heatmap. Columns are sorted by NMF group which is published in Motzer et al., *Cancer Cell* 2021. Rows are clustered with hierarchical clustering. Heatmap made using the complex heatmap package (Gu et al., 2016) For Figures 3.15 G/H, 3.17 C/D, log transformed expression of the genes of interested was plotted.

Cancer Immu Database Analysis

Cancer Immu has combined multiple datasets where patient genomic and transcriptomic data are correlated to outcome on anti-PD1 and/or anti-CTLA4 therapy

(http://129.59.197.30:3838/Cancer-Immu/) (Yang et al., 2021). To generate a cohort similar to the size of Motzer et al. 2021, all the melanoma datasets with pretreatment biopsies were collated. In total this represent 219 patients. *HK3* RNA levels were examined in responding and non-responding patients. Additionally, the impact of *HK3* on patient overall survival was analyzed.

Chapter 5: Discussion

The implications of this dissertation are wide reaching in the practice of human medicine and basic cancer biology. The mainstay technique developed in this work, to trace glucose (or any F18-based tracer into different cell fractions in a tissue microenvironments), pushes *in vivo* metabolic studies into the single cell era of biology. For the past 150 years, whether they be histological, genomic, transcriptomic, metabolomic, or proteomic analysis, bulk tissues have been used in the field of cancer biology. Thus, it has been difficult to tease out how the diverse cell population of a tumor contributes to any described phenotype. Only recently (the last 10 years) have single cell (sc) studies become commonplace and those are mostly currently restricted to RNA or DNA sequencing (Gohil et al., 2021). Today, applying these technologies spatially across tissue specimens is occurring more frequently, but still is rare (B. Chen et al., 2021; Hoch et al., 2022). Therefore, we still do not understand the metabolic programs of individual cell subsets in the TME today.

Technical advances in dissecting cell population metabolic programs

There are limitations with current technologies that restrict our ability to decern individual cell metabolic programs. Conducting single cell studies for ultimate metabolomic analysis is challenging because many metabolites have short half-lives (seconds to minutes) and thus require immediate freezing of the tissue to make precise and accurate measurements. This rapid procurement of tissue prevents single cell digestion, flow sorting, or other mechanisms to separate cell population prior to analysis. Therefore, our understanding of the metabolic TME until this time is a weighted average

of metabolic program activity in each cell type multiplied by the tissue abundance of that cell of interest. So, it is possible to see significant changes in a specific metabolic pathway, without any specific cell type increasing that program much greater than baseline. For example, Faubert et al. 2017 demonstrates that in lung tumors circulating lactate is consumed and used as metabolic substrate (Faubert et al., 2017). However, we have little idea at this moment which cells are performing this specific metabolic task. Is it the transformed tumor cells or is it the infiltrating or supporting stroma metabolizing the lactate? There is recent evidence that M1 macrophages can use lactate molecules to modify their histones and drive transcription of M2 genes (D. Zhang et al., 2019) to have a more pro-tumor pheontype. Therefore, it would not surprising if tumor infiltrating myeloid cells were using this lactate for their suppressive function and thus contributing to the labeling pattern seen by Faubert et al. 2017.

To address the previous generation of bulk metabolomics in the TME, this project undertook a novel technological advancement to evaluate metabolic uptake across cell subtypes in the TME. By using F18 tracers like FDG, these studies are inherently clinically relevant given the widespread adoption of this technology. Another benefit of this approach is that radioactive substrates are given at tracer doses. By not using saturating concentrations, there is less concern that administration of the compound of interest changes activity of cellular enzymes and glucose hormonal regulation due to the exogenous supplementation of tracer of interest. This contrasts with C13 labeling patterns which often follow patterns of mass action (Li et al., 2022). For the purpose of this work, Li and colleagues demonstrates that increasing C13-glucose intravenously alters insulin levels in the mice where they are performing metabolic flux analysis. Additionally, some

tracers like FDG are functionally inert once taken up by cells (end-tracers). Therefore, concern about metabolite turnover becomes negligible in the final reading of cellular radioactivity.

Using this new set of tools, we were able to observe that myeloid cells consume more glucose than other cells in both the TME (Reinfeld et al., 2021) and inflammatory microenvironments (Chapter 3). This observation (which at first seems paradoxical to the Warburg effect) has been validated by numerous groups in the time around and following its publication. FDG^{hi} lung tumors were shown to have overall higher levels of CD68 (Leitner et al., 2022), a pan macrophage marker. Josh Rabinowitz's group examined the fate of C13 glucose across mouse organs and observed that immune organs are the only location where C13-gluocse is rapidly consumed into glycolytic intermediates (TeSlaa et al., 2021). These immune tissues (spleen and blood) are inherently rich in myeloid cells when compared to solid organs. Additionally, a group examined FDG uptake in the Alzheimer's brain, and demonstrate that the CD11b+ phagocytic microglia are glucose consuming in this disease state (Xiang et al., 2021). Therefore, our observation that these myeloid cells are programed to constantly consume glucose appears to be a hallmark of many biological systems.

It is worth noting, that at the time, other groups are employing diverse techniques to profile the metabolism of individual cell populations. These technologies have been used on flow sorted bone marrow (DeVilbiss et al., 2021), C13 labeling *in vivo* (Lau et al., 2020), as well as spatial MALDI-TOF imaging combined with C13 labeling (Wang et al., 2022). These studies support our study's insights into the notion that individual cell populations have unique metabolic properties that promote their physiological function.

Additionally, these groups have used these studies to illustrate that *in vivo* metabolic labeling patterns differ profoundly from previous metabolic understandings derived from *in vitro* studies. Ma et al. 2019 demonstrated that T Cells in antigen response oxidize more glucose than expected while Lau et al. 2020 elucidated that cancer associated fibroblasts can drive mitochondrial oxidation of glucose in cancer cells. These findings were not previously appreciated because cell culture media contains supraphysiological concentrations of most substrates that when provided at those doses can alter metabolic activity and pathway reliance (Cantor et al., 2017; Rossiter et al., 2021). The focus on culturing cells in isolation *in vitro* creates interpretable data but prevents an understanding of how heterotypic cell interactions drive metabolic programs. Ultimately this effort for reproducible models (by having single cell types cultured in metabolic excess) limits the translatability of many previous papers in the field of cancer metabolism when the *in vivo* microenvironment is rich in diverse cell types, has orders of magnitude differences in some metabolites and has three-dimensional structure. These three features are not considered in traditional cell culture today even though all known to alter cancer cell behavior and aggressiveness

Given the heretical nature of our myeloid increased glucose uptake finding, it is important to discuss the historical evidence that supports this work. Warburg's initial observations, both that tumors continue to make lactate in the presence of oxygen and that lactate accumulates in tumor draining veins, suffer from experimental design limitations of his time. These observations occurred in bulk tissue in immunocompetent animals. Therefore, it is possible that myeloid and lymphoid cells in these models were contributing to the values he observed. Additionally, Warburg's manometry studies where

he observed that tumors do not respirate as expected happened *ex vivo* in tumor slices rich with immune cells in solutions with excess metabolic substrate. His work was not modeling the physiological glucose concentration (0.5 mM-2mM). Realistically, the phenotypes he observed could have been from saturating metabolic pathways and not replicating the actual *in vivo* concentrations. Therefore, the data put forth in this thesis may support Warburg's original view of the TME. Glucose is constantly consumed, and lactate is made in the space Virchow and later Dvorak noted as "the wound that would not heal" (Dvorak, 1986). We observe that in every model we tested, the tumor FDG uptake is greater on a per cell basis than the spleen. This work suggest that the myeloid cells contribute significantly to the glucose consumption, yet it remains unclear which cell population is directly responsible for the lactate accumulation.

Therefore, a main future direction of this work is to repeat similar studies but with infusing C13 as opposed to F18 metabolites. The power of C13 in these types of studies would allow our group to see if glucose has different cellular fate in these TME resident cell types. Based on the differences in HK isoform usage across cell times, I would hypothesize that, these diverse cells do ultimately flux glucose into different subcellular metabolic pathways. Myeloid cells are most likely diverting glucose into more cytosolic metabolic programs (like the PPP), while lymphoid cells and cancer cells are oxidizing this vital nutrient and using in the mitochondria. However, we cannot make those claims based on our F18 studies because they solely demonstrate metabolic uptake.

As alluded to previously, Lau et al. 2020 used C13 glucose *in vivo* in an approach to see how individual cell population use glucose in the pancreas cancer TME. In this work, mice were labeled overnight, tumors were digested at 37ºC, and then the single cell

suspensions were flow sorted to obtain populations of interest. They examined C13 labeling in macromolecules (like cell membranes and overall protein content) to describe differential metabolic activity across divergent cell types. The overnight labeling was necessary to increase C13 label in large macromolecule end products that would not degrade throughout the process of obtaining pure single cell populations. This minimizes potential artifacts that can occur during the 37ºC tissue digestion and room temperature flow sorting process. Since that work was published, Sigma-Aldrich now sells a collagenase that works at 4ºC. Therefore, the same studies in Chapter 2 could be conducted in the cold room, to evaluate the contribution of serum glucose glycolytic intermediates within these different TME resident populations. The labeling could happen over a shorter time (with 40 minutes-1 hour) in alignment with the human studies from the DeBerardinis lab (Courtney, Bezwada, et al., 2018; Faubert et al., 2017; Johnston et al., 2021). In this approach, one could theoretically look at intermediate metabolites directly, which the Vander Heiden group was unable to do. As mentioned previously, Rabinowiz group (Wang et al., 2022) has now also developed iso-imaging, where the isotopically labeled glucose is infused in the mice, organs are harvested and then MALDI-TOF spatial mass spectrometry is performed on the tissue. By staining serial sections with immune markers, it could be possible to see differences in labeling in immune rich sections of tumors vs immune poor. However, this technology has a relatively large resolution (50 uM) so it would be unable to say if a given metabolite went into a tumor macrophage or a cancer cell specifically. Their recent publication can analyze the intermediate metabolites (like lactate). The Rabinowitz group used this technology to validate their previous finding that kidney tissue can uptake exogenous citrate to stock the Kreb's Cycle

(Jang et al., 2019). With the MALDI-TOF imaging, this group beautifully demonstrated that it is the kidney cortical epithelia, which undergo the citrate catabolism while the medullary cells do not consuming this available metabolite.

Another interesting comparison would be to feed the mice C13-glucose chow and compare the observations of consumed isotopes versus infused isotope. The implementation of dietary manipulation as the treatment of cancer is a rapidly growing field, yet little interest is garnered from basic science discoveries and rigorous pre-clinical models. It would behoove the field to understand how metabolites consumed in the diet contribute to the biomass of the TME for doctors to provide patients with appropriate council on diet. Understanding these differences, would help contextualize many of the current claims made based on pre-clinical studies that use infused tracers or examine steady state metabolomic profiles.

A major limitation to the F18 technique is the relatively sort half-life and the institutional barriers to flow sort populations of interest. The short half-life restricts how many successive bead sorts can be performed. Based on our studies, it appears that 2-3 consecutive sorts can be performed to ensure that enough radioactive signal is present to have reliable data that demonstrates biologically significant differences. Increasing the amount of bead sorts and thus increasing the number of half-lives prior to reading the samples, would create smaller differences between the cell fractions. Besides the time aspect of using the beads purification, they are limitations in that enrichment of rare populations is not technically possible for low abundant cell types. Maximally, the commercial beads result in a 5-10x fold enrichment. So, if a desired cell population is less than 1% of the total TME, it is hard to generate very pure fractions. We observed this

phenomenon when bead sorting for the CD103+, CD11c+ conventional dendritic cell 1 (cDC1). There is significant enrichment for this cell type, and we observe increase glucose uptake in the cDC1 enriched fraction, however, it is not an ideal average purity to make strong claims (approximately 20% of the events). Understandably the VUMC flow core will not permit us to use radioactive material on their machines. With a flow sorter, we could get at least 5, if not more, very pure, and very specific populations of interest, in a shorter amount of time. However, we would probably have to stagger mouse injections and standardize the time difference between mouse injection and reading the samples on the Hidex gamma counter to eliminate all sources of variability. With this type of equipment in hand, we could make stronger assertions about the glucose uptake capacity of different myeloid and T Cell subsets. Additionally, we could evaluate glucose uptake in the non-tumor non CD45+ compartment like fibroblasts or endothelial cells.

Improving clinical imaging to better reflect cancer cell specific metabolic programs

Moving forward, this work conceptually can contribute to the field of molecular diagnostics. FDG-PET imaging is a hallmark of cancer care. Interestingly, it can also be used to diagnose different inflammatory conditions that lack any proliferating malignant cells (Love et al., 2005). However, it is not an effective imaging modality in all tumor types, in conflict with Warburg's original postulate that increased glucose uptake is a hallmark of cancer. The most striking example is the lack of clinical utility of PET imaging in ccRCC (Liu, 2016) . This disease is quintessentially a metabolic tumor type (Linehan et al., 2019). Almost all patients lose VHL functionality, thus stabilizing the metabolic transcription factor (HIF). Recently, *in vivo* C13 glucose studies from the DeBerardinis group confirmed

increased *in vivo* glycolytic flux into lactate labeling in 5 human ccRCC patients (Courtney, Bezwada, et al., 2018). Even though FDG imaging has been demonstrated to not be helpful clinically, in research studies it has been noted that patients with very aggressive often metastatic ccRCC (which is known to have even more inflammation) have FDG PET positive tumors and metastases (Majhail et al., 2003). This profoundly confusing fact led to the generation of the experimental schema implemented in Chapter 2 where our group sought strategies to evaluate the cellular uptake of FDG in immune and tumor cells from the TME.

Our data suggest that FDG uptake can be a surrogate for many processes other than cancer cell proliferation in the TME. The DeBerardinis group has published that there is in fact little correlation between FDG uptake and glycolytic C13 labeling in human lung cancer patients (Kernstine et al., 2020). In this study, FDG avidity did positively correlate with proliferation (Ki67), tumor size, and lactate uptake. Therefore, it may not be surprising that FDG signal could indicate large immune infiltrates, and/or myeloid cells disposing of dead cellular debris from the wasteland which is the TME. Additionally, in today's world of clinical immuno-oncology, a new therapeutic paradigm that is being ushered in across tumor types is to ultimately activate the patient's immune system to recognize their malignancy. Therefore, it has been that documented that some patients may have increases in FDG uptake on immunotherapy agents (as if their tumor was progressing), but ultimately demonstrate a positive response to therapy (Aide et al., 2019). This is one of the many paradigms of pseudoprogression that make traditional radiographic tumor assessment difficult in an age of cancer immunotherapy.

Given this possibility for lack of clinical correlation with traditional views on FDG uptake (where increase in signal is a correlate for tumor progression), there is a focus on the development of immune specific tracers. Groups have added radioactive nuclides (e.g., Zr89 or Ga68) to antibodies/nanobodies that recognize key immune oncology targets (e.g., PD1, PDL1 (Niemeijer et al., 2018) , and CD8 (Tavare et al., 2016)). These tools may be useful in selecting patients to receive therapy (i.e., if the tumor is PD1 PET positive), the target is present in the TME. However, these tools face large barriers to track patient response to therapy, which is a large source of clinical ambiguity. CD8 T cells are prognostic in almost all tumor types but are anti prognostic in ccRCC. PDL1 and PD-1 also have apposing prognostic significance across disease subtypes. It remains unclear how these types of markers will change while a patient is on therapy and how that might differ in responding and non-responding patients. We also currently do not appreciate whether those changes are consistent across histotypes of cancer and locations of metastasis. It can be hypothesized that in each tumor type where immunotherapy is used today, the PD1/PDL1/CD8 PET could be divergent. In one tumor type, these markers of immune activation all increase as a patient's tumor shrinks and, in another subtype, the markers decrease as the patient's tumor continues to grow. Certain biomarkers, like tumor mutational burden and tissue PD-L1 expression, demonstrate histotype specific benefits. So, it is reasonable to predict that similar limitations may exist when radioactive antibodies are used to evaluate the same targets. This perspective originates from the fact that neither PD-L1 nor TMB are predictive of ccRCC checkpoint blockade response. Zero percent of ccRCC patients have a TMB > 10 mutation

/Megabase (the FDA approved tissue agnostic biomarker for αPD-1 treatment). However, these drugs do provide survival benefit in unselected ccRCC patients (Valero et al., 2021).

Additionally, in clinical medicine today there is little infrastructure for the implementation of Zr89 or Ga68 across 100,000s of patients. These checkpoint blockade therapies are currently the most widely and most adopted therapy in oncology. The demand will only increase as these drugs are used in earlier stages of treatment. Therefore, companion imaging diagnostics need to rely on infrastructure that are already widely abundant. Since FDG is the most common PET scan in clinical medicine today, cyclotrons and clinical protocols already exist for F18 based tracers. F18 is the preferred radionuclide to attach metabolic substrates and thus makes them more translatable for patients today. Due to F18 having a relatively short half-life (110 minutes), it is less ideal to use this radionucleotide with antibodies or protein binding moieties that have different binding kinetics then small molecule catabolism.

Therefore, an approach that specifically image cancer cell metabolism may be the best method to track the diverse landscape of cancer therapeutics today. In clinical oncology in 2022, clinicians use a variety of immunotherapy, radiotherapy, targeted therapy, and chemotherapeutics. Ultimately, clinicians need imaging modalities that communicate whether the tumor cells are growing or dying. Does the patient in front of me require more therapy or is it safe to stop this therapy to prevent more toxicities? It appears understanding cancer cell metabolism within the TME *in vivo*, can allow for this type of diagnostic. It is not a novel concept to use more diverse radioactive metabolic substrates to examine tumor growth: groups have developed tracers that examine other metabolic pathways *in vivo*. Our studies in Chapter 2, use a F18-Gln that has been used

to image patients in many studies (Li et al., 2019; Schulte et al., 2017). However, these types of metabolic tracers have not been rationally designed. Instead, groups have used models of cancer cell metabolism where the transformed cell is the dominate consumer of all metabolic substrate. Therefore, any widely available metabolite could be an ideal imaging tool in cancer. I coin this view of cancer metabolism as “the hungry hungry hippo hypothesis” (H^4). Cancer cells continue to consume all available nutrients with little regard for the TME and other selective pressures that exist within it.

Our studies suggest that this notion is not true for all metabolites. At least for some metabolites (like glucose), individual cell populations (CD11b+ myeloid) have gene transcriptional programs that promote consumption of one metabolite instead of another. Using the H^4 model is problematic to select an ideal tracer because the TME is filled with proliferating lymphocytes, myeloid cells, endothelial cells, fibroblasts and thus metabolites that are associated with pro-growth, pro-proliferation programs may be uptake by multiple cell types (similar to FDG) (Andrejeva & Rathmell, 2017). These types of proliferation associated metabolic tracers would not help a clinician or radiologist decern between cancer cell and immune cell activation.

Another common mechanism to evaluate the feasibility of a metabolic tracer is in examining bulk RNA sequencing data and validating these metabolic trends with tissue IHC from the mouse tumor models or human tumor type of interest. These analyses, however, are insufficient to argue if that the catabolism of the metabolite of interest would be performed by transformed cells or by the cast of infiltrating stroma. Groups today are improving their target validation processes with conducting co-immunohistochemistry/immunofluorescence to examine which cell types are expressing

the catabolic enzyme or transporter of interest. Sadly, these types of tissue studies are not truly necessary to design and synthesize new tracers. It is worth noting that Glut1 protein levels were much higher on the MC38 tumor cells *in vivo* than any immune cell population (as assessed by flow cytometry). Yet, these cancer cells do not retain elevated levels of FDG. This suggests that the rate limiting enzymes for tracer metabolism (in the case of FDG, the HKs) may be a better predictor of cell fate than the transporters themselves.

Our data would suggest that tracers that examine fatty acid catabolism or glutamine catabolism would be more specific for evaluating tumor growth. We evaluated the F18-glutamine uptake in a series of mouse tumor models but did not evaluate the F18 fatty acids like oleate which has been used previously in pre-clinical studies (DeGrado et al., 2010; Witney et al., 2014). Additionally, the C16-BODIPY study conducted in Chapter 2 occurred *ex vivo*, thereby decreasing the translational aspect of that finding. Dr. Marcia Haigis' group, however, did publish similar findings, that fatty acids are consumed by CD45- tumor cells (Ringel et al., 2020). This increase in fatty acid catabolism contributes to the increase in tumor aggressiveness in obesity.

The framework used in Chapter 2 can be used to find develop tumor specific metabolic substrate. Historically papers would suggest that RNA transcriptomics has little role in predicting functional metabolic patterns (Aird et al., 2021; Lee et al., 2014). Interestingly, this was not observed in our work. Our NanoString metabolism data would predict that the myeloid cells consume glucose and cancer cells metabolize glutamine and fatty acids. Using a series of different approaches, we did in fact see that unique pattern that was predict by the NanoString analysis. Why could there be divergence in

our case where the transcriptomics conducted reliably predict metabolic labeling patterns? One reason is that prior attempts to validate RNA transcriptomics and metabolomics originated from bulk RNA-sequencing where there is contamination from the many diverse cell populations in the TME. Additionally, groups have tried to implement *in vitro* derived signatures in non-physiological media on plastic substrates and applied them to bulk *in vivo* data sets. Our approach is quite different in that we separated out the cells of interest from an *in vivo* model, subsequently performed deep transcriptomic characterization and then followed that up by cellular tracing techniques. This provides promise that as scRNA sequencing technology improves to ultimately provide deeper, richer datasets, we can predict and thus evaluate more specific metabolic tracers for the detection and monitoring of cancer cell progression. Today, it is very difficult to use 10x's sc data to appropriately do so because of the small amount of UMIs/cell returned in this platform. Another area for growth in the integration of single cell transcriptomics and metabolic assessment is spatial scRNA sequencing. However, the ROIs on the 10x Visium assay as well as the Nanostring Geomx platform are relatively large (50 μm). Thus each ROI contains multiple cell types in different proportions, creating a situation where deconvolution is necessary to find cell type specific metabolic programs. This is like the limitations presented by spatial metabolomics at this junction(Wang et al., 2022). It is worth noting that both companies claim to be unveiling subcellular tissue-based RNA-transcriptomic platforms in the Fall of 2022, (CosMx and Visium HD) unfortunately after the completion of this thesis (He et al., 2022). But these high definition platforms will be immensely helpful for further metabolic probing of the TME.

It is worth considering that our CD45- tumor cell fraction is heterogenous and compromised of important CD45- stromal cells like fibroblasts and endothelial cell populations. We created Thy1.1+ MC38 cell line and show that when these modified MC38 are specifically enriched with Thy1.1 beads, we observe the same phenotype, that immune cells consume more per cell glucose than transformed tumor cells. This approach can be further used and modified to go deeper into the metabolic programs of cancer cells. Cancer cell lines are easily amendable to lentiviral transduction or piggybac transposon insertion of this gene,Thy1.1. Thy1.1 is preferred in comparison to other tumor cell labeling strategies because other groups have shown that this congenic marker is less immunogenic (McKenna et al., 2011) (in comparison to GFP or other florescent proteins (Day et al., 2014; Grzelak et al., 2022)). Therefore, the generation of more syngeneic Thy1.1+ cancer cell lines would be helpful with the goal of harvesting RNA specifically from these Thy1.1+ cells after growth *in vivo*. With RNA collected specifically from these Thy1.1+ cancer cells from the TME, it would be possible to directly compare *in vitro* vs *in vivo* RNA programs. Additionally, one could experimentally alter numerous *in vitro* variables (growth media, 3D cultures, co-culture with immune cells) and interrogate how these culture modifications can alter cancer cell metabolism and transcriptomes to align more with the observed *in vivo* phenotypes.

A potential use for a series of Thy1.1+ murine cancer cell models would be to evaluate if there are shared metabolic programs across cancer types or if a disease specific approach may be needed to develop more ideal radiotracers. By purifying bona-fide tumor cells from relatively viable *in vivo* tumor models (MC38, RenCa, MLLAF9, EMT6) and then performing next generation RNA-seq, it would be powerful to examine

metabolic phenotype across cell lineages and mouse backgrounds. If enrichment of the same metabolic pathway were observed across these heterogenous cancer model, it would support the notion that there are shared metabolic features of oncogenic transformation. I would hypothesize an increase in glutamine catabolism is shared by all of these models based on our prior F18 experiment. Additionally, there may be quite divergent programs that are cell line specific and thus present opportunities for validation and new tracer development.

With these new cell lines, it would also be possible to examine the protein content or metabolic content (using techniques alluded to earlier by Lau et al. 2020) of these Thy1.1+ cells specifically using Thy1.1+ beads to lessen the cell stress during purification. Conducting these studies in immunocompetent and immunodeficient hosts (or with depleting antibodies) could allow for a dissection in how individual immune cell population alter cancer cell metabolic processes and/or protein expression.

Impact of cancer cell lineage on metabolic program

In collecting data for Chapter 2, I was surprised by the results from a study implementing a melanoma tumor model, YUMM, because it did not follow our typical pattern of myeloid glucose enrichment. In a study in collaboration with Ann Richmond's lab, we evaluated FDG uptake in one of the YUMM mouse melanoma models on anti-glutamine therapy (V9302). In this model, which is rich in myeloid cells, we see equal glucose uptake between the YUMM melanoma cells and the CD11b+ cells. Here we see again that this Warburgian H[4] is not true, because myeloid cells and tumor cells have equivalent glucose consumption. The YUMM cancer cells are not the dominate consumer of glucose on a live per cell basis. However, it was striking that these YUMM cells per cell

glucose uptake was much higher than the other models we used in our studies. The YUMM model is the only non-epithelial derived cancer model we examined; therefore, it becomes a natural question to ask whether cell of origin impacts metabolic phenotype. Melanomas are derived from neural crest stem cells, and thus it may not be surprising that they can engage in a transcriptional program that allows for heightened cellular glucose uptake whereas our other models were derived from mutant epithelia. The brain is an FDG positive organ at baseline, therefore certain transcriptional and phenotypic aspects of this lineage may promote glucose uptake at baseline.

With that observation where melanomas may have increased glucose uptake when compared to epithelial tumors, it would be intriguing to examine glucose uptake in tumors that originate from other stem cell populations. There are robust mouse models of acute lymphoid and myeloid leukemias (Kohnken et al., 2017) (ALL and AML respectively). AMLs arise in cells that are HK2+ elevated at baseline and have the ability to express HK3. Therefore, I would hypothesize that these tumor models take up more glucose than the infiltrating myeloid cells. Using an ALL model would be an appropriate control to evaluate whether all hematopoietic tumors cell can be highly glycolytic or that it is endowed to a certain subset of hematopoietic derived tumors. It would also be of interest to compare the labeling patterns in models of chronic myeloid leukemias vs acute leukemias given the basal difference in proliferation rate. A similar experiment could be done comparing more acute B cell leukemias, indolent lymphomas (follicular-like, aggressive lymphomas (diffuse large B cell), and multiple myeloma models. In each of these B Cell malignancies, a different progenitor drives disease progression. Therefore,

this study could act a surrogate to see the effect of developmental stage on malignant cell metabolism.

The Bosenberg lab at Yale has derived the YUMM cell lines from primary mouse melanomas with many different combinations of BRAF, PTEN, P53, Ras, etc. mutations to phenocopy the diversity of the tumors seen in the melanoma cancer genome atlas project (Meeth et al., 2016). Therefore, this set of tools presents an opportunity to evaluate the role of cancer mutation on tumor cell metabolic phenotype *in vivo*. A hallmark of modern cancer biology is the notion these distinctive genetic mutations dictate cancer cell phenotype. This observation has driven the development of personalized genomic therapies for cancer. However, there are very few situations where genomic mutation alone predicts response to therapy. Usually, inhibitor sensitivity requires the patient to harbor the druggable mutation **and** for that mutation to be in a tumor of a specific tissue type. For example, Vemurafenib (a BRAF V600E specific inhibitor) results in durable responses to melanoma and a few other rare tumor types (sarcomas, gliomas, etc.), however, as a single agent, it has mimical efficacy in V600E+ gastrointestinal malignancies (Subbiah et al., 2020). Additionally, recent advances in sequencing technology have allowed groups to deeply sequence histologically normal tissue. To the surprise of most cancer geneticists, histologically normal tissue from patients of all ages is enriched with mutations known to drive tumor formation (Martincorena et al., 2018; Moore et al., 2020). In combination, these observations suggest that mutation alone is insufficient to drive an oncogenic phenotype.

Given these recent findings, I hypothesize that the cell of origin has a greater impact on cell metabolism than the different mutations. In the line with the notion that

YUMM cell lines could behave quite similarly, even though they harbor different mutations, Meeth et al. 2016 demonstrated minimal differences in immune infiltrate in four of the YUMM cell lines they examined. Therefore, I would expect to see all the YUMM cancer cell lines to exhibit glucose uptake to a similar level to myeloid cells regardless of the gene mutation the cell line possesses. No one mutation in the YUMM cells would ultimately alter the degree of glucose uptake. Another set of exciting experiments would be to make these same oncogenic mutations in lung cancer models, and compare the uptake pattern across tumors that are genetically identical but derived from different cell lineages. This would be in line with recent data from Richard White's group that the basis for different mutational events in acral melanoma vs cutaneous melanoma is the oncogenic transforming capacity of the stem cell of origin (Weiss et al., 2022). They used zebrafish models of melanoma to show that acral melanoma oncogenes only cause tumors in the fish fins, whereas cutaneous melanoma oncogenes cannot induce transformation in the fin. Interestingly, the fish fin shares developmental lineage as the soul of the human foot, and thus provides compelling evidence in solid tumors that the stem cell of origin dictates whether an oncogenic event can be transforming. Similar work has been done in acute myeloid leukemias, where it is clear than only some progenitor states can be permissive for oncogenic transformation (Fisher et al., 2019). Therefore, I would support a model where the stem cell, or more broadly the histotype of tumor origin dictates the metabolic phenotype of the malignancy of interest. This does not, however, contradict our potential search for a cancer cell specific tracer. Given the shared nature of the program for cancer invasion and metastasis and that almost all cancer mutations

activate downstream mTOR signalling, it could be possible to find an upregulated metabolic pathway that could be targeted or imaged across malignancy.

It would also be potentially of interest to compare the metabolic uptake of the same cell line in different organs (like the lungs, brain, or kidney). It has recently been appreciated that certain tissue microenvironments can restrict metastasis. The oxidative microenvironment of skeletal muscles prevents breast cancer cells from successful colonization (Crist et al., 2022). Therefore, one can imagine the unique metabolic milieu of each organ driving selective pressures that force alterations in the cancer cell or immune cell metabolic program. I would imagine given the amount of data we and other groups have generated, that the myeloid cells would be glucose consuming in all tissues (as seen with the intrarenal RenCa model, and the validation of the MC38/CT26 phenotype in the AOM/DSS model). But for other metabolites, the organ metabolic set point, may drive new catabolic programs. Using genetically defined cell lines that metastasize to many organs could help interrogate some of those questions.

Enhanced cancer cell glycolytic reserve as a barrier to therapeutic targeting

Another peculiar observation when conducting these series of experiments occurred when conducting the Seahorse Glycolysis stress test on fractions purified from the MC38 TME. From a historical perspective, the Glycolysis Stress Test is the most similar assay to Warburg's original manometry studies. In the seahorse analyzer, cells are provided glucose acutely while the probes record the oxygen consumption and lactate formation that occurs in response to providing exogenous glucose. All the cell types from the tumor microenvironment can convert this extracellular glucose (10 mM, ~10x greater than what is available in the TME) into lactate to a similar degree. Then after glucose

stimulation, oligomycin (a mitochondrial complex five inhibitor) is provided to examine the magnitude of reserve glycolysis. What become noticeable in this assay is that all immune cell populations from the TME have negligible reserve glycolysis. However, the CD45- cancer cells do have a significant amount of glycolysis reserve. Similar results have been seen by the Beckerman lab, where oligomycin has minimal impact on the ECAR of tumor infiltrating lymphocytes in the Glycolysis Stress test (Beckermann et al., 2020). This experiment in total demonstrates that even though these MC38 cells are consuming less glucose than the myeloid cells (as seen in our FDG assay), when given an opportunity, they can increase glucose catabolism to a level greater than infiltrating cells. This assay, however, could be an artifact of the supraphysiological dose of glucose provided. A hallmark of any seahorse assay is to give these high doses of metabolic substrate to prevent the cells from running out of biochemical fuel during the experiment. However, it would be interesting to phenocopy the tumor glucose level by decreasing the concentration of glucose in the first injection and see how altering the exogenous glucose levels impacts ECAR as well as the spare glycolytic reserve.

This finding has profound implications for targeting cancer cell metabolism in the TME. It may indicate that cancer cells have more flexibility when their metabolic substrates are limited. How is this flexibility is endowed and what pathways are these substrates being shunted into during times of stress is yet to be determined. It appreciated that genetic mutations in cancer cells promote more primordial epigenetic states that allow cancer cells to engage in a wide variety of cellular programs that should not be accessible to a healthy mature cell population (phenotypic plasticity).

It also may be concerning that immune cells have minimal spare glycolysis ability. Therefore, immune cells may be exquisitely sensitive to anti-glycolysis agents. This provides some evidence why previous pharmacological attempts to develop anti-glycolysis agents like 2DG and 3-BPA may have not worked in human tumors. This class of drugs may ultimately exhibit anti-inflammatory properties like killing tumor resident T cells and promoting Treg differentiation before anti-tumor immunity or tumor cell death can be induced.

Targeting Cancer Specific Glutamine Metabolism

Our work suggests that glutamine metabolism is significantly elevated in the malignant epithelia at a transcriptomic and functional metabolic level. What is striking is that all aspects of glutamine metabolism are increased in the CD45- compartment: Glutamine uptake, glutaminolysis as well as general amino acid synthesis. This suggest that targeting only one aspect of glutamine metabolism (e.g. CB839 for the specific blockade of GLS) may be insufficient at reducing tumor burden. Instead, more broad anti-glutamine approaches would be needed to induce tumor regression. Dr. Johns Powell's group has extensively worked with DON and similar derivates (JHU-DON) to block all glutamine utilizing enzymes (Leone et al., 2019; Oh et al., 2020). However, this strategy has been quite toxic. It is yet to be seen how JHU-DON potentially alters the safety prolife of these glutamine antagonist agents. This molecules is still in early phase clinical trials.

Recently it has been noted that moonlighting abilities of metabolic enzymes may contribute to cancer cell growth more than their enzymatic function (Zhao et al., 2022). This finding suggests that solely targeting enzymatic activity with molecules like DON and

CB839 (a GLS inhiibtor) may be insufficient to induce cell death. Our NanoString transcriptomic analysis does provide intriguing anti-glutamine targets in the tumor TME with potentially fewer side effects than the pan anti-glutamine strategy of DON. Also, these targets do not rely on enzymatic function of individual metabolic genes. We observed increases in two crucial glutamine regulating transcription factors, Mycn and Atf4 in the CD45- cells. MYCN/Mycn is not expressed in the T cell or myeloid immune compartments (NanoString, Immpress database, Klemm et al. 2020), while ATF4/Atf4 activation in immune cells is known to promote tumor growth and generally be immunosuppressive (Chen & Cubillos-Ruiz, 2021; Cubillos-Ruiz et al., 2017; Cubillos-Ruiz et al., 2015; Song et al., 2018). It is worth noting that there is some expression of Mycn in NK cells, in line with the role of glutamine in NK cell activation (Loftus et al., 2018). In previous generations of medicinal chemistry, targeting transcription factors like Mycn and Atf4 was the holy grail. However recent advances in degrader technology make this much more possible today than in previous years (Hanzl & Winter, 2020). Groups have already found natural products that result in the proteasomal degradation of the glycolytic myc isoform, c-myc. (Losuwannarak et al., 2020; Sriratanasak et al., 2020). Therefore, a degrader-based approach for tumor cell specific glutamine catabolism transcription factors may lead to anti-metabolic strategies that do not focus on enzymatic activity, but rather restrict expression of whole clusters of metabolic genes.

Structure and function of hexokinases impact whole organismal health

The hexokinases are some of the most widely studied genes in human biology. Glucose fixation and metabolism are some of the earliest discoveries in biology at the

turn of the 20th century. The original work mostly done in bacteria could not predict the variety of mechanisms in which eukaryotic organisms would perform such a seemingly simple biochemical task (phosphorylation of glucose). Multicellular organism do so by implementing multiple HK isoforms with unique biochemical properties and regulatory elements. The clinical entity of diabetes lead to the molecular understanding of glucokinase (GCK, the high K_m hexokinase that is mostly beta cell specific), which demonstrates how evolutionarily fine-tuned these enzymes are to maintain organismal homeostasis. The understanding of beta cell biology and the role GCK plays in sensing blood glucose became essential to understanding the clinical phenotype of both type 1 and type two diabetes. When patient's lose beta cells due to inflammatory cell death (type 1), or when their beta cells no longer appropriately sense blood glucose (type 2), there is insufficient blood insulin to drive glucose catabolism in the entire the organism. The inflammation associated with diabetes has been recently described to alter GCK activity via citrullination, leading to beta cell glucose insensitivity (Yang et al., 2022). Therefore, it reasonable to assert that understanding the biological role, cell type specific nature as well as the post translational modifications of the other hexokinases is important to organismal function as well as disease pathogenesis.

HK1 and HK2 have been a large focus of biology because they are expressed across all cell types and sit at the intersection of glucose and mitochondrial metabolism. Their canonical role in metabolic pathways is to phosphorylate glucose while sensing mitochondrial ATP pools. If there is insufficient ATP or too much G6P (the end-product of its reaction), glycolysis is halted. Interestingly, these enzymes can have moonlighting functions where they perform tasks not in line with glucose catabolism. For example, HK2

is described as a pattern recognition receptor able to sense some subtypes of bacterial cell walls (Wolf et al., 2016). Because glucose metabolism is known to cause divergent cell function and fate, these enzymes are linchpins for phenotypic development across many human biological systems.

HK2 has been a large source of focus because of its unique regulation by mTOR. It is canonically thought of as a hypoxia inducible gene (Garcia et al., 2019). Therefore, its expression is increased in cancer cells (which have mTOR activating events from genetic alterations in EGFR, RAS, PI3K, LKB1, TSC1/2, AKT ,PTEN)(Reinfeld et al., 2022). Additionally, HK2 expression increases in active immune cells that are rich in the TME as well as many human immunopathologies. T Cell receptor engagement, B cell receptor ligation, macrophage PAMP activation, NK cell degranulation, and dendritic cell antigen presentation are all associated with increases in pS6, and HIF stabilization (even in normoxia, see Chapter 1). Therefore, the role of glucose in these crucial immune activating events has been examined extensively across immunology

Uncovering HK3's myeloid specific nature via deep bulk transcriptomic analysis on flow sorted populations

The discovery of HK3 as a myeloid specific interferon gamma induced gene has wide implications for myeloid immunometabolism and cancer biomarkers. As our work suggests myeloid cells are incredibly glucose consuming in the TME. The underlying mechanism is in part due to increased mTOR signaling (as seen by elevated pS6 and HK2 protein via flow cytometry) that these cells possess basally. However, blocking mTOR signaling was only able to partially decrease the elevated glycolytic phenotype in these cells.

Our NanoString analysis demonstrated that these CD11b+ cells have a unique enrichment in glycolytic genes at baseline. The most interesting enrichment is of the white blood cell Hexokinase, *HK3*. This gene has a log 6.5-fold increase in HK3. This gene has a log fold increase in the same order of magnitude with other widely accepted myeloid specific genes like CD68 and components of MHCII. We implemented many bioinformatic approaches to validate this finding across mouse and human biology. We see a stringkly similar pattern in the TME and some inflammatory microenvironments.

A crucial question is how this gene has been overlooked over the past forty years. A relatively crude explanation is a true lack of commercially available reagents that can detect HK3 specifically. These enzymes have high amounts of homology (>80%) and very similar catalytic domains, making it difficult to generate an isoform specific antibody. Non-specific antibodies that recognize HK3 would not pose a problem in the study of HK1/2 because of the limited expression of this one isoform across eukaryotic cells (Wilson, 2003). Additionally, the unique pattern of expression combined with the need to stimulate the cells with an inflammatory cytokine to get robust induction, makes it more difficult to study. But still, many approaches examine *HK3* at the RNA level, while mass spectrometry proteomics do not rely on antibodies for isoform detection. Based on our group's experience in performing transcriptomic analysis on the RenCa and MC38 model, HK3 expression is minimal when examining the whole tumor single cell suspensions. This is intuitive because myeloid cells make up a minority of the population. Therefore, to appreciate this enzyme's uniquely limited expression, flow sorting of myeloid and non-myeloid populations of interest are required.

Flow sorting can allow for understanding of individual cell populations in the TME, however most groups are not interested in transcriptomic changes across cell types from different lineages. In most studies, RNA is purified from the same cell type (like a T cell) either from different treatment condition (+/- checkpoint blockade), with differential expression of a marker ($Lag3^{hi}$vs $Lag3^{lo}$) or with a known phenotypic difference (T_{EMRA} vs T_{scm}). Therefore, groups have not developed significant many datasets that would allow for metabolic comparison across cell types. Klemm *Cell* 2020 did follow a similar scheme as our MC38 NanoString study, and at the gene level, *HK3* demonstrates the identical trend. It is only detectable in CD11b+ cells in the human TME across multiple disease setting. Interestingly in this data we also observe that *MYCN* is elevated in the primary glioma cells in comparison to the infiltrating CD45+ cells, suggesting that our flow sorting approach maybe more robust than previously appreciated. In accordance with elevated glioma *MYCN*, Craig Thompson's group has described that radioactive glutamine is a suitable approach to image primary brain tumors (Venneti et al., 2015).

A reasonable response would be that scRNA sequencing could overcome the issue of lack of comparison across cell lineages. With the latest technology from 10x Genomics, in one experimental condition it is possible to characterize the transcriptome of 1000s-10000s diverse cells without requiring the bias of flow sorting for a population of interest. This in theory solves the problem that myeloid cells, T cells, and cancer cells will be compared to each other. Technically, this is true, yet the lack of sequencing depth currently available on the 10x Genomics platform hampers its ability to characterize metabolic cell state. There are only 50k reads that align to 1000-2000 unique genes per cell (Wang et al., 2021). This is only 5-10% of the entire proteome that is captured via this

method. Additionally, genes associated with cell phenotype like CD11b and CD3ε, will represent an overwhelming amount of reads in each cell. Therefore, on the 10x platform most of the genes in each cell will not be characterized. For the many of the genes that are captured, only a handful of reads will be observed. This ultimately makes comparisons across cell type or treatment groups difficult and statistically unpowered, even though it is economically feasible.

Not surprisingly, given that metabolic genes are not often associated with cell phenotype and function and are often viewed as housekeeping genes, these metabolic enzymes are not preferentially expressed in the top 5-10% of genes in a cell. Therefore, metabolic genes may suffer from extreme drop out in many of these datasets. For example, our lab has generated preliminary data by performing single nucleus sequencing on 3 human ccRCC. In these samples, across all TME cell types, detection of *HK1*/*HK2*/*HK3* is minimal. There are no differences in expression across cell type clusters because the genes are so rarely detected. Single nucleus sequencing is regarded as a better tool at dissecting cell specific programs because nuclear RNA is more linked to cell type and to purify the nuclei requires minimal tissue processing, handling, and flow sorting/bead enrichment. Additionally, it can be easily conducted on cryo-preserved tissue slices that many groups have already banked for other analyses. Nuclei purification does bias towards capturing epithelial and myeloid cells nuclei and underrepresents lymphoid populations in solid tumors (Slyper et al., 2020). I have directly compared scRNAseq and snRNAseq in mouse kidneys from the Humphrey's lab and snSeq is better at detecting the myeloid specific nature of *Hk3*. This gives credence to the potential usefulness of this sequencing approach in comparison to single cell

methods. However, in the case of our ccRCC tumors and expression hexokinases, due to low coverage available on the 10x platform, snSeq is still insufficient to capture these enzymes.

Additionally, we probed for the expression of the three low K_m HKs in the scRNA from Obradovic et al. 2021 and once again, see minimal expression of these metabolic. The approach implemented in this used to ultimately uncover TREM2+ macrophages as a driver of disease pathogenesis was VIPER, which allowed for imputation of protein activity. This approach seems ideal to examine metabolic gene activity across cell types in the TME. However, since these HKs were never found in the original scRNA sequencing (just like in our labs snRNA approach), the protein activity could not be imputed. In total, these results illustrate the technical limitations of the 10x platform to probe cell metabolic state.

There is an alternative (yet more expensive) approach, the Smartseq platform. This technology increases the reads two log fold (2-4 million reads per cell, on average) however that technology only allows for a few 100s of cells to be sequenced (Wang et al., 2021). With more reads approximately, 5000 genes can be found in each cell (1/4 of the proteome). This Smartseq platform is more likely to replicate information gained from bulk transcriptomics, but by only probing the transcriptome of so few cells, one is unable to fully characterize the tissue microenvironment that one is studying.

While scRNAseq is still powerful and can generate future populations of interest whose metabolic program can be dissected using other assays, it is insufficient to directly probe cell metabolic state. If one is to conduct a scRNAseq study to examine metabolic program, the Smartseq platform is probably better due to better coverage of the whole

transcriptome combined with deeper sequencing. However, the small number of cells ultimately sequenced on the Smartseq platform may make it difficult to probe the inter and intracell type heterogeneity. So, it may be worthwhile to flow sort individual populations to ensure that the cell type of interest is included in this (expensive) experiment. And thus, we have returned to square one, where flow sorting was necessary prior to our NanoString analysis, which provided robust and easy to interpret data.

HK3's unique properties drive further mechanistic study

What aspects of HK3 biology support its further study? (1) HK3 has the lowest K_m for glucose. Thus, the cells this isoform should be able to bind more glucose. We in fact see that myeloid cells do consume more glucose in tumors, in the inflamed lung, while other groups have shown this phenotype in the brain (Xiang et al., 2021) (2) Additionally, HK3 appears to evolutionarily split off from HK1/2 at an earlier time, suggesting that other evolutionary forces may shape its functional role (Cardenas et al., 1998; Ureta et al., 1987). (3) HK3's is expressed in a very narrow subset of cells. It appears across organisms, that myeloid cells (monocytes, macrophages, neutrophils, dendritic cells, eosinophils) specifically transcribe this enzyme. These facts together support that it may have an entirely different role in cell function. An interesting proxy for these unique features comes from a recent pre-print that evaluated the ability for human glycolytic enzymes to complement a yeast strain deficient in cellular glycolysis. Of the 25 enzymes of glycolysis that this group probed, only one ortholog was unable to support cellular growth on glycolytic substrate, HK3. This result suggests that HK3 has little to do with producing pyruvate but rather plays another role in the cell (Boonekamp et al., 2021).

Since yeast are a single cell organism, it also suggests that HK3 may be linked to the formation of multi-cellular organisms with diverse cell compartments that divide biological tasks.

To describe new aspects of HK3 biology, I over expressed GFP-tagged human HK3 in the immortalized mouse macrophage cell line and the mouse colorectal cancer cell line MC38. The original goal was to use these cell lines to conduct GFP pulldowns and describe HK3s unique binding partners as well as post translational modifications that impact its cellular localization or function. However, to my surprise, even with puro selection, both cell lines lost expression of the HK3-GFP construct over time. The empty-GFP vector however remained 100% GFP-positive. Differing methods of splitting and passaging the cells all the while in puromycin, the isogenic HK3 OE cell lines would fluctuate between 40-60% GFP-positivity in both cell backgrounds. This preliminary data further supports that HK3, even though it performs glucose phosphorylation, may differ from its isozymes.

HK3 as a tumor suppressor?

It does not appear as if the HK3 OE lead to a growth advantage but instead these cultures would demonstrate massive cell death when HK3 was overexpressed. These results, though frustrating and surprising are quite interesting. HK1 and HK2 have been over expressed in many cell lines and are associated with a pro-growth and anti-apoptosis phenotype. Glucose and its catabolism are traditionally viewed as oncogenic components of cancer proliferation and progression. When over expressing the human HK3 in mouse cell lines, I have observed that the mouse HK1/2 isoforms decrease, demonstrating that the cells are least maintaining or potentially increasing their glucose uptake. However, in

these two cell lines, this ability to handle this glucose is disentangled from a pro-growth phenotype. This suggests that the fate of glucose after fixation by HK3, is not associated with cell growth (in line with the yeast complementation data). One possibility is that HK3 V_{max} does decrease as glucose concentration rises above 1 mM glucose concentrations, therefore overall cellular HK activity may be less when this enzyme becomes the dominate cellular isoform (via lentiviral over expression) (Su & Wilson, 2002). This possibility can be further explored by conducting commercially available hexokinase activity assays. If HK3 substrate inhibition comprises cell proliferation, one would expect to see less total HK activity in the OE lines in comparison to the empty vector. Additionally, I attempted to expand these cultures in glucose abundant conditions (25 mM). It may be worthwhile to see if the %GFP positivity of the HK-GFP OE cells increases as the glucose concentration is lowered. It could be hypothesized that HK3 in glucose abundance is not advantageous to growth but may be important as the glucose concentration decreases to concentrations that replicate the tissues, where the cells who express this enzyme perform their function.

These experimental observations are in line with the fact that HK3 is never expressed in the cancer cell compartment across human and mouse cell lines. Cancer cells are widely accepted to have altered epigenetic states that allow for the misexpression of proteins that should developmentally be restricted to them. This ability is the basis of immuno-oncology therapies which target the expression of melanoma associated antigens (MAGEs) (Weon & Potts, 2015). MAGEs are placental and germ cell genes that are mis-expressed by melanoma tumors and have been shown to evoke

immune responses. Additionally in the TME there are many inflamatory cytokines that one could imagine induce this enzyme.

Based on the notion that increase glucose metabolism drives cancer cell proliferation, HK3 inherently should be oncogenic. One would expect that cancer cells (maybe even to a greater myeloid leukemias) would enhance the expression of this enzyme. But across the TCGA, mouse tumor models, scRNA datasets, and even in myeloid disease, cancer cells do not upregulate *HK3*, especially in comparison to the myeloid cells that infiltrate these diverse settings.

So wh ycould increasing *HK3* be ultimately deleterious to cancer cell function? Work from the DeBerardinis group and others have recently described that mitochondrial metabolism of glucose is necessary for aggressive tumor phenotypes in mice and humans (Hensley et al., 2016; Johnston et al., 2021). Intriguingly, Data that Dr. DeBerardinis has shared in many talks, but not yet publish convincingly demonstrates that patients with lung tumors with increased C13-glucose→citrate labeling have a shorter overall survival than patients who demonstrate more canonical glucose to lactate labeling. Interestingly, this enhanced C13 citrate enrichment does not correlate to any known prognostic indicator like tumor mutational subtype or tumor stage, suggesting that this increase in mitochondrial metabolism may be a clinically useful biomarker for selecting patients with aggressive disease. Additionally, other groups have shown that mitochondrial deficient cancer cell lines when injected into mice do not form tumors until they coopt host mitochondrion (A. S. Tan et al., 2015). Human AML leukemia PDXs do the same process where when grown in NOD-SCID mice, they hijack the host mitochondria in the process of engraftment (Moschoi et al., 2016). This previously

overlooked aspect of tumor metabolism can now be imaged *in vivo*. A group at UCLA developed an OXPHOS detecting F18 tracer and demonstrate that this novel imaging agent accumulates in genetically engineered models of mouse lung cancer (Momcilovic et al., 2019). This data in concert do suggest that mitochondrial itself as well as the catabolism of glucose into the TCA cycle is a feature of aggressive malignancy. These data directly challenge another of Warburg's key contribution to the cancer literature. Warburg argued that mitochondrial dysfunction was a commonality between all tumors. However, his manometry studies do not necessarily demonstrate dysfunction of whole mitochondrion in heterogenous tumor slices, instead they demonstrate a preference for turning available glucose substrate into lactate when stimulated with supraphysiological doses of this sugar.

Cytosolic glucose processing as a myeloid specific cell program

Therefore, could the downstream consequences of HK3 activity be opposed to mitochondrial metabolism? HK3 , lacking the mitochondrial domain, may be diverting glucose into other glycolytic pathways like the PPP. The Ardehali group has demonstrated that blocking HK1's mitochondrial binding increase C13 glucose a labeling into the PPP and diverts the label away from glycolytic intermediates and citrate (De Jesus et al., 2022). Given that HK3 is inherently disassociated with the mitochondria (given its lack of MBS), it can be hypothesized that its basal function is to potentially divert glucose carbons in the PPP. To test that hypothesis, C13-glucose labeling studies could be conducted with the HK3 OE vs empty vector cell lines I have created. Even though these cells proliferate less, I would expect PPP intermediates to have an enriched labeling pattern in the OE cells vs the empty vector cells. Alongside, HK1 and HK2 could be overexpressed in the

same background, and if the labeling is restricted in glycolytic intermediates when HK1/HK2 are overexpressed, it would strongly suggest that HK3 diverts glucoses cellular fate away from the mitochondria in contrast to its isozymes. It may be crucial to conduct these studies at lower, more physiological glucose concentrations, to increase the activity of HK3 and thus observe the labeling differences.

Given that HK3 expression is tightly related to myeloid fate, a simple question is there evidence that myeloid cells are inherently sensitive to alterations in HK activity? The simplest answer is by looking at inborn errors of metabolism. Neutropenia is a described clinical component of disorders where patients are lacking G6PT transporter (SLC37A4) or the endoplasmic reticular G6P phosphatase, G6PC3. These mutations result in a well-known syndrome known as Glycogen Storage Diseases (GSD1b). In the G6PT deficient patients, a crucial ER transporter is lost and thus there is accumulation of a G6P-like bacterially derived molecule (anhydroglucitol) in the cytoplasm. This molecule then becomes phosphorylated by endogenous cytoplasmic HKs to become 1,5-anhydroglucitol-6-phosphate and then intern inhibiting the family of low K_m Hexokinases (Veiga-da-Cunha et al., 2019). Recently a small clinical trial employed empagliflozin (a SGLT2 inhibitor) to block anhydroglucitol uptake in patients with GSD1b. The group observed restoration of neutrophil function and clinical benefit in all four patients on trial, indicating that modifications to neutrophil glucose flux can alter immune function (Wortmann et al., 2020). A similar pathophysiologic sequence of events arises in patients who lose G6PC3, where they cannot decrease cytoplasmic G6P levels enzymatically (Kiykim et al., 2015). Therefore, the accumulation of G6P directly inhibits the HKs. Both defects are somatic, and thus should theoretically impact all the cells in the host.

However, the main phenotype in both patient cohorts is a potentially fatal neutropenia. This suggests that neutrophils (a subtype of myeloid cell) are exquisitely sensitive to inhibition of the HKs and thus it could be hypothesized that HK3 supports their fate and function. Mature neutrophils have very minimal mitochondrial content or oxidative respiration (Maianski et al., 2004). This may underlie their exquisite sensitivity to cytoplasmic HK inhibition due to G6P accumulation where other cells have mostly mitochondrial HKs. Thus, the compartmentalization of these enzymes s protects an overwhelming majority of the host cells from the toxic effects of G6P in patients with or loss of function mutations in G6PC3 or G6PT.

Another set of myeloid specific inborn errors of metabolism that may be relevant to HK3 function is the family of chronic granulomatous diseases (Arnold & Heimall, 2017). Patients present with a host of atypical infections due to loss of phagocytic efficacy in myeloid cells. The phagocytic defect arises from non-functional NADPH oxidases and thus cannot generate anti-microbial superoxide. To generate this cellular superoxide, myeloid cells must generate increased NADPH. NADPH is made in the from the oxidative PPP, and thus would be secondary to HK3 cytosolic glucose phosphorylation. Therefore, HK3 may be restricted to myeloid cells to increase cellular supply of NADPH to support their anti-microbial cellular function.

Recently myeloid cells have been described to have an intact NAD synthesis via the kynurenine pathway and NAD salvage pathway at rest (Minhas et al., 2019). Previously, the salvage has been extensively studied because primordial cancer cells upregulate this pathway to support their increased growth phenotype. It appears that this increase in NAD generation is occurring while these myeloid cells have a basal elevated

glycolytic rate. Yet these cells are not as proliferative and do not divide as often as cancer cells. So, why would these two seemingly distant metabolic pathways be linked myeloid cells? The Vander Heiden's group has described that cellular NAD levels support a cell's ability to continually ferment lactate (i.e., aerobic glycolysis). Essentially pyruvate to lactate oxidation continues at elevated rates in metabolically active cells to generate free NAD (Luengo et al., 2021). Therefore, it is possible to imagine that HK3 levels are elevated in myeloid cells to help assist in increased NAD levels to support continual glucose metabolism (which is basally elevated due to HK2/HK3 dual positivity). Additionally, this newly synthesized NAD can be the substrate for more NADPH generation which as mentioned above is crucial in the fate and function of myeloid cells.

There is evidence that HK3 may play a role in this enhanced ability to generate NAD. Recently the human blood proteoform atlas has been published with data demonstrating immune cell specific to protein expression and protein binding partners (Melani et al., 2022). (https://blood-proteoform-atlas.org/proteins). HK1 has no described binding partners in this data and its expression is in lymphocytes (specifically T cells). This is the same trend we observed in the MC38 TME at the RNA level (adding credence to the robust nature of our NanoString approach). HK3 demonstrates the expected enrichment in neutrophils, eosinophils, monocytes and unexpectedly in HSCs. In this dataset, HK3 is found to have 11 binding partners where the only metabolic enzyme it interacts with is PRPS1. PRPS1 synthesizes PRPP, which has two crucial enzymatic roles that may play a part in the HK3-myeloid immunometabolism paradigm. PRPP is the first product after the oxidative PPP and can be diverted into *de novo* nucleotide synthesis. PRPP is also the necessary co-factor for NAMPT (a crucial member of the

NAD salvage pathway, which mentioned above is utilized by myeloid cells basally) to generate NMN from NAM (Hove-Jensen et al., 2017). PRPS1 has been described as a target of the main fructose hexokinases (ketohexokinase (Li et al., 2016)) and its activity can be regulated by AMPK in brain tumor cells (Qian et al., 2018). Preliminary data from our group demonstrates that HK3 expression is the most elevated when iBMDMs are exposed both to IFNγ and metabolic stress (1 mM glucose or 10 mM rapamycin treatment). In both situations, pS6 is significantly decreased. We have not yet probed or altered the AMPK axis, but the decrease in pS6 is suggestive that AMPK may be more active. These features taken together could suggest that active AMPK+ IFNγ synergize to increases HK3 expression which then diverts glucose into the PPP, all the while potentially activating PRPS1 to increase NAD synthesis to further support the glycolytic nature of these cells during a period of metabolic and microbial stress. There is evidence that *de novo* nucleotide synthesis (which could be the product of increases PRPS1 activity and thus more PRPP) is enhanced in TAMs. Hallbook et al. demonstrates that TAMs in pancreatic cancer have higher rates of *de novo* nucleotide synthesis and export these newly synthesized DNA precursors into the TME interstitial space and cell culture media (Halbrook et al., 2019). They find that this increase in nucleotides promotes tumor resistance to the FDA approved anti-nucleotide chemotherapy, gemcitabine. This paper comments that this behavior seems wasteful in terms of diverting a large source of carbon to export a biosynthetic molecule that these typically non-proliferating cells do not need. However, now understanding myeloid specific expression of HK3, it is intriguing to hypothesize that this accumulation in nucleotides may be a byproduct of a metabolic

program focused on generating sufficient NAD to sustain their immunosuppressive glycolytic function in the harsh environment of the TME.

Hk3$^{-/-}$ mice demonstrate no alterations in anti-tumor immunity, but suggest role of this isozyme in granulocytes

In pursuit of demonstrating the role of HK3, we used bone marrow from *HK3*$^{-/-}$ mice to reconstitute RAG hosts. After 12 weeks, we implanted MC38 tumors in these mice, with the hypothesis that HK3 loss would result in larger tumors. HK3 as a marker of M1 macrophages may be a component of an anti-tumor phagocytic response. Therefore, these tumor-associated myeloid cells would have decreased anti-tumor function, and thus the mice would have larger tumors. However, the MC38 tumors grew to similar sizes in the *HK3* WT and KO mice. In these tumors, we conducted our FDG uptake assay as well as extensive flow cytometry analysis to characterize the infiltrate. In line with the lack of growth phenotype, there were no difference in glucose uptake across tumor fractions. The only statistically significant alteration across 14 flow panels, was an increase in Ly6G+ PMN-MDSC Ki67+ in both the tumors and the blood. This interestingly correlated with a decrease in neutrophils in the blood prior to tumor implantation. These data hint that Hk3 may have a greater role in granulocytes (PMN-MDSCs and neutrophils) than monocytes. This is in line with a decades old observation that hexokinase in granulocytes is almost completely cytoplasmic where other leukocytes have hexokinases activity in mitochondrial fractions (Rijksen et al., 1982). This also is in accordance with the clinical neutropenia seen GSD1b and G6PC3 deficiency where decrease in cytoplasmic HK activity (due to G6P accumulate) results in a selective neutrophil defect. These patients do not have monocyte deficiencies. The increased cytoplasmic HK activity was published

prior to the understanding of the sequence of these three low K_m isoforms and their unique regulation. Unfortunately, PMN-MDSCs and neutrophils are not very abundant in the MC38 TME. They are more represented in other tumor models (especially those in the Balbc background, such as RenCa and 4T1). Therefore, it is not surprising that losing a granulocyte specific gene and thus altering granulocyte function had no impact on overall tumor growth or T cell immunity in this C57B6 tumor model.

The expression of *HK3* in many of these datasets analyzed in Chapter 3 appears enriched in monocytes and macrophages. However, with the above results, it became apparent to ask whether *HK3* levels are different between monocytic and granulocytic cells. A contributory reason to the minimal amount of data concerning neutrophils/granulocyte *HK3* levels is that these cells are notoriously difficult to study and purify from tissues because small disturbances can cause their activation and induce their degranulation. Degranulated neutrophils form neutrophil extracellular traps (NETs). These extracellular structures are DNA rich structures and are used to prevent bacteria from invading the host. It is technically not feasible to perform flow cytometry or RNA seq on these neutrophils that have undergone NETosis. Therefore, in single cell tissue dissociations these neutrophils rarely make it to through the tissue processing to ultimately be clustered on the UMAP or detected via flow cytometry. Additionally, PBMCs which are often used for in these studies are prepared using Ficoll gradients and thus granulocytes (like neutrophils) are inherently excluded from the analysis. However, in one instance, we do see that *HK3* is much higher in TME neutrophils even compared to other CD11b cells (Klemm et al., 2020). Recently in our group, another graduate student (Melissa Wolf) conducted deep RNA sequencing on M-MDSCs, PMN-MDSCs, and TAMS

from the RenCa model. It is very clear that *Hk3* is many times higher in the PMN MDSCs in comparison to the monocytic MDSCs and their more mature counter the TAMs. Future *in vivo* studies with HK3 should focus on tumor models where tumor associated neutrophils play a role in tumor progression.

It has been recently established that Glut1 is elevated in neutrophils when compared to other CD45+ cells in mouse tumor models and mouse blood. This increase in Ly6g+ Glut1 is associated with a glycolytic phenotype that supports tumor growth. Loss of Glut1, specifically in these granulocytes, results in less tumor growth and increased response to radiotherapy in genetically engineered models of primary lung cancer (Ancey et al., 2021). Therefore, it would be hypothesized that HK3 as the main HK in these neutrophils could play a role in tumor immunity and metastatic progression. Interestingly, a group has recently published that HK3 elevation is a predictor of immune response in lung cancer (Tuo et al., 2020), although this group attributes *HK3* expression to the transformed cancer cells and not the TME infiltrating immunocytes even though *HK3* levels anti-correlate to tumor purity.

HK3 prognostic role in ccRCC

Uniquely, HK3 expression appears to correlate with poor prognosis in ccRCC. In this tumor type, it is widely established that increased tumor associated inflammation correlate with worse disease outcomes and tumor progression. Therefore, it is not surprising that HK3 as an inflammatory myeloid gene correlates with poor prognosis. An ongoing question is whether elevated HK3 is a marker of a certain type of myeloid cell in the TME. Across many datasets, *HK3* expression correlates with the gene CD16 (FCGR3a). This gene is expressed highly on neutrophils, granulocytic MDSCs, non-

classical monocytes and NK cells. Based on the GTEX and scRNAseq data, we can assume that the expression in minimal in the NK cells. In scRNA sequencing data it appears to be more associated with the non-classical monocyte program, however this may be due to the lack of neutrophils at the time of sample processing due to the technical difficulties alluded to above.

There are recent studies that implicate myeloid cells in the ccRCC TME. Mass cytometry demonstrates that myeloid cells are the second most abundant cells in the TME after CD8 T cells (Chevrier et al., 2017). Groups have taken IHC approaches to show that both M1 and M2 markers predict poor prognosis (Dannenmann et al., 2013; Xu et al., 2014) . We now also appreciate via scRNA approaches that TREM2+ C1q macrophages (Braun et al., 2021; Obradovic et al., 2021) increase with stage and grade, aligning with our HK3 result in the Vanderbilt TMA and the TCGA.

Intriguingly, there is historical literature that examines the clinical value of neutrophil to lymphocyte ratio in RCC. This metric can predict patient outcomes prior to treatment as well as patients undergoing immune-checkpoint blockade. Meta-analyses demonstrate that increased neutrophil to lymphocyte ratio is an indicator of poor prognosis in all RCC patients (X. Chen et al., 2021). Traditionally in oncology, increased neutrophils and decreased lymphocyte counts demonstrate underlying bone marrow output that would be expected in patients with advanced disease (and thus higher NLR rations). Recent studies have shown that if the NLR ratio decreases on checkpoint blockade, patients are more likely to respond (Lalani et al., 2018). This intuitively makes sense given that these patients with decrease NLRs are most likely having increases in lymphocytes and thus getting the desired anti-tumor immunity associated with generating

more lymphoid immune cells. Yost et al. 2019 demonstrates that the T Cell responding to checkpoint blockade are not the clones in the tumor prior to treatment, but rather blood-based clones repopulating the TME (Yost et al., 2019). So, increases in these lymphocytic cells peripherally may suggest this population is growing and then infiltrating into in the TME. Even though there are many studies investigating NLR and ccRCC, there is only one study that evaluates neutrophils on RCC growth (Song et al., 2015). This study demonstrates aggressive disease has an increase in CD66b in the RCC tumor tissue. CD66b can be a marker of both granulocytic MDSCs and neutrophils, but in total this finding suggests that granulocytes play a role in the RCC TME that has been overlooked. Mechanistically, this group evaluated the impact of neutrophils on RCC cell lines in co-culture assays and demonstrate that neutrophils can increase the HIF2α signaling axis in ccRCC cell lines, increasing their proliferation rate. Therefore, the contribution of ccRCC tumor associated neutrophils may be already targeted with the generation of new HIF2α inhibitors (recently approved for VHL patients and under trial for the treatment of RCC in combo with TKIs and ICB).

A first pass at the ccRCC TCGA dataset demonstrates that many neutrophilic/granulocytic markers are elevated in the ccRCC microenvironment. There are genes related to neutrophil chemotaxis (CCL4, CXCL8, CXCL16) as well as genes related to neutrophilic phenotype (CD16, CD32, CD33, CD15, Lox1, CD84, CD64, MIF, MMP9 and CXCR6). The neutrophilic chemoattractant CXCL8/IL8 has been implicated in ccRCC patient response to immunotherapy (Yuen et al., 2020). Given the elevated HK3 in the ccRCC TME and its correlation with poor outcome, it is warranted to conduct tissue studies, flow cytometry on primary tumors and blood to evaluate the role of granulocytic

MDSCs and neutrophils in ccRCC. It would be worthwhile to stain for more granulocytic markers (e.g., CD66b, CD15, and CD16) as well as NETs in the tumor tissue. Future studies conducting spatial RNA sequencing may be able to disentangle the myeloid heterogeneity in RCC and how these cells contribute to the necrotic core and hyper-vascular periphery of ccRCC. With our HK3 findings, I would hypothesize that these granulocytic cells are elevated in patients with more advanced disease (higher grade and stage) as well as in metastatic vs primary tumors. I would anticipate that patients responding to IO will have increases in the lymphoid compartment and decreases in these cells both in the blood and primary tumor. This paradigm is worthwhile to study in RCC because tumor associated neutrophils in other disease types often are associated with increases in tumor angiogenesis. These granulocytes can often be larger sources of VEGF in part due to their HIF active metabolic program. We observed that an intertumoral ncreases in *HK3* in patients receiving VEGF TKI. These agents are thought to kill ccRCC cells, by increasing hypoxia due to vascular collapse. However, the only low K_m HK that demonstrates a treatment effect if this *HK3*. This could be hypothesized due to increase in neutrophil infiltration thus supplying additional VEGF to ultimately circumvent VEGF pathway inhibition.

Going forward, with the knowledge of HK3 as potential granulocyte specific gene, a key aspect will be between articulating the role of granulocytic MDSCs vs neutrophils in RCC. These cells have very little differences that can be established on a protein level, making them challenging to study. Many of the markers mentioned above overlap between these two cell types. Therefore, it remains unclear where cell may be driving the prognostic features of HK3 in ccRCC. It is worth noting, however that these cells do have

different densities where in PBMC the G-MDSCs are purified with other immune cells, and the neutrophils are below the Ficoll gradient. Therefore, granulocytic markers can be observed in the PBMC of cancer patients. Future work should focus on evaluating protein and RNA expression from both cell types to see if HK3 goes up with terminal neutrophilic differentiation or whether it is heightened in this protumor intermediate G-MDSC stage.

HK3 uniquely appears to be relevant in ccRCC. Why is that the case? ccRCC has a unique mutational profile that may drive this relationship. ccRCC is the only tumor type with VHL mutations in the TCGA. Patients with hereditary VHL syndrome get a series of rare tumors (hemangioblastomas, pheochromocytomas) and ccRCC. Therefore, loss of function of this tumor suppressor is associated with a narrow set of malignancy unlike other tumor predisposition syndromes like Li-Fraumeni (somatic p53 loss) where patients develop tumors in almost all organ systems. This phenotype suggests that there is interplay between the tumor stem cell of origin, the organ of tumor origin, mutational event and immune microenvironment that ultimately contribute to ccRCC pathogenesis.

Targeting HK3^{hi} cells using new therapeutic paradigms

Ultimately with the pharmacological tools of the 21st century, it is possible to target HK3 specifically and potentially modify the immune landscape of the TME. In this era of immune oncology, the field focuses on hot or cold TMEs. However, this perspective is narrow in scope give that tumor “hotness” is typically defined by T cell related gene sets or the crucial anti-tumor cytokine IFNγ. Although often overlooked, almost all tumors are rich in myeloid infiltrate. This returns to another foundational cancer observation by the pathologist Rudolf Virchow, where he observed that cancer is the chronic wound. He

noted the neutrophils and monocytes that are often responsible for tissue repair after injury are also abundant in tumors. Therefore, strategies that alter myeloid biology may even have broader scope than the paradigm changing immune checkpoint blockade therapy.

Given the result that Glut1 KO in granulocytes results in smaller lung tumors and better response to radiation therapy, decreasing granulocyte glycolysis is potentially a worthwhile TME target. Neutrophils decrease in the periphery and have elevated proliferation markers to when *Hk3* is specifically knocked out in the bone marrow. Previous attempts to target TME glycolysis have been too broad and not focused on eliminating cell-type specific metabolic programs. Both pre-clinical and clinical models have employed 2DG to block hexokinase activity in all cell types in the TME. This approach is too toxic due to the glycolytic nature of human brain tissue. Additionally, groups have developed GLUT1 or GLUT1/3 inhibitors. However, based on our data and data from autoimmune models, it would be hypothesized that these drugs could ultimately limit anti-tumor efficacy prior to inducing tumor cell death (Healey et al., 2021). This approach may also abolish T cell memory, which may be underlying successful therapeutic responses in non-immunotherapeutic paradigms like radiotherapy, chemotherapy, and targeted therapy. The unique metabolic features of granulocytes ($Mito^{Lo}$, cytoplasmic HK^{hi}) combined with the viability of the mice embryos deficient in HK3 suggest that with targeted approaches, the protumor impact of neutrophils can be targeted safely.

The success of mRNA technologies for the induction of robust COVID immunity demonstrate that nucleic acid therapy can be given to humans with minimal adverse

effects (Polack et al., 2020). These nucleic acids payloads can induce a productive and profound immune response. Recently, the treatment of Spinal Muscular Atrophy has been revolutionized by the antisense RNA treatment that results in appropriate gene splicing (Finkel et al., 2017). These children who were born with fatal motor neuron diseases now are reaching ages never previously seen. Given the success of both paradigms, it is reasonable to imagine treatment with RNAi technologies that can decrease HK3 expression acutely. The acute depletion of HK3 may be necessary to see a biological effect. In our mouse model, we used a model of chronic HK3 depletion, which may have allowed for altered HK1/2 dynamics to support myeloid cell biology. Acutely knocking down this gene down at the time of tumor formation may exhibit greater benefit because of the potential compensation from other isoforms. HK1 and HK2 can be expressed as isoforms that lack the mitochondrial-binding domain. These truncated splice variants have been shown to be elevated in diseases like obesity and diabetes (De Jesus et al., 2022). The exquisite specificity of HK3 for myeloid cells would limit the potential of off target effects. Additionally, the exogenous RNA may activate PRRs in the TME and enhance anti-tumor immunity.

Another benefit of the RNA approach is that multiples targets can be engaged simultaneously. We observe that the non-granulocytic myeloid cells additionally have higher levels of HK2. It is appreciated in cancer biology that HK2 is a pro-proliferative gene. Yet, in T cells, the HK2 specific deletion has no impact on any *in vivo* or *in vitro* phenotype (Mehta et al., 2018). This work clearly demonstrates that HK2 is robustly induced with TCR stimulation, however its loss is negligible to T cell phenotype or function in a plethora of models. From our analysis across tumor types, HK1 is the dominate T cell

hexokinase (seen in our Nanostring as well as the human Proteoform database). Therefore, combined targeting of TME HK2/HK3 with RNAi technologies may have a desirable impact of decreasing myeloid and tumor cell glycolysis while leaving T cell glycolysis intact.

Increasing the number of targets would theoretically increase the potential risk of off target effects. The dose limiting toxicity of 2DG was neurological and it would be unexpected that lipid nanoparticles can cross the blood brain barrier whereas 2DG is a glucose analog. More specificity can be added to this RNAi strategy by adding mannosylated sugars to only target M2 macrophages (binding via CD206) as done by the Yull/Gorgio groups at Vanderbilt (Ortega et al., 2016).

Another new pharmacological approach is using targeted protein degradation (Hanzl & Winter, 2020). This paradigm relies on relatively large molecules that have two biologically active components, one binding a ubiquitin ligase and another component binding a protein of interest. These molecules promote proteasomal degradation of proteins in a specific manner by forcing the addition of ubiquitin on the protein of interest. The most successful example of molecules in this class are thalidomide and it family of immunomodulatory drugs (IMiDs). IMiDs work by targeted degradation of the B cell specific transcription factors IZKF1/3 and thus these molecules are biologically active in plasma cell malignancies like multiple myeloma (Kronke et al., 2014). This degrader approach also overcomes the similarity of the ATP binding pockets across HK1/2/3. The homology between these domains would have made it difficult to generate small molecules against the catalytic domain of each isozyme. Additionally, these enzymes can have moonlighting functions that would not be inhibited by ATP mimetics.

The degrader paradigm is exciting because these molecules only need to bind a protein surface or pocket, not an active site. Therefore, small molecules can be generated against the unique HK3 N-terminus and then placed on degrader scaffolds that promote VHL or CRBN binding to promote proteasomal degradation. In ccRCC, it would be compelling to use a VHL dependent degrader because these molecules would cause no degradation in the VHL-/- cancer cells but would promote degradation in the surrounding VHL+ stroma. This strategy could demonstrate that targeting a stromal associated program has anti-tumor efficacy, like αPD1 inhibition. This in contrast to mutation specific TKIs or chemotherapy in which the mechanism of action is by inducing apoptosis of rapidly proliferating cells.

It is interesting to note that of all the previously FDA approved therapies for ccRCC (IL2, VEGF TKI, αPD1, IFNα), direct cancer cell cytotoxicity is not a major mechanism of action. Instead, these therapies alter TME constituents to promote cell death via hypoxia or via immune activation. However, this may not be the paradigm for ccRCC permanently. Currently HIF2α inhibitors are in advanced stage clinical trials and have demonstrated signs of efficacy. They effectively control ccRCCs in VHL disease patients and have been approved in that setting recently (Jonasch et al., 2021). It is known that myeloid HIF2α can contribute to cancer development (Imtiyaz et al., 2010). So, these therapies may also decrease myeloid glycolysis and thus myeloid immunosuppression. In total, these observations, support HK3 as a target in ccRCC because it fits a paradigm where altering TME gene programs can ultimately impact ccRCC patient outcomes.

Another pharmacological strategy can rely on targeting different post translational modifications (PTM) that drive the differences in localization of HK1/2 vs HK3. This

paradigm has been used in the inhibition of RAS isoforms in malignancy. There are three RAS isoforms in humans: HRAS, NRAS, and KRAS. A series of lipid installing events occur post translationally that help traffic this oncogene to the cell membrane (Rowinsky et al., 1999). As this field progressed, much interest was in the development of farnesyltransferase inhibitors that would prevent these three isoforms from being placed on the inner leaflet of cell membrane. With this mis-trafficking it was hypothesized that RAS would no longer be able to transduce its pro-growth signals. However, these drugs failed in KRAS and NRAS mutated tumors because other lipoyl-transferases can bypass the farnesylation mark. (like adding a geranylgeranylation mark) (Storck et al., 2019; Whyte et al., 1997). This geranylgeranyl permits KRAS/NRAS to reach the cell membrane and to constitutively signal. HRAS however is singularly reliant on the farnseyl group and thus these inhibitors do have clinical benefit in HRAS mutated tumors (Gilardi et al., 2020). Unfortunately, HRAS is the least mutated of the RAS isoforms in cancer, This example demonstrates that it may be possible to target HK3 by understanding its unique PTMs and how this isoforms traffics from ribosomes into the cytoplasm. Performing IP/Mass spectrometry in the HK3-GFP cell lines discussed earlier will be helpful in identifying those marks and potentially targeting to decrease cytoplasmic HK3 activity.

References

For tables 1.1/1.2

1. Osthus, R.C., et al., *Deregulation of glucose transporter 1 and glycolytic gene expression by c-Myc.* J Biol Chem, 2000. **275**(29): p. 21797-800.
2. Kim, J.W., et al., *Evaluation of myc E-box phylogenetic footprints in glycolytic genes by chromatin immunoprecipitation assays.* Mol Cell Biol, 2004. **24**(13): p. 5923-36.
3. Tateishi, K., et al., *Myc-Driven Glycolysis Is a Therapeutic Target in Glioblastoma.* Clin Cancer Res, 2016. **22**(17): p. 4452-65.
4. Satoh, K., et al., *Global metabolic reprogramming of colorectal cancer occurs at adenoma stage and is induced by MYC.* Proc Natl Acad Sci U S A, 2017. **114**(37): p. E7697-E7706.
5. Elstrom, R.L., et al., *Akt stimulates aerobic glycolysis in cancer cells.* Cancer Res, 2004. **64**(11): p. 3892-9.
6. Edinger, A.L. and C.B. Thompson, *Akt maintains cell size and survival by increasing mTOR-dependent nutrient uptake.* Mol Biol Cell, 2002. **13**(7): p. 2276-88.
7. Hung, Y.P., et al., *Akt regulation of glycolysis mediates bioenergetic stability in epithelial cells.* Elife, 2017. **6**.
8. Nogueira, V., K.C. Patra, and N. Hay, *Selective eradication of cancer displaying hyperactive Akt by exploiting the metabolic consequences of Akt activation.* Elife, 2018. **7**.
9. Dupuy, F., et al., *PDK1-Dependent Metabolic Reprogramming Dictates Metastatic Potential in Breast Cancer.* Cell Metab, 2015. **22**(4): p. 577-89.
10. Maurer, M., et al., *3-Phosphoinositide-dependent kinase 1 potentiates upstream lesions on the phosphatidylinositol 3-kinase pathway in breast carcinoma.* Cancer Res, 2009. **69**(15): p. 6299-306.
11. McFate, T., et al., *Pyruvate dehydrogenase complex activity controls metabolic and malignant phenotype in cancer cells.* J Biol Chem, 2008. **283**(33): p. 22700-8.
12. Hao, Y., et al., *Oncogenic PIK3CA mutations reprogram glutamine metabolism in colorectal cancer.* Nat Commun, 2016. **7**: p. 11971.
13. Hopkins, B.D., et al., *Suppression of insulin feedback enhances the efficacy of PI3K inhibitors.* Nature, 2018. **560**(7719): p. 499-503.
14. Magometschnigg, H., et al., *PIK3CA Mutational Status Is Associated with High Glycolytic Activity in ER+/HER2- Early Invasive Breast Cancer: a Molecular Imaging Study Using [(18)F]FDG PET/CT.* Mol Imaging Biol, 2019. **21**(5): p. 991-1002.
15. Jiang, W., et al., *The PIK3CA E542K and E545K mutations promote glycolysis and proliferation via induction of the beta-catenin/SIRT3 signaling pathway in cervical cancer.* J Hematol Oncol, 2018. **11**(1): p. 139.
16. Ciraolo, E., et al., *Phosphoinositide 3-kinase p110beta activity: key role in metabolism and mammary gland cancer but not development.* Sci Signal, 2008. **1**(36): p. ra3.
17. Jia, S., et al., *Essential roles of PI(3)K-p110beta in cell growth, metabolism and tumorigenesis.* Nature, 2008. **454**(7205): p. 776-9.
18. Gopal, A.K., et al., *PI3Kdelta inhibition by idelalisib in patients with relapsed indolent lymphoma.* N Engl J Med, 2014. **370**(11): p. 1008-18.
19. Kurmi, K., et al., *Tyrosine Phosphorylation of Mitochondrial Creatine Kinase 1 Enhances a Druggable Tumor Energy Shuttle Pathway.* Cell Metab, 2018. **28**(6): p. 833-847 e8.
20. Kim, S.M., et al., *Glycolysis inhibition sensitizes non-small cell lung cancer with T790M mutation to irreversible EGFR inhibitors via translational suppression of Mcl-1 by AMPK activation.* Mol Cancer Ther, 2013. **12**(10): p. 2145-56.
21. Kim, J.H., et al., *Enhanced Glycolysis Supports Cell Survival in EGFR-Mutant Lung Adenocarcinoma by Inhibiting Autophagy-Mediated EGFR Degradation.* Cancer Res, 2018. **78**(16): p. 4482-4496.
22. Yang, W., et al., *EGFR-induced and PKCepsilon monoubiquitylation-dependent NF-kappaB activation upregulates PKM2 expression and promotes tumorigenesis.* Mol Cell, 2012. **48**(5): p. 771-84.
23. Mazure, N.M., et al., *Oncogenic transformation and hypoxia synergistically act to modulate vascular endothelial growth factor expression.* Cancer Res, 1996. **56**(15): p. 3436-40.
24. Santana-Codina, N., et al., *Oncogenic KRAS supports pancreatic cancer through regulation of nucleotide synthesis.* Nat Commun, 2018. **9**(1): p. 4945.
25. Viale, A., et al., *Oncogene ablation-resistant pancreatic cancer cells depend on mitochondrial function.* Nature, 2014. **514**(7524): p. 628-32.
26. Zhang, H., et al., *HIF-1 inhibits mitochondrial biogenesis and cellular respiration in VHL-deficient renal cell carcinoma by repression of C-MYC activity.* Cancer Cell, 2007. **11**(5): p. 407-20.
27. Thomas, G.V., et al., *Hypoxia-inducible factor determines sensitivity to inhibitors of mTOR in kidney cancer.* Nat Med, 2006. **12**(1): p. 122-7.
28. Courtney, K.D., et al., *Isotope Tracing of Human Clear Cell Renal Cell Carcinomas Demonstrates Suppressed Glucose Oxidation In Vivo.* Cell Metab, 2018. **28**(5): p. 793-800 e2.
29. Matoba, S., et al., *p53 regulates mitochondrial respiration.* Science, 2006. **312**(5780): p. 1650-3.

30. Schwartzenberg-Bar-Yoseph, F., M. Armoni, and E. Karnieli, *The tumor suppressor p53 down-regulates glucose transporters GLUT1 and GLUT4 gene expression.* Cancer Res, 2004. **64**(7): p. 2627-33.
31. Kawauchi, K., et al., *p53 regulates glucose metabolism through an IKK-NF-kappaB pathway and inhibits cell transformation.* Nat Cell Biol, 2008. **10**(5): p. 611-8.
32. Bensaad, K., et al., *TIGAR, a p53-inducible regulator of glycolysis and apoptosis.* Cell, 2006. **126**(1): p. 107-20.
33. Jiang, P., et al., *p53 regulates biosynthesis through direct inactivation of glucose-6-phosphate dehydrogenase.* Nat Cell Biol, 2011. **13**(3): p. 310-6.
34. Boidot, R., et al., *Regulation of monocarboxylate transporter MCT1 expression by p53 mediates inward and outward lactate fluxes in tumors.* Cancer Res, 2012. **72**(4): p. 939-48.
35. Sun, S., et al., *Constitutive Activation of mTORC1 in Endothelial Cells Leads to the Development and Progression of Lymphangiosarcoma through VEGF Autocrine Signaling.* Cancer Cell, 2015. **28**(6): p. 758-772.
36. Sun, Q., et al., *Mammalian target of rapamycin up-regulation of pyruvate kinase isoenzyme type M2 is critical for aerobic glycolysis and tumor growth.* Proc Natl Acad Sci U S A, 2011. **108**(10): p. 4129-34.
37. Jiang, X., H.L. Kenerson, and R.S. Yeung, *Glucose deprivation in tuberous sclerosis complex-related tumors.* Cell Biosci, 2011. **1**: p. 34.
38. Parkhitko, A.A., et al., *Autophagy-dependent metabolic reprogramming sensitizes TSC2-deficient cells to the antimetabolite 6-aminonicotinamide.* M ol Cancer Res, 2014. **12**(1): p. 48-57.
39. Faubert, B., et al., *Loss of the tumor suppressor LKB1 promotes metabolic reprogramming of cancer cells via HIF-1alpha.* Proc Natl Acad Sci U S A, 2014. **111**(7): p. 2554-9.
40. Mahoney, C.L., et al., *LKB1/KRAS mutant lung cancers constitute a genetic subset of NSCLC with increased sensitivity to MAPK and mTOR signalling inhibition.* Br J Cancer, 2009. **100**(2): p. 370-5.
41. Poffenberger, M.C., et al., *LKB1 deficiency in T cells promotes the development of gastrointestinal polyposis.* Science, 2018. **361**(6400): p. 406-411.
42. Yang, Y., et al., *UOK 262 cell line, fumarate hydratase deficient (FH-/FH-) hereditary leiomyomatosis renal cell carcinoma: in vitro and in vivo model of an aberrant energy metabolic pathway in human cancer.* Cancer Genet Cytogenet, 2010. **196**(1): p. 45-55.
43. Baysal, B.E., et al., *Mutations in SDHD, a mitochondrial complex II gene, in hereditary paraganglioma.* Science, 2000. **287**(5454): p. 848-51.
44. Dang, L., et al., *Cancer-associated IDH1 mutations produce 2-hydroxyglutarate.* Nature, 2009. **462**(7274): p. 739-44.
45. Bunse, L., et al., *Suppression of antitumor T cell immunity by the oncometabolite (R)-2-hydroxyglutarate.* Nat Med, 2018. **24**(8): p. 1192-1203.
46. Cascone, T., et al., *Increased Tumor Glycolysis Characterizes Immune Resistance to Adoptive T Cell Therapy.* Cell Metab, 2018. **27**(5): p. 977-987 e4.
47. Lynch, J.T., et al., *Inhibiting PI3Kbeta with AZD8186 Regulates Key Metabolic Pathways in PTEN-Null Tumors.* Clin Cancer Res, 2017. **23**(24): p. 7584-7595.
48. Cordero-Espinoza, L. and T. Hagen, *Increased concentrations of fructose 2,6-bisphosphate contribute to the Warburg effect in phosphatase and tensin homolog (PTEN)-deficient cells.* J Biol Chem, 2013. **288**(50): p. 36020-8.
49. Wang, L., et al., *Hexokinase 2-mediated Warburg effect is required for PTEN- and p53-deficiency-driven prostate cancer growth.* Cell Rep, 2014. **8**(5): p. 1461-74.
50. Qian, X., et al., *PTEN Suppresses Glycolysis by Dephosphorylating and Inhibiting Autophosphorylated PGK1.* Mol Cell, 2019. **76**(3): p. 516-527 e7.

For thesis body

Abu-Eid, R., Samara, R. N., Ozbun, L., Abdalla, M. Y., Berzofsky, J. A., Friedman, K. M., Mkrtichyan, M., & Khleif, S. N. (2014). Selective inhibition of regulatory T cells by targeting the PI3K-Akt pathway. *Cancer Immunol Res*, *2*(11), 1080-1089. https://doi.org/10.1158/2326-6066.CIR-14-0095

Acosta-Iborra, B., Elorza, A., Olazabal, I. M., Martin-Cofreces, N. B., Martin-Puig, S., Miro, M., Calzada, M. J., Aragones, J., Sanchez-Madrid, F., & Landazuri, M. O. (2009). Macrophage oxygen sensing modulates antigen presentation and phagocytic functions involving IFN-gamma production through the HIF-1 alpha transcription factor. *J Immunol*, *182*(5), 3155-3164. https://doi.org/10.4049/jimmunol.0801710

Aide, N., Hicks, R. J., Le Tourneau, C., Lheureux, S., Fanti, S., & Lopci, E. (2019). FDG PET/CT for assessing tumour response to immunotherapy : Report on the EANM symposium on immune modulation and recent review of the literature. *Eur J Nucl Med Mol Imaging*, *46*(1), 238-250. https://doi.org/10.1007/s00259-018-4171-4

Aird, T. P., Farquharson, A. J., Bermingham, K. M., O'Sulllivan, A., Drew, J. E., & Carson, B. P. (2021). Divergent serum metabolomic, skeletal muscle signaling, transcriptomic, and performance adaptations to fasted versus whey protein-fed sprint interval training. *Am J Physiol Endocrinol Metab*, *321*(6), E802-E820. https://doi.org/10.1152/ajpendo.00265.2021

Alessi, D. R., James, S. R., Downes, C. P., Holmes, A. B., Gaffney, P. R., Reese, C. B., & Cohen, P. (1997). Characterization of a 3-phosphoinositide-dependent protein kinase which phosphorylates and activates protein kinase Balpha. *Curr Biol*, *7*(4), 261-269. https://doi.org/10.1016/s0960-9822(06)00122-9

Allard, B., Pommey, S., Smyth, M. J., & Stagg, J. (2013). Targeting CD73 enhances the antitumor activity of anti-PD-1 and anti-CTLA-4 mAbs. *Clin Cancer Res*, *19*(20), 5626-5635. https://doi.org/10.1158/1078-0432.CCR-13-0545

Altman, B. J., Stine, Z. E., & Dang, C. V. (2016). From Krebs to clinic: glutamine metabolism to cancer therapy. *Nat Rev Cancer*, *16*(10), 619-634. https://doi.org/10.1038/nrc.2016.71

Ancey, P. B., Contat, C., Boivin, G., Sabatino, S., Pascual, J., Zangger, N., Perentes, J. Y., Peters, S., Abel, E. D., Kirsch, D. G., Rathmell, J. C., Vozenin, M. C., & Meylan, E. (2021). GLUT1 Expression in Tumor-Associated Neutrophils Promotes Lung Cancer Growth and Resistance to Radiotherapy. *Cancer Res*, *81*(9), 2345-2357. https://doi.org/10.1158/0008-5472.CAN-20-2870

Andrejeva, G., & Rathmell, J. C. (2017). Similarities and Distinctions of Cancer and Immune Metabolism in Inflammation and Tumors. *Cell Metab*, *26*(1), 49-70. https://doi.org/10.1016/j.cmet.2017.06.004

Angelin, A., Gil-de-Gomez, L., Dahiya, S., Jiao, J., Guo, L., Levine, M. H., Wang, Z., Quinn, W. J., 3rd, Kopinski, P. K., Wang, L., Akimova, T., Liu, Y., Bhatti, T. R., Han, R., Laskin, B. L., Baur, J. A., Blair, I. A., Wallace, D. C., Hancock, W. W., & Beier, U. H. (2017). Foxp3 Reprograms T Cell Metabolism to Function in Low-Glucose, High-Lactate Environments. *Cell Metab*, *25*(6), 1282-1293 e1287. https://doi.org/10.1016/j.cmet.2016.12.018

Arnold, D. E., & Heimall, J. R. (2017). A Review of Chronic Granulomatous Disease. *Adv Ther*, *34*(12), 2543-2557. https://doi.org/10.1007/s12325-017-0636-2

Assmann, N., O'Brien, K. L., Donnelly, R. P., Dyck, L., Zaiatz-Bittencourt, V., Loftus, R. M., Heinrich, P., Oefner, P. J., Lynch, L., Gardiner, C. M., Dettmer, K., & Finlay, D. K. (2017). Srebp-controlled glucose metabolism is essential for NK cell functional responses. *Nat Immunol*, *18*(11), 1197-1206. https://doi.org/10.1038/ni.3838

Aune, T. M., Crooke, P. S., 3rd, Patrick, A. E., Tossberg, J. T., Olsen, N. J., & Spurlock, C. F., 3rd. (2017). Expression of long non-coding RNAs in autoimmunity and linkage to enhancer function and autoimmune disease risk genetic variants. *J Autoimmun*, *81*, 99-109. https://doi.org/10.1016/j.jaut.2017.03.014

Azuma, T., Yao, S., Zhu, G., Flies, A. S., Flies, S. J., & Chen, L. (2008). B7-H1 is a ubiquitous antiapoptotic receptor on cancer cells. *Blood*, *111*(7), 3635-3643. https://doi.org/10.1182/blood-2007-11-123141

Bachem, A., Guttler, S., Hartung, E., Ebstein, F., Schaefer, M., Tannert, A., Salama, A., Movassaghi, K., Opitz, C., Mages, H. W., Henn, V., Kloetzel, P. M., Gurka, S., & Kroczek, R. A. (2010). Superior antigen cross-presentation and XCR1 expression define human CD11c+CD141+ cells as homologues of mouse CD8+ dendritic cells. *J Exp Med*, *207*(6), 1273-1281. https://doi.org/10.1084/jem.20100348

Balko, J. M. A., M.L. Meijers W.C. et al. . (2022). Cytotoxic T cells specific for alpha-myosin drive immunotherapy related myocarditis. *Research Square*. https://doi.org/ [https://doi.org/10.21203/rs.3.rs-1315661/v1]

Barbi, J., Cummings, H. E., Lu, B., Oghumu, S., Ruckle, T., Rommel, C., Lafuse, W., Whitacre, C. C., & Satoskar, A. R. (2008). PI3Kgamma (PI3Kgamma) is essential for efficient induction of CXCR3 on activated T cells. *Blood*, *112*(8), 3048-3051. https://doi.org/10.1182/blood-2008-02-135715

Barry, K. C., Hsu, J., Broz, M. L., Cueto, F. J., Binnewies, M., Combes, A. J., Nelson, A. E., Loo, K., Kumar, R., Rosenblum, M. D., Alvarado, M. D., Wolf, D. M., Bogunovic, D., Bhardwaj, N., Daud, A. I., Ha, P. K., Ryan, W. R., Pollack, J. L., Samad, B., . . . Krummel, M. F. (2018). A natural killer-dendritic cell axis defines checkpoint therapy-responsive tumor microenvironments. *Nat Med*, *24*(8), 1178-1191. https://doi.org/10.1038/s41591-018-0085-8

Barsoum, I. B., Smallwood, C. A., Siemens, D. R., & Graham, C. H. (2014). A mechanism of hypoxia-mediated escape from adaptive immunity in cancer cells. *Cancer Res*, *74*(3), 665-674. https://doi.org/10.1158/0008-5472.CAN-13-0992

Basu, S., Hubbard, B., & Shevach, E. M. (2015). Foxp3-mediated inhibition of Akt inhibits Glut1 (glucose transporter 1) expression in human T regulatory cells. *J Leukoc Biol*, *97*(2), 279-283. https://doi.org/10.1189/jlb.2AB0514-273RR

Baumann, T., Dunkel, A., Schmid, C., Schmitt, S., Hiltensperger, M., Lohr, K., Laketa, V., Donakonda, S., Ahting, U., Lorenz-Depiereux, B., Heil, J. E., Schredelseker, J., Simeoni, L., Fecher, C., Korber, N., Bauer, T., Huser, N., Hartmann, D., Laschinger, M., . . . Hochst, B. (2020). Regulatory myeloid cells paralyze T cells through cell-cell transfer of the metabolite methylglyoxal. *Nat Immunol*, *21*(5), 555-566. https://doi.org/10.1038/s41590-020-0666-9

Becker, C., Fantini, M. C., Wirtz, S., Nikolaev, A., Kiesslich, R., Lehr, H. A., Galle, P. R., & Neurath, M. F. (2005). In vivo imaging of colitis and colon cancer development in mice using high resolution chromoendoscopy. *Gut*, *54*(7), 950-954. https://doi.org/10.1136/gut.2004.061283

Beckermann, K. E., Hongo, R., Ye, X., Young, K., Carbonell, K., Healey, D. C. C., Siska, P. J., Barone, S., Roe, C. E., Smith, C. C., Vincent, B. G., Mason, F. M., Irish, J. M., Rathmell, W. K., & Rathmell, J. C. (2020). CD28 costimulation drives tumor-infiltrating T cell glycolysis to promote inflammation. *JCI Insight*, *5*(16). https://doi.org/10.1172/jci.insight.138729

Beharry, Z., Mahajan, S., Zemskova, M., Lin, Y. W., Tholanikunnel, B. G., Xia, Z., Smith, C. D., & Kraft, A. S. (2011). The Pim protein kinases regulate energy metabolism and cell growth. *Proc Natl Acad Sci U S A*, *108*(2), 528-533. https://doi.org/10.1073/pnas.1013214108

Bensaad, K., Tsuruta, A., Selak, M. A., Vidal, M. N., Nakano, K., Bartrons, R., Gottlieb, E., & Vousden, K. H. (2006). TIGAR, a p53-inducible regulator of glycolysis and apoptosis. *Cell*, *126*(1), 107-120. https://doi.org/10.1016/j.cell.2006.05.036

Bhandari, T., Olson, J., Johnson, R. S., & Nizet, V. (2013). HIF-1alpha influences myeloid cell antigen presentation and response to subcutaneous OVA vaccination. *J Mol Med (Berl)*, *91*(10), 1199-1205. https://doi.org/10.1007/s00109-013-1052-y

Bi, K., He, M. X., Bakouny, Z., Kanodia, A., Napolitano, S., Wu, J., Grimaldi, G., Braun, D. A., Cuoco, M. S., Mayorga, A., DelloStritto, L., Bouchard, G., Steinharter, J., Tewari, A. K., Vokes, N. I., Shannon, E., Sun, M., Park, J., Chang, S. L., . . . Van Allen, E. M. (2021). Tumor and immune reprogramming during immunotherapy in advanced renal cell carcinoma. *Cancer Cell*, *39*(5), 649-661 e645. https://doi.org/10.1016/j.ccell.2021.02.015

Bian, Y., Li, W., Kremer, D. M., Sajjakulnukit, P., Li, S., Crespo, J., Nwosu, Z. C., Zhang, L., Czerwonka, A., Pawlowska, A., Xia, H., Li, J., Liao, P., Yu, J., Vatan, L., Szeliga, W., Wei, S., Grove, S., Liu, J. R., . . . Zou, W. (2020). Cancer SLC43A2 alters T cell methionine metabolism and histone methylation. *Nature*, *585*(7824), 277-282. https://doi.org/10.1038/s41586-020-2682-1

Blouin, C. C., Page, E. L., Soucy, G. M., & Richard, D. E. (2004). Hypoxic gene activation by lipopolysaccharide in macrophages: implication of hypoxia-inducible factor 1alpha. *Blood*, *103*(3), 1124-1130. https://doi.org/10.1182/blood-2003-07-2427

Boonekamp, F. J., Knibbe, E., Vieira-Lara, M. A., Wijsman, M., Luttik, M. A. H., van Eunen, K., den Ridder, M., Bron, R., Almonacid Suarez, A. M., van Rijn, P., Wolters, J. C., Pabst, M., Daran, J.-M., Bakker, B., & Daran-Lapujade, P. (2021). A yeast with muscle doesn't run faster: full humanization of the glycolytic pathway in Saccharomyces cerevisiae. *bioRxiv*, 2021.2009.2028.462164. https://doi.org/10.1101/2021.09.28.462164

Borges da Silva, H., Beura, L. K., Wang, H., Hanse, E. A., Gore, R., Scott, M. C., Walsh, D. A., Block, K. E., Fonseca, R., Yan, Y., Hippen, K. L., Blazar, B. R., Masopust, D., Kelekar, A., Vulchanova, L., Hogquist, K. A., & Jameson, S. C. (2018). The purinergic receptor P2RX7 directs metabolic fitness of long-lived memory CD8(+) T cells. *Nature*, *559*(7713), 264-268. https://doi.org/10.1038/s41586-018-0282-0

Bottcher, J. P., Bonavita, E., Chakravarty, P., Blees, H., Cabeza-Cabrerizo, M., Sammicheli, S., Rogers, N. C., Sahai, E., Zelenay, S., & Reis e Sousa, C. (2018). NK Cells Stimulate Recruitment of cDC1 into the Tumor Microenvironment Promoting Cancer Immune Control. *Cell*, *172*(5), 1022-1037 e1014. https://doi.org/10.1016/j.cell.2018.01.004

Bougneres, L., Helft, J., Tiwari, S., Vargas, P., Chang, B. H., Chan, L., Campisi, L., Lauvau, G., Hugues, S., Kumar, P., Kamphorst, A. O., Dumenil, A. M., Nussenzweig, M., MacMicking, J. D., Amigorena, S., & Guermonprez, P. (2009). A role for lipid bodies in the cross-presentation of phagocytosed antigens by MHC class I in dendritic cells. *Immunity*, *31*(2), 232-244. https://doi.org/10.1016/j.immuni.2009.06.022

Boussiotis, V. A., Chatterjee, P., & Li, L. (2014). Biochemical signaling of PD-1 on T cells and its functional implications. *Cancer J*, *20*(4), 265-271. https://doi.org/10.1097/PPO.0000000000000059

Brand, A., Singer, K., Koehl, G. E., Kolitzus, M., Schoenhammer, G., Thiel, A., Matos, C., Bruss, C., Klobuch, S., Peter, K., Kastenberger, M., Bogdan, C., Schleicher, U., Mackensen, A., Ullrich, E., Fichtner-Feigl, S., Kesselring, R., Mack, M., Ritter, U., . . . Kreutz, M. (2016). LDHA-Associated Lactic Acid Production Blunts

Tumor Immunosurveillance by T and NK Cells. *Cell Metab*, *24*(5), 657-671. https://doi.org/10.1016/j.cmet.2016.08.011
Braun, D. A., Street, K., Burke, K. P., Cookmeyer, D. L., Denize, T., Pedersen, C. B., Gohil, S. H., Schindler, N., Pomerance, L., Hirsch, L., Bakouny, Z., Hou, Y., Forman, J., Huang, T., Li, S., Cui, A., Keskin, D. B., Steinharter, J., Bouchard, G., . . . Wu, C. J. (2021). Progressive immune dysfunction with advancing disease stage in renal cell carcinoma. *Cancer Cell*, *39*(5), 632-648 e638. https://doi.org/10.1016/j.ccell.2021.02.013
Briercheck, E. L., Trotta, R., Chen, L., Hartlage, A. S., Cole, J. P., Cole, T. D., Mao, C., Banerjee, P. P., Hsu, H. T., Mace, E. M., Ciarlariello, D., Mundy-Bosse, B. L., Garcia-Cao, I., Scoville, S. D., Yu, L., Pilarski, R., Carson, W. E., 3rd, Leone, G., Pandolfi, P. P., . . . Caligiuri, M. A. (2015). PTEN is a negative regulator of NK cell cytolytic function. *J Immunol*, *194*(4), 1832-1840. https://doi.org/10.4049/jimmunol.1401224
Brown, C. C., Gudjonson, H., Pritykin, Y., Deep, D., Lavallee, V. P., Mendoza, A., Fromme, R., Mazutis, L., Ariyan, C., Leslie, C., Pe'er, D., & Rudensky, A. Y. (2019). Transcriptional Basis of Mouse and Human Dendritic Cell Heterogeneity. *Cell*, *179*(4), 846-863 e824. https://doi.org/10.1016/j.cell.2019.09.035
Bryant, K. L., Mancias, J. D., Kimmelman, A. C., & Der, C. J. (2014). KRAS: feeding pancreatic cancer proliferation. *Trends Biochem Sci*, *39*(2), 91-100. https://doi.org/10.1016/j.tibs.2013.12.004
Buchan, S. L., Fallatah, M., Thirdborough, S. M., Taraban, V. Y., Rogel, A., Thomas, L. J., Penfold, C. A., He, L. Z., Curran, M. A., Keler, T., & Al-Shamkhani, A. (2018). PD-1 Blockade and CD27 Stimulation Activate Distinct Transcriptional Programs That Synergize for CD8(+) T-Cell-Driven Antitumor Immunity. *Clin Cancer Res*, *24*(10), 2383-2394. https://doi.org/10.1158/1078-0432.CCR-17-3057
Byles, V., Covarrubias, A. J., Ben-Sahra, I., Lamming, D. W., Sabatini, D. M., Manning, B. D., & Horng, T. (2013). The TSC-mTOR pathway regulates macrophage polarization. *Nat Commun*, *4*, 2834. https://doi.org/10.1038/ncomms3834
Byun, J. K., Park, M., Lee, S., Yun, J. W., Lee, J., Kim, J. S., Cho, S. J., Jeon, H. J., Lee, I. K., Choi, Y. K., & Park, K. G. (2020). Inhibition of Glutamine Utilization Synergizes with Immune Checkpoint Inhibitor to Promote Antitumor Immunity. *Mol Cell*, *80*(4), 592-606 e598. https://doi.org/10.1016/j.molcel.2020.10.015
Cai, T. T., Ye, S. B., Liu, Y. N., He, J., Chen, Q. Y., Mai, H. Q., Zhang, C. X., Cui, J., Zhang, X. S., Busson, P., Zeng, Y. X., & Li, J. (2017). LMP1-mediated glycolysis induces myeloid-derived suppressor cell expansion in nasopharyngeal carcinoma. *PLoS Pathog*, *13*(7), e1006503. https://doi.org/10.1371/journal.ppat.1006503
Calcinotto, A., Filipazzi, P., Grioni, M., Iero, M., De Milito, A., Ricupito, A., Cova, A., Canese, R., Jachetti, E., Rossetti, M., Huber, V., Parmiani, G., Generoso, L., Santinami, M., Borghi, M., Fais, S., Bellone, M., & Rivoltini, L. (2012). Modulation of microenvironment acidity reverses anergy in human and murine tumor-infiltrating T lymphocytes. *Cancer Res*, *72*(11), 2746-2756. https://doi.org/10.1158/0008-5472.CAN-11-1272
Cancer Genome Atlas Research, N. (2013). Comprehensive molecular characterization of clear cell renal cell carcinoma. *Nature*, *499*(7456), 43-49. https://doi.org/10.1038/nature12222
Canouil, M., Bouland, G. A., Bonnefond, A., Froguel, P., t Hart, L. M., & Slieker, R. C. (2020). NACHO: an R package for quality control of NanoString nCounter data. *Bioinformatics*, *36*(3), 970-971. https://doi.org/10.1093/bioinformatics/btz647
Cantor, J. R., Abu-Remaileh, M., Kanarek, N., Freinkman, E., Gao, X., Louissaint, A., Jr., Lewis, C. A., & Sabatini, D. M. (2017). Physiologic Medium Rewires Cellular Metabolism and Reveals Uric Acid as an Endogenous Inhibitor of UMP Synthase. *Cell*, *169*(2), 258-272 e217. https://doi.org/10.1016/j.cell.2017.03.023
Cao, D., Qi, Z., Pang, Y., Li, H., Xie, H., Wu, J., Huang, Y., Zhu, Y., Shen, Y., Zhu, Y., Dai, B., Hu, X., Ye, D., & Wang, Z. (2019). Retinoic Acid-Related Orphan Receptor C Regulates Proliferation, Glycolysis, and Chemoresistance via the PD-L1/ITGB6/STAT3 Signaling Axis in Bladder Cancer. *Cancer Res*, *79*(10), 2604-2618. https://doi.org/10.1158/0008-5472.CAN-18-3842
Cao, L., Che, X., Qiu, X., Li, Z., Yang, B., Wang, S., Hou, K., Fan, Y., Qu, X., & Liu, Y. (2019). M2 macrophage infiltration into tumor islets leads to poor prognosis in non-small-cell lung cancer. *Cancer Manag Res*, *11*, 6125-6138. https://doi.org/10.2147/CMAR.S199832
Cardenas, M. L., Cornish-Bowden, A., & Ureta, T. (1998). Evolution and regulatory role of the hexokinases. *Biochim Biophys Acta*, *1401*(3), 242-264. https://doi.org/10.1016/s0167-4889(97)00150-x
Cascone, T., McKenzie, J. A., Mbofung, R. M., Punt, S., Wang, Z., Xu, C., Williams, L. J., Wang, Z., Bristow, C. A., Carugo, A., Peoples, M. D., Li, L., Karpinets, T., Huang, L., Malu, S., Creasy, C., Leahey, S. E., Chen, J., Chen, Y., . . . Peng, W. (2018). Increased Tumor Glycolysis Characterizes Immune Resistance to Adoptive T Cell Therapy. *Cell Metab*, *27*(5), 977-987 e974. https://doi.org/10.1016/j.cmet.2018.02.024
Chafe, S. C., Lou, Y., Sceneay, J., Vallejo, M., Hamilton, M. J., McDonald, P. C., Bennewith, K. L., Moller, A., & Dedhar, S. (2015). Carbonic anhydrase IX promotes myeloid-derived suppressor cell mobilization and establishment of a metastatic niche by stimulating G-CSF production. *Cancer Res*, *75*(6), 996-1008. https://doi.org/10.1158/0008-5472.CAN-14-3000
Chafe, S. C., McDonald, P. C., Saberi, S., Nemirovsky, O., Venkateswaran, G., Burugu, S., Gao, D., Delaidelli, A., Kyle, A. H., Baker, J. H. E., Gillespie, J. A., Bashashati, A., Minchinton, A. I., Zhou, Y., Shah, S. P., & Dedhar, S. (2019). Targeting Hypoxia-Induced Carbonic Anhydrase IX Enhances Immune-Checkpoint Blockade Locally and Systemically. *Cancer Immunol Res*, *7*(7), 1064-1078. https://doi.org/10.1158/2326-6066.CIR-18-0657

Chan, D. A., Sutphin, P. D., Nguyen, P., Turcotte, S., Lai, E. W., Banh, A., Reynolds, G. E., Chi, J. T., Wu, J., Solow-Cordero, D. E., Bonnet, M., Flanagan, J. U., Bouley, D. M., Graves, E. E., Denny, W. A., Hay, M. P., & Giaccia, A. J. (2011). Targeting GLUT1 and the Warburg effect in renal cell carcinoma by chemical synthetic lethality. *Sci Transl Med*, *3*(94), 94ra70. https://doi.org/10.1126/scitranslmed.3002394

Chang, C. H., Qiu, J., O'Sullivan, D., Buck, M. D., Noguchi, T., Curtis, J. D., Chen, Q., Gindin, M., Gubin, M. M., van der Windt, G. J., Tonc, E., Schreiber, R. D., Pearce, E. J., & Pearce, E. L. (2015). Metabolic Competition in the Tumor Microenvironment Is a Driver of Cancer Progression. *Cell*, *162*(6), 1229-1241. https://doi.org/10.1016/j.cell.2015.08.016

Chellappa, S., Kushekhar, K., Munthe, L. A., Tjonnfjord, G. E., Aandahl, E. M., Okkenhaug, K., & Tasken, K. (2019). The PI3K p110delta Isoform Inhibitor Idelalisib Preferentially Inhibits Human Regulatory T Cell Function. *J Immunol*, *202*(5), 1397-1405. https://doi.org/10.4049/jimmunol.1701703

Chen, B., Scurrah, C. R., McKinley, E. T., Simmons, A. J., Ramirez-Solano, M. A., Zhu, X., Markham, N. O., Heiser, C. N., Vega, P. N., Rolong, A., Kim, H., Sheng, Q., Drewes, J. L., Zhou, Y., Southard-Smith, A. N., Xu, Y., Ro, J., Jones, A. L., Revetta, F., . . . Lau, K. S. (2021). Differential pre-malignant programs and microenvironment chart distinct paths to malignancy in human colorectal polyps. *Cell*, *184*(26), 6262-6280 e6226. https://doi.org/10.1016/j.cell.2021.11.031

Chen, D. S., & Mellman, I. (2013). Oncology meets immunology: the cancer-immunity cycle. *Immunity*, *39*(1), 1-10. https://doi.org/10.1016/j.immuni.2013.07.012

Chen, W., Hill, H., Christie, A., Kim, M. S., Holloman, E., Pavia-Jimenez, A., Homayoun, F., Ma, Y., Patel, N., Yell, P., Hao, G., Yousuf, Q., Joyce, A., Pedrosa, I., Geiger, H., Zhang, H., Chang, J., Gardner, K. H., Bruick, R. K., . . . Brugarolas, J. (2016). Targeting renal cell carcinoma with a HIF-2 antagonist. *Nature*, *539*(7627), 112-117. https://doi.org/10.1038/nature19796

Chen, X., & Cubillos-Ruiz, J. R. (2021). Endoplasmic reticulum stress signals in the tumour and its microenvironment. *Nat Rev Cancer*, *21*(2), 71-88. https://doi.org/10.1038/s41568-020-00312-2

Chen, X., Meng, F., & Jiang, R. (2021). Neutrophil-to-Lymphocyte Ratio as a Prognostic Biomarker for Patients With Metastatic Renal Cell Carcinoma Treated With Immune Checkpoint Inhibitors: A Systematic Review and Meta-Analysis. *Front Oncol*, *11*, 746976. https://doi.org/10.3389/fonc.2021.746976

Chen, Y. W., Tekle, C., & Fodstad, O. (2008). The immunoregulatory protein human B7H3 is a tumor-associated antigen that regulates tumor cell migration and invasion. *Curr Cancer Drug Targets*, *8*(5), 404-413. https://doi.org/10.2174/156800908785133141

Chevrier, S., Levine, J. H., Zanotelli, V. R. T., Silina, K., Schulz, D., Bacac, M., Ries, C. H., Ailles, L., Jewett, M. A. S., Moch, H., van den Broek, M., Beisel, C., Stadler, M. B., Gedye, C., Reis, B., Pe'er, D., & Bodenmiller, B. (2017). An Immune Atlas of Clear Cell Renal Cell Carcinoma. *Cell*, *169*(4), 736-749 e718. https://doi.org/10.1016/j.cell.2017.04.016

Chiu, D. K., Tse, A. P., Xu, I. M., Di Cui, J., Lai, R. K., Li, L. L., Koh, H. Y., Tsang, F. H., Wei, L. L., Wong, C. M., Ng, I. O., & Wong, C. C. (2017). Hypoxia inducible factor HIF-1 promotes myeloid-derived suppressor cells accumulation through ENTPD2/CD39L1 in hepatocellular carcinoma. *Nat Commun*, *8*(1), 517. https://doi.org/10.1038/s41467-017-00530-7

Cho, H., Du, X., Rizzi, J. P., Liberzon, E., Chakraborty, A. A., Gao, W., Carvo, I., Signoretti, S., Bruick, R. K., Josey, J. A., Wallace, E. M., & Kaelin, W. G. (2016). On-target efficacy of a HIF-2alpha antagonist in preclinical kidney cancer models. *Nature*, *539*(7627), 107-111. https://doi.org/10.1038/nature19795

Choi, B. K., Lee, D. Y., Lee, D. G., Kim, Y. H., Kim, S. H., Oh, H. S., Han, C., & Kwon, B. S. (2017). 4-1BB signaling activates glucose and fatty acid metabolism to enhance CD8(+) T cell proliferation. *Cell Mol Immunol*, *14*(9), 748-757. https://doi.org/10.1038/cmi.2016.02

Choueiri, T. K., Bauer, T. M., Papadopoulos, K. P., Plimack, E. R., Merchan, J. R., McDermott, D. F., Michaelson, M. D., Appleman, L. J., Thamake, S., Perini, R. F., Zojwalla, N. J., & Jonasch, E. (2021). Inhibition of hypoxia-inducible factor-2alpha in renal cell carcinoma with belzutifan: a phase 1 trial and biomarker analysis. *Nat Med*. https://doi.org/10.1038/s41591-021-01324-7

Chow, M. T., Ozga, A. J., Servis, R. L., Frederick, D. T., Lo, J. A., Fisher, D. E., Freeman, G. J., Boland, G. M., & Luster, A. D. (2019). Intratumoral Activity of the CXCR3 Chemokine System Is Required for the Efficacy of Anti-PD-1 Therapy. *Immunity*, *50*(6), 1498-1512 e1495. https://doi.org/10.1016/j.immuni.2019.04.010

Ciscato, F., Ferrone, L., Masgras, I., Laquatra, C., & Rasola, A. (2021). Hexokinase 2 in Cancer: A Prima Donna Playing Multiple Characters. *Int J Mol Sci*, *22*(9). https://doi.org/10.3390/ijms22094716

Clark, D. J., Dhanasekaran, S. M., Petralia, F., Pan, J., Song, X., Hu, Y., da Veiga Leprevost, F., Reva, B., Lih, T. M., Chang, H. Y., Ma, W., Huang, C., Ricketts, C. J., Chen, L., Krek, A., Li, Y., Rykunov, D., Li, Q. K., Chen, L. S., . . . Clinical Proteomic Tumor Analysis, C. (2019). Integrated Proteogenomic Characterization of Clear Cell Renal Cell Carcinoma. *Cell*, *179*(4), 964-983 e931. https://doi.org/10.1016/j.cell.2019.10.007

Clever, D., Roychoudhuri, R., Constantinides, M. G., Askenase, M. H., Sukumar, M., Klebanoff, C. A., Eil, R. L., Hickman, H. D., Yu, Z., Pan, J. H., Palmer, D. C., Phan, A. T., Goulding, J., Gattinoni, L., Goldrath, A. W., Belkaid, Y., & Restifo, N. P. (2016). Oxygen Sensing by T Cells Establishes an Immunologically Tolerant Metastatic Niche. *Cell*, *166*(5), 1117-1131 e1114. https://doi.org/10.1016/j.cell.2016.07.032

Colegio, O. R., Chu, N. Q., Szabo, A. L., Chu, T., Rhebergen, A. M., Jairam, V., Cyrus, N., Brokowski, C. E., Eisenbarth, S. C., Phillips, G. M., Cline, G. W., Phillips, A. J., & Medzhitov, R. (2014). Functional polarization of tumour-associated macrophages by tumour-derived lactic acid. *Nature*, *513*(7519), 559-563. https://doi.org/10.1038/nature13490

Cong, J., Wang, X., Zheng, X., Wang, D., Fu, B., Sun, R., Tian, Z., & Wei, H. (2018). Dysfunction of Natural Killer Cells by FBP1-Induced Inhibition of Glycolysis during Lung Cancer Progression. *Cell Metab*, *28*(2), 243-255 e245. https://doi.org/10.1016/j.cmet.2018.06.021

Contat, C., Ancey, P. B., Zangger, N., Sabatino, S., Pascual, J., Escrig, S., Jensen, L., Goepfert, C., Lanz, B., Lepore, M., Gruetter, R., Rossier, A., Berezowska, S., Neppl, C., Zlobec, I., Clerc-Rosset, S., Knott, G. W., Rathmell, J. C., Abel, E. D., . . . Meylan, E. (2020). Combined deletion of Glut1 and Glut3 impairs lung adenocarcinoma growth. *Elife*, *9*. https://doi.org/10.7554/eLife.53618

Cortese, N., Capretti, G., Barbagallo, M., Rigamonti, A., Takis, P. G., Castino, G. F., Vignali, D., Maggi, G., Gavazzi, F., Ridolfi, C., Nappo, G., Donisi, G., Erreni, M., Avigni, R., Rahal, D., Spaggiari, P., Roncalli, M., Cappello, P., Novelli, F., . . . Marchesi, F. (2020). Metabolome of Pancreatic Juice Delineates Distinct Clinical Profiles of Pancreatic Cancer and Reveals a Link between Glucose Metabolism and PD-1(+) Cells. *Cancer Immunol Res*, *8*(4), 493-505. https://doi.org/10.1158/2326-6066.CIR-19-0403

Corzo, C. A., Condamine, T., Lu, L., Cotter, M. J., Youn, J. I., Cheng, P., Cho, H. I., Celis, E., Quiceno, D. G., Padhya, T., McCaffrey, T. V., McCaffrey, J. C., & Gabrilovich, D. I. (2010). HIF-1alpha regulates function and differentiation of myeloid-derived suppressor cells in the tumor microenvironment. *J Exp Med*, *207*(11), 2439-2453. https://doi.org/10.1084/jem.20100587

Courtney, K. D., Bezwada, D., Mashimo, T., Pichumani, K., Vemireddy, V., Funk, A. M., Wimberly, J., McNeil, S. S., Kapur, P., Lotan, Y., Margulis, V., Cadeddu, J. A., Pedrosa, I., DeBerardinis, R. J., Malloy, C. R., Bachoo, R. M., & Maher, E. A. (2018). Isotope Tracing of Human Clear Cell Renal Cell Carcinomas Demonstrates Suppressed Glucose Oxidation In Vivo. *Cell Metab*, *28*(5), 793-800 e792. https://doi.org/10.1016/j.cmet.2018.07.020

Courtney, K. D., Corcoran, R. B., & Engelman, J. A. (2010). The PI3K pathway as drug target in human cancer. *J Clin Oncol*, *28*(6), 1075-1083. https://doi.org/10.1200/JCO.2009.25.3641

Courtney, K. D., Infante, J. R., Lam, E. T., Figlin, R. A., Rini, B. I., Brugarolas, J., Zojwalla, N. J., Lowe, A. M., Wang, K., Wallace, E. M., Josey, J. A., & Choueiri, T. K. (2018). Phase I Dose-Escalation Trial of PT2385, a First-in-Class Hypoxia-Inducible Factor-2alpha Antagonist in Patients With Previously Treated Advanced Clear Cell Renal Cell Carcinoma. *J Clin Oncol*, *36*(9), 867-874. https://doi.org/10.1200/JCO.2017.74.2627

Cramer, T., Yamanishi, Y., Clausen, B. E., Forster, I., Pawlinski, R., Mackman, N., Haase, V. H., Jaenisch, R., Corr, M., Nizet, V., Firestein, G. S., Gerber, H. P., Ferrara, N., & Johnson, R. S. (2003). HIF-1alpha is essential for myeloid cell-mediated inflammation. *Cell*, *112*(5), 645-657. https://doi.org/10.1016/s0092-8674(03)00154-5

Crist, S. B., Nemkov, T., Dumpit, R. F., Dai, J., Tapscott, S. J., True, L. D., Swarbrick, A., Sullivan, L. B., Nelson, P. S., Hansen, K. C., & Ghajar, C. M. (2022). Unchecked oxidative stress in skeletal muscle prevents outgrowth of disseminated tumour cells. *Nat Cell Biol*. https://doi.org/10.1038/s41556-022-00881-4

Crompton, J. G., Sukumar, M., Roychoudhuri, R., Clever, D., Gros, A., Eil, R. L., Tran, E., Hanada, K., Yu, Z., Palmer, D. C., Kerkar, S. P., Michalek, R. D., Upham, T., Leonardi, A., Acquavella, N., Wang, E., Marincola, F. M., Gattinoni, L., Muranski, P., . . . Restifo, N. P. (2015). Akt inhibition enhances expansion of potent tumor-specific lymphocytes with memory cell characteristics. *Cancer Res*, *75*(2), 296-305. https://doi.org/10.1158/0008-5472.CAN-14-2277

Crooks, D. R., Maio, N., Lang, M., Ricketts, C. J., Vocke, C. D., Gurram, S., Turan, S., Kim, Y. Y., Cawthon, G. M., Sohelian, F., De Val, N., Pfeiffer, R. M., Jailwala, P., Tandon, M., Tran, B., Fan, T. W., Lane, A. N., Ried, T., Wangsa, D., . . . Linehan, W. M. (2021). Mitochondrial DNA alterations underlie an irreversible shift to aerobic glycolysis in fumarate hydratase-deficient renal cancer. *Sci Signal*, *14*(664). https://doi.org/10.1126/scisignal.abc4436

Crozat, K., Guiton, R., Contreras, V., Feuillet, V., Dutertre, C. A., Ventre, E., Vu Manh, T. P., Baranek, T., Storset, A. K., Marvel, J., Boudinot, P., Hosmalin, A., Schwartz-Cornil, I., & Dalod, M. (2010). The XC chemokine receptor 1 is a conserved selective marker of mammalian cells homologous to mouse CD8alpha+ dendritic cells. *J Exp Med*, *207*(6), 1283-1292. https://doi.org/10.1084/jem.20100223

Cubillos-Ruiz, J. R., Bettigole, S. E., & Glimcher, L. H. (2017). Tumorigenic and Immunosuppressive Effects of Endoplasmic Reticulum Stress in Cancer. *Cell*, *168*(4), 692-706. https://doi.org/10.1016/j.cell.2016.12.004

Cubillos-Ruiz, J. R., Silberman, P. C., Rutkowski, M. R., Chopra, S., Perales-Puchalt, A., Song, M., Zhang, S., Bettigole, S. E., Gupta, D., Holcomb, K., Ellenson, L. H., Caputo, T., Lee, A. H., Conejo-Garcia, J. R., & Glimcher, L. H. (2015). ER Stress Sensor XBP1 Controls Anti-tumor Immunity by Disrupting Dendritic Cell Homeostasis. *Cell*, *161*(7), 1527-1538. https://doi.org/10.1016/j.cell.2015.05.025

D'Souza, L. J., Wright, S. H., & Bhattacharya, D. (2021). Genetic evidence that uptake of the fluorescent analog 2NBDG occurs independently of known glucose transporters. *bioRxiv*, 2021.2012.2013.472409. https://doi.org/10.1101/2021.12.13.472409

da Cunha Santos, G., Shepherd, F. A., & Tsao, M. S. (2011). EGFR mutations and lung cancer. *Annu Rev Pathol*, *6*, 49-69. https://doi.org/10.1146/annurev-pathol-011110-130206

Danial, N. N., Gramm, C. F., Scorrano, L., Zhang, C. Y., Krauss, S., Ranger, A. M., Datta, S. R., Greenberg, M. E., Licklider, L. J., Lowell, B. B., Gygi, S. P., & Korsmeyer, S. J. (2003). BAD and glucokinase reside in a mitochondrial complex that integrates glycolysis and apoptosis. *Nature*, *424*(6951), 952-956. https://doi.org/10.1038/nature01825

Dannenmann, S. R., Thielicke, J., Stockli, M., Matter, C., von Boehmer, L., Cecconi, V., Hermanns, T., Hefermehl, L., Schraml, P., Moch, H., Knuth, A., & van den Broek, M. (2013). Tumor-associated macrophages subvert T-cell function and correlate with reduced survival in clear cell renal cell carcinoma. *Oncoimmunology*, *2*(3), e23562. https://doi.org/10.4161/onci.23562

Davis, R. J., Moore, E. C., Clavijo, P. E., Friedman, J., Cash, H., Chen, Z., Silvin, C., Van Waes, C., & Allen, C. (2017). Anti-PD-L1 Efficacy Can Be Enhanced by Inhibition of Myeloid-Derived Suppressor Cells with a Selective Inhibitor of PI3Kdelta/gamma. *Cancer Res*, *77*(10), 2607-2619. https://doi.org/10.1158/0008-5472.CAN-16-2534

Day, C. P., Carter, J., Weaver Ohler, Z., Bonomi, C., El Meskini, R., Martin, P., Graff-Cherry, C., Feigenbaum, L., Tuting, T., Van Dyke, T., Hollingshead, M., & Merlino, G. (2014). "Glowing head" mice: a genetic tool enabling reliable preclinical image-based evaluation of cancers in immunocompetent allografts. *PLoS One*, *9*(11), e109956. https://doi.org/10.1371/journal.pone.0109956

De Henau, O., Rausch, M., Winkler, D., Campesato, L. F., Liu, C., Cymerman, D. H., Budhu, S., Ghosh, A., Pink, M., Tchaicha, J., Douglas, M., Tibbitts, T., Sharma, S., Proctor, J., Kosmider, N., White, K., Stern, H., Soglia, J., Adams, J., . . . Merghoub, T. (2016). Overcoming resistance to checkpoint blockade therapy by targeting PI3Kgamma in myeloid cells. *Nature*, *539*(7629), 443-447. https://doi.org/10.1038/nature20554

De Jesus, A., Keyhani-Nejad, F., Pusec, C. M., Goodman, L., Geier, J. A., Stoolman, J. S., Stanczyk, P. J., Nguyen, T., Xu, K., Suresh, K. V., Chen, Y., Rodriguez, A. E., Shapiro, J. S., Chang, H. C., Chen, C., Shah, K. P., Ben-Sahra, I., Layden, B. T., Chandel, N. S., . . . Ardehali, H. (2022). Hexokinase 1 cellular localization regulates the metabolic fate of glucose. *Mol Cell*, *82*(7), 1261-1277 e1269. https://doi.org/10.1016/j.molcel.2022.02.028

DeGrado, T. R., Bhattacharyya, F., Pandey, M. K., Belanger, A. P., & Wang, S. (2010). Synthesis and preliminary evaluation of 18-(18)F-fluoro-4-thia-oleate as a PET probe of fatty acid oxidation. *J Nucl Med*, *51*(8), 1310-1317. https://doi.org/10.2967/jnumed.109.074245

Delorey, T. M., Ziegler, C. G. K., Heimberg, G., Normand, R., Yang, Y., Segerstolpe, A., Abbondanza, D., Fleming, S. J., Subramanian, A., Montoro, D. T., Jagadeesh, K. A., Dey, K. K., Sen, P., Slyper, M., Pita-Juárez, Y. H., Phillips, D., Bloom-Ackerman, Z., Barkas, N., Ganna, A., . . . Regev, A. (2021). A single-cell and spatial atlas of autopsy tissues reveals pathology and cellular targets of SARS-CoV-2. *bioRxiv*, 2021.2002.2025.430130. https://doi.org/10.1101/2021.02.25.430130

den Brok, M. H., Bull, C., Wassink, M., de Graaf, A. M., Wagenaars, J. A., Minderman, M., Thakur, M., Amigorena, S., Rijke, E. O., Schrier, C. C., & Adema, G. J. (2016). Saponin-based adjuvants induce cross-presentation in dendritic cells by intracellular lipid body formation. *Nat Commun*, *7*, 13324. https://doi.org/10.1038/ncomms13324

Deng, Y., Yang, J., Luo, F., Qian, J., Liu, R., Zhang, D., Yu, H., & Chu, Y. (2018). mTOR-mediated glycolysis contributes to the enhanced suppressive function of murine tumor-infiltrating monocytic myeloid-derived suppressor cells. *Cancer Immunol Immunother*, *67*(9), 1355-1364. https://doi.org/10.1007/s00262-018-2177-1

Deprez, J., Vertommen, D., Alessi, D. R., Hue, L., & Rider, M. H. (1997). Phosphorylation and activation of heart 6-phosphofructo-2-kinase by protein kinase B and other protein kinases of the insulin signaling cascades. *J Biol Chem*, *272*(28), 17269-17275. https://doi.org/10.1074/jbc.272.28.17269

DeVilbiss, A. W., Zhao, Z., Martin-Sandoval, M. S., Ubellacker, J. M., Tasdogan, A., Agathocleous, M., Mathews, T. P., & Morrison, S. J. (2021). Metabolomic profiling of rare cell populations isolated by flow cytometry from tissues. *Elife*, *10*. https://doi.org/10.7554/eLife.61980

Diaz-Montero, C. M., Rini, B. I., & Finke, J. H. (2020). The immunology of renal cell carcinoma. *Nat Rev Nephrol*, *16*(12), 721-735. https://doi.org/10.1038/s41581-020-0316-3

Dietl, K., Renner, K., Dettmer, K., Timischl, B., Eberhart, K., Dorn, C., Hellerbrand, C., Kastenberger, M., Kunz-Schughart, L. A., Oefner, P. J., Andreesen, R., Gottfried, E., & Kreutz, M. P. (2010). Lactic acid and acidification inhibit TNF secretion and glycolysis of human monocytes. *J Immunol*, *184*(3), 1200-1209. https://doi.org/10.4049/jimmunol.0902584

Ding, C., Sun, X., Wu, C., Hu, X., Zhang, H. G., & Yan, J. (2019). Tumor Microenvironment Modulates Immunological Outcomes of Myeloid Cells with mTORC1 Disruption. *J Immunol*, *202*(5), 1623-1634. https://doi.org/10.4049/jimmunol.1801112

Doedens, A. L., Phan, A. T., Stradner, M. H., Fujimoto, J. K., Nguyen, J. V., Yang, E., Johnson, R. S., & Goldrath, A. W. (2013). Hypoxia-inducible factors enhance the effector responses of CD8(+) T cells to persistent antigen. *Nat Immunol*, *14*(11), 1173-1182. https://doi.org/10.1038/ni.2714

Doedens, A. L., Stockmann, C., Rubinstein, M. P., Liao, D., Zhang, N., DeNardo, D. G., Coussens, L. M., Karin, M., Goldrath, A. W., & Johnson, R. S. (2010). Macrophage expression of hypoxia-inducible factor-1 alpha

suppresses T-cell function and promotes tumor progression. *Cancer Res*, *70*(19), 7465-7475. https://doi.org/10.1158/0008-5472.CAN-10-1439

Dong, H., Strome, S. E., Salomao, D. R., Tamura, H., Hirano, F., Flies, D. B., Roche, P. C., Lu, J., Zhu, G., Tamada, K., Lennon, V. A., Celis, E., & Chen, L. (2002). Tumor-associated B7-H1 promotes T-cell apoptosis: a potential mechanism of immune evasion. *Nat Med*, *8*(8), 793-800. https://doi.org/10.1038/nm730

Donnelly, R. P., Loftus, R. M., Keating, S. E., Liou, K. T., Biron, C. A., Gardiner, C. M., & Finlay, D. K. (2014). mTORC1-dependent metabolic reprogramming is a prerequisite for NK cell effector function. *J Immunol*, *193*(9), 4477-4484. https://doi.org/10.4049/jimmunol.1401558

Du, X., Wen, J., Wang, Y., Karmaus, P. W. F., Khatamian, A., Tan, H., Li, Y., Guy, C., Nguyen, T. M., Dhungana, Y., Neale, G., Peng, J., Yu, J., & Chi, H. (2018). Hippo/Mst signalling couples metabolic state and immune function of CD8alpha(+) dendritic cells. *Nature*, *558*(7708), 141-145. https://doi.org/10.1038/s41586-018-0177-0

Durai, V., Bagadia, P., Granja, J. M., Satpathy, A. T., Kulkarni, D. H., Davidson, J. T. t., Wu, R., Patel, S. J., Iwata, A., Liu, T. T., Huang, X., Briseno, C. G., Grajales-Reyes, G. E., Wohner, M., Tagoh, H., Kee, B. L., Newberry, R. D., Busslinger, M., Chang, H. Y., . . . Murphy, K. M. (2019). Cryptic activation of an Irf8 enhancer governs cDC1 fate specification. *Nat Immunol*, *20*(9), 1161-1173. https://doi.org/10.1038/s41590-019-0450-x

Duvel, K., Yecies, J. L., Menon, S., Raman, P., Lipovsky, A. I., Souza, A. L., Triantafellow, E., Ma, Q., Gorski, R., Cleaver, S., Vander Heiden, M. G., MacKeigan, J. P., Finan, P. M., Clish, C. B., Murphy, L. O., & Manning, B. D. (2010). Activation of a metabolic gene regulatory network downstream of mTOR complex 1. *Mol Cell*, *39*(2), 171-183. https://doi.org/10.1016/j.molcel.2010.06.022

Dvorak, H. F. (1986). Tumors: wounds that do not heal. Similarities between tumor stroma generation and wound healing. *N Engl J Med*, *315*(26), 1650-1659. https://doi.org/10.1056/NEJM198612253152606

Dwyer, C. J., Arhontoulis, D. C., Rangel Rivera, G. O., Knochelmann, H. M., Smith, A. S., Wyatt, M. M., Rubinstein, M. P., Atkinson, C., Thaxton, J. E., Neskey, D. M., & Paulos, C. M. (2020). Ex vivo blockade of PI3K gamma or delta signaling enhances the antitumor potency of adoptively transferred CD8(+) T cells. *Eur J Immunol*, *50*(9), 1386-1399. https://doi.org/10.1002/eji.201948455

Edwards, D. N., Ngwa, V. M., Raybuck, A. L., Wang, S., Hwang, Y., Kim, L. C., Cho, S. H., Paik, Y., Wang, Q., Zhang, S., Manning, H. C., Rathmell, J. C., Cook, R. S., Boothby, M. R., & Chen, J. (2021). Selective glutamine metabolism inhibition in tumor cells improves antitumor T lymphocyte activity in triple-negative breast cancer. *J Clin Invest*, *131*(4). https://doi.org/10.1172/JCI140100

Elstrom, R. L., Bauer, D. E., Buzzai, M., Karnauskas, R., Harris, M. H., Plas, D. R., Zhuang, H., Cinalli, R. M., Alavi, A., Rudin, C. M., & Thompson, C. B. (2004). Akt stimulates aerobic glycolysis in cancer cells. *Cancer Res*, *64*(11), 3892-3899. https://doi.org/10.1158/0008-5472.CAN-03-2904

Epstein, A. C., Gleadle, J. M., McNeill, L. A., Hewitson, K. S., O'Rourke, J., Mole, D. R., Mukherji, M., Metzen, E., Wilson, M. I., Dhanda, A., Tian, Y. M., Masson, N., Hamilton, D. L., Jaakkola, P., Barstead, R., Hodgkin, J., Maxwell, P. H., Pugh, C. W., Schofield, C. J., & Ratcliffe, P. J. (2001). C. elegans EGL-9 and mammalian homologs define a family of dioxygenases that regulate HIF by prolyl hydroxylation. *Cell*, *107*(1), 43-54. https://doi.org/10.1016/s0092-8674(01)00507-4

Errea, A., Cayet, D., Marchetti, P., Tang, C., Kluza, J., Offermanns, S., Sirard, J. C., & Rumbo, M. (2016). Lactate Inhibits the Pro-Inflammatory Response and Metabolic Reprogramming in Murine Macrophages in a GPR81-Independent Manner. *PLoS One*, *11*(11), e0163694. https://doi.org/10.1371/journal.pone.0163694

Evans, C. A., Liu, T., Lescarbeau, A., Nair, S. J., Grenier, L., Pradeilles, J. A., Glenadel, Q., Tibbitts, T., Rowley, A. M., DiNitto, J. P., Brophy, E. E., O'Hearn, E. L., Ali, J. A., Winkler, D. G., Goldstein, S. I., O'Hearn, P., Martin, C. M., Hoyt, J. G., Soglia, J. R., . . . Castro, A. C. (2016). Discovery of a Selective Phosphoinositide-3-Kinase (PI3K)-gamma Inhibitor (IPI-549) as an Immuno-Oncology Clinical Candidate. *ACS Med Chem Lett*, *7*(9), 862-867. https://doi.org/10.1021/acsmedchemlett.6b00238

Everts, B., Amiel, E., Huang, S. C., Smith, A. M., Chang, C. H., Lam, W. Y., Redmann, V., Freitas, T. C., Blagih, J., van der Windt, G. J., Artyomov, M. N., Jones, R. G., Pearce, E. L., & Pearce, E. J. (2014). TLR-driven early glycolytic reprogramming via the kinases TBK1-IKKvarepsilon supports the anabolic demands of dendritic cell activation. *Nat Immunol*, *15*(4), 323-332. https://doi.org/10.1038/ni.2833

Fakih, M., Ouyang, C., Wang, C., Tu, T. Y., Gozo, M. C., Cho, M., Sy, M., Longmate, J. A., & Lee, P. P. (2019). Immune overdrive signature in colorectal tumor subset predicts poor clinical outcome. *J Clin Invest*, *129*(10), 4464-4476. https://doi.org/10.1172/JCI127046

Faubert, B., Li, K. Y., Cai, L., Hensley, C. T., Kim, J., Zacharias, L. G., Yang, C., Do, Q. N., Doucette, S., Burguete, D., Li, H., Huet, G., Yuan, Q., Wigal, T., Butt, Y., Ni, M., Torrealba, J., Oliver, D., Lenkinski, R. E., . . . DeBerardinis, R. J. (2017). Lactate Metabolism in Human Lung Tumors. *Cell*, *171*(2), 358-371 e359. https://doi.org/10.1016/j.cell.2017.09.019

Faubert, B., Vincent, E. E., Griss, T., Samborska, B., Izreig, S., Svensson, R. U., Mamer, O. A., Avizonis, D., Shackelford, D. B., Shaw, R. J., & Jones, R. G. (2014). Loss of the tumor suppressor LKB1 promotes metabolic reprogramming of cancer cells via HIF-1alpha. *Proc Natl Acad Sci U S A*, *111*(7), 2554-2559. https://doi.org/10.1073/pnas.1312570111

Federzoni, E. A., Humbert, M., Torbett, B. E., Behre, G., Fey, M. F., & Tschan, M. P. (2014). CEBPA-dependent HK3 and KLF5 expression in primary AML and during AML differentiation. *Sci Rep*, *4*, 4261. https://doi.org/10.1038/srep04261
Federzoni, E. A., Valk, P. J., Torbett, B. E., Haferlach, T., Lowenberg, B., Fey, M. F., & Tschan, M. P. (2012). PU.1 is linking the glycolytic enzyme HK3 in neutrophil differentiation and survival of APL cells. *Blood*, *119*(21), 4963-4970. https://doi.org/10.1182/blood-2011-09-378117
Finke, J., Ko, J., Rini, B., Rayman, P., Ireland, J., & Cohen, P. (2011). MDSC as a mechanism of tumor escape from sunitinib mediated anti-angiogenic therapy. *Int Immunopharmacol*, *11*(7), 856-861. https://doi.org/10.1016/j.intimp.2011.01.030
Finkel, R. S., Mercuri, E., Darras, B. T., Connolly, A. M., Kuntz, N. L., Kirschner, J., Chiriboga, C. A., Saito, K., Servais, L., Tizzano, E., Topaloglu, H., Tulinius, M., Montes, J., Glanzman, A. M., Bishop, K., Zhong, Z. J., Gheuens, S., Bennett, C. F., Schneider, E., . . . Group, E. S. (2017). Nusinersen versus Sham Control in Infantile-Onset Spinal Muscular Atrophy. *N Engl J Med*, *377*(18), 1723-1732. https://doi.org/10.1056/NEJMoa1702752
Firth, J. D., Ebert, B. L., & Ratcliffe, P. J. (1995). Hypoxic regulation of lactate dehydrogenase A. Interaction between hypoxia-inducible factor 1 and cAMP response elements. *J Biol Chem*, *270*(36), 21021-21027. https://doi.org/10.1074/jbc.270.36.21021
Fischer, K., Hoffmann, P., Voelkl, S., Meidenbauer, N., Ammer, J., Edinger, M., Gottfried, E., Schwarz, S., Rothe, G., Hoves, S., Renner, K., Timischl, B., Mackensen, A., Kunz-Schughart, L., Andreesen, R., Krause, S. W., & Kreutz, M. (2007). Inhibitory effect of tumor cell-derived lactic acid on human T cells. *Blood*, *109*(9), 3812-3819. https://doi.org/10.1182/blood-2006-07-035972
Fisher, J. N., Kalleda, N., Stavropoulou, V., & Schwaller, J. (2019). The Impact of the Cellular Origin in Acute Myeloid Leukemia: Learning From Mouse Models. *Hemasphere*, *3*(1), e152. https://doi.org/10.1097/HS9.0000000000000152
Fong, L., Hotson, A., Powderly, J. D., Sznol, M., Heist, R. S., Choueiri, T. K., George, S., Hughes, B. G. M., Hellmann, M. D., Shepard, D. R., Rini, B. I., Kummar, S., Weise, A. M., Riese, M. J., Markman, B., Emens, L. A., Mahadevan, D., Luke, J. J., Laport, G., . . . Miller, R. A. (2020). Adenosine 2A Receptor Blockade as an Immunotherapy for Treatment-Refractory Renal Cell Cancer. *Cancer Discov*, *10*(1), 40-53. https://doi.org/10.1158/2159-8290.CD-19-0980
Foubert, P., Kaneda, M. M., & Varner, J. A. (2017). PI3Kgamma Activates Integrin alpha4 and Promotes Immune Suppressive Myeloid Cell Polarization during Tumor Progression. *Cancer Immunol Res*, *5*(11), 957-968. https://doi.org/10.1158/2326-6066.CIR-17-0143
Frauwirth, K. A., Riley, J. L., Harris, M. H., Parry, R. V., Rathmell, J. C., Plas, D. R., Elstrom, R. L., June, C. H., & Thompson, C. B. (2002). The CD28 signaling pathway regulates glucose metabolism. *Immunity*, *16*(6), 769-777. https://doi.org/10.1016/s1074-7613(02)00323-0
Freeman, G. J., Long, A. J., Iwai, Y., Bourque, K., Chernova, T., Nishimura, H., Fitz, L. J., Malenkovich, N., Okazaki, T., Byrne, M. C., Horton, H. F., Fouser, L., Carter, L., Ling, V., Bowman, M. R., Carreno, B. M., Collins, M., Wood, C. R., & Honjo, T. (2000). Engagement of the PD-1 immunoinhibitory receptor by a novel B7 family member leads to negative regulation of lymphocyte activation. *J Exp Med*, *192*(7), 1027-1034. https://doi.org/10.1084/jem.192.7.1027
Freemerman, A. J., Johnson, A. R., Sacks, G. N., Milner, J. J., Kirk, E. L., Troester, M. A., Macintyre, A. N., Goraksha-Hicks, P., Rathmell, J. C., & Makowski, L. (2014). Metabolic reprogramming of macrophages: glucose transporter 1 (GLUT1)-mediated glucose metabolism drives a proinflammatory phenotype. *J Biol Chem*, *289*(11), 7884-7896. https://doi.org/10.1074/jbc.M113.522037
Freemerman, A. J., Zhao, L., Pingili, A. K., Teng, B., Cozzo, A. J., Fuller, A. M., Johnson, A. R., Milner, J. J., Lim, M. F., Galanko, J. A., Beck, M. A., Bear, J. E., Rotty, J. D., Bezavada, L., Smallwood, H. S., Puchowicz, M. A., Liu, J., Locasale, J. W., Lee, D. P., . . . Makowski, L. (2019). Myeloid Slc2a1-Deficient Murine Model Revealed Macrophage Activation and Metabolic Phenotype Are Fueled by GLUT1. *J Immunol*, *202*(4), 1265-1286. https://doi.org/10.4049/jimmunol.1800002
Fridman, W. H., Pages, F., Sautes-Fridman, C., & Galon, J. (2012). The immune contexture in human tumours: impact on clinical outcome. *Nat Rev Cancer*, *12*(4), 298-306. https://doi.org/10.1038/nrc3245
Fridman, W. H., Zitvogel, L., Sautes-Fridman, C., & Kroemer, G. (2017). The immune contexture in cancer prognosis and treatment. *Nat Rev Clin Oncol*, *14*(12), 717-734. https://doi.org/10.1038/nrclinonc.2017.101
Fruman, D. A., Chiu, H., Hopkins, B. D., Bagrodia, S., Cantley, L. C., & Abraham, R. T. (2017). The PI3K Pathway in Human Disease. *Cell*, *170*(4), 605-635. https://doi.org/10.1016/j.cell.2017.07.029
Fuertes, M. B., Kacha, A. K., Kline, J., Woo, S. R., Kranz, D. M., Murphy, K. M., & Gajewski, T. F. (2011). Host type I IFN signals are required for antitumor CD8+ T cell responses through CD8{alpha}+ dendritic cells. *J Exp Med*, *208*(10), 2005-2016. https://doi.org/10.1084/jem.20101159
Fukuzumi, M., Shinomiya, H., Shimizu, Y., Ohishi, K., & Utsumi, S. (1996). Endotoxin-induced enhancement of glucose influx into murine peritoneal macrophages via GLUT1. *Infect Immun*, *64*(1), 108-112. https://doi.org/10.1128/iai.64.1.108-112.1996

Gabrilovich, D., Ishida, T., Oyama, T., Ran, S., Kravtsov, V., Nadaf, S., & Carbone, D. P. (1998). Vascular endothelial growth factor inhibits the development of dendritic cells and dramatically affects the differentiation of multiple hematopoietic lineages in vivo. *Blood*, *92*(11), 4150-4166. https://www.ncbi.nlm.nih.gov/pubmed/9834220
Galluzzi, L., Chan, T. A., Kroemer, G., Wolchok, J. D., & Lopez-Soto, A. (2018). The hallmarks of successful anticancer immunotherapy. *Sci Transl Med*, *10*(459). https://doi.org/10.1126/scitranslmed.aat7807
Gandhi, L., Rodriguez-Abreu, D., Gadgeel, S., Esteban, E., Felip, E., De Angelis, F., Domine, M., Clingan, P., Hochmair, M. J., Powell, S. F., Cheng, S. Y., Bischoff, H. G., Peled, N., Grossi, F., Jennens, R. R., Reck, M., Hui, R., Garon, E. B., Boyer, M., . . . Investigators, K.-. (2018). Pembrolizumab plus Chemotherapy in Metastatic Non-Small-Cell Lung Cancer. *N Engl J Med*, *378*(22), 2078-2092. https://doi.org/10.1056/NEJMoa1801005
Gao, X., Sanderson, S. M., Dai, Z., Reid, M. A., Cooper, D. E., Lu, M., Richie, J. P., Jr., Ciccarella, A., Calcagnotto, A., Mikhael, P. G., Mentch, S. J., Liu, J., Ables, G., Kirsch, D. G., Hsu, D. S., Nichenametla, S. N., & Locasale, J. W. (2019). Dietary methionine influences therapy in mouse cancer models and alters human metabolism. *Nature*, *572*(7769), 397-401. https://doi.org/10.1038/s41586-019-1437-3
Garcia, S. N., Guedes, R. C., & Marques, M. M. (2019). Unlocking the Potential of HK2 in Cancer Metabolism and Therapeutics. *Curr Med Chem*, *26*(41), 7285-7322. https://doi.org/10.2174/0929867326666181213092652
Gavalas, N. G., Tsiatas, M., Tsitsilonis, O., Politi, E., Ioannou, K., Ziogas, A. C., Rodolakis, A., Vlahos, G., Thomakos, N., Haidopoulos, D., Terpos, E., Antsaklis, A., Dimopoulos, M. A., & Bamias, A. (2012). VEGF directly suppresses activation of T cells from ascites secondary to ovarian cancer via VEGF receptor type 2. *Br J Cancer*, *107*(11), 1869-1875. https://doi.org/10.1038/bjc.2012.468
Ge, X., Li, M., Yin, J., Shi, Z., Fu, Y., Zhao, N., Chen, H., Meng, L., Li, X., Hu, Z., Zhao, X., Guo, H., & Qian, X. (2022). Fumarate inhibits PTEN to promote tumorigenesis and therapeutic resistance of type2 papillary renal cell carcinoma. *Mol Cell*, *82*(7), 1249-1260 e1247. https://doi.org/10.1016/j.molcel.2022.01.029
Geeraerts, X., Fernandez-Garcia, J., Hartmann, F. J., de Goede, K. E., Martens, L., Elkrim, Y., Debraekeleer, A., Stijlemans, B., Vandekeere, A., Rinaldi, G., De Rycke, R., Planque, M., Broekaert, D., Meinster, E., Clappaert, E., Bardet, P., Murgaski, A., Gysemans, C., Nana, F. A., . . . Van Ginderachter, J. A. (2021). Macrophages are metabolically heterogeneous within the tumor microenvironment. *Cell Rep*, *37*(13), 110171. https://doi.org/10.1016/j.celrep.2021.110171
Gemta, L. F., Siska, P. J., Nelson, M. E., Gao, X., Liu, X., Locasale, J. W., Yagita, H., Slingluff, C. L., Jr., Hoehn, K. L., Rathmell, J. C., & Bullock, T. N. J. (2019). Impaired enolase 1 glycolytic activity restrains effector functions of tumor-infiltrating CD8(+) T cells. *Sci Immunol*, *4*(31). https://doi.org/10.1126/sciimmunol.aap9520
Gerriets, V. A., Kishton, R. J., Johnson, M. O., Cohen, S., Siska, P. J., Nichols, A. G., Warmoes, M. O., de Cubas, A. A., MacIver, N. J., Locasale, J. W., Turka, L. A., Wells, A. D., & Rathmell, J. C. (2016). Foxp3 and Toll-like receptor signaling balance Treg cell anabolic metabolism for suppression. *Nat Immunol*, *17*(12), 1459-1466. https://doi.org/10.1038/ni.3577
Gerriets, V. A., Kishton, R. J., Nichols, A. G., Macintyre, A. N., Inoue, M., Ilkayeva, O., Winter, P. S., Liu, X., Priyadharshini, B., Slawinska, M. E., Haeberli, L., Huck, C., Turka, L. A., Wood, K. C., Hale, L. P., Smith, P. A., Schneider, M. A., MacIver, N. J., Locasale, J. W., . . . Rathmell, J. C. (2015). Metabolic programming and PDHK1 control CD4+ T cell subsets and inflammation. *J Clin Invest*, *125*(1), 194-207. https://doi.org/10.1172/JCI76012
Gilardi, M., Wang, Z., Proietto, M., Chilla, A., Calleja-Valera, J. L., Goto, Y., Vanoni, M., Janes, M. R., Mikulski, Z., Gualberto, A., Molinolo, A. A., Ferrara, N., Gutkind, J. S., & Burrows, F. (2020). Tipifarnib as a Precision Therapy for HRAS-Mutant Head and Neck Squamous Cell Carcinomas. *Mol Cancer Ther*, *19*(9), 1784-1796. https://doi.org/10.1158/1535-7163.MCT-19-0958
Goffaux, G., Hammami, I., & Jolicoeur, M. (2017). A Dynamic Metabolic Flux Analysis of Myeloid-Derived Suppressor Cells Confirms Immunosuppression-Related Metabolic Plasticity. *Sci Rep*, *7*(1), 9850. https://doi.org/10.1038/s41598-017-10464-1
Gohil, S. H., Iorgulescu, J. B., Braun, D. A., Keskin, D. B., & Livak, K. J. (2021). Applying high-dimensional single-cell technologies to the analysis of cancer immunotherapy. *Nat Rev Clin Oncol*, *18*(4), 244-256. https://doi.org/10.1038/s41571-020-00449-x
Gonzalez-Garcia, A., Sanchez-Ruiz, J., Flores, J. M., & Carrera, A. C. (2010). Phosphatidylinositol 3-kinase gamma inhibition ameliorates inflammation and tumor growth in a model of colitis-associated cancer. *Gastroenterology*, *138*(4), 1374-1383. https://doi.org/10.1053/j.gastro.2009.12.001
Gottfried, E., Kunz-Schughart, L. A., Ebner, S., Mueller-Klieser, W., Hoves, S., Andreesen, R., Mackensen, A., & Kreutz, M. (2006). Tumor-derived lactic acid modulates dendritic cell activation and antigen expression. *Blood*, *107*(5), 2013-2021. https://doi.org/10.1182/blood-2005-05-1795
Granstein, R. D., Ding, W., Huang, J., Holzer, A., Gallo, R. L., Di Nardo, A., & Wagner, J. A. (2005). Augmentation of cutaneous immune responses by ATP gamma S: purinergic agonists define a novel class of immunologic adjuvants. *J Immunol*, *174*(12), 7725-7731. https://doi.org/10.4049/jimmunol.174.12.7725
Grzelak, C. A., Goddard, E. T., Lederer, E. E., Rajaram, K., Dai, J., Shor, R. E., Lim, A. R., Kim, J., Beronja, S., Funnell, A. P. W., & Ghajar, C. M. (2022). Elimination of fluorescent protein immunogenicity permits

modeling of metastasis in immune-competent settings. *Cancer Cell*, *40*(1), 1-2. https://doi.org/10.1016/j.ccell.2021.11.004
Gu, Z., Eils, R., & Schlesner, M. (2016). Complex heatmaps reveal patterns and correlations in multidimensional genomic data. *Bioinformatics*, *32*(18), 2847-2849. https://doi.org/10.1093/bioinformatics/btw313
Guak, H., Al Habyan, S., Ma, E. H., Aldossary, H., Al-Masri, M., Won, S. Y., Ying, T., Fixman, E. D., Jones, R. G., McCaffrey, L. M., & Krawczyk, C. M. (2018). Glycolytic metabolism is essential for CCR7 oligomerization and dendritic cell migration. *Nat Commun*, *9*(1), 2463. https://doi.org/10.1038/s41467-018-04804-6
Guilliams, M., Dutertre, C. A., Scott, C. L., McGovern, N., Sichien, D., Chakarov, S., Van Gassen, S., Chen, J., Poidinger, M., De Prijck, S., Tavernier, S. J., Low, I., Irac, S. E., Mattar, C. N., Sumatoh, H. R., Low, G. H. L., Chung, T. J. K., Chan, D. K. H., Tan, K. K., . . . Ginhoux, F. (2016). Unsupervised High-Dimensional Analysis Aligns Dendritic Cells across Tissues and Species. *Immunity*, *45*(3), 669-684. https://doi.org/10.1016/j.immuni.2016.08.015
Gyori, D., Chessa, T., Hawkins, P. T., & Stephens, L. R. (2017). Class (I) Phosphoinositide 3-Kinases in the Tumor Microenvironment. *Cancers (Basel)*, *9*(3). https://doi.org/10.3390/cancers9030024
Hackstein, H., Taner, T., Zahorchak, A. F., Morelli, A. E., Logar, A. J., Gessner, A., & Thomson, A. W. (2003). Rapamycin inhibits IL-4--induced dendritic cell maturation in vitro and dendritic cell mobilization and function in vivo. *Blood*, *101*(11), 4457-4463. https://doi.org/10.1182/blood-2002-11-3370
Halbrook, C. J., Pontious, C., Kovalenko, I., Lapienyte, L., Dreyer, S., Lee, H. J., Thurston, G., Zhang, Y., Lazarus, J., Sajjakulnukit, P., Hong, H. S., Kremer, D. M., Nelson, B. S., Kemp, S., Zhang, L., Chang, D., Biankin, A., Shi, J., Frankel, T. L., . . . Lyssiotis, C. A. (2019). Macrophage-Released Pyrimidines Inhibit Gemcitabine Therapy in Pancreatic Cancer. *Cell Metab*, *29*(6), 1390-1399 e1396. https://doi.org/10.1016/j.cmet.2019.02.001
Haluska, F. G., Finver, S., Tsujimoto, Y., & Croce, C. M. (1986). The t(8; 14) chromosomal translocation occurring in B-cell malignancies results from mistakes in V-D-J joining. *Nature*, *324*(6093), 158-161. https://doi.org/10.1038/324158a0
Hammami, I., Chen, J., Murschel, F., Bronte, V., De Crescenzo, G., & Jolicoeur, M. (2012). Immunosuppressive activity enhances central carbon metabolism and bioenergetics in myeloid-derived suppressor cells in vitro models. *BMC Cell Biol*, *13*, 18. https://doi.org/10.1186/1471-2121-13-18
Hammerich, L., Marron, T. U., Upadhyay, R., Svensson-Arvelund, J., Dhainaut, M., Hussein, S., Zhan, Y., Ostrowski, D., Yellin, M., Marsh, H., Salazar, A. M., Rahman, A. H., Brown, B. D., Merad, M., & Brody, J. D. (2019). Systemic clinical tumor regressions and potentiation of PD1 blockade with in situ vaccination. *Nat Med*, *25*(5), 814-824. https://doi.org/10.1038/s41591-019-0410-x
Hanahan, D., & Weinberg, R. A. (2011). Hallmarks of cancer: the next generation. *Cell*, *144*(5), 646-674. https://doi.org/10.1016/j.cell.2011.02.013
Hanzl, A., & Winter, G. E. (2020). Targeted protein degradation: current and future challenges. *Curr Opin Chem Biol*, *56*, 35-41. https://doi.org/10.1016/j.cbpa.2019.11.012
Hard, G. C. (1970). Some biochemical aspects of the immune macrophage. *Br J Exp Pathol*, *51*(1), 97-105. https://www.ncbi.nlm.nih.gov/pubmed/5434449
Haschemi, A., Kosma, P., Gille, L., Evans, C. R., Burant, C. F., Starkl, P., Knapp, B., Haas, R., Schmid, J. A., Jandl, C., Amir, S., Lubec, G., Park, J., Esterbauer, H., Bilban, M., Brizuela, L., Pospisilik, J. A., Otterbein, L. E., & Wagner, O. (2012). The sedoheptulose kinase CARKL directs macrophage polarization through control of glucose metabolism. *Cell Metab*, *15*(6), 813-826. https://doi.org/10.1016/j.cmet.2012.04.023
Hassanein, M., Hight, M. R., Buck, J. R., Tantawy, M. N., Nickels, M. L., Hoeksema, M. D., Harris, B. K., Boyd, K., Massion, P. P., & Manning, H. C. (2016). Preclinical Evaluation of 4-[18F]Fluoroglutamine PET to Assess ASCT2 Expression in Lung Cancer. *Mol Imaging Biol*, *18*(1), 18-23. https://doi.org/10.1007/s11307-015-0862-4
Hatfield, S. M., Kjaergaard, J., Lukashev, D., Schreiber, T. H., Belikoff, B., Abbott, R., Sethumadhavan, S., Philbrook, P., Ko, K., Cannici, R., Thayer, M., Rodig, S., Kutok, J. L., Jackson, E. K., Karger, B., Podack, E. R., Ohta, A., & Sitkovsky, M. V. (2015). Immunological mechanisms of the antitumor effects of supplemental oxygenation. *Sci Transl Med*, *7*(277), 277ra230. https://doi.org/10.1126/scitranslmed.aaa1260
Hay, S. B., Ferchen, K., Chetal, K., Grimes, H. L., & Salomonis, N. (2018). The Human Cell Atlas bone marrow single-cell interactive web portal. *Exp Hematol*, *68*, 51-61. https://doi.org/10.1016/j.exphem.2018.09.004
He, J., Wang, Y., Liu, T., Liu, G., Chen, S., Li, Q., Quan, Y., Yang, H., Feng, J., Wang, S., Yang, M., & Dong, Z. (2019). Stage-specific requirement of kinase PDK1 for NK cells development and activation. *Cell Death Differ*, *26*(10), 1918-1928. https://doi.org/10.1038/s41418-018-0263-8
He, S., Bhatt, R., Brown, C., Brown, E. A., Buhr, D. L., Chantranuvatana, K., Danaher, P., Dunaway, D., Garrison, R. G., Geiss, G., Gregory, M. T., Hoang, M. L., Khafizov, R., Killingbeck, E. E., Kim, D., Kim, T. K., Kim, Y., Klock, A., Korukonda, M., . . . Beechem, J. M. (2022). High-plex Multiomic Analysis in FFPE at Subcellular Level by Spatial Molecular Imaging. *bioRxiv*, 2021.2011.2003.467020. https://doi.org/10.1101/2021.11.03.467020
He, W., Zhang, H., Han, F., Chen, X., Lin, R., Wang, W., Qiu, H., Zhuang, Z., Liao, Q., Zhang, W., Cai, Q., Cui, Y., Jiang, W., Wang, H., & Ke, Z. (2017). CD155T/TIGIT Signaling Regulates CD8(+) T-cell Metabolism and

Promotes Tumor Progression in Human Gastric Cancer. *Cancer Res*, *77*(22), 6375-6388. https://doi.org/10.1158/0008-5472.CAN-17-0381

Healey, D. C. C., Cephus, J. Y., Barone, S. M., Chowdhury, N. U., Dahunsi, D. O., Madden, M. Z., Ye, X., Yu, X., Olszewski, K., Young, K., Gerriets, V. A., Siska, P. J., Dworski, R., Hemler, J., Locasale, J. W., Poyurovsky, M. V., Peebles, R. S., Jr., Irish, J. M., Newcomb, D. C., & Rathmell, J. C. (2021). Targeting In Vivo Metabolic Vulnerabilities of Th2 and Th17 Cells Reduces Airway Inflammation. *J Immunol*, *206*(6), 1127-1139. https://doi.org/10.4049/jimmunol.2001029

Hensley, C. T., Faubert, B., Yuan, Q., Lev-Cohain, N., Jin, E., Kim, J., Jiang, L., Ko, B., Skelton, R., Loudat, L., Wodzak, M., Klimko, C., McMillan, E., Butt, Y., Ni, M., Oliver, D., Torrealba, J., Malloy, C. R., Kernstine, K., . . . DeBerardinis, R. J. (2016). Metabolic Heterogeneity in Human Lung Tumors. *Cell*, *164*(4), 681-694. https://doi.org/10.1016/j.cell.2015.12.034

Herber, D. L., Cao, W., Nefedova, Y., Novitskiy, S. V., Nagaraj, S., Tyurin, V. A., Corzo, A., Cho, H. I., Celis, E., Lennox, B., Knight, S. C., Padhya, T., McCaffrey, T. V., McCaffrey, J. C., Antonia, S., Fishman, M., Ferris, R. L., Kagan, V. E., & Gabrilovich, D. I. (2010). Lipid accumulation and dendritic cell dysfunction in cancer. *Nat Med*, *16*(8), 880-886. https://doi.org/10.1038/nm.2172

Hesketh, R. L., Wang, J., Wright, A. J., Lewis, D. Y., Denton, A. E., Grenfell, R., Miller, J. L., Bielik, R., Gehrung, M., Fala, M., Ros, S., Xie, B., Hu, D. E., & Brindle, K. M. (2019). Magnetic Resonance Imaging Is More Sensitive Than PET for Detecting Treatment-Induced Cell Death-Dependent Changes in Glycolysis. *Cancer Res*, *79*(14), 3557-3569. https://doi.org/10.1158/0008-5472.CAN-19-0182

Hinshaw, D. C., Hanna, A., Lama-Sherpa, T., Metge, B., Kammerud, S. C., Benavides, G. A., Kumar, A., Alsheikh, H. A., Mota, M., Chen, D., Ballinger, S. W., Rathmell, J. C., Ponnazhagan, S., Darley-Usmar, V., Samant, R. S., & Shevde, L. A. (2021). Hedgehog Signaling Regulates Metabolism and Polarization of Mammary Tumor-Associated Macrophages. *Cancer Res*, *81*(21), 5425-5437. https://doi.org/10.1158/0008-5472.CAN-20-1723

Hirayama, S., Ishii, G., Nagai, K., Ono, S., Kojima, M., Yamauchi, C., Aokage, K., Hishida, T., Yoshida, J., Suzuki, K., & Ochiai, A. (2012). Prognostic impact of CD204-positive macrophages in lung squamous cell carcinoma: possible contribution of Cd204-positive macrophages to the tumor-promoting microenvironment. *J Thorac Oncol*, *7*(12), 1790-1797. https://doi.org/10.1097/JTO.0b013e3182745968

Ho, P. C., Bihuniak, J. D., Macintyre, A. N., Staron, M., Liu, X., Amezquita, R., Tsui, Y. C., Cui, G., Micevic, G., Perales, J. C., Kleinstein, S. H., Abel, E. D., Insogna, K. L., Feske, S., Locasale, J. W., Bosenberg, M. W., Rathmell, J. C., & Kaech, S. M. (2015). Phosphoenolpyruvate Is a Metabolic Checkpoint of Anti-tumor T Cell Responses. *Cell*, *162*(6), 1217-1228. https://doi.org/10.1016/j.cell.2015.08.012

Hoch, T., Schulz, D., Eling, N., Gomez, J. M., Levesque, M. P., & Bodenmiller, B. (2022). Multiplexed imaging mass cytometry of the chemokine milieus in melanoma characterizes features of the response to immunotherapy. *Sci Immunol*, *7*(70), eabk1692. https://doi.org/10.1126/sciimmunol.abk1692

Hochrein, S. M., Wu, H., Eckstein, M., Arrigoni, L., Herman, J. S., Schumacher, F., Gerecke, C., Rosenfeldt, M., Grun, D., Kleuser, B., Gasteiger, G., Kastenmuller, W., Ghesquiere, B., Van den Bossche, J., Abel, E. D., & Vaeth, M. (2022). The glucose transporter GLUT3 controls T helper 17 cell responses through glycolytic-epigenetic reprogramming. *Cell Metab*, *34*(4), 516-532 e511. https://doi.org/10.1016/j.cmet.2022.02.015

Holmquist-Mengelbier, L., Fredlund, E., Lofstedt, T., Noguera, R., Navarro, S., Nilsson, H., Pietras, A., Vallon-Christersson, J., Borg, A., Gradin, K., Poellinger, L., & Pahlman, S. (2006). Recruitment of HIF-1alpha and HIF-2alpha to common target genes is differentially regulated in neuroblastoma: HIF-2alpha promotes an aggressive phenotype. *Cancer Cell*, *10*(5), 413-423. https://doi.org/10.1016/j.ccr.2006.08.026

Hove-Jensen, B., Andersen, K. R., Kilstrup, M., Martinussen, J., Switzer, R. L., & Willemoes, M. (2017). Phosphoribosyl Diphosphate (PRPP): Biosynthesis, Enzymology, Utilization, and Metabolic Significance. *Microbiol Mol Biol Rev*, *81*(1). https://doi.org/10.1128/MMBR.00040-16

Hsu, J., Hodgins, J. J., Marathe, M., Nicolai, C. J., Bourgeois-Daigneault, M. C., Trevino, T. N., Azimi, C. S., Scheer, A. K., Randolph, H. E., Thompson, T. W., Zhang, L., Iannello, A., Mathur, N., Jardine, K. E., Kirn, G. A., Bell, J. C., McBurney, M. W., Raulet, D. H., & Ardolino, M. (2018). Contribution of NK cells to immunotherapy mediated by PD-1/PD-L1 blockade. *J Clin Invest*, *128*(10), 4654-4668. https://doi.org/10.1172/JCI99317

Huang, A., Peng, D., Guo, H., Ben, Y., Zuo, X., Wu, F., Yang, X., Teng, F., Li, Z., Qian, X., & Qin, F. X. (2017). A human programmed death-ligand 1-expressing mouse tumor model for evaluating the therapeutic efficacy of anti-human PD-L1 antibodies. *Sci Rep*, *7*, 42687. https://doi.org/10.1038/srep42687

Huang, S. C., Everts, B., Ivanova, Y., O'Sullivan, D., Nascimento, M., Smith, A. M., Beatty, W., Love-Gregory, L., Lam, W. Y., O'Neill, C. M., Yan, C., Du, H., Abumrad, N. A., Urban, J. F., Jr., Artyomov, M. N., Pearce, E. L., & Pearce, E. J. (2014). Cell-intrinsic lysosomal lipolysis is essential for alternative activation of macrophages. *Nat Immunol*, *15*(9), 846-855. https://doi.org/10.1038/ni.2956

Huang, T., Cheng, X., Chahoud, J., Sarhan, A., Tamboli, P., Rao, P., Guo, M., Manyam, G., Zhang, L., Xiang, Y., Han, L., Shang, X., Deng, P., Luo, Y., Lu, X., Feng, S., Ferrer, M. M., Alan Wang, Y., DePinho, R. A., . . . Lu, X. (2020). Effective combinatorial immunotherapy for penile squamous cell carcinoma. *Nat Commun*, *11*(1), 2124. https://doi.org/10.1038/s41467-020-15980-9

Hubert, M., Gobbini, E., Couillault, C., Manh, T. V., Doffin, A. C., Berthet, J., Rodriguez, C., Ollion, V., Kielbassa, J., Sajous, C., Treilleux, I., Tredan, O., Dubois, B., Dalod, M., Bendriss-Vermare, N., Caux, C., & Valladeau-

Guilemond, J. (2020). IFN-III is selectively produced by cDC1 and predicts good clinical outcome in breast cancer. *Sci Immunol*, *5*(46). https://doi.org/10.1126/sciimmunol.aav3942
Huynh, A., DuPage, M., Priyadharshini, B., Sage, P. T., Quiros, J., Borges, C. M., Townamchai, N., Gerriets, V. A., Rathmell, J. C., Sharpe, A. H., Bluestone, J. A., & Turka, L. A. (2015). Control of PI(3) kinase in Treg cells maintains homeostasis and lineage stability. *Nat Immunol*, *16*(2), 188-196. https://doi.org/10.1038/ni.3077
Iannone, R., Miele, L., Maiolino, P., Pinto, A., & Morello, S. (2013). Blockade of A2b adenosine receptor reduces tumor growth and immune suppression mediated by myeloid-derived suppressor cells in a mouse model of melanoma. *Neoplasia*, *15*(12), 1400-1409. https://doi.org/10.1593/neo.131748
Ibrahim, J., Nguyen, A. H., Rehman, A., Ochi, A., Jamal, M., Graffeo, C. S., Henning, J. R., Zambirinis, C. P., Fallon, N. C., Barilla, R., Badar, S., Mitchell, A., Rao, R. S., Acehan, D., Frey, A. B., & Miller, G. (2012). Dendritic cell populations with different concentrations of lipid regulate tolerance and immunity in mouse and human liver. *Gastroenterology*, *143*(4), 1061-1072. https://doi.org/10.1053/j.gastro.2012.06.003
Im, S. S., Yousef, L., Blaschitz, C., Liu, J. Z., Edwards, R. A., Young, S. G., Raffatellu, M., & Osborne, T. F. (2011). Linking lipid metabolism to the innate immune response in macrophages through sterol regulatory element binding protein-1a. *Cell Metab*, *13*(5), 540-549. https://doi.org/10.1016/j.cmet.2011.04.001
Imtiyaz, H. Z., Williams, E. P., Hickey, M. M., Patel, S. A., Durham, A. C., Yuan, L. J., Hammond, R., Gimotty, P. A., Keith, B., & Simon, M. C. (2010). Hypoxia-inducible factor 2alpha regulates macrophage function in mouse models of acute and tumor inflammation. *J Clin Invest*, *120*(8), 2699-2714. https://doi.org/10.1172/JCI39506
Infantino, V., Iacobazzi, V., Menga, A., Avantaggiati, M. L., & Palmieri, F. (2014). A key role of the mitochondrial citrate carrier (SLC25A1) in TNFalpha- and IFNgamma-triggered inflammation. *Biochim Biophys Acta*, *1839*(11), 1217-1225. https://doi.org/10.1016/j.bbagrm.2014.07.013
Inoki, K., Li, Y., Zhu, T., Wu, J., & Guan, K. L. (2002). TSC2 is phosphorylated and inhibited by Akt and suppresses mTOR signalling. *Nat Cell Biol*, *4*(9), 648-657. https://doi.org/10.1038/ncb839
Isaacs, J. S., Jung, Y. J., Mole, D. R., Lee, S., Torres-Cabala, C., Chung, Y. L., Merino, M., Trepel, J., Zbar, B., Toro, J., Ratcliffe, P. J., Linehan, W. M., & Neckers, L. (2005). HIF overexpression correlates with biallelic loss of fumarate hydratase in renal cancer: novel role of fumarate in regulation of HIF stability. *Cancer Cell*, *8*(2), 143-153. https://doi.org/10.1016/j.ccr.2005.06.017
Ivan, M., Kondo, K., Yang, H., Kim, W., Valiando, J., Ohh, M., Salic, A., Asara, J. M., Lane, W. S., & Kaelin, W. G., Jr. (2001). HIFalpha targeted for VHL-mediated destruction by proline hydroxylation: implications for O2 sensing. *Science*, *292*(5516), 464-468. https://doi.org/10.1126/science.1059817
Jaakkola, P., Mole, D. R., Tian, Y. M., Wilson, M. I., Gielbert, J., Gaskell, S. J., von Kriegsheim, A., Hebestreit, H. F., Mukherji, M., Schofield, C. J., Maxwell, P. H., Pugh, C. W., & Ratcliffe, P. J. (2001). Targeting of HIF-alpha to the von Hippel-Lindau ubiquitylation complex by O2-regulated prolyl hydroxylation. *Science*, *292*(5516), 468-472. https://doi.org/10.1126/science.1059796
Jaiswal, A. R., Liu, A. J., Pudakalakatti, S., Dutta, P., Jayaprakash, P., Bartkowiak, T., Ager, C. R., Wang, Z. Q., Reuben, A., Cooper, Z. A., Ivan, C., Ju, Z., Nwajei, F., Wang, J., Davies, M. A., Davis, R. E., Wargo, J. A., Bhattacharya, P. K., Hong, D. S., & Curran, M. A. (2020). Melanoma Evolves Complete Immunotherapy Resistance through the Acquisition of a Hypermetabolic Phenotype. *Cancer Immunol Res*, *8*(11), 1365-1380. https://doi.org/10.1158/2326-6066.CIR-19-0005
Jalali, S., Price-Troska, T., Bothun, C., Villasboas, J., Kim, H. J., Yang, Z. Z., Novak, A. J., Dong, H., & Ansell, S. M. (2019). Reverse signaling via PD-L1 supports malignant cell growth and survival in classical Hodgkin lymphoma. *Blood Cancer J*, *9*(3), 22. https://doi.org/10.1038/s41408-019-0185-9
Jang, C., Hui, S., Zeng, X., Cowan, A. J., Wang, L., Chen, L., Morscher, R. J., Reyes, J., Frezza, C., Hwang, H. Y., Imai, A., Saito, Y., Okamoto, K., Vaspoli, C., Kasprenski, L., Zsido, G. A., 2nd, Gorman, J. H., 3rd, Gorman, R. C., & Rabinowitz, J. D. (2019). Metabolite Exchange between Mammalian Organs Quantified in Pigs. *Cell Metab*, *30*(3), 594-606 e593. https://doi.org/10.1016/j.cmet.2019.06.002
Jeong, H., Kim, S., Hong, B. J., Lee, C. J., Kim, Y. E., Bok, S., Oh, J. M., Gwak, S. H., Yoo, M. Y., Lee, M. S., Chung, S. J., Defrene, J., Tessier, P., Pelletier, M., Jeon, H., Roh, T. Y., Kim, B., Kim, K. H., Ju, J. H., . . . Ahn, G. O. (2019). Tumor-Associated Macrophages Enhance Tumor Hypoxia and Aerobic Glycolysis. *Cancer Res*, *79*(4), 795-806. https://doi.org/10.1158/0008-5472.CAN-18-2545
Jha, A. K., Huang, S. C., Sergushichev, A., Lampropoulou, V., Ivanova, Y., Loginicheva, E., Chmielewski, K., Stewart, K. M., Ashall, J., Everts, B., Pearce, E. J., Driggers, E. M., & Artyomov, M. N. (2015). Network integration of parallel metabolic and transcriptional data reveals metabolic modules that regulate macrophage polarization. *Immunity*, *42*(3), 419-430. https://doi.org/10.1016/j.immuni.2015.02.005
Jian, S. L., Chen, W. W., Su, Y. C., Su, Y. W., Chuang, T. H., Hsu, S. C., & Huang, L. R. (2017). Glycolysis regulates the expansion of myeloid-derived suppressor cells in tumor-bearing hosts through prevention of ROS-mediated apoptosis. *Cell Death Dis*, *8*(5), e2779. https://doi.org/10.1038/cddis.2017.192
Jiang, P., Du, W., Wang, X., Mancuso, A., Gao, X., Wu, M., & Yang, X. (2011). p53 regulates biosynthesis through direct inactivation of glucose-6-phosphate dehydrogenase. *Nat Cell Biol*, *13*(3), 310-316. https://doi.org/10.1038/ncb2172
Johnson, M. O., Wolf, M. M., Madden, M. Z., Andrejeva, G., Sugiura, A., Contreras, D. C., Maseda, D., Liberti, M. V., Paz, K., Kishton, R. J., Johnson, M. E., de Cubas, A. A., Wu, P., Li, G., Zhang, Y., Newcomb, D. C., Wells,

A. D., Restifo, N. P., Rathmell, W. K., . . . Rathmell, J. C. (2018). Distinct Regulation of Th17 and Th1 Cell Differentiation by Glutaminase-Dependent Metabolism. *Cell*, *175*(7), 1780-1795 e1719. https://doi.org/10.1016/j.cell.2018.10.001

Johnston, K., Pachnis, P., Tasdogan, A., Faubert, B., Zacharias, L. G., Vu, H. S., Rodgers-Augustyniak, L., Johnson, A., Huang, F., Ricciardo, S., Zhao, Z., Mathews, T. P., Watt, T., Leavey, P., & DeBerardinis, R. J. (2021). Isotope tracing reveals glycolysis and oxidative metabolism in childhood tumors of multiple histologies. *Med (N Y)*, *2*(4), 395-410. https://doi.org/10.1016/j.medj.2021.01.002

Jonasch, E., Donskov, F., Iliopoulos, O., Rathmell, W. K., Narayan, V. K., Maughan, B. L., Oudard, S., Else, T., Maranchie, J. K., Welsh, S. J., Thamake, S., Park, E. K., Perini, R. F., Linehan, W. M., Srinivasan, R., & Investigators, M. K. (2021). Belzutifan for Renal Cell Carcinoma in von Hippel-Lindau Disease. *N Engl J Med*, *385*(22), 2036-2046. https://doi.org/10.1056/NEJMoa2103425

Joshi, S., Singh, A. R., Liu, K. X., Pham, T. V., Zulcic, M., Skola, D., Chun, H. B., Glass, C. K., Morales, G. A., Garlich, J. R., & Durden, D. L. (2019). SF2523: Dual PI3K/BRD4 Inhibitor Blocks Tumor Immunosuppression and Promotes Adaptive Immune Responses in Cancer. *Mol Cancer Ther*, *18*(6), 1036-1044. https://doi.org/10.1158/1535-7163.MCT-18-1206

julian.knight@well.ox.ac.uk, C. O.-M.-o. B. A. C. E. a., & Consortium, C. O.-M.-o. B. A. (2022). A blood atlas of COVID-19 defines hallmarks of disease severity and specificity. *Cell*, *185*(5), 916-938 e958. https://doi.org/10.1016/j.cell.2022.01.012

Kaneda, M. M., Cappello, P., Nguyen, A. V., Ralainirina, N., Hardamon, C. R., Foubert, P., Schmid, M. C., Sun, P., Mose, E., Bouvet, M., Lowy, A. M., Valasek, M. A., Sasik, R., Novelli, F., Hirsch, E., & Varner, J. A. (2016). Macrophage PI3Kgamma Drives Pancreatic Ductal Adenocarcinoma Progression. *Cancer Discov*, *6*(8), 870-885. https://doi.org/10.1158/2159-8290.CD-15-1346

Kaneda, M. M., Messer, K. S., Ralainirina, N., Li, H., Leem, C. J., Gorjestani, S., Woo, G., Nguyen, A. V., Figueiredo, C. C., Foubert, P., Schmid, M. C., Pink, M., Winkler, D. G., Rausch, M., Palombella, V. J., Kutok, J., McGovern, K., Frazer, K. A., Wu, X., . . . Varner, J. A. (2016). PI3Kgamma is a molecular switch that controls immune suppression. *Nature*, *539*(7629), 437-442. https://doi.org/10.1038/nature19834

Karmaus, P. W. F., Herrada, A. A., Guy, C., Neale, G., Dhungana, Y., Long, L., Vogel, P., Avila, J., Clish, C. B., & Chi, H. (2017). Critical roles of mTORC1 signaling and metabolic reprogramming for M-CSF-mediated myelopoiesis. *J Exp Med*, *214*(9), 2629-2647. https://doi.org/10.1084/jem.20161855

Kartha, V. K., Duarte, F. M., Hu, Y., Ma, S., Chew, J. G., Lareau, C. A., Earl, A., Burkett, Z. D., Kohlway, A. S., Lebofsky, R., & Buenrostro, J. D. (2021). Functional Inference of Gene Regulation using Single-Cell Multi-Omics. *bioRxiv*, 2021.2007.2028.453784. https://doi.org/10.1101/2021.07.28.453784

Katholnig, K., Schutz, B., Fritsch, S. D., Schorghofer, D., Linke, M., Sukhbaatar, N., Matschinger, J. M., Unterleuthner, D., Hirtl, M., Lang, M., Herac, M., Spittler, A., Bergthaler, A., Schabbauer, G., Bergmann, M., Dolznig, H., Hengstschlager, M., Magnuson, M. A., Mikula, M., & Weichhart, T. (2019). Inactivation of mTORC2 in macrophages is a signature of colorectal cancer that promotes tumorigenesis. *JCI Insight*, *4*(20). https://doi.org/10.1172/jci.insight.124164

Katzen, H. M., & Schimke, R. T. (1965). Multiple forms of hexokinase in the rat: tissue distribution, age dependency, and properties. *Proc Natl Acad Sci U S A*, *54*(4), 1218-1225. https://doi.org/10.1073/pnas.54.4.1218

Katzenelenbogen, Y., Sheban, F., Yalin, A., Yofe, I., Svetlichnyy, D., Jaitin, D. A., Bornstein, C., Moshe, A., Keren-Shaul, H., Cohen, M., Wang, S. Y., Li, B., David, E., Salame, T. M., Weiner, A., & Amit, I. (2020). Coupled scRNA-Seq and Intracellular Protein Activity Reveal an Immunosuppressive Role of TREM2 in Cancer. *Cell*, *182*(4), 872-885 e819. https://doi.org/10.1016/j.cell.2020.06.032

Kawalekar, O. U., O'Connor, R. S., Fraietta, J. A., Guo, L., McGettigan, S. E., Posey, A. D., Jr., Patel, P. R., Guedan, S., Scholler, J., Keith, B., Snyder, N. W., Blair, I. A., Milone, M. C., & June, C. H. (2016). Distinct Signaling of Coreceptors Regulates Specific Metabolism Pathways and Impacts Memory Development in CAR T Cells. *Immunity*, *44*(2), 380-390. https://doi.org/10.1016/j.immuni.2016.01.021

Kawauchi, K., Araki, K., Tobiume, K., & Tanaka, N. (2008). p53 regulates glucose metabolism through an IKK-NF-kappaB pathway and inhibits cell transformation. *Nat Cell Biol*, *10*(5), 611-618. https://doi.org/10.1038/ncb1724

Kaymak, I., Williams, K. S., Cantor, J. R., & Jones, R. G. (2021). Immunometabolic Interplay in the Tumor Microenvironment. *Cancer Cell*, *39*(1), 28-37. https://doi.org/10.1016/j.ccell.2020.09.004

Kc, W., Satpathy, A. T., Rapaport, A. S., Briseno, C. G., Wu, X., Albring, J. C., Russler-Germain, E. V., Kretzer, N. M., Durai, V., Persaud, S. P., Edelson, B. T., Loschko, J., Cella, M., Allen, P. M., Nussenzweig, M. C., Colonna, M., Sleckman, B. P., Murphy, T. L., & Murphy, K. M. (2014). L-Myc expression by dendritic cells is required for optimal T-cell priming. *Nature*, *507*(7491), 243-247. https://doi.org/10.1038/nature12967

Keating, S. E., Zaiatz-Bittencourt, V., Loftus, R. M., Keane, C., Brennan, K., Finlay, D. K., & Gardiner, C. M. (2016). Metabolic Reprogramming Supports IFN-gamma Production by CD56bright NK Cells. *J Immunol*, *196*(6), 2552-2560. https://doi.org/10.4049/jimmunol.1501783

Keith, B., Johnson, R. S., & Simon, M. C. (2011). HIF1alpha and HIF2alpha: sibling rivalry in hypoxic tumour growth and progression. *Nat Rev Cancer*, *12*(1), 9-22. https://doi.org/10.1038/nrc3183

Kelley, T. W., Graham, M. M., Doseff, A. I., Pomerantz, R. W., Lau, S. M., Ostrowski, M. C., Franke, T. F., & Marsh, C. B. (1999). Macrophage colony-stimulating factor promotes cell survival through Akt/protein kinase B. *J Biol Chem*, *274*(37), 26393-26398. https://doi.org/10.1074/jbc.274.37.26393
Keppel, M. P., Saucier, N., Mah, A. Y., Vogel, T. P., & Cooper, M. A. (2015). Activation-specific metabolic requirements for NK Cell IFN-gamma production. *J Immunol*, *194*(4), 1954-1962. https://doi.org/10.4049/jimmunol.1402099
Kernstine, K. H., Faubert, B., Do, Q. N., Rogers, T. J., Hensley, C. T., Cai, L., Torrealba, J., Oliver, D., Wachsmann, J. W., Lenkinski, R. E., Malloy, C. R., & Deberardinis, R. J. (2020). Does Tumor FDG-PET Avidity Represent Enhanced Glycolytic Metabolism in Non-Small Cell Lung Cancer? *Ann Thorac Surg*, *109*(4), 1019-1025. https://doi.org/10.1016/j.athoracsur.2019.10.061
Kilgour, M. K., MacPherson, S., Zacharias, L. G., Ellis, A. E., Sheldon, R. D., Liu, E. Y., Keyes, S., Pauly, B., Carleton, G., Allard, B., Smazynski, J., Williams, K. S., Watson, P. H., Stagg, J., Nelson, B. H., DeBerardinis, R. J., Jones, R. G., Hamilton, P. T., & Lum, J. J. (2021). 1-Methylnicotinamide is an immune regulatory metabolite in human ovarian cancer. *Sci Adv*, *7*(4). https://doi.org/10.1126/sciadv.abe1174
Kim, J., Lee, J. H., & Iyer, V. R. (2008). Global identification of Myc target genes reveals its direct role in mitochondrial biogenesis and its E-box usage in vivo. *PLoS One*, *3*(3), e1798. https://doi.org/10.1371/journal.pone.0001798
Kim, J. W., Zeller, K. I., Wang, Y., Jegga, A. G., Aronow, B. J., O'Donnell, K. A., & Dang, C. V. (2004). Evaluation of myc E-box phylogenetic footprints in glycolytic genes by chromatin immunoprecipitation assays. *Mol Cell Biol*, *24*(13), 5923-5936. https://doi.org/10.1128/MCB.24.13.5923-5936.2004
Kim, S. M., Yun, M. R., Hong, Y. K., Solca, F., Kim, J. H., Kim, H. J., & Cho, B. C. (2013). Glycolysis inhibition sensitizes non-small cell lung cancer with T790M mutation to irreversible EGFR inhibitors via translational suppression of Mcl-1 by AMPK activation. *Mol Cancer Ther*, *12*(10), 2145-2156. https://doi.org/10.1158/1535-7163.MCT-12-1188
Kiykim, A., Baris, S., Karakoc-Aydiner, E., Ozen, A. O., Ogulur, I., Bozkurt, S., Ataizi, C. C., Boztug, K., & Barlan, I. B. (2015). G6PC3 Deficiency: Primary Immune Deficiency Beyond Just Neutropenia. *J Pediatr Hematol Oncol*, *37*(8), 616-622. https://doi.org/10.1097/MPH.0000000000000441
Klemm, F., Maas, R. R., Bowman, R. L., Kornete, M., Soukup, K., Nassiri, S., Brouland, J. P., Iacobuzio-Donahue, C. A., Brennan, C., Tabar, V., Gutin, P. H., Daniel, R. T., Hegi, M. E., & Joyce, J. A. (2020). Interrogation of the Microenvironmental Landscape in Brain Tumors Reveals Disease-Specific Alterations of Immune Cells. *Cell*, *181*(7), 1643-1660 e1617. https://doi.org/10.1016/j.cell.2020.05.007
Klose, R., Krzywinska, E., Castells, M., Gotthardt, D., Putz, E. M., Kantari-Mimoun, C., Chikdene, N., Meinecke, A. K., Schrodter, K., Helfrich, I., Fandrey, J., Sexl, V., & Stockmann, C. (2016). Targeting VEGF-A in myeloid cells enhances natural killer cell responses to chemotherapy and ameliorates cachexia. *Nat Commun*, *7*, 12528. https://doi.org/10.1038/ncomms12528
Ko, J. S., Zea, A. H., Rini, B. I., Ireland, J. L., Elson, P., Cohen, P., Golshayan, A., Rayman, P. A., Wood, L., Garcia, J., Dreicer, R., Bukowski, R., & Finke, J. H. (2009). Sunitinib mediates reversal of myeloid-derived suppressor cell accumulation in renal cell carcinoma patients. *Clin Cancer Res*, *15*(6), 2148-2157. https://doi.org/10.1158/1078-0432.CCR-08-1332
Kohn, A. D., Barthel, A., Kovacina, K. S., Boge, A., Wallach, B., Summers, S. A., Birnbaum, M. J., Scott, P. H., Lawrence, J. C., Jr., & Roth, R. A. (1998). Construction and characterization of a conditionally active version of the serine/threonine kinase Akt. *J Biol Chem*, *273*(19), 11937-11943. https://doi.org/10.1074/jbc.273.19.11937
Kohnken, R., Porcu, P., & Mishra, A. (2017). Overview of the Use of Murine Models in Leukemia and Lymphoma Research. *Front Oncol*, *7*, 22. https://doi.org/10.3389/fonc.2017.00022
Kono, M., Yoshida, N., Maeda, K., Suarez-Fueyo, A., Kyttaris, V. C., & Tsokos, G. C. (2019). Glutaminase 1 Inhibition Reduces Glycolysis and Ameliorates Lupus-like Disease in MRL/lpr Mice and Experimental Autoimmune Encephalomyelitis. *Arthritis Rheumatol*, *71*(11), 1869-1878. https://doi.org/10.1002/art.41019
Kovacina, K. S., Park, G. Y., Bae, S. S., Guzzetta, A. W., Schaefer, E., Birnbaum, M. J., & Roth, R. A. (2003). Identification of a proline-rich Akt substrate as a 14-3-3 binding partner. *J Biol Chem*, *278*(12), 10189-10194. https://doi.org/10.1074/jbc.M210837200
Kratchmarov, R., Viragova, S., Kim, M. J., Rothman, N. J., Liu, K., Reizis, B., & Reiner, S. L. (2018). Metabolic control of cell fate bifurcations in a hematopoietic progenitor population. *Immunol Cell Biol*, *96*(8), 863-871. https://doi.org/10.1111/imcb.12040
Kronke, J., Udeshi, N. D., Narla, A., Grauman, P., Hurst, S. N., McConkey, M., Svinkina, T., Heckl, D., Comer, E., Li, X., Ciarlo, C., Hartman, E., Munshi, N., Schenone, M., Schreiber, S. L., Carr, S. A., & Ebert, B. L. (2014). Lenalidomide causes selective degradation of IKZF1 and IKZF3 in multiple myeloma cells. *Science*, *343*(6168), 301-305. https://doi.org/10.1126/science.1244851
Kumagai, S., Koyama, S., Itahashi, K., Tanegashima, T., Lin, Y. T., Togashi, Y., Kamada, T., Irie, T., Okumura, G., Kono, H., Ito, D., Fujii, R., Watanabe, S., Sai, A., Fukuoka, S., Sugiyama, E., Watanabe, G., Owari, T., Nishinakamura, H., . . . Nishikawa, H. (2022). Lactic acid promotes PD-1 expression in regulatory T cells in

highly glycolytic tumor microenvironments. *Cancer Cell*, *40*(2), 201-218 e209. https://doi.org/10.1016/j.ccell.2022.01.001
Kurotaki, D., Kawase, W., Sasaki, H., Nakabayashi, J., Nishiyama, A., Morse, H. C., 3rd, Ozato, K., Suzuki, Y., & Tamura, T. (2019). Epigenetic control of early dendritic cell lineage specification by the transcription factor IRF8 in mice. *Blood*, *133*(17), 1803-1813. https://doi.org/10.1182/blood-2018-06-857789
LaFave, L. M., Kartha, V. K., Ma, S., Meli, K., Del Priore, I., Lareau, C., Naranjo, S., Westcott, P. M. K., Duarte, F. M., Sankar, V., Chiang, Z., Brack, A., Law, T., Hauck, H., Okimoto, A., Regev, A., Buenrostro, J. D., & Jacks, T. (2020). Epigenomic State Transitions Characterize Tumor Progression in Mouse Lung Adenocarcinoma. *Cancer Cell*, *38*(2), 212-228 e213. https://doi.org/10.1016/j.ccell.2020.06.006
Lalani, A. A., Xie, W., Martini, D. J., Steinharter, J. A., Norton, C. K., Krajewski, K. M., Duquette, A., Bosse, D., Bellmunt, J., Van Allen, E. M., McGregor, B. A., Creighton, C. J., Harshman, L. C., & Choueiri, T. K. (2018). Change in Neutrophil-to-lymphocyte ratio (NLR) in response to immune checkpoint blockade for metastatic renal cell carcinoma. *J Immunother Cancer*, *6*(1), 5. https://doi.org/10.1186/s40425-018-0315-0
Land, S. C., & Tee, A. R. (2007). Hypoxia-inducible factor 1alpha is regulated by the mammalian target of rapamycin (mTOR) via an mTOR signaling motif. *J Biol Chem*, *282*(28), 20534-20543. https://doi.org/10.1074/jbc.M611782200
Laoui, D., Keirsse, J., Morias, Y., Van Overmeire, E., Geeraerts, X., Elkrim, Y., Kiss, M., Bolli, E., Lahmar, Q., Sichien, D., Serneels, J., Scott, C. L., Boon, L., De Baetselier, P., Mazzone, M., Guilliams, M., & Van Ginderachter, J. A. (2016). The tumour microenvironment harbours ontogenically distinct dendritic cell populations with opposing effects on tumour immunity. *Nat Commun*, *7*, 13720. https://doi.org/10.1038/ncomms13720
Larkin, J., Chiarion-Sileni, V., Gonzalez, R., Grob, J. J., Cowey, C. L., Lao, C. D., Schadendorf, D., Dummer, R., Smylie, M., Rutkowski, P., Ferrucci, P. F., Hill, A., Wagstaff, J., Carlino, M. S., Haanen, J. B., Maio, M., Marquez-Rodas, I., McArthur, G. A., Ascierto, P. A., . . . Wolchok, J. D. (2015). Combined Nivolumab and Ipilimumab or Monotherapy in Untreated Melanoma. *N Engl J Med*, *373*(1), 23-34. https://doi.org/10.1056/NEJMoa1504030
Lau, A. N., Li, Z., Danai, L. V., Westermark, A. M., Darnell, A. M., Ferreira, R., Gocheva, V., Sivanand, S., Lien, E. C., Sapp, K. M., Mayers, J. R., Biffi, G., Chin, C. R., Davidson, S. M., Tuveson, D. A., Jacks, T., Matheson, N. J., Yilmaz, O., & Vander Heiden, M. G. (2020). Dissecting cell-type-specific metabolism in pancreatic ductal adenocarcinoma. *Elife*, *9*. https://doi.org/10.7554/eLife.56782
Lauterbach, M. A., Hanke, J. E., Serefidou, M., Mangan, M. S. J., Kolbe, C. C., Hess, T., Rothe, M., Kaiser, R., Hoss, F., Gehlen, J., Engels, G., Kreutzenbeck, M., Schmidt, S. V., Christ, A., Imhof, A., Hiller, K., & Latz, E. (2019). Toll-like Receptor Signaling Rewires Macrophage Metabolism and Promotes Histone Acetylation via ATP-Citrate Lyase. *Immunity*, *51*(6), 997-1011 e1017. https://doi.org/10.1016/j.immuni.2019.11.009
Lee, K. J., Yin, W., Arafat, D., Tang, Y., Uppal, K., Tran, V., Cabrera-Mora, M., Lapp, S., Moreno, A., Meyer, E., DeBarry, J. D., Pakala, S., Nayak, V., Kissinger, J. C., Jones, D. P., Galinski, M., Styczynski, M. P., & Gibson, G. (2014). Comparative transcriptomics and metabolomics in a rhesus macaque drug administration study. *Front Cell Dev Biol*, *2*, 54. https://doi.org/10.3389/fcell.2014.00054
Lee, M. J., Yun, S. J., Lee, B., Jeong, E., Yoon, G., Kim, K., & Park, S. (2020). Association of TIM-3 expression with glucose metabolism in Jurkat T cells. *BMC Immunol*, *21*(1), 48. https://doi.org/10.1186/s12865-020-00377-6
Leitner, B. P., Givechian, K. B., Ospanova, S., Beisenbayeva, A., Politi, K., & Perry, R. J. (2022). Multimodal analysis suggests differential immuno-metabolic crosstalk in lung squamous cell carcinoma and adenocarcinoma. *NPJ Precis Oncol*, *6*(1), 8. https://doi.org/10.1038/s41698-021-00248-2
Leone, R. D., Zhao, L., Englert, J. M., Sun, I. M., Oh, M. H., Sun, I. H., Arwood, M. L., Bettencourt, I. A., Patel, C. H., Wen, J., Tam, A., Blosser, R. L., Prchalova, E., Alt, J., Rais, R., Slusher, B. S., & Powell, J. D. (2019). Glutamine blockade induces divergent metabolic programs to overcome tumor immune evasion. *Science*, *366*(6468), 1013-1021. https://doi.org/10.1126/science.aav2588
Li, C., Huang, S., Guo, J., Wang, C., Huang, Z., Huang, R., Liu, L., Liang, S., & Wang, H. (2019). Metabolic Evaluation of MYCN-Amplified Neuroblastoma by 4-[(18)F]FGln PET Imaging. *Mol Imaging Biol*, *21*(6), 1117-1126. https://doi.org/10.1007/s11307-019-01330-9
Li, C., Wang, Y., Li, Y., Yu, Q., Jin, X., Wang, X., Jia, A., Hu, Y., Han, L., Wang, J., Yang, H., Yan, D., Bi, Y., & Liu, G. (2018). HIF1alpha-dependent glycolysis promotes macrophage functional activities in protecting against bacterial and fungal infection. *Sci Rep*, *8*(1), 3603. https://doi.org/10.1038/s41598-018-22039-9
LÍ, S., Josse, J., & Husson, F. (2008). FactoMineR: An R Package for Multivariate Analysis. *Journal of Statistical Software*, *25*, 1-18.
Li, W., Tanikawa, T., Kryczek, I., Xia, H., Li, G., Wu, K., Wei, S., Zhao, L., Vatan, L., Wen, B., Shu, P., Sun, D., Kleer, C., Wicha, M., Sabel, M., Tao, K., Wang, G., & Zou, W. (2018). Aerobic Glycolysis Controls Myeloid-Derived Suppressor Cells and Tumor Immunity via a Specific CEBPB Isoform in Triple-Negative Breast Cancer. *Cell Metab*, *28*(1), 87-103 e106. https://doi.org/10.1016/j.cmet.2018.04.022
Li, X., Hui, S., Mirek, E. T., Jonsson, W. O., Anthony, T. G., Lee, W. D., Zeng, X., Jang, C., & Rabinowitz, J. D. (2022). Circulating metabolite homeostasis achieved through mass action. *Nat Metab*, *4*(1), 141-152. https://doi.org/10.1038/s42255-021-00517-1

Li, X., Qian, X., Peng, L. X., Jiang, Y., Hawke, D. H., Zheng, Y., Xia, Y., Lee, J. H., Cote, G., Wang, H., Wang, L., Qian, C. N., & Lu, Z. (2016). A splicing switch from ketohexokinase-C to ketohexokinase-A drives hepatocellular carcinoma formation. *Nat Cell Biol*, *18*(5), 561-571. https://doi.org/10.1038/ncb3338
Lim, S., Liu, H., Madeira da Silva, L., Arora, R., Liu, Z., Phillips, J. B., Schmitt, D. C., Vu, T., McClellan, S., Lin, Y., Lin, W., Piazza, G. A., Fodstad, O., & Tan, M. (2016). Immunoregulatory Protein B7-H3 Reprograms Glucose Metabolism in Cancer Cells by ROS-Mediated Stabilization of HIF1alpha. *Cancer Res*, *76*(8), 2231-2242. https://doi.org/10.1158/0008-5472.CAN-15-1538
Linehan, W. M., Schmidt, L. S., Crooks, D. R., Wei, D., Srinivasan, R., Lang, M., & Ricketts, C. J. (2019). The Metabolic Basis of Kidney Cancer. *Cancer Discov*, *9*(8), 1006-1021. https://doi.org/10.1158/2159-8290.CD-18-1354
Liu, D., Chang, C., Lu, N., Wang, X., Lu, Q., Ren, X., Ren, P., Zhao, D., Wang, L., Zhu, Y., He, F., & Tang, L. (2017). Comprehensive Proteomics Analysis Reveals Metabolic Reprogramming of Tumor-Associated Macrophages Stimulated by the Tumor Microenvironment. *J Proteome Res*, *16*(1), 288-297. https://doi.org/10.1021/acs.jproteome.6b00604
Liu, E., Marin, D., Banerjee, P., Macapinlac, H. A., Thompson, P., Basar, R., Nassif Kerbauy, L., Overman, B., Thall, P., Kaplan, M., Nandivada, V., Kaur, I., Nunez Cortes, A., Cao, K., Daher, M., Hosing, C., Cohen, E. N., Kebriaei, P., Mehta, R., . . . Rezvani, K. (2020). Use of CAR-Transduced Natural Killer Cells in CD19-Positive Lymphoid Tumors. *N Engl J Med*, *382*(6), 545-553. https://doi.org/10.1056/NEJMoa1910607
Liu, G., Bi, Y., Shen, B., Yang, H., Zhang, Y., Wang, X., Liu, H., Lu, Y., Liao, J., Chen, X., & Chu, Y. (2014). SIRT1 limits the function and fate of myeloid-derived suppressor cells in tumors by orchestrating HIF-1alpha-dependent glycolysis. *Cancer Res*, *74*(3), 727-737. https://doi.org/10.1158/0008-5472.CAN-13-2584
Liu, H., Tekle, C., Chen, Y. W., Kristian, A., Zhao, Y., Zhou, M., Liu, Z., Ding, Y., Wang, B., Maelandsmo, G. M., Nesland, J. M., Fodstad, O., & Tan, M. (2011). B7-H3 silencing increases paclitaxel sensitivity by abrogating Jak2/Stat3 phosphorylation. *Mol Cancer Ther*, *10*(6), 960-971. https://doi.org/10.1158/1535-7163.MCT-11-0072
Liu, L., Lu, Y., Martinez, J., Bi, Y., Lian, G., Wang, T., Milasta, S., Wang, J., Yang, M., Liu, G., Green, D. R., & Wang, R. (2016). Proinflammatory signal suppresses proliferation and shifts macrophage metabolism from Myc-dependent to HIF1alpha-dependent. *Proc Natl Acad Sci U S A*, *113*(6), 1564-1569. https://doi.org/10.1073/pnas.1518000113
Liu, M., Tong, Z., Ding, C., Luo, F., Wu, S., Wu, C., Albeituni, S., He, L., Hu, X., Tieri, D., Rouchka, E. C., Hamada, M., Takahashi, S., Gibb, A. A., Kloecker, G., Zhang, H. G., Bousamra, M., 2nd, Hill, B. G., Zhang, X., & Yan, J. (2020). Transcription factor c-Maf is a checkpoint that programs macrophages in lung cancer. *J Clin Invest*, *130*(4), 2081-2096. https://doi.org/10.1172/JCI131335
Liu, P. S., Wang, H., Li, X., Chao, T., Teav, T., Christen, S., Di Conza, G., Cheng, W. C., Chou, C. H., Vavakova, M., Muret, C., Debackere, K., Mazzone, M., Huang, H. D., Fendt, S. M., Ivanisevic, J., & Ho, P. C. (2017). alpha-ketoglutarate orchestrates macrophage activation through metabolic and epigenetic reprogramming. *Nat Immunol*, *18*(9), 985-994. https://doi.org/10.1038/ni.3796
Liu, Y. (2016). The Place of FDG PET/CT in Renal Cell Carcinoma: Value and Limitations. *Front Oncol*, *6*, 201. https://doi.org/10.3389/fonc.2016.00201
Loftus, R. M., Assmann, N., Kedia-Mehta, N., O'Brien, K. L., Garcia, A., Gillespie, C., Hukelmann, J. L., Oefner, P. J., Lamond, A. I., Gardiner, C. M., Dettmer, K., Cantrell, D. A., Sinclair, L. V., & Finlay, D. K. (2018). Amino acid-dependent cMyc expression is essential for NK cell metabolic and functional responses in mice. *Nat Commun*, *9*(1), 2341. https://doi.org/10.1038/s41467-018-04719-2
Loibl, S., & Gianni, L. (2017). HER2-positive breast cancer. *Lancet*, *389*(10087), 2415-2429. https://doi.org/10.1016/S0140-6736(16)32417-5
Lokshin, A., Raskovalova, T., Huang, X., Zacharia, L. C., Jackson, E. K., & Gorelik, E. (2006). Adenosine-mediated inhibition of the cytotoxic activity and cytokine production by activated natural killer cells. *Cancer Res*, *66*(15), 7758-7765. https://doi.org/10.1158/0008-5472.CAN-06-0478
Long, A. H., Haso, W. M., Shern, J. F., Wanhainen, K. M., Murgai, M., Ingaramo, M., Smith, J. P., Walker, A. J., Kohler, M. E., Venkateshwara, V. R., Kaplan, R. N., Patterson, G. H., Fry, T. J., Orentas, R. J., & Mackall, C. L. (2015). 4-1BB costimulation ameliorates T cell exhaustion induced by tonic signaling of chimeric antigen receptors. *Nat Med*, *21*(6), 581-590. https://doi.org/10.1038/nm.3838
Losuwannarak, N., Roytrakul, S., & Chanvorachote, P. (2020). Gigantol Targets MYC for Ubiquitin-proteasomal Degradation and Suppresses Lung Cancer Cell Growth. *Cancer Genomics Proteomics*, *17*(6), 781-793. https://doi.org/10.21873/cgp.20232
Love, C., Tomas, M. B., Tronco, G. G., & Palestro, C. J. (2005). FDG PET of infection and inflammation. *Radiographics*, *25*(5), 1357-1368. https://doi.org/10.1148/rg.255045122
Love, M. I., Huber, W., & Anders, S. (2014). Moderated estimation of fold change and dispersion for RNA-seq data with DESeq2. *Genome Biol*, *15*(12), 550. https://doi.org/10.1186/s13059-014-0550-8
Luengo, A., Li, Z., Gui, D. Y., Sullivan, L. B., Zagorulya, M., Do, B. T., Ferreira, R., Naamati, A., Ali, A., Lewis, C. A., Thomas, C. J., Spranger, S., Matheson, N. J., & Vander Heiden, M. G. (2021). Increased demand for

NAD(+) relative to ATP drives aerobic glycolysis. *Mol Cell*, *81*(4), 691-707 e696. https://doi.org/10.1016/j.molcel.2020.12.012
Ma, E. H., Verway, M. J., Johnson, R. M., Roy, D. G., Steadman, M., Hayes, S., Williams, K. S., Sheldon, R. D., Samborska, B., Kosinski, P. A., Kim, H., Griss, T., Faubert, B., Condotta, S. A., Krawczyk, C. M., DeBerardinis, R. J., Stewart, K. M., Richer, M. J., Chubukov, V., . . . Jones, R. G. (2019). Metabolic Profiling Using Stable Isotope Tracing Reveals Distinct Patterns of Glucose Utilization by Physiologically Activated CD8(+) T Cells. *Immunity*, *51*(5), 856-870 e855. https://doi.org/10.1016/j.immuni.2019.09.003
Mabuchi, S., Komura, N., Sasano, T., Shimura, K., Yokoi, E., Kozasa, K., Kuroda, H., Takahashi, R., Kawano, M., Matsumoto, Y., Kato, H., Hatazawa, J., & Kimura, T. (2020). Pretreatment tumor-related leukocytosis misleads positron emission tomography-computed tomography during lymph node staging in gynecological malignancies. *Nat Commun*, *11*(1), 1364. https://doi.org/10.1038/s41467-020-15186-z
MacDonald, P. E., Joseph, J. W., & Rorsman, P. (2005). Glucose-sensing mechanisms in pancreatic beta-cells. *Philos Trans R Soc Lond B Biol Sci*, *360*(1464), 2211-2225. https://doi.org/10.1098/rstb.2005.1762
Macintyre, A. N., Gerriets, V. A., Nichols, A. G., Michalek, R. D., Rudolph, M. C., Deoliveira, D., Anderson, S. M., Abel, E. D., Chen, B. J., Hale, L. P., & Rathmell, J. C. (2014). The glucose transporter Glut1 is selectively essential for CD4 T cell activation and effector function. *Cell Metab*, *20*(1), 61-72. https://doi.org/10.1016/j.cmet.2014.05.004
Mah, A. Y., Rashidi, A., Keppel, M. P., Saucier, N., Moore, E. K., Alinger, J. B., Tripathy, S. K., Agarwal, S. K., Jeng, E. K., Wong, H. C., Miller, J. S., Fehniger, T. A., Mace, E. M., French, A. R., & Cooper, M. A. (2017). Glycolytic requirement for NK cell cytotoxicity and cytomegalovirus control. *JCI Insight*, *2*(23). https://doi.org/10.1172/jci.insight.95128
Maianski, N. A., Geissler, J., Srinivasula, S. M., Alnemri, E. S., Roos, D., & Kuijpers, T. W. (2004). Functional characterization of mitochondria in neutrophils: a role restricted to apoptosis. *Cell Death Differ*, *11*(2), 143-153. https://doi.org/10.1038/sj.cdd.4401320
Majewski, N., Nogueira, V., Bhaskar, P., Coy, P. E., Skeen, J. E., Gottlob, K., Chandel, N. S., Thompson, C. B., Robey, R. B., & Hay, N. (2004). Hexokinase-mitochondria interaction mediated by Akt is required to inhibit apoptosis in the presence or absence of Bax and Bak. *Mol Cell*, *16*(5), 819-830. https://doi.org/10.1016/j.molcel.2004.11.014
Majhail, N. S., Urbain, J. L., Albani, J. M., Kanvinde, M. H., Rice, T. W., Novick, A. C., Mekhail, T. M., Olencki, T. E., Elson, P., & Bukowski, R. M. (2003). F-18 fluorodeoxyglucose positron emission tomography in the evaluation of distant metastases from renal cell carcinoma. *J Clin Oncol*, *21*(21), 3995-4000. https://doi.org/10.1200/JCO.2003.04.073
Malinoc, A., Sullivan, M., Wiech, T., Schmid, K. W., Jilg, C., Straeter, J., Deger, S., Hoffmann, M. M., Bosse, A., Rasp, G., Eng, C., & Neumann, H. P. (2012). Biallelic inactivation of the SDHC gene in renal carcinoma associated with paraganglioma syndrome type 3. *Endocr Relat Cancer*, *19*(3), 283-290. https://doi.org/10.1530/ERC-11-0324
Marcais, A., Cherfils-Vicini, J., Viant, C., Degouve, S., Viel, S., Fenis, A., Rabilloud, J., Mayol, K., Tavares, A., Bienvenu, J., Gangloff, Y. G., Gilson, E., Vivier, E., & Walzer, T. (2014). The metabolic checkpoint kinase mTOR is essential for IL-15 signaling during the development and activation of NK cells. *Nat Immunol*, *15*(8), 749-757. https://doi.org/10.1038/ni.2936
Marchingo, J. M., Sinclair, L. V., Howden, A. J., & Cantrell, D. A. (2020). Quantitative analysis of how Myc controls T cell proteomes and metabolic pathways during T cell activation. *Elife*, *9*. https://doi.org/10.7554/eLife.53725
Martincorena, I., Fowler, J. C., Wabik, A., Lawson, A. R. J., Abascal, F., Hall, M. W. J., Cagan, A., Murai, K., Mahbubani, K., Stratton, M. R., Fitzgerald, R. C., Handford, P. A., Campbell, P. J., Saeb-Parsy, K., & Jones, P. H. (2018). Somatic mutant clones colonize the human esophagus with age. *Science*, *362*(6417), 911-917. https://doi.org/10.1126/science.aau3879
Massimino, L., Lamparelli, L. A., Houshyar, Y., D'Alessio, S., Peyrin-Biroulet, L., Vetrano, S., Danese, S., & Ungaro, F. (2021). The Inflammatory Bowel Disease Transcriptome and Metatranscriptome Meta-Analysis (IBD TaMMA) framework. *Nature Computational Science*, *1*(8), 511-515. https://doi.org/10.1038/s43588-021-00114-y
Matoba, S., Kang, J. G., Patino, W. D., Wragg, A., Boehm, M., Gavrilova, O., Hurley, P. J., Bunz, F., & Hwang, P. M. (2006). p53 regulates mitochondrial respiration. *Science*, *312*(5780), 1650-1653. https://doi.org/10.1126/science.1126863
Mayer, C. T., Ghorbani, P., Nandan, A., Dudek, M., Arnold-Schrauf, C., Hesse, C., Berod, L., Stuve, P., Puttur, F., Merad, M., & Sparwasser, T. (2014). Selective and efficient generation of functional Batf3-dependent CD103+ dendritic cells from mouse bone marrow. *Blood*, *124*(20), 3081-3091. https://doi.org/10.1182/blood-2013-12-545772
Mazure, N. M., Chen, E. Y., Yeh, P., Laderoute, K. R., & Giaccia, A. J. (1996). Oncogenic transformation and hypoxia synergistically act to modulate vascular endothelial growth factor expression. *Cancer Res*, *56*(15), 3436-3440. https://www.ncbi.nlm.nih.gov/pubmed/8758908
McDermott, D. F., Huseni, M. A., Atkins, M. B., Motzer, R. J., Rini, B. I., Escudier, B., Fong, L., Joseph, R. W., Pal, S. K., Reeves, J. A., Sznol, M., Hainsworth, J., Rathmell, W. K., Stadler, W. M., Hutson, T., Gore, M. E.,

Ravaud, A., Bracarda, S., Suarez, C., . . . Powles, T. (2018). Clinical activity and molecular correlates of response to atezolizumab alone or in combination with bevacizumab versus sunitinib in renal cell carcinoma. *Nat Med*, *24*(6), 749-757. https://doi.org/10.1038/s41591-018-0053-3

McKenna, K. C., Vicetti Miguel, R. D., Beatty, K. M., & Bilonick, R. A. (2011). A caveat for T cell transfer studies: generation of cytotoxic anti-Thy1.2 antibodies in Thy1.1 congenic mice given Thy1.2+ tumors or T cells. *J Leukoc Biol*, *89*(2), 291-300. https://doi.org/10.1189/jlb.0610333

Meeth, K., Wang, J. X., Micevic, G., Damsky, W., & Bosenberg, M. W. (2016). The YUMM lines: a series of congenic mouse melanoma cell lines with defined genetic alterations. *Pigment Cell Melanoma Res*, *29*(5), 590-597. https://doi.org/10.1111/pcmr.12498

Mehta, M. M., Weinberg, S. E., Steinert, E. M., Chhiba, K., Martinez, C. A., Gao, P., Perlman, H. R., Bryce, P., Hay, N., & Chandel, N. S. (2018). Hexokinase 2 is dispensable for T cell-dependent immunity. *Cancer Metab*, *6*, 10. https://doi.org/10.1186/s40170-018-0184-5

Melani, R. D., Gerbasi, V. R., Anderson, L. C., Sikora, J. W., Toby, T. K., Hutton, J. E., Butcher, D. S., Negrao, F., Seckler, H. S., Srzentic, K., Fornelli, L., Camarillo, J. M., LeDuc, R. D., Cesnik, A. J., Lundberg, E., Greer, J. B., Fellers, R. T., Robey, M. T., DeHart, C. J., . . . Kelleher, N. L. (2022). The Blood Proteoform Atlas: A reference map of proteoforms in human hematopoietic cells. *Science*, *375*(6579), 411-418. https://doi.org/10.1126/science.aaz5284

Mendler, A. N., Hu, B., Prinz, P. U., Kreutz, M., Gottfried, E., & Noessner, E. (2012). Tumor lactic acidosis suppresses CTL function by inhibition of p38 and JNK/c-Jun activation. *Int J Cancer*, *131*(3), 633-640. https://doi.org/10.1002/ijc.26410

Menk, A. V., Scharping, N. E., Rivadeneira, D. B., Calderon, M. J., Watson, M. J., Dunstane, D., Watkins, S. C., & Delgoffe, G. M. (2018). 4-1BB costimulation induces T cell mitochondrial function and biogenesis enabling cancer immunotherapeutic responses. *J Exp Med*, *215*(4), 1091-1100. https://doi.org/10.1084/jem.20171068

Meric-Bernstam, F., Brusco, L., Shaw, K., Horombe, C., Kopetz, S., Davies, M. A., Routbort, M., Piha-Paul, S. A., Janku, F., Ueno, N., Hong, D., De Groot, J., Ravi, V., Li, Y., Luthra, R., Patel, K., Broaddus, R., Mendelsohn, J., & Mills, G. B. (2015). Feasibility of Large-Scale Genomic Testing to Facilitate Enrollment Onto Genomically Matched Clinical Trials. *J Clin Oncol*, *33*(25), 2753-2762. https://doi.org/10.1200/JCO.2014.60.4165

Meric-Bernstam, F., Lee, R. J., Carthon, B. C., Iliopoulos, O., Mier, J. W., Patel, M. R., Tannir, N. M., Owonikoko, T. K., Haas, N. B., Voss, M. H., Harding, J. J., Srinivasan, R., Shapiro, G., Telli, M. L., Munster, P. N., Carvajal, R. D., Jenkins, Y., Whiting, S. H., Bendell, J. C., & Bauer, T. M. (2019). CB-839, a glutaminase inhibitor, in combination with cabozantinib in patients with clear cell and papillary metastatic renal cell cancer (mRCC): Results of a phase I study. *Journal of Clinical Oncology*, *37*(7_suppl), 549-549. https://doi.org/10.1200/JCO.2019.37.7_suppl.549

Meyer, M. A., Baer, J. M., Knolhoff, B. L., Nywening, T. M., Panni, R. Z., Su, X., Weilbaecher, K. N., Hawkins, W. G., Ma, C., Fields, R. C., Linehan, D. C., Challen, G. A., Faccio, R., Aft, R. L., & DeNardo, D. G. (2018). Breast and pancreatic cancer interrupt IRF8-dependent dendritic cell development to overcome immune surveillance. *Nat Commun*, *9*(1), 1250. https://doi.org/10.1038/s41467-018-03600-6

Michl, J., Ohlbaum, D. J., & Silverstein, S. C. (1976). 2-Deoxyglucose selectively inhibits Fc and complement receptor-mediated phagocytosis in mouse peritoneal macrophages II. Dissociation of the inhibitory effects of 2-deoxyglucose on phagocytosis and ATP generation. *J Exp Med*, *144*(6), 1484-1493. https://doi.org/10.1084/jem.144.6.1484

Miller, T. W., Forbes, J. T., Shah, C., Wyatt, S. K., Manning, H. C., Olivares, M. G., Sanchez, V., Dugger, T. C., de Matos Granja, N., Narasanna, A., Cook, R. S., Kennedy, J. P., Lindsley, C. W., & Arteaga, C. L. (2009). Inhibition of mammalian target of rapamycin is required for optimal antitumor effect of HER2 inhibitors against HER2-overexpressing cancer cells. *Clin Cancer Res*, *15*(23), 7266-7276. https://doi.org/10.1158/1078-0432.CCR-09-1665

Mills, E. L., Kelly, B., Logan, A., Costa, A. S. H., Varma, M., Bryant, C. E., Tourlomousis, P., Dabritz, J. H. M., Gottlieb, E., Latorre, I., Corr, S. C., McManus, G., Ryan, D., Jacobs, H. T., Szibor, M., Xavier, R. J., Braun, T., Frezza, C., Murphy, M. P., & O'Neill, L. A. (2016). Succinate Dehydrogenase Supports Metabolic Repurposing of Mitochondria to Drive Inflammatory Macrophages. *Cell*, *167*(2), 457-470 e413. https://doi.org/10.1016/j.cell.2016.08.064

Minhas, P. S., Liu, L., Moon, P. K., Joshi, A. U., Dove, C., Mhatre, S., Contrepois, K., Wang, Q., Lee, B. A., Coronado, M., Bernstein, D., Snyder, M. P., Migaud, M., Majeti, R., Mochly-Rosen, D., Rabinowitz, J. D., & Andreasson, K. I. (2019). Macrophage de novo NAD(+) synthesis specifies immune function in aging and inflammation. *Nat Immunol*, *20*(1), 50-63. https://doi.org/10.1038/s41590-018-0255-3

Miranda-Goncalves, V., Granja, S., Martinho, O., Honavar, M., Pojo, M., Costa, B. M., Pires, M. M., Pinheiro, C., Cordeiro, M., Bebiano, G., Costa, P., Reis, R. M., & Baltazar, F. (2016). Hypoxia-mediated upregulation of MCT1 expression supports the glycolytic phenotype of glioblastomas. *Oncotarget*, *7*(29), 46335-46353. https://doi.org/10.18632/oncotarget.10114

Molgora, M., Esaulova, E., Vermi, W., Hou, J., Chen, Y., Luo, J., Brioschi, S., Bugatti, M., Omodei, A. S., Ricci, B., Fronick, C., Panda, S. K., Takeuchi, Y., Gubin, M. M., Faccio, R., Cella, M., Gilfillan, S., Unanue, E. R.,

Artyomov, M. N., . . . Colonna, M. (2020). TREM2 Modulation Remodels the Tumor Myeloid Landscape Enhancing Anti-PD-1 Immunotherapy. *Cell*, *182*(4), 886-900 e817. https://doi.org/10.1016/j.cell.2020.07.013

Momcilovic, M., Jones, A., Bailey, S. T., Waldmann, C. M., Li, R., Lee, J. T., Abdelhady, G., Gomez, A., Holloway, T., Schmid, E., Stout, D., Fishbein, M. C., Stiles, L., Dabir, D. V., Dubinett, S. M., Christofk, H., Shirihai, O., Koehler, C. M., Sadeghi, S., & Shackelford, D. B. (2019). In vivo imaging of mitochondrial membrane potential in non-small-cell lung cancer. *Nature*, *575*(7782), 380-384. https://doi.org/10.1038/s41586-019-1715-0

Mookerjee, S. A., Goncalves, R. L. S., Gerencser, A. A., Nicholls, D. G., & Brand, M. D. (2015). The contributions of respiration and glycolysis to extracellular acid production. *Biochim Biophys Acta*, *1847*(2), 171-181. https://doi.org/10.1016/j.bbabio.2014.10.005

Moore, L., Leongamornlert, D., Coorens, T. H. H., Sanders, M. A., Ellis, P., Dentro, S. C., Dawson, K. J., Butler, T., Rahbari, R., Mitchell, T. J., Maura, F., Nangalia, J., Tarpey, P. S., Brunner, S. F., Lee-Six, H., Hooks, Y., Moody, S., Mahbubani, K. T., Jimenez-Linan, M., . . . Stratton, M. R. (2020). The mutational landscape of normal human endometrial epithelium. *Nature*, *580*(7805), 640-646. https://doi.org/10.1038/s41586-020-2214-z

Mootha, V. K., Lindgren, C. M., Eriksson, K. F., Subramanian, A., Sihag, S., Lehar, J., Puigserver, P., Carlsson, E., Ridderstrale, M., Laurila, E., Houstis, N., Daly, M. J., Patterson, N., Mesirov, J. P., Golub, T. R., Tamayo, P., Spiegelman, B., Lander, E. S., Hirschhorn, J. N., . . . Groop, L. C. (2003). PGC-1alpha-responsive genes involved in oxidative phosphorylation are coordinately downregulated in human diabetes. *Nat Genet*, *34*(3), 267-273. https://doi.org/10.1038/ng1180

Morioka, S., Perry, J. S. A., Raymond, M. H., Medina, C. B., Zhu, Y., Zhao, L., Serbulea, V., Onengut-Gumuscu, S., Leitinger, N., Kucenas, S., Rathmell, J. C., Makowski, L., & Ravichandran, K. S. (2018). Efferocytosis induces a novel SLC program to promote glucose uptake and lactate release. *Nature*, *563*(7733), 714-718. https://doi.org/10.1038/s41586-018-0735-5

Moschoi, R., Imbert, V., Nebout, M., Chiche, J., Mary, D., Prebet, T., Saland, E., Castellano, R., Pouyet, L., Collette, Y., Vey, N., Chabannon, C., Recher, C., Sarry, J. E., Alcor, D., Peyron, J. F., & Griessinger, E. (2016). Protective mitochondrial transfer from bone marrow stromal cells to acute myeloid leukemic cells during chemotherapy. *Blood*, *128*(2), 253-264. https://doi.org/10.1182/blood-2015-07-655860

Motzer, R. J., Banchereau, R., Hamidi, H., Powles, T., McDermott, D., Atkins, M. B., Escudier, B., Liu, L. F., Leng, N., Abbas, A. R., Fan, J., Koeppen, H., Lin, J., Carroll, S., Hashimoto, K., Mariathasan, S., Green, M., Tayama, D., Hegde, P. S., . . . Rini, B. (2020). Molecular Subsets in Renal Cancer Determine Outcome to Checkpoint and Angiogenesis Blockade. *Cancer Cell*, *38*(6), 803-817 e804. https://doi.org/10.1016/j.ccell.2020.10.011

Motzer, R. J., Tannir, N. M., McDermott, D. F., Aren Frontera, O., Melichar, B., Choueiri, T. K., Plimack, E. R., Barthelemy, P., Porta, C., George, S., Powles, T., Donskov, F., Neiman, V., Kollmannsberger, C. K., Salman, P., Gurney, H., Hawkins, R., Ravaud, A., Grimm, M. O., . . . CheckMate, I. (2018). Nivolumab plus Ipilimumab versus Sunitinib in Advanced Renal-Cell Carcinoma. *N Engl J Med*, *378*(14), 1277-1290. https://doi.org/10.1056/NEJMoa1712126

Muller-Durovic, B., Lanna, A., Covre, L. P., Mills, R. S., Henson, S. M., & Akbar, A. N. (2016). Killer Cell Lectin-like Receptor G1 Inhibits NK Cell Function through Activation of Adenosine 5'-Monophosphate-Activated Protein Kinase. *J Immunol*, *197*(7), 2891-2899. https://doi.org/10.4049/jimmunol.1600590

Myers, M. P., Pass, I., Batty, I. H., Van der Kaay, J., Stolarov, J. P., Hemmings, B. A., Wigler, M. H., Downes, C. P., & Tonks, N. K. (1998). The lipid phosphatase activity of PTEN is critical for its tumor supressor function. *Proc Natl Acad Sci U S A*, *95*(23), 13513-13518. https://doi.org/10.1073/pnas.95.23.13513

Nagareddy, P. R., Murphy, A. J., Stirzaker, R. A., Hu, Y., Yu, S., Miller, R. G., Ramkhelawon, B., Distel, E., Westerterp, M., Huang, L. S., Schmidt, A. M., Orchard, T. J., Fisher, E. A., Tall, A. R., & Goldberg, I. J. (2013). Hyperglycemia promotes myelopoiesis and impairs the resolution of atherosclerosis. *Cell Metab*, *17*(5), 695-708. https://doi.org/10.1016/j.cmet.2013.04.001

Naik, S. H., Proietto, A. I., Wilson, N. S., Dakic, A., Schnorrer, P., Fuchsberger, M., Lahoud, M. H., O'Keeffe, M., Shao, Q. X., Chen, W. F., Villadangos, J. A., Shortman, K., & Wu, L. (2005). Cutting edge: generation of splenic CD8+ and CD8- dendritic cell equivalents in Fms-like tyrosine kinase 3 ligand bone marrow cultures. *J Immunol*, *174*(11), 6592-6597. https://doi.org/10.4049/jimmunol.174.11.6592

Nair-Gill, E., Wiltzius, S. M., Wei, X. X., Cheng, D., Riedinger, M., Radu, C. G., & Witte, O. N. (2010). PET probes for distinct metabolic pathways have different cell specificities during immune responses in mice. *J Clin Invest*, *120*(6), 2005-2015. https://doi.org/10.1172/JCI41250

Napoli, M., & Flores, E. R. (2017). The p53 family orchestrates the regulation of metabolism: physiological regulation and implications for cancer therapy. *Br J Cancer*, *116*(2), 149-155. https://doi.org/10.1038/bjc.2016.384

Newman, A. M., Steen, C. B., Liu, C. L., Gentles, A. J., Chaudhuri, A. A., Scherer, F., Khodadoust, M. S., Esfahani, M. S., Luca, B. A., Steiner, D., Diehn, M., & Alizadeh, A. A. (2019). Determining cell type abundance and expression from bulk tissues with digital cytometry. *Nat Biotechnol*, *37*(7), 773-782. https://doi.org/10.1038/s41587-019-0114-2

Niemeijer, A. N., Leung, D., Huisman, M. C., Bahce, I., Hoekstra, O. S., van Dongen, G., Boellaard, R., Du, S., Hayes, W., Smith, R., Windhorst, A. D., Hendrikse, N. H., Poot, A., Vugts, D. J., Thunnissen, E., Morin, P.,

Lipovsek, D., Donnelly, D. J., Bonacorsi, S. J., . . . de Langen, A. J. (2018). Whole body PD-1 and PD-L1 positron emission tomography in patients with non-small-cell lung cancer. *Nat Commun*, *9*(1), 4664. https://doi.org/10.1038/s41467-018-07131-y

Noman, M. Z., Desantis, G., Janji, B., Hasmim, M., Karray, S., Dessen, P., Bronte, V., & Chouaib, S. (2014). PD-L1 is a novel direct target of HIF-1alpha, and its blockade under hypoxia enhanced MDSC-mediated T cell activation. *J Exp Med*, *211*(5), 781-790. https://doi.org/10.1084/jem.20131916

Nunes-Xavier, C. E., Karlsen, K. F., Tekle, C., Pedersen, C., Oyjord, T., Hongisto, V., Nesland, J. M., Tan, M., Sahlberg, K. K., & Fodstad, O. (2016). Decreased expression of B7-H3 reduces the glycolytic capacity and sensitizes breast cancer cells to AKT/mTOR inhibitors. *Oncotarget*, *7*(6), 6891-6901. https://doi.org/10.18632/oncotarget.6902

O'Neil, R. T., Saha, S., Veach, R. A., Welch, R. C., Woodard, L. E., Rooney, C. M., & Wilson, M. H. (2018). Transposon-modified antigen-specific T lymphocytes for sustained therapeutic protein delivery in vivo. *Nat Commun*, *9*(1), 1325. https://doi.org/10.1038/s41467-018-03787-8

O'Neill, L. A., Kishton, R. J., & Rathmell, J. (2016). A guide to immunometabolism for immunologists. *Nat Rev Immunol*, *16*(9), 553-565. https://doi.org/10.1038/nri.2016.70

Obradovic, A., Chowdhury, N., Haake, S. M., Ager, C., Wang, V., Vlahos, L., Guo, X. V., Aggen, D. H., Rathmell, W. K., Jonasch, E., Johnson, J. E., Roth, M., Beckermann, K. E., Rini, B. I., McKiernan, J., Califano, A., & Drake, C. G. (2021). Single-cell protein activity analysis identifies recurrence-associated renal tumor macrophages. *Cell*, *184*(11), 2988-3005 e2916. https://doi.org/10.1016/j.cell.2021.04.038

Oh, M. H., Sun, I. H., Zhao, L., Leone, R. D., Sun, I. M., Xu, W., Collins, S. L., Tam, A. J., Blosser, R. L., Patel, C. H., Englert, J. M., Arwood, M. L., Wen, J., Chan-Li, Y., Tenora, L., Majer, P., Rais, R., Slusher, B. S., Horton, M. R., & Powell, J. D. (2020). Targeting glutamine metabolism enhances tumor-specific immunity by modulating suppressive myeloid cells. *J Clin Invest*, *130*(7), 3865-3884. https://doi.org/10.1172/JCI131859

Ohta, A., Gorelik, E., Prasad, S. J., Ronchese, F., Lukashev, D., Wong, M. K., Huang, X., Caldwell, S., Liu, K., Smith, P., Chen, J. F., Jackson, E. K., Apasov, S., Abrams, S., & Sitkovsky, M. (2006). A2A adenosine receptor protects tumors from antitumor T cells. *Proc Natl Acad Sci U S A*, *103*(35), 13132-13137. https://doi.org/10.1073/pnas.0605251103

Ohta, A., Ohta, A., Madasu, M., Kini, R., Subramanian, M., Goel, N., & Sitkovsky, M. (2009). A2A adenosine receptor may allow expansion of T cells lacking effector functions in extracellular adenosine-rich microenvironments. *J Immunol*, *183*(9), 5487-5493. https://doi.org/10.4049/jimmunol.0901247

Oki, S., Ohta, T., Shioi, G., Hatanaka, H., Ogasawara, O., Okuda, Y., Kawaji, H., Nakaki, R., Sese, J., & Meno, C. (2018). ChIP-Atlas: a data-mining suite powered by full integration of public ChIP-seq data. *EMBO Rep*, *19*(12). https://doi.org/10.15252/embr.201846255

Orozco, J. M., Krawczyk, P. A., Scaria, S. M., Cangelosi, A. L., Chan, S. H., Kunchok, T., Lewis, C. A., & Sabatini, D. M. (2020). Dihydroxyacetone phosphate signals glucose availability to mTORC1. *Nat Metab*, *2*(9), 893-901. https://doi.org/10.1038/s42255-020-0250-5

Ortega, R. A., Barham, W., Sharman, K., Tikhomirov, O., Giorgio, T. D., & Yull, F. E. (2016). Manipulating the NF-kappaB pathway in macrophages using mannosylated, siRNA-delivering nanoparticles can induce immunostimulatory and tumor cytotoxic functions. *Int J Nanomedicine*, *11*, 2163-2177. https://doi.org/10.2147/IJN.S93483

Osorio, F., Tavernier, S. J., Hoffmann, E., Saeys, Y., Martens, L., Vetters, J., Delrue, I., De Rycke, R., Parthoens, E., Pouliot, P., Iwawaki, T., Janssens, S., & Lambrecht, B. N. (2014). The unfolded-protein-response sensor IRE-1alpha regulates the function of CD8alpha+ dendritic cells. *Nat Immunol*, *15*(3), 248-257. https://doi.org/10.1038/ni.2808

Osthus, R. C., Shim, H., Kim, S., Li, Q., Reddy, R., Mukherjee, M., Xu, Y., Wonsey, D., Lee, L. A., & Dang, C. V. (2000). Deregulation of glucose transporter 1 and glycolytic gene expression by c-Myc. *J Biol Chem*, *275*(29), 21797-21800. https://doi.org/10.1074/jbc.C000023200

Pacella, I., Procaccini, C., Focaccetti, C., Miacci, S., Timperi, E., Faicchia, D., Severa, M., Rizzo, F., Coccia, E. M., Bonacina, F., Mitro, N., Norata, G. D., Rossetti, G., Ranzani, V., Pagani, M., Giorda, E., Wei, Y., Matarese, G., Barnaba, V., & Piconese, S. (2018). Fatty acid metabolism complements glycolysis in the selective regulatory T cell expansion during tumor growth. *Proc Natl Acad Sci U S A*, *115*(28), E6546-E6555. https://doi.org/10.1073/pnas.1720113115

Palazon, A., Tyrakis, P. A., Macias, D., Velica, P., Rundqvist, H., Fitzpatrick, S., Vojnovic, N., Phan, A. T., Loman, N., Hedenfalk, I., Hatschek, T., Lovrot, J., Foukakis, T., Goldrath, A. W., Bergh, J., & Johnson, R. S. (2017). An HIF-1alpha/VEGF-A Axis in Cytotoxic T Cells Regulates Tumor Progression. *Cancer Cell*, *32*(5), 669-683 e665. https://doi.org/10.1016/j.ccell.2017.10.003

Palmer, C. S., Duette, G. A., Wagner, M. C. E., Henstridge, D. C., Saleh, S., Pereira, C., Zhou, J., Simar, D., Lewin, S. R., Ostrowski, M., McCune, J. M., & Crowe, S. M. (2017). Metabolically active CD4+ T cells expressing Glut1 and OX40 preferentially harbor HIV during in vitro infection. *FEBS Lett*, *591*(20), 3319-3332. https://doi.org/10.1002/1873-3468.12843

Palmer, L. D., Maloney, K. N., Boyd, K. L., Goleniewska, A. K., Toki, S., Maxwell, C. N., Chazin, W. J., Peebles, R. S., Jr., Newcomb, D. C., & Skaar, E. P. (2019). The Innate Immune Protein S100A9 Protects from T-Helper

Cell Type 2-mediated Allergic Airway Inflammation. *Am J Respir Cell Mol Biol*, *61*(4), 459-468. https://doi.org/10.1165/rcmb.2018-0217OC

Palmieri, E. M., Menga, A., Martin-Perez, R., Quinto, A., Riera-Domingo, C., De Tullio, G., Hooper, D. C., Lamers, W. H., Ghesquiere, B., McVicar, D. W., Guarini, A., Mazzone, M., & Castegna, A. (2017). Pharmacologic or Genetic Targeting of Glutamine Synthetase Skews Macrophages toward an M1-like Phenotype and Inhibits Tumor Metastasis. *Cell Rep*, *20*(7), 1654-1666. https://doi.org/10.1016/j.celrep.2017.07.054

Palmieri, E. M., Spera, I., Menga, A., Infantino, V., Porcelli, V., Iacobazzi, V., Pierri, C. L., Hooper, D. C., Palmieri, F., & Castegna, A. (2015). Acetylation of human mitochondrial citrate carrier modulates mitochondrial citrate/malate exchange activity to sustain NADPH production during macrophage activation. *Biochim Biophys Acta*, *1847*(8), 729-738. https://doi.org/10.1016/j.bbabio.2015.04.009

Palsson-McDermott, E. M., Curtis, A. M., Goel, G., Lauterbach, M. A., Sheedy, F. J., Gleeson, L. E., van den Bosch, M. W., Quinn, S. R., Domingo-Fernandez, R., Johnston, D. G., Jiang, J. K., Israelsen, W. J., Keane, J., Thomas, C., Clish, C., Vander Heiden, M., Xavier, R. J., & O'Neill, L. A. (2015). Pyruvate kinase M2 regulates Hif-1alpha activity and IL-1beta induction and is a critical determinant of the warburg effect in LPS-activated macrophages. *Cell Metab*, *21*(1), 65-80. https://doi.org/10.1016/j.cmet.2014.12.005

Pan, M., Reid, M. A., Lowman, X. H., Kulkarni, R. P., Tran, T. Q., Liu, X., Yang, Y., Hernandez-Davies, J. E., Rosales, K. K., Li, H., Hugo, W., Song, C., Xu, X., Schones, D. E., Ann, D. K., Gradinaru, V., Lo, R. S., Locasale, J. W., & Kong, M. (2016). Regional glutamine deficiency in tumours promotes dedifferentiation through inhibition of histone demethylation. *Nat Cell Biol*, *18*(10), 1090-1101. https://doi.org/10.1038/ncb3410

Pantel, A., Teixeira, A., Haddad, E., Wood, E. G., Steinman, R. M., & Longhi, M. P. (2014). Direct type I IFN but not MDA5/TLR3 activation of dendritic cells is required for maturation and metabolic shift to glycolysis after poly IC stimulation. *PLoS Biol*, *12*(1), e1001759. https://doi.org/10.1371/journal.pbio.1001759

Parang, B., Barrett, C. W., & Williams, C. S. (2016). AOM/DSS Model of Colitis-Associated Cancer. *Methods Mol Biol*, *1422*, 297-307. https://doi.org/10.1007/978-1-4939-3603-8_26

Parmar, K., Mauch, P., Vergilio, J. A., Sackstein, R., & Down, J. D. (2007). Distribution of hematopoietic stem cells in the bone marrow according to regional hypoxia. *Proc Natl Acad Sci U S A*, *104*(13), 5431-5436. https://doi.org/10.1073/pnas.0701152104

Parry, R. V., Chemnitz, J. M., Frauwirth, K. A., Lanfranco, A. R., Braunstein, I., Kobayashi, S. V., Linsley, P. S., Thompson, C. B., & Riley, J. L. (2005). CTLA-4 and PD-1 receptors inhibit T-cell activation by distinct mechanisms. *Mol Cell Biol*, *25*(21), 9543-9553. https://doi.org/10.1128/MCB.25.21.9543-9553.2005

Parsons, D. W., Wang, T. L., Samuels, Y., Bardelli, A., Cummins, J. M., DeLong, L., Silliman, N., Ptak, J., Szabo, S., Willson, J. K., Markowitz, S., Kinzler, K. W., Vogelstein, B., Lengauer, C., & Velculescu, V. E. (2005). Colorectal cancer: mutations in a signalling pathway. *Nature*, *436*(7052), 792. https://doi.org/10.1038/436792a

Patsoukis, N., Bardhan, K., Chatterjee, P., Sari, D., Liu, B., Bell, L. N., Karoly, E. D., Freeman, G. J., Petkova, V., Seth, P., Li, L., & Boussiotis, V. A. (2015). PD-1 alters T-cell metabolic reprogramming by inhibiting glycolysis and promoting lipolysis and fatty acid oxidation. *Nat Commun*, *6*, 6692. https://doi.org/10.1038/ncomms7692

Pavlova, N. N., & Thompson, C. B. (2016). The Emerging Hallmarks of Cancer Metabolism. *Cell Metab*, *23*(1), 27-47. https://doi.org/10.1016/j.cmet.2015.12.006

Peperzak, V., Veraar, E. A., Keller, A. M., Xiao, Y., & Borst, J. (2010). The Pim kinase pathway contributes to survival signaling in primed CD8+ T cells upon CD27 costimulation. *J Immunol*, *185*(11), 6670-6678. https://doi.org/10.4049/jimmunol.1000159

Pilon-Thomas, S., Kodumudi, K. N., El-Kenawi, A. E., Russell, S., Weber, A. M., Luddy, K., Damaghi, M., Wojtkowiak, J. W., Mule, J. J., Ibrahim-Hashim, A., & Gillies, R. J. (2016). Neutralization of Tumor Acidity Improves Antitumor Responses to Immunotherapy. *Cancer Res*, *76*(6), 1381-1390. https://doi.org/10.1158/0008-5472.CAN-15-1743

Polack, F. P., Thomas, S. J., Kitchin, N., Absalon, J., Gurtman, A., Lockhart, S., Perez, J. L., Perez Marc, G., Moreira, E. D., Zerbini, C., Bailey, R., Swanson, K. A., Roychoudhury, S., Koury, K., Li, P., Kalina, W. V., Cooper, D., Frenck, R. W., Jr., Hammitt, L. L., . . . Group, C. C. T. (2020). Safety and Efficacy of the BNT162b2 mRNA Covid-19 Vaccine. *N Engl J Med*, *383*(27), 2603-2615. https://doi.org/10.1056/NEJMoa2034577

Pollard, P. J., Briere, J. J., Alam, N. A., Barwell, J., Barclay, E., Wortham, N. C., Hunt, T., Mitchell, M., Olpin, S., Moat, S. J., Hargreaves, I. P., Heales, S. J., Chung, Y. L., Griffiths, J. R., Dalgleish, A., McGrath, J. A., Gleeson, M. J., Hodgson, S. V., Poulsom, R., . . . Tomlinson, I. P. (2005). Accumulation of Krebs cycle intermediates and over-expression of HIF1alpha in tumours which result from germline FH and SDH mutations. *Hum Mol Genet*, *14*(15), 2231-2239. https://doi.org/10.1093/hmg/ddi227

Potzl, J., Roser, D., Bankel, L., Homberg, N., Geishauser, A., Brenner, C. D., Weigand, M., Rocken, M., & Mocikat, R. (2017). Reversal of tumor acidosis by systemic buffering reactivates NK cells to express IFN-gamma and induces NK cell-dependent lymphoma control without other immunotherapies. *Int J Cancer*, *140*(9), 2125-2133. https://doi.org/10.1002/ijc.30646

Poulin, L. F., Salio, M., Griessinger, E., Anjos-Afonso, F., Craciun, L., Chen, J. L., Keller, A. M., Joffre, O., Zelenay, S., Nye, E., Le Moine, A., Faure, F., Donckier, V., Sancho, D., Cerundolo, V., Bonnet, D., & Reis e Sousa, C. (2010). Characterization of human DNGR-1+ BDCA3+ leukocytes as putative equivalents of mouse CD8alpha+ dendritic cells. *J Exp Med*, *207*(6), 1261-1271. https://doi.org/10.1084/jem.20092618

Previte, D. M., Martins, C. P., O'Connor, E. C., Marre, M. L., Coudriet, G. M., Beck, N. W., Menk, A. V., Wright, R. H., Tse, H. M., Delgoffe, G. M., & Piganelli, J. D. (2019). Lymphocyte Activation Gene-3 Maintains Mitochondrial and Metabolic Quiescence in Naive CD4(+) T Cells. *Cell Rep*, *27*(1), 129-141 e124. https://doi.org/10.1016/j.celrep.2019.03.004

Puchalska, P., Huang, X., Martin, S. E., Han, X., Patti, G. J., & Crawford, P. A. (2018). Isotope Tracing Untargeted Metabolomics Reveals Macrophage Polarization-State-Specific Metabolic Coordination across Intracellular Compartments. *iScience*, *9*, 298-313. https://doi.org/10.1016/j.isci.2018.10.029

Qian, X., Li, X., Tan, L., Lee, J. H., Xia, Y., Cai, Q., Zheng, Y., Wang, H., Lorenzi, P. L., & Lu, Z. (2018). Conversion of PRPS Hexamer to Monomer by AMPK-Mediated Phosphorylation Inhibits Nucleotide Synthesis in Response to Energy Stress. *Cancer Discov*, *8*(1), 94-107. https://doi.org/10.1158/2159-8290.CD-17-0712

Qin, H., Yu, H., Sheng, J., Zhang, D., Shen, N., Liu, L., Tang, Z., & Chen, X. (2019). PI3Kgamma Inhibitor Attenuates Immunosuppressive Effect of Poly(l-Glutamic Acid)-Combretastatin A4 Conjugate in Metastatic Breast Cancer. *Adv Sci (Weinh)*, *6*(12), 1900327. https://doi.org/10.1002/advs.201900327

Rademakers, S. E., Lok, J., van der Kogel, A. J., Bussink, J., & Kaanders, J. H. (2011). Metabolic markers in relation to hypoxia; staining patterns and colocalization of pimonidazole, HIF-1alpha, CAIX, LDH-5, GLUT-1, MCT1 and MCT4. *BMC Cancer*, *11*, 167. https://doi.org/10.1186/1471-2407-11-167

Rahl, P. B., Lin, C. Y., Seila, A. C., Flynn, R. A., McCuine, S., Burge, C. B., Sharp, P. A., & Young, R. A. (2010). c-Myc regulates transcriptional pause release. *Cell*, *141*(3), 432-445. https://doi.org/10.1016/j.cell.2010.03.030

Rahman, M., Jackson, L. K., Johnson, W. E., Li, D. Y., Bild, A. H., & Piccolo, S. R. (2015). Alternative preprocessing of RNA-Sequencing data in The Cancer Genome Atlas leads to improved analysis results. *Bioinformatics*, *31*(22), 3666-3672. https://doi.org/10.1093/bioinformatics/btv377

Ramakrishnan, R., Tyurin, V. A., Veglia, F., Condamine, T., Amoscato, A., Mohammadyani, D., Johnson, J. J., Zhang, L. M., Klein-Seetharaman, J., Celis, E., Kagan, V. E., & Gabrilovich, D. I. (2014). Oxidized lipids block antigen cross-presentation by dendritic cells in cancer. *J Immunol*, *192*(6), 2920-2931. https://doi.org/10.4049/jimmunol.1302801

Rathmell, J. C., Fox, C. J., Plas, D. R., Hammerman, P. S., Cinalli, R. M., & Thompson, C. B. (2003). Akt-directed glucose metabolism can prevent Bax conformation change and promote growth factor-independent survival. *Mol Cell Biol*, *23*(20), 7315-7328. https://doi.org/10.1128/MCB.23.20.7315-7328.2003

Raudvere, U., Kolberg, L., Kuzmin, I., Arak, T., Adler, P., Peterson, H., & Vilo, J. (2019). g:Profiler: a web server for functional enrichment analysis and conversions of gene lists (2019 update). *Nucleic Acids Res*, *47*(W1), W191-W198. https://doi.org/10.1093/nar/gkz369

Reinfeld, B. I., Madden, M. Z., Wolf, M. M., Chytil, A., Bader, J. E., Patterson, A. R., Sugiura, A., Cohen, A. S., Ali, A., Do, B. T., Muir, A., Lewis, C. A., Hongo, R. A., Young, K. L., Brown, R. E., Todd, V. M., Huffstater, T., Abraham, A., O'Neil, R. T., . . . Rathmell, W. K. (2021). Cell-programmed nutrient partitioning in the tumour microenvironment. *Nature*, *593*(7858), 282-288. https://doi.org/10.1038/s41586-021-03442-1

Reinfeld, B. I., Rathmell, W. K., Kim, T. K., & Rathmell, J. C. (2022). The therapeutic implications of immunosuppressive tumor aerobic glycolysis. *Cell Mol Immunol*, *19*(1), 46-58. https://doi.org/10.1038/s41423-021-00727-3

Renner, K., Bruss, C., Schnell, A., Koehl, G., Becker, H. M., Fante, M., Menevse, A. N., Kauer, N., Blazquez, R., Hacker, L., Decking, S. M., Bohn, T., Faerber, S., Evert, K., Aigle, L., Amslinger, S., Landa, M., Krijgsman, O., Rozeman, E. A., . . . Kreutz, M. (2019). Restricting Glycolysis Preserves T Cell Effector Functions and Augments Checkpoint Therapy. *Cell Rep*, *29*(1), 135-150 e139. https://doi.org/10.1016/j.celrep.2019.08.068

Ribechini, E., Hutchinson, J. A., Hergovits, S., Heuer, M., Lucas, J., Schleicher, U., Jordan Garrote, A. L., Potter, S. J., Riquelme, P., Brackmann, H., Muller, N., Raifer, H., Berberich, I., Huber, M., Beilhack, A., Lohoff, M., Bogdan, C., Eyrich, M., Hermanns, H. M., . . . Lutz, M. B. (2017). Novel GM-CSF signals via IFN-gammaR/IRF-1 and AKT/mTOR license monocytes for suppressor function. *Blood Adv*, *1*(14), 947-960. https://doi.org/10.1182/bloodadvances.2017006858

Rijksen, G., Staal, G. E., Beks, P. J., Streefkerk, M., & Akkerman, J. W. (1982). Compartmentation of hexokinase in human blood cells. Characterization of soluble and particulate enzymes. *Biochim Biophys Acta*, *719*(3), 431-437. https://doi.org/10.1016/0304-4165(82)90230-6

Ringel, A. E., Drijvers, J. M., Baker, G. J., Catozzi, A., Garcia-Canaveras, J. C., Gassaway, B. M., Miller, B. C., Juneja, V. R., Nguyen, T. H., Joshi, S., Yao, C. H., Yoon, H., Sage, P. T., LaFleur, M. W., Trombley, J. D., Jacobson, C. A., Maliga, Z., Gygi, S. P., Sorger, P. K., . . . Haigis, M. C. (2020). Obesity Shapes Metabolism in the Tumor Microenvironment to Suppress Anti-Tumor Immunity. *Cell*, *183*(7), 1848-1866 e1826. https://doi.org/10.1016/j.cell.2020.11.009

Rini, B. I., Plimack, E. R., Stus, V., Gafanov, R., Hawkins, R., Nosov, D., Pouliot, F., Alekseev, B., Soulieres, D., Melichar, B., Vynnychenko, I., Kryzhanivska, A., Bondarenko, I., Azevedo, S. J., Borchiellini, D., Szczylik, C., Markus, M., McDermott, R. S., Bedke, J., . . . Investigators, K.-. (2019). Pembrolizumab plus Axitinib versus

Sunitinib for Advanced Renal-Cell Carcinoma. *N Engl J Med*, *380*(12), 1116-1127. https://doi.org/10.1056/NEJMoa1816714
Ritchie, M. E., Phipson, B., Wu, D., Hu, Y., Law, C. W., Shi, W., & Smyth, G. K. (2015). limma powers differential expression analyses for RNA-sequencing and microarray studies. *Nucleic Acids Res*, *43*(7), e47. https://doi.org/10.1093/nar/gkv007
Rius, J., Guma, M., Schachtrup, C., Akassoglou, K., Zinkernagel, A. S., Nizet, V., Johnson, R. S., Haddad, G. G., & Karin, M. (2008). NF-kappaB links innate immunity to the hypoxic response through transcriptional regulation of HIF-1alpha. *Nature*, *453*(7196), 807-811. https://doi.org/10.1038/nature06905
Robinson, M. D., McCarthy, D. J., & Smyth, G. K. (2010). edgeR: a Bioconductor package for differential expression analysis of digital gene expression data. *Bioinformatics*, *26*(1), 139-140. https://doi.org/10.1093/bioinformatics/btp616
Rodriguez-Prados, J. C., Traves, P. G., Cuenca, J., Rico, D., Aragones, J., Martin-Sanz, P., Cascante, M., & Bosca, L. (2010). Substrate fate in activated macrophages: a comparison between innate, classic, and alternative activation. *J Immunol*, *185*(1), 605-614. https://doi.org/10.4049/jimmunol.0901698
Rodriguez-Viciana, P., Warne, P. H., Vanhaesebroeck, B., Waterfield, M. D., & Downward, J. (1996). Activation of phosphoinositide 3-kinase by interaction with Ras and by point mutation. *EMBO J*, *15*(10), 2442-2451. https://www.ncbi.nlm.nih.gov/pubmed/8665852
Roman, M., Baraibar, I., Lopez, I., Nadal, E., Rolfo, C., Vicent, S., & Gil-Bazo, I. (2018). KRAS oncogene in non-small cell lung cancer: clinical perspectives on the treatment of an old target. *Mol Cancer*, *17*(1), 33. https://doi.org/10.1186/s12943-018-0789-x
Rossiter, N. J., Huggler, K. S., Adelmann, C. H., Keys, H. R., Soens, R. W., Sabatini, D. M., & Cantor, J. R. (2021). CRISPR screens in physiologic medium reveal conditionally essential genes in human cells. *Cell Metab*, *33*(6), 1248-1263 e1249. https://doi.org/10.1016/j.cmet.2021.02.005
Rowinsky, E. K., Windle, J. J., & Von Hoff, D. D. (1999). Ras protein farnesyltransferase: A strategic target for anticancer therapeutic development. *J Clin Oncol*, *17*(11), 3631-3652. https://doi.org/10.1200/JCO.1999.17.11.3631
Sabharwal, S. S., Rosen, D. B., Grein, J., Tedesco, D., Joyce-Shaikh, B., Ueda, R., Semana, M., Bauer, M., Bang, K., Stevenson, C., Cua, D. J., & Zuniga, L. A. (2018). GITR Agonism Enhances Cellular Metabolism to Support CD8(+) T-cell Proliferation and Effector Cytokine Production in a Mouse Tumor Model. *Cancer Immunol Res*, *6*(10), 1199-1211. https://doi.org/10.1158/2326-6066.CIR-17-0632
Saha, A., Taylor, P. A., Lees, C. J., Panoskaltsis-Mortari, A., Osborn, M. J., Feser, C. J., Thangavelu, G., Melchinger, W., Refaeli, Y., Hill, G. R., Munn, D. H., Murphy, W. J., Serody, J. S., Maillard, I., Kreymborg, K., van den Brink, M., Dong, C., Huang, S., Zang, X., . . . Blazar, B. R. (2019). Donor and host B7-H4 expression negatively regulates acute graft-versus-host disease lethality. *JCI Insight*, *4*(19). https://doi.org/10.1172/jci.insight.127716
Samudio, I., Rezvani, K., Shaim, H., Hofs, E., Ngom, M., Bu, L., Liu, G., Lee, J. T., Imren, S., Lam, V., Poon, G. F., Ghaedi, M., Takei, F., Humphries, K., Jia, W., & Krystal, G. (2016). UV-inactivated HSV-1 potently activates NK cell killing of leukemic cells. *Blood*, *127*(21), 2575-2586. https://doi.org/10.1182/blood-2015-04-639088
Sarbassov, D. D., Guertin, D. A., Ali, S. M., & Sabatini, D. M. (2005). Phosphorylation and regulation of Akt/PKB by the rictor-mTOR complex. *Science*, *307*(5712), 1098-1101. https://doi.org/10.1126/science.1106148
Sasaki, T., Irie-Sasaki, J., Jones, R. G., Oliveira-dos-Santos, A. J., Stanford, W. L., Bolon, B., Wakeham, A., Itie, A., Bouchard, D., Kozieradzki, I., Joza, N., Mak, T. W., Ohashi, P. S., Suzuki, A., & Penninger, J. M. (2000). Function of PI3Kgamma in thymocyte development, T cell activation, and neutrophil migration. *Science*, *287*(5455), 1040-1046. https://doi.org/10.1126/science.287.5455.1040
Sathaliyawala, T., O'Gorman, W. E., Greter, M., Bogunovic, M., Konjufca, V., Hou, Z. E., Nolan, G. P., Miller, M. J., Merad, M., & Reizis, B. (2010). Mammalian target of rapamycin controls dendritic cell development downstream of Flt3 ligand signaling. *Immunity*, *33*(4), 597-606. https://doi.org/10.1016/j.immuni.2010.09.012
Saudemont, A., Garcon, F., Yadi, H., Roche-Molina, M., Kim, N., Segonds-Pichon, A., Martin-Fontecha, A., Okkenhaug, K., & Colucci, F. (2009). p110gamma and p110delta isoforms of phosphoinositide 3-kinase differentially regulate natural killer cell migration in health and disease. *Proc Natl Acad Sci U S A*, *106*(14), 5795-5800. https://doi.org/10.1073/pnas.0808594106
Saxton, R. A., & Sabatini, D. M. (2017). mTOR Signaling in Growth, Metabolism, and Disease. *Cell*, *168*(6), 960-976. https://doi.org/10.1016/j.cell.2017.02.004
Schafer, J. R., Salzillo, T. C., Chakravarti, N., Kararoudi, M. N., Trikha, P., Foltz, J. A., Wang, R., Li, S., & Lee, D. A. (2019). Education-dependent activation of glycolysis promotes the cytolytic potency of licensed human natural killer cells. *J Allergy Clin Immunol*, *143*(1), 346-358 e346. https://doi.org/10.1016/j.jaci.2018.06.047
Scharping, N. E., Rivadeneira, D. B., Menk, A. V., Vignali, P. D. A., Ford, B. R., Rittenhouse, N. L., Peralta, R., Wang, Y., Wang, Y., DePeaux, K., Poholek, A. C., & Delgoffe, G. M. (2021). Mitochondrial stress induced by continuous stimulation under hypoxia rapidly drives T cell exhaustion. *Nat Immunol*, *22*(2), 205-215. https://doi.org/10.1038/s41590-020-00834-9

Scheffler, J. M., Sparber, F., Tripp, C. H., Herrmann, C., Humenberger, A., Blitz, J., Romani, N., Stoitzner, P., & Huber, L. A. (2014). LAMTOR2 regulates dendritic cell homeostasis through FLT3-dependent mTOR signalling. *Nat Commun*, *5*, 5138. https://doi.org/10.1038/ncomms6138
Schmid, M. C., Avraamides, C. J., Dippold, H. C., Franco, I., Foubert, P., Ellies, L. G., Acevedo, L. M., Manglicmot, J. R., Song, X., Wrasidlo, W., Blair, S. L., Ginsberg, M. H., Cheresh, D. A., Hirsch, E., Field, S. J., & Varner, J. A. (2011). Receptor tyrosine kinases and TLR/IL1Rs unexpectedly activate myeloid cell PI3kgamma, a single convergent point promoting tumor inflammation and progression. *Cancer Cell*, *19*(6), 715-727. https://doi.org/10.1016/j.ccr.2011.04.016
Schulte, M. L., Fu, A., Zhao, P., Li, J., Geng, L., Smith, S. T., Kondo, J., Coffey, R. J., Johnson, M. O., Rathmell, J. C., Sharick, J. T., Skala, M. C., Smith, J. A., Berlin, J., Washington, M. K., Nickels, M. L., & Manning, H. C. (2018). Pharmacological blockade of ASCT2-dependent glutamine transport leads to antitumor efficacy in preclinical models. *Nat Med*, *24*(2), 194-202. https://doi.org/10.1038/nm.4464
Schulte, M. L., Hight, M. R., Ayers, G. D., Liu, Q., Shyr, Y., Washington, M. K., & Manning, H. C. (2017). Non-Invasive Glutamine PET Reflects Pharmacological Inhibition of BRAF(V600E) In Vivo. *Mol Imaging Biol*, *19*(3), 421-428. https://doi.org/10.1007/s11307-016-1008-z
Schwartzenberg-Bar-Yoseph, F., Armoni, M., & Karnieli, E. (2004). The tumor suppressor p53 down-regulates glucose transporters GLUT1 and GLUT4 gene expression. *Cancer Res*, *64*(7), 2627-2633. https://doi.org/10.1158/0008-5472.can-03-0846
Selak, M. A., Armour, S. M., MacKenzie, E. D., Boulahbel, H., Watson, D. G., Mansfield, K. D., Pan, Y., Simon, M. C., Thompson, C. B., & Gottlieb, E. (2005). Succinate links TCA cycle dysfunction to oncogenesis by inhibiting HIF-alpha prolyl hydroxylase. *Cancer Cell*, *7*(1), 77-85. https://doi.org/10.1016/j.ccr.2004.11.022
Semenza, G. L., & Wang, G. L. (1992). A nuclear factor induced by hypoxia via de novo protein synthesis binds to the human erythropoietin gene enhancer at a site required for transcriptional activation. *Mol Cell Biol*, *12*(12), 5447-5454. https://doi.org/10.1128/mcb.12.12.5447-5454.1992
Sevigny, C. P., Li, L., Awad, A. S., Huang, L., McDuffie, M., Linden, J., Lobo, P. I., & Okusa, M. D. (2007). Activation of adenosine 2A receptors attenuates allograft rejection and alloantigen recognition. *J Immunol*, *178*(7), 4240-4249. https://doi.org/10.4049/jimmunol.178.7.4240
Sharma, P., & Allison, J. P. (2015). The future of immune checkpoint therapy. *Science*, *348*(6230), 56-61. https://doi.org/10.1126/science.aaa8172
Sharpe, A. H., & Pauken, K. E. (2018). The diverse functions of the PD1 inhibitory pathway. *Nat Rev Immunol*, *18*(3), 153-167. https://doi.org/10.1038/nri.2017.108
Shen, C., Beroukhim, R., Schumacher, S. E., Zhou, J., Chang, M., Signoretti, S., & Kaelin, W. G., Jr. (2011). Genetic and functional studies implicate HIF1alpha as a 14q kidney cancer suppressor gene. *Cancer Discov*, *1*(3), 222-235. https://doi.org/10.1158/2159-8290.CD-11-0098
Shi, T., Ma, Y., Cao, L., Zhan, S., Xu, Y., Fu, F., Liu, C., Zhang, G., Wang, Z., Wang, R., Lu, H., Lu, B., Chen, W., & Zhang, X. (2019). B7-H3 promotes aerobic glycolysis and chemoresistance in colorectal cancer cells by regulating HK2. *Cell Death Dis*, *10*(4), 308. https://doi.org/10.1038/s41419-019-1549-6
Shimoda, L. A., Fallon, M., Pisarcik, S., Wang, J., & Semenza, G. L. (2006). HIF-1 regulates hypoxic induction of NHE1 expression and alkalinization of intracellular pH in pulmonary arterial myocytes. *Am J Physiol Lung Cell Mol Physiol*, *291*(5), L941-949. https://doi.org/10.1152/ajplung.00528.2005
Shrestha, S., Yang, K., Guy, C., Vogel, P., Neale, G., & Chi, H. (2015). Treg cells require the phosphatase PTEN to restrain TH1 and TFH cell responses. *Nat Immunol*, *16*(2), 178-187. https://doi.org/10.1038/ni.3076
Sica, G. L., Choi, I. H., Zhu, G., Tamada, K., Wang, S. D., Tamura, H., Chapoval, A. I., Flies, D. B., Bajorath, J., & Chen, L. (2003). B7-H4, a molecule of the B7 family, negatively regulates T cell immunity. *Immunity*, *18*(6), 849-861. https://doi.org/10.1016/s1074-7613(03)00152-3
Sinclair, C., Bommakanti, G., Gardinassi, L., Loebbermann, J., Johnson, M. J., Hakimpour, P., Hagan, T., Benitez, L., Todor, A., Machiah, D., Oriss, T., Ray, A., Bosinger, S., Ravindran, R., Li, S., & Pulendran, B. (2017). mTOR regulates metabolic adaptation of APCs in the lung and controls the outcome of allergic inflammation. *Science*, *357*(6355), 1014-1021. https://doi.org/10.1126/science.aaj2155
Sinclair, L. V., Barthelemy, C., & Cantrell, D. A. (2020). Single Cell Glucose Uptake Assays: A Cautionary Tale. *Immunometabolism*, *2*(4), e200029. https://doi.org/10.20900/immunometab20200029
Sinclair, L. V., Howden, A. J., Brenes, A., Spinelli, L., Hukelmann, J. L., Macintyre, A. N., Liu, X., Thomson, S., Taylor, P. M., Rathmell, J. C., Locasale, J. W., Lamond, A. I., & Cantrell, D. A. (2019). Antigen receptor control of methionine metabolism in T cells. *Elife*, *8*. https://doi.org/10.7554/eLife.44210
Siska, P. J., Beckermann, K. E., Mason, F. M., Andrejeva, G., Greenplate, A. R., Sendor, A. B., Chiang, Y. J., Corona, A. L., Gemta, L. F., Vincent, B. G., Wang, R. C., Kim, B., Hong, J., Chen, C. L., Bullock, T. N., Irish, J. M., Rathmell, W. K., & Rathmell, J. C. (2017). Mitochondrial dysregulation and glycolytic insufficiency functionally impair CD8 T cells infiltrating human renal cell carcinoma. *JCI Insight*, *2*(12). https://doi.org/10.1172/jci.insight.93411
Slattery, K., Woods, E., Zaiatz-Bittencourt, V., Marks, S., Chew, S., Conroy, M., Goggin, C., MacEochagain, C., Kennedy, J., Lucas, S., Finlay, D. K., & Gardiner, C. M. (2021). TGFbeta drives NK cell metabolic

dysfunction in human metastatic breast cancer. *J Immunother Cancer*, *9*(2). https://doi.org/10.1136/jitc-2020-002044

Slyper, M., Porter, C. B. M., Ashenberg, O., Waldman, J., Drokhlyansky, E., Wakiro, I., Smillie, C., Smith-Rosario, G., Wu, J., Dionne, D., Vigneau, S., Jane-Valbuena, J., Tickle, T. L., Napolitano, S., Su, M. J., Patel, A. G., Karlstrom, A., Gritsch, S., Nomura, M., . . . Regev, A. (2020). A single-cell and single-nucleus RNA-Seq toolbox for fresh and frozen human tumors. *Nat Med*, *26*(5), 792-802. https://doi.org/10.1038/s41591-020-0844-1

Song, M., Sandoval, T. A., Chae, C. S., Chopra, S., Tan, C., Rutkowski, M. R., Raundhal, M., Chaurio, R. A., Payne, K. K., Konrad, C., Bettigole, S. E., Shin, H. R., Crowley, M. J. P., Cerliani, J. P., Kossenkov, A. V., Motorykin, I., Zhang, S., Manfredi, G., Zamarin, D., . . . Cubillos-Ruiz, J. R. (2018). IRE1alpha-XBP1 controls T cell function in ovarian cancer by regulating mitochondrial activity. *Nature*, *562*(7727), 423-428. https://doi.org/10.1038/s41586-018-0597-x

Song, Q., Hawkins, G. A., Wudel, L., Chou, P. C., Forbes, E., Pullikuth, A. K., Liu, L., Jin, G., Craddock, L., Topaloglu, U., Kucera, G., O'Neill, S., Levine, E. A., Sun, P., Watabe, K., Lu, Y., Alexander-Miller, M. A., Pasche, B., Miller, L. D., & Zhang, W. (2019). Dissecting intratumoral myeloid cell plasticity by single cell RNA-seq. *Cancer Med*, *8*(6), 3072-3085. https://doi.org/10.1002/cam4.2113

Song, W., Yeh, C. R., He, D., Wang, Y., Xie, H., Pang, S. T., Chang, L. S., Li, L., & Yeh, S. (2015). Infiltrating neutrophils promote renal cell carcinoma progression via VEGFa/HIF2alpha and estrogen receptor beta signals. *Oncotarget*, *6*(22), 19290-19304. https://doi.org/10.18632/oncotarget.4478

Sorrelle, N., Ganguly, D., Dominguez, A. T. A., Zhang, Y., Huang, H., Dahal, L. N., Burton, N., Ziemys, A., & Brekken, R. A. (2019). Improved Multiplex Immunohistochemistry for Immune Microenvironment Evaluation of Mouse Formalin-Fixed, Paraffin-Embedded Tissues. *J Immunol*, *202*(1), 292-299. https://doi.org/10.4049/jimmunol.1800878

Sorrentino, C., Miele, L., Porta, A., Pinto, A., & Morello, S. (2015). Myeloid-derived suppressor cells contribute to A2B adenosine receptor-induced VEGF production and angiogenesis in a mouse melanoma model. *Oncotarget*, *6*(29), 27478-27489. https://doi.org/10.18632/oncotarget.4393

Spranger, S., Bao, R., & Gajewski, T. F. (2015). Melanoma-intrinsic beta-catenin signalling prevents anti-tumour immunity. *Nature*, *523*(7559), 231-235. https://doi.org/10.1038/nature14404

Spranger, S., Dai, D., Horton, B., & Gajewski, T. F. (2017). Tumor-Residing Batf3 Dendritic Cells Are Required for Effector T Cell Trafficking and Adoptive T Cell Therapy. *Cancer Cell*, *31*(5), 711-723 e714. https://doi.org/10.1016/j.ccell.2017.04.003

Sriratanasak, N., Petsri, K., Laobuthee, A., Wattanathana, W., Vinayanuwattikun, C., Luanpitpong, S., & Chanvorachote, P. (2020). Novel c-Myc-Targeting Compound N, N-Bis (5-Ethyl-2-Hydroxybenzyl) Methylamine for Mediated c-Myc Ubiquitin-Proteasomal Degradation in Lung Cancer Cells. *Mol Pharmacol*, *98*(2), 130-142. https://doi.org/10.1124/mol.120.119719

Staron, M. M., Gray, S. M., Marshall, H. D., Parish, I. A., Chen, J. H., Perry, C. J., Cui, G., Li, M. O., & Kaech, S. M. (2014). The transcription factor FoxO1 sustains expression of the inhibitory receptor PD-1 and survival of antiviral CD8(+) T cells during chronic infection. *Immunity*, *41*(5), 802-814. https://doi.org/10.1016/j.immuni.2014.10.013

Storck, E. M., Morales-Sanfrutos, J., Serwa, R. A., Panyain, N., Lanyon-Hogg, T., Tolmachova, T., Ventimiglia, L. N., Martin-Serrano, J., Seabra, M. C., Wojciak-Stothard, B., & Tate, E. W. (2019). Dual chemical probes enable quantitative system-wide analysis of protein prenylation and prenylation dynamics. *Nat Chem*, *11*(6), 552-561. https://doi.org/10.1038/s41557-019-0237-6

Strauss, L., Sangaletti, S., Consonni, F. M., Szebeni, G., Morlacchi, S., Totaro, M. G., Porta, C., Anselmo, A., Tartari, S., Doni, A., Zitelli, F., Tripodo, C., Colombo, M. P., & Sica, A. (2015). RORC1 Regulates Tumor-Promoting "Emergency" Granulo-Monocytopoiesis. *Cancer Cell*, *28*(2), 253-269. https://doi.org/10.1016/j.ccell.2015.07.006

Su, D., & Wilson, J. E. (2002). Purification of the Type II and Type III isozymes of rat hexokinase, expressed in yeast. *Protein Expr Purif*, *24*(1), 83-89. https://doi.org/10.1006/prep.2001.1537

Subbiah, V., Puzanov, I., Blay, J. Y., Chau, I., Lockhart, A. C., Raje, N. S., Wolf, J., Baselga, J., Meric-Bernstam, F., Roszik, J., Diamond, E. L., Riely, G. J., Sherman, E. J., Riehl, T., Pitcher, B., & Hyman, D. M. (2020). Pan-Cancer Efficacy of Vemurafenib in BRAF (V600)-Mutant Non-Melanoma Cancers. *Cancer Discov*, *10*(5), 657-663. https://doi.org/10.1158/2159-8290.CD-19-1265

Subramanian, A., Tamayo, P., Mootha, V. K., Mukherjee, S., Ebert, B. L., Gillette, M. A., Paulovich, A., Pomeroy, S. L., Golub, T. R., Lander, E. S., & Mesirov, J. P. (2005). Gene set enrichment analysis: a knowledge-based approach for interpreting genome-wide expression profiles. *Proc Natl Acad Sci U S A*, *102*(43), 15545-15550. https://doi.org/10.1073/pnas.0506580102

Sukumar, M., Liu, J., Ji, Y., Subramanian, M., Crompton, J. G., Yu, Z., Roychoudhuri, R., Palmer, D. C., Muranski, P., Karoly, E. D., Mohney, R. P., Klebanoff, C. A., Lal, A., Finkel, T., Restifo, N. P., & Gattinoni, L. (2013). Inhibiting glycolytic metabolism enhances CD8+ T cell memory and antitumor function. *J Clin Invest*, *123*(10), 4479-4488. https://doi.org/10.1172/JCI69589

Sullivan, M. R., Danai, L. V., Lewis, C. A., Chan, S. H., Gui, D. Y., Kunchok, T., Dennstedt, E. A., Vander Heiden, M. G., & Muir, A. (2019). Quantification of microenvironmental metabolites in murine cancers reveals determinants of tumor nutrient availability. *Elife*, *8*. https://doi.org/10.7554/eLife.44235

Sun, D., Wang, J., Han, Y., Dong, X., Ge, J., Zheng, R., Shi, X., Wang, B., Li, Z., Ren, P., Sun, L., Yan, Y., Zhang, P., Zhang, F., Li, T., & Wang, C. (2021). TISCH: a comprehensive web resource enabling interactive single-cell transcriptome visualization of tumor microenvironment. *Nucleic Acids Res*, *49*(D1), D1420-D1430. https://doi.org/10.1093/nar/gkaa1020

Sun, Q., Chen, X., Ma, J., Peng, H., Wang, F., Zha, X., Wang, Y., Jing, Y., Yang, H., Chen, R., Chang, L., Zhang, Y., Goto, J., Onda, H., Chen, T., Wang, M. R., Lu, Y., You, H., Kwiatkowski, D., & Zhang, H. (2011). Mammalian target of rapamycin up-regulation of pyruvate kinase isoenzyme type M2 is critical for aerobic glycolysis and tumor growth. *Proc Natl Acad Sci U S A*, *108*(10), 4129-4134. https://doi.org/10.1073/pnas.1014769108

Sun, S., Chen, S., Liu, F., Wu, H., McHugh, J., Bergin, I. L., Gupta, A., Adams, D., & Guan, J. L. (2015). Constitutive Activation of mTORC1 in Endothelial Cells Leads to the Development and Progression of Lymphangiosarcoma through VEGF Autocrine Signaling. *Cancer Cell*, *28*(6), 758-772. https://doi.org/10.1016/j.ccell.2015.10.004

Svastova, E., Hulikova, A., Rafajova, M., Zat'ovicova, M., Gibadulinova, A., Casini, A., Cecchi, A., Scozzafava, A., Supuran, C. T., Pastorek, J., & Pastorekova, S. (2004). Hypoxia activates the capacity of tumor-associated carbonic anhydrase IX to acidify extracellular pH. *FEBS Lett*, *577*(3), 439-445. https://doi.org/10.1016/j.febslet.2004.10.043

Synnestvedt, K., Furuta, G. T., Comerford, K. M., Louis, N., Karhausen, J., Eltzschig, H. K., Hansen, K. R., Thompson, L. F., & Colgan, S. P. (2002). Ecto-5'-nucleotidase (CD73) regulation by hypoxia-inducible factor-1 mediates permeability changes in intestinal epithelia. *J Clin Invest*, *110*(7), 993-1002. https://doi.org/10.1172/JCI15337

Tabancay, A. P., Jr., Gau, C. L., Machado, I. M., Uhlmann, E. J., Gutmann, D. H., Guo, L., & Tamanoi, F. (2003). Identification of dominant negative mutants of Rheb GTPase and their use to implicate the involvement of human Rheb in the activation of p70S6K. *J Biol Chem*, *278*(41), 39921-39930. https://doi.org/10.1074/jbc.M306553200

Tan, A. S., Baty, J. W., Dong, L. F., Bezawork-Geleta, A., Endaya, B., Goodwin, J., Bajzikova, M., Kovarova, J., Peterka, M., Yan, B., Pesdar, E. A., Sobol, M., Filimonenko, A., Stuart, S., Vondrusova, M., Kluckova, K., Sachaphibulkij, K., Rohlena, J., Hozak, P., . . . Berridge, M. V. (2015). Mitochondrial genome acquisition restores respiratory function and tumorigenic potential of cancer cells without mitochondrial DNA. *Cell Metab*, *21*(1), 81-94. https://doi.org/10.1016/j.cmet.2014.12.003

Tan, Z., Xie, N., Banerjee, S., Cui, H., Fu, M., Thannickal, V. J., & Liu, G. (2015). The monocarboxylate transporter 4 is required for glycolytic reprogramming and inflammatory response in macrophages. *J Biol Chem*, *290*(1), 46-55. https://doi.org/10.1074/jbc.M114.603589

Tan, Z., Xie, N., Cui, H., Moellering, D. R., Abraham, E., Thannickal, V. J., & Liu, G. (2015). Pyruvate dehydrogenase kinase 1 participates in macrophage polarization via regulating glucose metabolism. *J Immunol*, *194*(12), 6082-6089. https://doi.org/10.4049/jimmunol.1402469

Tang, Z., Li, C., Kang, B., Gao, G., Li, C., & Zhang, Z. (2017). GEPIA: a web server for cancer and normal gene expression profiling and interactive analyses. *Nucleic Acids Res*, *45*(W1), W98-W102. https://doi.org/10.1093/nar/gkx247

Tassi, I., Cella, M., Gilfillan, S., Turnbull, I., Diacovo, T. G., Penninger, J. M., & Colonna, M. (2007). p110gamma and p110delta phosphoinositide 3-kinase signaling pathways synergize to control development and functions of murine NK cells. *Immunity*, *27*(2), 214-227. https://doi.org/10.1016/j.immuni.2007.07.014

Tateishi, K., Iafrate, A. J., Ho, Q., Curry, W. T., Batchelor, T. T., Flaherty, K. T., Onozato, M. L., Lelic, N., Sundaram, S., Cahill, D. P., Chi, A. S., & Wakimoto, H. (2016). Myc-Driven Glycolysis Is a Therapeutic Target in Glioblastoma. *Clin Cancer Res*, *22*(17), 4452-4465. https://doi.org/10.1158/1078-0432.CCR-15-2274

Tavakoli, S., Short, J. D., Downs, K., Nguyen, H. N., Lai, Y., Zhang, W., Jerabek, P., Goins, B., Sadeghi, M. M., & Asmis, R. (2017). Differential Regulation of Macrophage Glucose Metabolism by Macrophage Colony-stimulating Factor and Granulocyte-Macrophage Colony-stimulating Factor: Implications for (18)F FDG PET Imaging of Vessel Wall Inflammation. *Radiology*, *283*(1), 87-97. https://doi.org/10.1148/radiol.2016160839

Tavare, R., Escuin-Ordinas, H., Mok, S., McCracken, M. N., Zettlitz, K. A., Salazar, F. B., Witte, O. N., Ribas, A., & Wu, A. M. (2016). An Effective Immuno-PET Imaging Method to Monitor CD8-Dependent Responses to Immunotherapy. *Cancer Res*, *76*(1), 73-82. https://doi.org/10.1158/0008-5472.CAN-15-1707

Tcyganov, E., Mastio, J., Chen, E., & Gabrilovich, D. I. (2018). Plasticity of myeloid-derived suppressor cells in cancer. *Curr Opin Immunol*, *51*, 76-82. https://doi.org/10.1016/j.coi.2018.03.009

Tee, A. R., Manning, B. D., Roux, P. P., Cantley, L. C., & Blenis, J. (2003). Tuberous sclerosis complex gene products, Tuberin and Hamartin, control mTOR signaling by acting as a GTPase-activating protein complex toward Rheb. *Curr Biol*, *13*(15), 1259-1268. https://doi.org/10.1016/s0960-9822(03)00506-2

Tekle, C., Nygren, M. K., Chen, Y. W., Dybsjord, I., Nesland, J. M., Maelandsmo, G. M., & Fodstad, O. (2012). B7-H3 contributes to the metastatic capacity of melanoma cells by modulation of known metastasis-associated genes. *Int J Cancer*, *130*(10), 2282-2290. https://doi.org/10.1002/ijc.26238

TeSlaa, T., Bartman, C. R., Jankowski, C. S. R., Zhang, Z., Xu, X., Xing, X., Wang, L., Lu, W., Hui, S., & Rabinowitz, J. D. (2021). The Source of Glycolytic Intermediates in Mammalian Tissues. *Cell Metab*, *33*(2), 367-378 e365. https://doi.org/10.1016/j.cmet.2020.12.020

Thomas, G. V., Tran, C., Mellinghoff, I. K., Welsbie, D. S., Chan, E., Fueger, B., Czernin, J., & Sawyers, C. L. (2006). Hypoxia-inducible factor determines sensitivity to inhibitors of mTOR in kidney cancer. *Nat Med*, *12*(1), 122-127. https://doi.org/10.1038/nm1337

Tirosh, I., Izar, B., Prakadan, S. M., Wadsworth, M. H., 2nd, Treacy, D., Trombetta, J. J., Rotem, A., Rodman, C., Lian, C., Murphy, G., Fallahi-Sichani, M., Dutton-Regester, K., Lin, J. R., Cohen, O., Shah, P., Lu, D., Genshaft, A. S., Hughes, T. K., Ziegler, C. G., . . . Garraway, L. A. (2016). Dissecting the multicellular ecosystem of metastatic melanoma by single-cell RNA-seq. *Science*, *352*(6282), 189-196. https://doi.org/10.1126/science.aad0501

Tomlinson, I. P., Alam, N. A., Rowan, A. J., Barclay, E., Jaeger, E. E., Kelsell, D., Leigh, I., Gorman, P., Lamlum, H., Rahman, S., Roylance, R. R., Olpin, S., Bevan, S., Barker, K., Hearle, N., Houlston, R. S., Kiuru, M., Lehtonen, R., Karhu, A., . . . Multiple Leiomyoma, C. (2002). Germline mutations in FH predispose to dominantly inherited uterine fibroids, skin leiomyomata and papillary renal cell cancer. *Nat Genet*, *30*(4), 406-410. https://doi.org/10.1038/ng849

Torres, C., Mancinelli, G., Cordoba-Chacon, J., Viswakarma, N., Castellanos, K., Grimaldo, S., Kumar, S., Principe, D., Dorman, M. J., McKinney, R., Hirsch, E., Dawson, D., Munshi, H. G., Rana, A., & Grippo, P. J. (2019). p110gamma deficiency protects against pancreatic carcinogenesis yet predisposes to diet-induced hepatotoxicity. *Proc Natl Acad Sci U S A*, *116*(29), 14724-14733. https://doi.org/10.1073/pnas.1813012116

Tracz, A., Mastri, M., Lee, C. R., Pili, R., & Ebos, J. M. (2014). Modeling spontaneous metastatic renal cell carcinoma (mRCC) in mice following nephrectomy. *J Vis Exp*(86). https://doi.org/10.3791/51485

Tuo, Z., Zheng, X., Zong, Y., Li, J., Zou, C., Lv, Y., & Liu, J. (2020). HK3 is correlated with immune infiltrates and predicts response to immunotherapy in non-small cell lung cancer. *Clin Transl Med*, *10*(1), 319-330. https://doi.org/10.1002/ctm2.6

Turajlic, S., Xu, H., Litchfield, K., Rowan, A., Chambers, T., Lopez, J. I., Nicol, D., O'Brien, T., Larkin, J., Horswell, S., Stares, M., Au, L., Jamal-Hanjani, M., Challacombe, B., Chandra, A., Hazell, S., Eichler-Jonsson, C., Soultati, A., Chowdhury, S., . . . Consortium, T. R. R. (2018). Tracking Cancer Evolution Reveals Constrained Routes to Metastases: TRACERx Renal. *Cell*, *173*(3), 581-594 e512. https://doi.org/10.1016/j.cell.2018.03.057

Uehara, M., McGrath, M. M., Ohori, S., Solhjou, Z., Banouni, N., Routray, S., Evans, C., DiNitto, J. P., Elkhal, A., Turka, L. A., Strom, T. B., Tullius, S. G., Winkler, D. G., Azzi, J., & Abdi, R. (2017). Regulation of T cell alloimmunity by PI3Kgamma and PI3Kdelta. *Nat Commun*, *8*(1), 951. https://doi.org/10.1038/s41467-017-00982-x

Ullah, M. S., Davies, A. J., & Halestrap, A. P. (2006). The plasma membrane lactate transporter MCT4, but not MCT1, is up-regulated by hypoxia through a HIF-1alpha-dependent mechanism. *J Biol Chem*, *281*(14), 9030-9037. https://doi.org/10.1074/jbc.M511397200

Ureta, T., Medina, C., & Preller, A. (1987). The evolution of hexokinases. *Arch Biol Med Exp*, *20*(3-4), 343-357. https://www.ncbi.nlm.nih.gov/pubmed/8816075

Valero, C., Lee, M., Hoen, D., Zehir, A., Berger, M. F., Seshan, V. E., Chan, T. A., & Morris, L. G. T. (2021). Response Rates to Anti-PD-1 Immunotherapy in Microsatellite-Stable Solid Tumors With 10 or More Mutations per Megabase. *JAMA Oncol*, *7*(5), 739-743. https://doi.org/10.1001/jamaoncol.2020.7684

Van den Bossche, J., Baardman, J., Otto, N. A., van der Velden, S., Neele, A. E., van den Berg, S. M., Luque-Martin, R., Chen, H. J., Boshuizen, M. C., Ahmed, M., Hoeksema, M. A., de Vos, A. F., & de Winther, M. P. (2016). Mitochondrial Dysfunction Prevents Repolarization of Inflammatory Macrophages. *Cell Rep*, *17*(3), 684-696. https://doi.org/10.1016/j.celrep.2016.09.008

Vander Heiden, M. G., Cantley, L. C., & Thompson, C. B. (2009). Understanding the Warburg effect: the metabolic requirements of cell proliferation. *Science*, *324*(5930), 1029-1033. https://doi.org/10.1126/science.1160809

Vander Heiden, M. G., & DeBerardinis, R. J. (2017). Understanding the Intersections between Metabolism and Cancer Biology. *Cell*, *168*(4), 657-669. https://doi.org/10.1016/j.cell.2016.12.039

Vanharanta, S., Buchta, M., McWhinney, S. R., Virta, S. K., Peczkowska, M., Morrison, C. D., Lehtonen, R., Januszewicz, A., Jarvinen, H., Juhola, M., Mecklin, J. P., Pukkala, E., Herva, R., Kiuru, M., Nupponen, N. N., Aaltonen, L. A., Neumann, H. P., & Eng, C. (2004). Early-onset renal cell carcinoma as a novel extraparaganglial component of SDHB-associated heritable paraganglioma. *Am J Hum Genet*, *74*(1), 153-159. https://doi.org/10.1086/381054

Vats, D., Mukundan, L., Odegaard, J. I., Zhang, L., Smith, K. L., Morel, C. R., Wagner, R. A., Greaves, D. R., Murray, P. J., & Chawla, A. (2006). Oxidative metabolism and PGC-1beta attenuate macrophage-mediated inflammation. *Cell Metab*, *4*(1), 13-24. https://doi.org/10.1016/j.cmet.2006.05.011

Veglia, F., Tyurin, V. A., Mohammadyani, D., Blasi, M., Duperret, E. K., Donthireddy, L., Hashimoto, A., Kapralov, A., Amoscato, A., Angelini, R., Patel, S., Alicea-Torres, K., Weiner, D., Murphy, M. E., Klein-Seetharaman, J., Celis, E., Kagan, V. E., & Gabrilovich, D. I. (2017). Lipid bodies containing oxidatively truncated lipids block

antigen cross-presentation by dendritic cells in cancer. *Nat Commun*, *8*(1), 2122. https://doi.org/10.1038/s41467-017-02186-9
Veiga-da-Cunha, M., Chevalier, N., Stephenne, X., Defour, J. P., Paczia, N., Ferster, A., Achouri, Y., Dewulf, J. P., Linster, C. L., Bommer, G. T., & Van Schaftingen, E. (2019). Failure to eliminate a phosphorylated glucose analog leads to neutropenia in patients with G6PT and G6PC3 deficiency. *Proc Natl Acad Sci U S A*, *116*(4), 1241-1250. https://doi.org/10.1073/pnas.1816143116
Venneti, S., Dunphy, M. P., Zhang, H., Pitter, K. L., Zanzonico, P., Campos, C., Carlin, S. D., La Rocca, G., Lyashchenko, S., Ploessl, K., Rohle, D., Omuro, A. M., Cross, J. R., Brennan, C. W., Weber, W. A., Holland, E. C., Mellinghoff, I. K., Kung, H. F., Lewis, J. S., & Thompson, C. B. (2015). Glutamine-based PET imaging facilitates enhanced metabolic evaluation of gliomas in vivo. *Sci Transl Med*, *7*(274), 274ra217. https://doi.org/10.1126/scitranslmed.aaa1009
Voron, T., Colussi, O., Marcheteau, E., Pernot, S., Nizard, M., Pointet, A. L., Latreche, S., Bergaya, S., Benhamouda, N., Tanchot, C., Stockmann, C., Combe, P., Berger, A., Zinzindohoue, F., Yagita, H., Tartour, E., Taieb, J., & Terme, M. (2015). VEGF-A modulates expression of inhibitory checkpoints on CD8+ T cells in tumors. *J Exp Med*, *212*(2), 139-148. https://doi.org/10.1084/jem.20140559
Waickman, A. T., & Powell, J. D. (2012). mTOR, metabolism, and the regulation of T-cell differentiation and function. *Immunol Rev*, *249*(1), 43-58. https://doi.org/10.1111/j.1600-065X.2012.01152.x
Wang, F., Zhang, S., Vuckovic, I., Jeon, R., Lerman, A., Folmes, C. D., Dzeja, P. P., & Herrmann, J. (2018). Glycolytic Stimulation Is Not a Requirement for M2 Macrophage Differentiation. *Cell Metab*, *28*(3), 463-475 e464. https://doi.org/10.1016/j.cmet.2018.08.012
Wang, J., Ye, C., Chen, C., Xiong, H., Xie, B., Zhou, J., Chen, Y., Zheng, S., & Wang, L. (2017). Glucose transporter GLUT1 expression and clinical outcome in solid tumors: a systematic review and meta-analysis. *Oncotarget*, *8*(10), 16875-16886. https://doi.org/10.18632/oncotarget.15171
Wang, L., Kang, F. B., & Shan, B. E. (2014). B7-H3-mediated tumor immunology: Friend or foe? *Int J Cancer*, *134*(12), 2764-2771. https://doi.org/10.1002/ijc.28474
Wang, L., Xing, X., Zeng, X., Jackson, S. R., TeSlaa, T., Al-Dalahmah, O., Samarah, L. Z., Goodwin, K., Yang, L., McReynolds, M. R., Li, X., Wolff, J. J., Rabinowitz, J. D., & Davidson, S. M. (2022). Spatially resolved isotope tracing reveals tissue metabolic activity. *Nat Methods*, *19*(2), 223-230. https://doi.org/10.1038/s41592-021-01378-y
Wang, R., Dillon, C. P., Shi, L. Z., Milasta, S., Carter, R., Finkelstein, D., McCormick, L. L., Fitzgerald, P., Chi, H., Munger, J., & Green, D. R. (2011). The transcription factor Myc controls metabolic reprogramming upon T lymphocyte activation. *Immunity*, *35*(6), 871-882. https://doi.org/10.1016/j.immuni.2011.09.021
Wang, T., Liu, H., Lian, G., Zhang, S. Y., Wang, X., & Jiang, C. (2017). HIF1alpha-Induced Glycolysis Metabolism Is Essential to the Activation of Inflammatory Macrophages. *Mediators Inflamm*, *2017*, 9029327. https://doi.org/10.1155/2017/9029327
Wang, X., He, Y., Zhang, Q., Ren, X., & Zhang, Z. (2021). Direct Comparative Analyses of 10X Genomics Chromium and Smart-seq2. *Genomics Proteomics Bioinformatics*, *19*(2), 253-266. https://doi.org/10.1016/j.gpb.2020.02.005
Warburg, O. (1956). On the origin of cancer cells. *Science*, *123*(3191), 309-314. https://doi.org/10.1126/science.123.3191.309
Warburg, O., Negelein, E., & Posener, K. (1924). Versuche an Überlebendem Carcinomgewebe. *Klinische Wochenschrift*, *3*(24), 1062-1064. https://doi.org/10.1007/BF01736087
Ward, P. S., & Thompson, C. B. (2012). Signaling in control of cell growth and metabolism. *Cold Spring Harb Perspect Biol*, *4*(7), a006783. https://doi.org/10.1101/cshperspect.a006783
Waskow, C., Liu, K., Darrasse-Jeze, G., Guermonprez, P., Ginhoux, F., Merad, M., Shengelia, T., Yao, K., & Nussenzweig, M. (2008). The receptor tyrosine kinase Flt3 is required for dendritic cell development in peripheral lymphoid tissues. *Nat Immunol*, *9*(6), 676-683. https://doi.org/10.1038/ni.1615
Watson, M. J., Vignali, P. D. A., Mullett, S. J., Overacre-Delgoffe, A. E., Peralta, R. M., Grebinoski, S., Menk, A. V., Rittenhouse, N. L., DePeaux, K., Whetstone, R. D., Vignali, D. A. A., Hand, T. W., Poholek, A. C., Morrison, B. M., Rothstein, J. D., Wendell, S. G., & Delgoffe, G. M. (2021). Metabolic support of tumour-infiltrating regulatory T cells by lactic acid. *Nature*, *591*(7851), 645-651. https://doi.org/10.1038/s41586-020-03045-2
Wculek, S. K., Amores-Iniesta, J., Conde-Garrosa, R., Khouili, S. C., Melero, I., & Sancho, D. (2019). Effective cancer immunotherapy by natural mouse conventional type-1 dendritic cells bearing dead tumor antigen. *J Immunother Cancer*, *7*(1), 100. https://doi.org/10.1186/s40425-019-0565-5
Wei, S. C., Meijers, W. C., Axelrod, M. L., Anang, N. A. S., Screever, E. M., Wescott, E. C., Johnson, D. B., Whitley, E., Lehmann, L., Courand, P. Y., Mancuso, J. J., Himmel, L. E., Lebrun-Vignes, B., Wleklinski, M. J., Knollmann, B. C., Srinivasan, J., Li, Y., Atolagbe, O. T., Rao, X., . . . Allison, J. P. (2021). A Genetic Mouse Model Recapitulates Immune Checkpoint Inhibitor-Associated Myocarditis and Supports a Mechanism-Based Therapeutic Intervention. *Cancer Discov*, *11*(3), 614-625. https://doi.org/10.1158/2159-8290.CD-20-0856
Weinberg, S. E., Singer, B. D., Steinert, E. M., Martinez, C. A., Mehta, M. M., Martinez-Reyes, I., Gao, P., Helmin, K. A., Abdala-Valencia, H., Sena, L. A., Schumacker, P. T., Turka, L. A., & Chandel, N. S. (2019).

Mitochondrial complex III is essential for suppressive function of regulatory T cells. *Nature*, *565*(7740), 495-499. https://doi.org/10.1038/s41586-018-0846-z
Weiss, J. M., Hunter, M. V., Cruz, N. M., Baggiolini, A., Tagore, M., Ma, Y., Misale, S., Marasco, M., Simon-Vermot, T., Campbell, N. R., Newell, F., Wilmott, J. S., Johansson, P. A., Thompson, J. F., Long, G. V., Pearson, J. V., Mann, G. J., Scolyer, R. A., Waddell, N., . . . White, R. M. (2022). Anatomic position determines oncogenic specificity in melanoma. *Nature*. https://doi.org/10.1038/s41586-022-04584-6
Wenes, M., Shang, M., Di Matteo, M., Goveia, J., Martin-Perez, R., Serneels, J., Prenen, H., Ghesquiere, B., Carmeliet, P., & Mazzone, M. (2016). Macrophage Metabolism Controls Tumor Blood Vessel Morphogenesis and Metastasis. *Cell Metab*, *24*(5), 701-715. https://doi.org/10.1016/j.cmet.2016.09.008
Weon, J. L., & Potts, P. R. (2015). The MAGE protein family and cancer. *Curr Opin Cell Biol*, *37*, 1-8. https://doi.org/10.1016/j.ceb.2015.08.002
Whyte, D. B., Kirschmeier, P., Hockenberry, T. N., Nunez-Oliva, I., James, L., Catino, J. J., Bishop, W. R., & Pai, J. K. (1997). K- and N-Ras are geranylgeranylated in cells treated with farnesyl protein transferase inhibitors. *J Biol Chem*, *272*(22), 14459-14464. https://doi.org/10.1074/jbc.272.22.14459
Wilson, J. E. (2003). Isozymes of mammalian hexokinase: structure, subcellular localization and metabolic function. *J Exp Biol*, *206*(Pt 12), 2049-2057. https://doi.org/10.1242/jeb.00241
Wise, D. R., DeBerardinis, R. J., Mancuso, A., Sayed, N., Zhang, X. Y., Pfeiffer, H. K., Nissim, I., Daikhin, E., Yudkoff, M., McMahon, S. B., & Thompson, C. B. (2008). Myc regulates a transcriptional program that stimulates mitochondrial glutaminolysis and leads to glutamine addiction. *Proc Natl Acad Sci U S A*, *105*(48), 18782-18787. https://doi.org/10.1073/pnas.0810199105
Witney, T. H., Pisaneschi, F., Alam, I. S., Trousil, S., Kaliszczak, M., Twyman, F., Brickute, D., Nguyen, Q. D., Schug, Z., Gottlieb, E., & Aboagye, E. O. (2014). Preclinical evaluation of 3-18F-fluoro-2,2-dimethylpropionic acid as an imaging agent for tumor detection. *J Nucl Med*, *55*(9), 1506-1512. https://doi.org/10.2967/jnumed.114.140343
Wolf, A. J., Reyes, C. N., Liang, W., Becker, C., Shimada, K., Wheeler, M. L., Cho, H. C., Popescu, N. I., Coggeshall, K. M., Arditi, M., & Underhill, D. M. (2016). Hexokinase Is an Innate Immune Receptor for the Detection of Bacterial Peptidoglycan. *Cell*, *166*(3), 624-636. https://doi.org/10.1016/j.cell.2016.05.076
Wolfson, R. L., & Sabatini, D. M. (2017). The Dawn of the Age of Amino Acid Sensors for the mTORC1 Pathway. *Cell Metab*, *26*(2), 301-309. https://doi.org/10.1016/j.cmet.2017.07.001
Wood, C. G., Ferguson, J. E., 3rd, Parker, J. S., Moore, D. T., Whisenant, J. G., Maygarden, S. J., Wallen, E. M., Kim, W. Y., Milowsky, M. I., Beckermann, K. E., Davis, N. B., Haake, S. M., Karam, J. A., Bortone, D. S., Vincent, B. G., Powles, T., & Rathmell, W. K. (2020). Neoadjuvant pazopanib and molecular analysis of tissue response in renal cell carcinoma. *JCI Insight*, *5*(22). https://doi.org/10.1172/jci.insight.132852
Wortmann, S. B., Van Hove, J. L. K., Derks, T. G. J., Chevalier, N., Knight, V., Koller, A., Oussoren, E., Mayr, J. A., van Spronsen, F. J., Lagler, F. B., Gaughan, S., Van Schaftingen, E., & Veiga-da-Cunha, M. (2020). Treating neutropenia and neutrophil dysfunction in glycogen storage disease type Ib with an SGLT2 inhibitor. *Blood*, *136*(9), 1033-1043. https://doi.org/10.1182/blood.2019004465
Wu, D., Sanin, D. E., Everts, B., Chen, Q., Qiu, J., Buck, M. D., Patterson, A., Smith, A. M., Chang, C. H., Liu, Z., Artyomov, M. N., Pearce, E. L., Cella, M., & Pearce, E. J. (2016). Type 1 Interferons Induce Changes in Core Metabolism that Are Critical for Immune Function. *Immunity*, *44*(6), 1325-1336. https://doi.org/10.1016/j.immuni.2016.06.006
Wu, H., Estrella, V., Beatty, M., Abrahams, D., El-Kenawi, A., Russell, S., Ibrahim-Hashim, A., Longo, D. L., Reshetnyak, Y. K., Moshnikova, A., Andreev, O. A., Luddy, K., Damaghi, M., Kodumudi, K., Pillai, S. R., Enriquez-Navas, P., Pilon-Thomas, S., Swietach, P., & Gillies, R. J. (2020). T-cells produce acidic niches in lymph nodes to suppress their own effector functions. *Nat Commun*, *11*(1), 4113. https://doi.org/10.1038/s41467-020-17756-7
Wu, T., Zhao, Y., Wang, H., Li, Y., Shao, L., Wang, R., Lu, J., Yang, Z., Wang, J., & Zhao, Y. (2016). mTOR masters monocytic myeloid-derived suppressor cells in mice with allografts or tumors. *Sci Rep*, *6*, 20250. https://doi.org/10.1038/srep20250
Wu, W. C., Sun, H. W., Chen, J., OuYang, H. Y., Yu, X. J., Chen, H. T., Shuang, Z. Y., Shi, M., Wang, Z., & Zheng, L. (2019). Immunosuppressive Immature Myeloid Cell Generation Is Controlled by Glutamine Metabolism in Human Cancer. *Cancer Immunol Res*, *7*(10), 1605-1618. https://doi.org/10.1158/2326-6066.CIR-18-0902
Wyatt, E., Wu, R., Rabeh, W., Park, H. W., Ghanefar, M., & Ardehali, H. (2010). Regulation and cytoprotective role of hexokinase III. *PLoS One*, *5*(11), e13823. https://doi.org/10.1371/journal.pone.0013823
Xiang, X., Wind, K., Wiedemann, T., Blume, T., Shi, Y., Briel, N., Beyer, L., Biechele, G., Eckenweber, F., Zatcepin, A., Lammich, S., Ribicic, S., Tahirovic, S., Willem, M., Deussing, M., Palleis, C., Rauchmann, B. S., Gildehaus, F. J., Lindner, S., . . . Brendel, M. (2021). Microglial activation states drive glucose uptake and FDG-PET alterations in neurodegenerative diseases. *Sci Transl Med*, *13*(615), eabe5640. https://doi.org/10.1126/scitranslmed.abe5640
Xiao, Z., Dai, Z., & Locasale, J. W. (2019). Metabolic landscape of the tumor microenvironment at single cell resolution. *Nat Commun*, *10*(1), 3763. https://doi.org/10.1038/s41467-019-11738-0

Xin Yu, J., Hodge, J. P., Oliva, C., Neftelinov, S. T., Hubbard-Lucey, V. M., & Tang, J. (2020). Trends in clinical development for PD-1/PD-L1 inhibitors. *Nat Rev Drug Discov*, *19*(3), 163-164. https://doi.org/10.1038/d41573-019-00182-w

Xu, L., Zhu, Y., Chen, L., An, H., Zhang, W., Wang, G., Lin, Z., & Xu, J. (2014). Prognostic value of diametrically polarized tumor-associated macrophages in renal cell carcinoma. *Ann Surg Oncol*, *21*(9), 3142-3150. https://doi.org/10.1245/s10434-014-3601-1

Xu, W., Liu, W. R., Xu, Y., Tian, X., Anwaier, A., Su, J. Q., Zhu, W. K., Shi, G. H., Wei, G. M., Huang, Y. P., Qu, Y. Y., Zhang, H. L., & Ye, D. W. (2021). Hexokinase 3 dysfunction promotes tumorigenesis and immune escape by upregulating monocyte/macrophage infiltration into the clear cell renal cell carcinoma microenvironment. *Int J Biol Sci*, *17*(9), 2205-2222. https://doi.org/10.7150/ijbs.58295

Xu, W., Yang, H., Liu, Y., Yang, Y., Wang, P., Kim, S. H., Ito, S., Yang, C., Wang, P., Xiao, M. T., Liu, L. X., Jiang, W. Q., Liu, J., Zhang, J. Y., Wang, B., Frye, S., Zhang, Y., Xu, Y. H., Lei, Q. Y., . . . Xiong, Y. (2011). Oncometabolite 2-hydroxyglutarate is a competitive inhibitor of alpha-ketoglutarate-dependent dioxygenases. *Cancer Cell*, *19*(1), 17-30. https://doi.org/10.1016/j.ccr.2010.12.014

Yadav, A., Matson, K. J. E., Li, L., Hua, I., Gaur, P., Alkaslasi, M. R., Hasan, S., Galuta, A., Dedek, A., Ameri, S., Parnell, J., Alshardan, M. M., Qumqumji, F. A., Alhamad, S. M., Wang, A. P., Poulen, G., Lonjon, N., Vachiery-Lahaye, F., Nalls, M. A., . . . Levine, A. J. (2022). The Human Motoneuron Expression Signature is Defined by ALS-Related Genes. *bioRxiv*, 2022.2003.2025.485808. https://doi.org/10.1101/2022.03.25.485808

Yang, J., Zhao, S., Wang, J., Sheng, Q., Liu, Q., & Shyr, Y. (2021). A pan-cancer immunogenomic atlas for immune checkpoint blockade immunotherapy. *Cancer Res*. https://doi.org/10.1158/0008-5472.CAN-21-2335

Yang, M., Li, D., Chang, Z., Yang, Z., Tian, Z., & Dong, Z. (2015). PDK1 orchestrates early NK cell development through induction of E4BP4 expression and maintenance of IL-15 responsiveness. *J Exp Med*, *212*(2), 253-265. https://doi.org/10.1084/jem.20141703

Yang, M. L., Horstman, S., Gee, R., Guyer, P., Lam, T. T., Kanyo, J., Perdigoto, A. L., Speake, C., Greenbaum, C. J., Callebaut, A., Overbergh, L., Kibbey, R. G., Herold, K. C., James, E. A., & Mamula, M. J. (2022). Citrullination of glucokinase is linked to autoimmune diabetes. *Nat Commun*, *13*(1), 1870. https://doi.org/10.1038/s41467-022-29512-0

Yarden, Y. (2001). Biology of HER2 and its importance in breast cancer. *Oncology*, *61 Suppl 2*, 1-13. https://doi.org/10.1159/000055396

Yoshida, G. J. (2020). Beyond the Warburg Effect: N-Myc Contributes to Metabolic Reprogramming in Cancer Cells. *Front Oncol*, *10*, 791. https://doi.org/10.3389/fonc.2020.00791

Yoshida, H., Lareau, C. A., Ramirez, R. N., Rose, S. A., Maier, B., Wroblewska, A., Desland, F., Chudnovskiy, A., Mortha, A., Dominguez, C., Tellier, J., Kim, E., Dwyer, D., Shinton, S., Nabekura, T., Qi, Y., Yu, B., Robinette, M., Kim, K. W., . . . Immunological Genome, P. (2019). The cis-Regulatory Atlas of the Mouse Immune System. *Cell*, *176*(4), 897-912 e820. https://doi.org/10.1016/j.cell.2018.12.036

Yost, K. E., Satpathy, A. T., Wells, D. K., Qi, Y., Wang, C., Kageyama, R., McNamara, K. L., Granja, J. M., Sarin, K. Y., Brown, R. A., Gupta, R. K., Curtis, C., Bucktrout, S. L., Davis, M. M., Chang, A. L. S., & Chang, H. Y. (2019). Clonal replacement of tumor-specific T cells following PD-1 blockade. *Nat Med*, *25*(8), 1251-1259. https://doi.org/10.1038/s41591-019-0522-3

Young, A., Ngiow, S. F., Gao, Y., Patch, A. M., Barkauskas, D. S., Messaoudene, M., Lin, G., Coudert, J. D., Stannard, K. A., Zitvogel, L., Degli-Esposti, M. A., Vivier, E., Waddell, N., Linden, J., Huntington, N. D., Souza-Fonseca-Guimaraes, F., & Smyth, M. J. (2018). A2AR Adenosine Signaling Suppresses Natural Killer Cell Maturation in the Tumor Microenvironment. *Cancer Res*, *78*(4), 1003-1016. https://doi.org/10.1158/0008-5472.CAN-17-2826

Yu, F., White, S. B., Zhao, Q., & Lee, F. S. (2001). HIF-1alpha binding to VHL is regulated by stimulus-sensitive proline hydroxylation. *Proc Natl Acad Sci U S A*, *98*(17), 9630-9635. https://doi.org/10.1073/pnas.181341498

Yu, M., Yongzhi, H., Chen, S., Luo, X., Lin, Y., Zhou, Y., Jin, H., Hou, B., Deng, Y., Tu, L., & Jian, Z. (2017). The prognostic value of GLUT1 in cancers: a systematic review and meta-analysis. *Oncotarget*, *8*(26), 43356-43367. https://doi.org/10.18632/oncotarget.17445

Yuen, K. C., Liu, L. F., Gupta, V., Madireddi, S., Keerthivasan, S., Li, C., Rishipathak, D., Williams, P., Kadel, E. E., 3rd, Koeppen, H., Chen, Y. J., Modrusan, Z., Grogan, J. L., Banchereau, R., Leng, N., Thastrom, A., Shen, X., Hashimoto, K., Tayama, D., . . . Mariathasan, S. (2020). High systemic and tumor-associated IL-8 correlates with reduced clinical benefit of PD-L1 blockade. *Nat Med*, *26*(5), 693-698. https://doi.org/10.1038/s41591-020-0860-1

Zack, T. I., Schumacher, S. E., Carter, S. L., Cherniack, A. D., Saksena, G., Tabak, B., Lawrence, M. S., Zhsng, C. Z., Wala, J., Mermel, C. H., Sougnez, C., Gabriel, S. B., Hernandez, B., Shen, H., Laird, P. W., Getz, G., Meyerson, M., & Beroukhim, R. (2013). Pan-cancer patterns of somatic copy number alteration. *Nat Genet*, *45*(10), 1134-1140. https://doi.org/10.1038/ng.2760

Zappasodi, R., Serganova, I., Cohen, I. J., Maeda, M., Shindo, M., Senbabaoglu, Y., Watson, M. J., Leftin, A., Maniyar, R., Verma, S., Lubin, M., Ko, M., Mane, M. M., Zhong, H., Liu, C., Ghosh, A., Abu-Akeel, M.,

Ackerstaff, E., Koutcher, J. A., . . . Merghoub, T. (2021). CTLA-4 blockade drives loss of Treg stability in glycolysis-low tumours. *Nature*, *591*(7851), 652-658. https://doi.org/10.1038/s41586-021-03326-4

Zawacka-Pankau, J., Grinkevich, V. V., Hunten, S., Nikulenkov, F., Gluch, A., Li, H., Enge, M., Kel, A., & Selivanova, G. (2011). Inhibition of glycolytic enzymes mediated by pharmacologically activated p53: targeting Warburg effect to fight cancer. *J Biol Chem*, *286*(48), 41600-41615. https://doi.org/10.1074/jbc.M111.240812

Zeng, H., Cohen, S., Guy, C., Shrestha, S., Neale, G., Brown, S. A., Cloer, C., Kishton, R. J., Gao, X., Youngblood, B., Do, M., Li, M. O., Locasale, J. W., Rathmell, J. C., & Chi, H. (2016). mTORC1 and mTORC2 Kinase Signaling and Glucose Metabolism Drive Follicular Helper T Cell Differentiation. *Immunity*, *45*(3), 540-554. https://doi.org/10.1016/j.immuni.2016.08.017

Zhang, B., Yao, G., Zhang, Y., Gao, J., Yang, B., Rao, Z., & Gao, J. (2011). M2-polarized tumor-associated macrophages are associated with poor prognoses resulting from accelerated lymphangiogenesis in lung adenocarcinoma. *Clinics (Sao Paulo)*, *66*(11), 1879-1886. https://doi.org/10.1590/s1807-59322011001100006

Zhang, D., Tang, Z., Huang, H., Zhou, G., Cui, C., Weng, Y., Liu, W., Kim, S., Lee, S., Perez-Neut, M., Ding, J., Czyz, D., Hu, R., Ye, Z., He, M., Zheng, Y. G., Shuman, H. A., Dai, L., Ren, B., . . . Zhao, Y. (2019). Metabolic regulation of gene expression by histone lactylation. *Nature*, *574*(7779), 575-580. https://doi.org/10.1038/s41586-019-1678-1

Zhang, H., Gao, P., Fukuda, R., Kumar, G., Krishnamachary, B., Zeller, K. I., Dang, C. V., & Semenza, G. L. (2007). HIF-1 inhibits mitochondrial biogenesis and cellular respiration in VHL-deficient renal cell carcinoma by repression of C-MYC activity. *Cancer Cell*, *11*(5), 407-420. https://doi.org/10.1016/j.ccr.2007.04.001

Zhang, L., Li, Z., Skrzypczynska, K. M., Fang, Q., Zhang, W., O'Brien, S. A., He, Y., Wang, L., Zhang, Q., Kim, A., Gao, R., Orf, J., Wang, T., Sawant, D., Kang, J., Bhatt, D., Lu, D., Li, C. M., Rapaport, A. S., . . . Yu, X. (2020). Single-Cell Analyses Inform Mechanisms of Myeloid-Targeted Therapies in Colon Cancer. *Cell*, *181*(2), 442-459 e429. https://doi.org/10.1016/j.cell.2020.03.048

Zhang, X., Shen, L., Liu, Q., Hou, L., & Huang, L. (2019). Inhibiting PI3 kinase-gamma in both myeloid and plasma cells remodels the suppressive tumor microenvironment in desmoplastic tumors. *J Control Release*, *309*, 173-180. https://doi.org/10.1016/j.jconrel.2019.07.039

Zhang, Y., Gao, X., Saucedo, L. J., Ru, B., Edgar, B. A., & Pan, D. (2003). Rheb is a direct target of the tuberous sclerosis tumour suppressor proteins. *Nat Cell Biol*, *5*(6), 578-581. https://doi.org/10.1038/ncb999

Zhang, Y., Kurupati, R., Liu, L., Zhou, X. Y., Zhang, G., Hudaihed, A., Filisio, F., Giles-Davis, W., Xu, X., Karakousis, G. C., Schuchter, L. M., Xu, W., Amaravadi, R., Xiao, M., Sadek, N., Krepler, C., Herlyn, M., Freeman, G. J., Rabinowitz, J. D., & Ertl, H. C. J. (2017). Enhancing CD8(+) T Cell Fatty Acid Catabolism within a Metabolically Challenging Tumor Microenvironment Increases the Efficacy of Melanoma Immunotherapy. *Cancer Cell*, *32*(3), 377-391 e379. https://doi.org/10.1016/j.ccell.2017.08.004

Zhao, F., Xiao, C., Evans, K. S., Theivanthiran, T., DeVito, N., Holtzhausen, A., Liu, J., Liu, X., Boczkowski, D., Nair, S., Locasale, J. W., & Hanks, B. A. (2018). Paracrine Wnt5a-beta-Catenin Signaling Triggers a Metabolic Program that Drives Dendritic Cell Tolerization. *Immunity*, *48*(1), 147-160 e147. https://doi.org/10.1016/j.immuni.2017.12.004

Zhao, J. S., Shi, S., Qu, H. Y., Keckesova, Z., Cao, Z. J., Yang, L. X., Yu, X., Feng, L., Shi, Z., Krakowiak, J., Mao, R. Y., Shen, Y. T., Fan, Y. M., Fu, T. M., Ye, C., Xu, D., Gao, X., You, J., Li, W., . . . Feng, Y. X. (2022). Glutamine synthetase licenses APC/C-mediated mitotic progression to drive cell growth. *Nat Metab*, *4*(2), 239-253. https://doi.org/10.1038/s42255-021-00524-2

Zhao, X., Li, D. C., Zhu, X. G., Gan, W. J., Li, Z., Xiong, F., Zhang, Z. X., Zhang, G. B., Zhang, X. G., & Zhao, H. (2013). B7-H3 overexpression in pancreatic cancer promotes tumor progression. *Int J Mol Med*, *31*(2), 283-291. https://doi.org/10.3892/ijmm.2012.1212

Zhao, X., Zhang, G. B., Gan, W. J., Xiong, F., Li, Z., Zhao, H., Zhu, D. M., Zhang, B., Zhang, X. G., & Li, D. C. (2013). Silencing of B7-H3 increases gemcitabine sensitivity by promoting apoptosis in pancreatic carcinoma. *Oncol Lett*, *5*(3), 805-812. https://doi.org/10.3892/ol.2013.1118

Zhou, R., Pantel, A. R., Li, S., Lieberman, B. P., Ploessl, K., Choi, H., Blankemeyer, E., Lee, H., Kung, H. F., Mach, R. H., & Mankoff, D. A. (2017). [(18)F](2S,4R)4-Fluoroglutamine PET Detects Glutamine Pool Size Changes in Triple-Negative Breast Cancer in Response to Glutaminase Inhibition. *Cancer Res*, *77*(6), 1476-1484. https://doi.org/10.1158/0008-5472.CAN-16-1945